77-FM-36 JSC-12957

OFT-1 Reference Flight Profile

(NASA-TM-74939) OFT-1 REFERENCE FLIGHT PROFILE. DEORBIT THROUGH LANDING (NASA) 160 p HC A08/MF A01 CSCL 22A

N77-31215

Unclas

G3/12 47394

Deorbit Through Landing

Mission Planning and Analysis Division

August 1977

NASA

National Aeronautics and
Space Administration

Lyndon B. Johnson Space Center
Houston, Texas

77-FM-36 JSC-12957

SHUTTLE PROGRAM

OFT-1 REFERENCE FLIGHT PROFILE

DEORBIT THROUGH LANDING

By David Heath, Lazarus Gonzales, and Moises Montez,
Flight Analysis Branch; James M. Hiott, Roger Ruda,
and Howard C. Kyle, McDonnell Douglas Technical Service Co., Inc.

Approved: Claude A. Graves, Jr.
Claude A. Graves, Jr., Assistant Chief
Flight Analysis Branch

Approved: Ronald L. Berry
Ronald L. Berry, Chief
Mission Planning and Analysis Division

National Aeronautics and Space Administration

Lyndon B. Johnson Space Center

Mission Planning and Analysis Division

Houston, Texas

August 1977

ACKNOWLEDGMENTS

The following organizations have contributed to this document through participation in the OFT Entry-Through-Landing Working Group.

Astronaut Office

Avionics Systems Engineering Division

Crew Training and Procedures Division

Engineering Analysis Division

Flight Control Division

Ground Data Systems Division

McDonnell Douglas Technical Services Company

Mission Planning and Analysis Division

NOAA National Weather Service

Orbiter Project Engineering Office

Program Operations Office

Rockwell International

Space Shuttle Program Office

Structures and Mechanics Division

CONTENTS

TABLES

FIGURES

Figure		Page

OFT-1 REFERENCE FLIGHT PROFILE

DEORBIT THROUGH LANDING

By David Heath, Lazarus Gonzales, and Moises Montez,
Flight Analysis Branch; James M. Hiott, Roger Ruda, and
Howard C. Kyle, McDonnell Douglas Technical Services Co., Inc.

1.0 SUMMARY

This document presents the Orbital Flight Test Number One (OFT-1) deorbit-through-landing reference flight profile. This profile updates the preliminary OFT-1 deorbit-through-landing reference flight profile (ref. 1). Detailed descriptions and the rationale for the shaping of each phase are included.

Since reference 1 was published, the projected Orbiter weight during entry has increased from 181 450 pounds to 183 839.8 pounds, and the circular orbital altitude prior to deorbit has increased from approximately 120 nautical miles to approximately 150 nautical miles. The deorbit-through-landing reference flight profile described in this document has been reshaped to accommodate these changes and to provide compatibility with manual flight in the approach and landing phase. In addition, the angle-of-attack profile during the transition phase of entry has been modified slightly.

The Orbiter surface temperatures during entry for this profile have been maintained at approximately the same Orbiter surface temperatures of the previous profile (ref. 1). Consequently, the heat load during entry for this profile has increased slightly from that of the previous profile because of the energy that must be dissipated during entry as a result of increased Orbiter weight and orbital altitude.

Providing compatibility with manual flight for the approach and landing phase results in changes to the outer and inner glideslopes from 24 degrees and 3 degrees to 22 degrees and 1.5 degrees, respectively. The modified angle-of-attack profile during the transition phase of entry provides improved trajectory control at initiation of the ramp from the 40-degree angle of attack required for the high heating region of entry to the lower angle of attack required at the entry/terminal area energy management (TAEM) interface and provides more margin for dispersions at the entry/TAEM interface.

The TAEM flight profile has been reshaped to accommodate the 22-degree glideslope at the TAEM/approach and landing interface, to accommodate the lower dynamic pressure and higher angle of attack at entry/TAEM interface caused by

the modified angle-of-attack profile during entry, and to provide better flight control conditions in the TAEM phase.

The analysis performed in shaping the OFT-1 deorbit-through-landing profile has resulted in requirements to modify the entry and TAEM guidance software. A modification to the entry guidance software is required to provide better control of phugoid damping for the higher drag levels necessary because of increased orbiter weight and increased orbiter altitudes. A TAEM guidance software modification is necessary to provide a better match between the reference profile defined by the entry guidance logic and the reference profile defined by the TAEM guidance logic at the entry/TAEM interface.

The modification to the entry guidance software has been approved by the Orbiter Avionics Software Control Board (OASCB). A change request for the modifications to the TAEM guidance has been submitted to the OASCB.

OFT-1 will be launched from Kennedy Space Center (KSC) into an approximate 150-nautical mile altitude circular orbit with a 38-degree inclination. The deorbit maneuver is initiated at 29 hours 40 minutes 03 seconds ground elapsed time (GET) during the 20th orbit, with subsequent landing on runway 17 left on Rogers Lake bed at Edwards Air Force Base (EAFB) at 10 hours 58 minutes 50 seconds local time. The 20th orbit was selected for deorbit because this deorbit opportunity provides communications and tracking by the Guam station between deorbit and entry interface and an opportunity for backup deorbit on the following orbit. Following this backup deorbit opportunity, the next deorbit possibility is about 17.7 hours later during the 33rd orbit. The entry ground tracks are generally north of, and clear of, the densely populated Los Angeles area for deorbit during orbits 17 through 21.

The deorbit targeting is biased to provide the capability to achieve the desired entry interface state vector with two orbiter maneuvering system (OMS) engines as planned for the normal deorbit maneuver or with one OMS engine in contingency situations. The minimum deorbit ΔV for this biased targeting is 364 fps. However, the OMS tanks are loaded and the OMS propellant is budgeted to provide a deorbit capability if the propellant in one OMS tank is unavailable for deorbit, provided a minimum ΔV of 100 fps is available from the reaction control system (RCS) propellant. The availability of this RCS propellant for deorbit using this current loading philosophy, however, is an issue. With this OMS propellant budget, it is necessary to use 3280 pounds excess OMS propellant to achieve the desired longitudinal center of gravity position of 66.25 percent during entry with a resulting orbiter entry weight of 183 839.8 pounds. This propellant wasting is accomplished by an out-of-plane component of the deorbit maneuver resulting in a total ΔV of 528 fps. This deorbit maneuver is 4 minutes 18.4 seconds in duration with 19 minutes 38.8 seconds free-flight time from the end of the deorbit maneuver to the entry interface. For the one-OMS backup deorbit, the maneuver is 8 minutes 36.8 seconds duration with 15 minutes 18.4 seconds free-flight between the end of the deorbit maneuver and the entry interface. Nominal conditions at entry interface are 3066 nautical miles range-to-go, 25 684 fps inertial velocity, and -1.527 degrees inertial flightpath angle.

The entry profile uses a 40-degree angle-of-attack profile to improve the thermal environment to accommodate potential early transition from laminar to turbulent flow on the orbiter underside. The criteria used to shape the entry profile were to ensure structural integrity by limiting the structural temperatures at the expense of higher thermal protection system (TPS) surface temperatures. This may result in the need for TPS tile replacement after the first flight in limited areas of the orbiter. The temperature control phase of the entry profile has been reshaped to accommodate the increased weight and to maintain Orbiter surface temperature to approximately the same temperature as the previous profile (ref. 1). The increased orbiter weight and the higher deorbit altitude, discussed previously, result in an increased heat load for the OFT-1 profile. To help alleviate this increase in heat load, the drag acceleration level in the constant drag phase of entry has been increased 2 fps^2 to 33 fps^2. The net result of these changes is an increase of 978 Btu/ft^2 in heat load with about 1.6 degrees increase in backface temperature. The increase in drag acceleration during the constant drag phase resulted in the need for a modification of the entry logic to provide a better control of the phugoid damping after bank reversals. In addition, the entry-through-landing profile is shaped to satisfy flight control system, structural, and sonic boom guidelines and constraints, and yet provide margins to accommodate the effects of dispersions while providing for trajectory control to damp the phugoid motion induced by bank reversals required for crossrange control. The transition subphase of the entry profile is shaped to provide smooth transition into the TAEM phase and to provide runway redesignation capability as late as possible in the entry phase. The entry/TAEM interface occurs at a relative velocity of 2500 fps.

During entry, the angle-of-attack profile is ramped from 40 degrees at 14 500 fps relative velocity to 13.6 degrees at 2500 fps relative velocity. This represents a slight modification from the preliminary reference flight profile (ref. 1) and provides a smoother drag profile at the initiation of the angle-of-attack ramp, a lower dynamic pressure in the 6000 to 4000 fps relative velocity region, and more margin for dispersions near the entry/TAEM interface. With this angle-of-attack profile, a maximum crossrange of 550 nautical miles is achievable with margins included for first orbital flight dispersions.

The TAEM phase is shaped within the TAEM flight corridor to provide maneuver margins to compensate for winds and trajectory and aerodynamic dispersions while maintaining descent rates and trajectory turning rates acceptable for compartment venting and sonic boom overpressures. The dynamic pressure at initiation of the TAEM guidance is 215 psf and is approximately constant throughout the supersonic flight regime. The dynamic pressure in this regime is higher than that of the previous profile (ref. 1) and causes a lower angle-of-attack profile to be flown during TAEM thus providing improved flight control conditions. This update is dependent on the implementation of a modification to the TAEM guidance flight software, which provides an additional linear reference dynamic pressure as a function of range. The profile is biased toward the undershoot boundary of the TAEM corridor in the transonic region to provide maneuver capability to account for dispersions at the expense of slightly higher sonic boom overpressures. The profile is then ramped to 285 lb/ft^2 dynamic pressure at the end of the TAEM phase as required by the approach and landing phase. This ramp to 285 lb/ft^2 dynamic pressure differs from the preliminary reference flight profile (ref. 1) that was ramped to 300 lb/ft^2 dynamic pressure. This change was required to accommodate an update to a 22-degree steep glideslope in the approach and landing phase. The resulting angle-of-attack profile provides the best conditions possible for the flight control considerations of rolloff, nose slice, lateral directional hysteresis, and aileron hysteresis consistent with maneuver margins and flight corridor limits resulting from other constraints and guidelines. Shaping the TAEM flight profile required an update to the TAEM guidance flight software to include a linear altitude versus range reference profile at the initiation of the TAEM guidance. This logic was necessary to better match the slope of the entry profile at entry/TAEM interface thus minimizing trajectory transients at this interface.

The approach and landing phase flight profile has been completely reshaped since the preliminary reference flight profile (ref. 1) was published and is designed to provide compatibility with manual flight. The criteria used to design the approach and landing phase profile were to fly the outer glideslope as shallow as possible while maintaining adequate performance margins, to provide 10 seconds or more flight time on the inner glideslope, and to provide an energy reserve at nominal touchdown corresponding to 5 seconds of flight time. In addition, the approach and landing phase profile has been shaped to accommodate 50-percent design headwinds and precludes conditions for tailscrape.

Based on these criteria, the approach and landing phase is designed to fly a 22-degree outer glideslope followed by a preflare maneuver onto a 1.5-degree inner glideslope. The 22-degree outer glideslope was chosen because it provides speedbrake settings near midrange capability to account for dispersions at a dynamic pressure of 285 psf. The 285 psf dynamic pressure is necessary to provide 10 seconds of flight time on the inner glideslope and the 5 seconds of energy reserve required at touchdown. Speedbrake retraction occurs at 1800 feet altitude for no-wind and at 4000 feet altitude for 50-percent design head winds. The actual flight time on the 1.5-degree glideslope is 9 seconds. Touchdown occurs at 202 KEAS at a 7.09-degree pitch angle for the no-wind case.

The location of the outer glideslope ground intersect point was chosen to provide touchdown at about 2500 feet down the runway, which ensures that adequate microwave scanning beam landing system (MSBLS) coverage is available until stable conditions on the 1.5-degree inner glideslope are achieved. This geometry also provides conditions for acceptable radar altimeter data when the orbiter is about 4000 feet from the runway threshold.

In shaping the OFT-1 approach and landing profile, tradeoff studies between zero- and 50-degree design headwind cases were examined. The normal load factor during the preflare maneuver for the zero-wind case using the OFT-1 autoland guidance constants is marginal. This is an issue that must be resolved.

Open issues to be resolved are OASCB decisions on the proposed guidance software modifications, reevaluation of the OMS loading philosophy, examination of the effects of trajectory variations on sonic boom overpressures, redefining angle-of-attack profiles as flight control considerations are better understood, determining the Orbiter maneuver capability during the TAEM phase, determining the TAEM heading alinement circle (HAC) geometry for optimum MSBLS acquisition and TAEM guidance performance, defining the wind criteria and the corresponding erasable memory data for the two sets of guidance constants required for the

TAEM and approach and landing phases, performing communications and tracking analysis of the deorbit-through-landing trajectory to verify that communication and tracking coverage predicted from simplified models is adequate, and performing orbiter systems analysis of the deorbit-through-landing profile to verify the orbiter's capability to fly the profile.

Issues that have been resolved since the OFT-1 Preliminary Reference Flight Profile for Deorbit Through Landing document (ref. 1) was published are to provide abort-once-around (AOA) landing capability at EAFB by providing yaw ascent steering and to provide compatibility with the manual flight mode by reshaping the approach and landing flight profile.

2.0 INTRODUCTION

This document presents the Orbiter OFT-1 deorbit-through-landing flight profile that supersedes the Preliminary OFT-1 deorbit-through-landing flight profile (ref. 1). The purpose of this profile is to define the OFT-1 trajectory data for the Orbiter system and subsystem evaluation, flight and Mission Control Center software development and verification, mission techniques development, time-line development, and evaluation of operational suitability.

The OFT-1 profile development was coordinated through the OFT-1 entry-through-landing working group (ref. 2) established by the flight operations panel (FOP) for the purpose of developing the entry-through-landing profiles for the OFT flights. This profile departs from the expected operational profiles in order to minimize the effects of the thermal environment during entry. This is to accommodate the uncertainties in the thermal environment for the first flight, particularly the uncertainty in the point of transition from laminar to turbulent flow on the Orbiter underside. To accomplish this, the 40-degree angle-of-attack profile used for the early part of entry for operational flights is maintained longer in the entry phase for OFT-1 so that energy can be dissipated during entry through the larger drag coefficient for the higher angle of attack, rather than through increased atmospheric density by flying at lower altitudes.

Maintaining the 40-degree angle-of-attack profile through a longer period of the entry significantly reduces the entry crossrange capability of the Orbiter. This reduction is so large that an AOA return to EAFB requires yaw steering during ascent to reduce the crossrange for AOA.

The OFT-1 mission will be launched from KSC into an approximate 150-nautical mile altitude circular orbit at 38 degrees inclination. The OFT-1 deorbit-through-landing flight profile will be updated periodically as open issues are resolved and to reflect the results of assessments by the systems, flight design, and flight operations groups.

Since reference 1 was published, the orbit altitude for OFT-1 has increased from an approximate 120 nautical miles to an approximate 150 nautical miles. This increased orbit altitude provides improved onorbit tracking and communications and is necessary to provide acceptable free-fall time between deorbit and entry interface for mission termination from nominal or backup deorbit opportunities if OMS propellant is loaded to provide deorbit capability using OMS propellant from only one set of tanks. The Orbiter entry weight has also increased from 181 499 pounds to 183 839.8 pounds. The deorbit-through-landing flight profile discussed in this document has been designed to accommodate these changes and to provide compatibility with manual flight. In addition, the ramp in the angle-of-attack profile from the 40 degrees during the high heating region of entry to the lower angle of attack required at entry/TAEM interface has been modified slightly.

The consequence of a higher orbital altitude and a heavier weight Orbiter is reflected in an increase in heat load during the entry phase, which causes slightly higher backface temperatures than those of the preliminary reference flight profile (ref. 1). To help alleviate the increasing heat load, a higher drag acceleration level has been designed for the constant drag phase of entry.

The modification to the entry angle-of-attack profile provides better trajectory control at initiation of the ramp in the angle-of-attack profile and provides improved capability to accommodate dispersions in the 5000 fps to 2500 fps relative velocity region.

The flight profile for the TAEM phase has been reshaped to accommodate the changes in conditions at entry/TAEM interface caused by the modified entry angle-of-attack profile and the conditions at TAEM/approach and landing interface required for a 22-degree outer glideslope for the approach and landing phase. The dynamic pressure at initiation of the TAEM guidance is 215 psf and is approximately constant throughout the supersonic regime to provide improved flight control conditions. Holding the dynamic pressure constant during the supersonic regime is desirable, and a modification to the TAEM guidance software to provide an additional linear reference dynamic pressure versus range segment has been submitted to the OASCB to accommodate this update. The flight profile for the TAEM phase is based on a proposed modification to the TAEM guidance software to provide a linear reference altitude range segment at initiation of the TAEM guidance. This modification is necessary to better match the slope of the entry profile at the TAEM interface and thus minimize transients at the entry/TAEM interface. The TAEM dynamic pressure profile is ramped to 285 psf at the end of the TAEM phase to accommodate a 22-degree outer glideslope for the approach and landing phase.

Providing compatibility with manual flight has resulted in a complete update to the approach and landing flight profile (ref. 1). The outer and inner glideslopes have been changed from 24 degrees and 3 degrees, respectively to 22 degrees and 1.5 degrees, respectively. In addition, the profile is designed to provide 10 seconds of flight time on the inner glideslope with an energy reserve at nominal touchdown corresponding to 5 seconds of flight time. The approach and landing phase profile is also designed to accommodate zero to 50 percent headwinds.

Yaw steering during ascent, which has been implemented to provide AOA landing capability at EAFB, also resulted in improved postdeorbit tracking by the Guam station as reflected in an increase in maximum elevation angle from 4.3 degrees for the previous profile to 26.3 degrees for this profile and an increase in tracking time from 3 minutes 21 seconds to 6 minutes.

During the 20th orbit at 29 hours 40 minutes 02.9 seconds GET, a two-OMS deorbit maneuver targeted to provide a one-OMS backup capability is used to initiate entry with subsequent landing on runway 17 left on Rogers Lake bed at EAFB.

3.0 ACRONYMS

AOA	abort once around
AOS	acquisition of signal
APU	auxiliary power unit
DAP	digital autopilot
EAFB	Edwards Air Force Base
FCS	flight control system
FOP	flight operations panel
fps	feet per second
g	gravity acceleration
GET	ground elasped time
HAC	heading alinement circle
HRSI	high-temperature reusable surface insulation
JSC	Johnson Space Center
KSC	Kennedy Space Center
KEAS	knots equivalent airspeed
LOS	loss of signal
MSBLS	microwave scanning beam landing system
NASA	National Aeronautics and Space Administration
OFT-1	orbital flight test number one
OMS	Orbiter maneuvering system
psf	pounds per square foot
RCC	reinforced carbon-carbon
RCS	reaction control system
RI	Rockwell International
RTLS	return to landing site

STDN	Spaceflight Tracking and Data Network
SVDS	space vehicle dynamics simulation
TAEM	terminal area energy management
TPS	thermal protection system
Ve	relative velocity
ΔV	velocity increment

4.0 PROFILE DESCRIPTION

The guidelines and constraints for shaping the OFT-1 deorbit-through-landing profile are presented in the Appendix. The guideline for landing before 1000 hours local time could not be met for a deorbit that provides tracking and communications between the end of deorbit and the entry interface.

A detailed description of the simulation and performance data used in developing the deorbit-through-landing profile is presented in section 4.1. Detailed discussion of the deorbit, entry, TAEM, and approach and landing phases is presented in sections 4.2 through 4.5. An overall sequence of events is presented in table 4-I. The deorbit-through-landing groundtrack is presented in figure 4-1.

4.1 Simulation Data

The Orbiter weights and balance data used to design the OFT-1 deorbit-through-landing flight profile are presented in reference 3 (table 4.1-I). The OMS loading is summarized in table 4.1-II. The OMS system is loaded to provide a backup deorbit capability if the propellant in one OMS tank is not available for deorbit. This is achieved by using 100 fps ΔV from the RCS propellant tanks and combining this with 82 fps extra ΔV loaded in each OMS propellant tank. For a nominal deorbit with minimum ΔV, this extra OMS propellant results in the longitudinal center of gravity being too far aft. Therefore, the nominal deorbit maneuver has an out-of-plane component to use 3280 pounds excess OMS propellant to achieve the desired 66.25 percent longitudinal center-of-gravity position. This results in an Orbiter weight at the entry interface of 183 839.8 pounds. However, since the design of the OFT-1 profile was initiated, the amount of RCS propellant available for deorbit, using the philosophy of table 4.1-II, is in the process of being revised. In addition, the amount of RCS propellant (ref. 4) used for onorbit maneuvering has increased. Hence, the OMS loading philosophy must be reevaluated.

The OFT-1 deorbit-through-landing trajectory was generated using the space vehicle dynamics simulation (SVDS) program (ref. 5). The flight profile is based on zero winds, the 1962 United States standard atmosphere, and the aerodynamic data defined in the December 1976 Design Data Book (ref. 6). The attitude control system for the entry phase is simulated using a 3-degree-of-freedom model to represent the Orbiter rotational dynamics. The sideslip angle is assumed to be zero and the angle of attack and bank angle are simulated assuming a 5.0-deg/sec pitch rate, a 1.0-deg/sec^2 pitch acceleration, a 5.0-deg/sec roll rate, a 3-degree deadband in entry digital autopilot (DAP), and a 0.85-deg/sec^2 roll acceleration. The flight control system for the TAEM and the approach and landing phase for 3 degrees-of-freedom is simulated by calculating a vehicle inertial attitude matrix and speedbrake deflection by integrating body rate response and speedbrake rate that is based on guidance commands and appropriate limits on the control surface deflection rates. The simulation program used to define the autoland guidance constants was a 6-degree-of-freedom program that utilized the December 1976 aerodynamic data (ref. 6), 50-percent design headwinds, and the flight control system defined in reference 7. Thermal models used to define TPS surface and backface temperatures are the simplified models described in reference 8. The entry, TAEM, and approach and landing guidance used in simulating the OFT-1 profile is defined in reference 9. The navigation simulation used in this reference trajectory is defined in reference 10. The covariance matrix, atmospheric density model, and system constraint limits used in simulating the navigation are presented in tables 4.1-III and 4.1-IV.

The prime landing site for OFT-1 is runway 17 left on Rogers Lake bed at EAFB. The runway azimuth and the coordinate systems origin with respect to the Fischer 1960 spheroid for runway 17 are 190.06 degrees east of north, 34.902 degrees north geodetic latitude, and 117.842 degrees west longitude, and 2220.6 feet altitude (ref. 11).

4.2 Deorbit

The nominal deorbit maneuver occurs during the 20th orbit at 29 hours 40 minutes 02.9 seconds GET at 22.88 degrees south latitude and 103.64 degrees east longitude. At deorbit, the Orbiter is in a 38-degree inclination orbit with apogee and perigee altitudes of 149 nautical miles and 154 nautical miles, respectively. Table 4.2-I (ref. 4) presents the OFT-1 orbits that have deorbit opportunities with subsequent landings at EAFB. The 20th orbit was chosen for the deorbit maneuver because it provides 6 minutes of Guam station tracking and communications with the Orbiter following the deorbit maneuver. The backup deorbit opportunity from the 21st orbit provides about 3 minutes postdeorbit tracking and communications with the Guam station. Deorbit from orbits 17, 18, and 19 have no postburn tracking or communications prior to entry interface. Following the 21st orbit, the next opportunity to deorbit and land at EAFB is about 17.7 hours later on the 33rd orbit. Deorbit on the 20th orbit results in landing at 10 hours 35 minutes 5 seconds local time, which is inconsistent with the ground rule for landing prior to 1000 hours local time (see Appendix). Landing before 1000 hours in the morning results in a higher probability of low magnitude winds and turbulence at low altitudes. Deorbit on orbits 17 through 21 results in entry groundtracks north of the densely populated Los Angeles area.

The deorbit targeting is biased to provide the capability to achieve the desired entry interface state vector with either a two-OMS nominal deorbit maneuver or a one-OMS contingency deorbit maneuver. The minimum deorbit ΔV for this biased targeting is 364 fps. However, the OMS tanks are loaded, and the OMS propellant is budgeted to provide a deorbit capability if the propellant in one OMS tank is unavailable for deorbit, provided a minimum ΔV of 100 fps is available from the RCS propellant. Utilizing the consumable budgets that were baselined for the trajectory computation, it is necessary to use 3280 pounds excess OMS fuel to achieve the desired entry longitudinal center-of-gravity position of 66.25 percent with a resulting Orbiter entry weight of 183 838.9 pounds. This propellant wasting is accomplished by an out-of-plane component during the deorbit maneuver. The deorbit maneuver, including propellant wasting, requires a total ΔV of 528 fps with a burn duration of 4 minutes 18.4 seconds. The free-fall time from the end of thrust termination to entry interface is 19 minutes 38.8 seconds. For the one-OMS contingency backup deorbit, the maneuver is 8 minutes 36.8 seconds in duration with a free-fall time of 15 minutes 18.4 seconds. Significant deorbit parameters are summarized in table 4.2-II. Since the design of the OFT-1 profile presented in this document was initiated, the availability of the required RCS propellant for deorbit for one OMS engine failure using the current loading philosophy has become questionable. In addition, the amount of RCS propellant used for onorbit maneuvers has increased. Therefore, the OMS loading requirements will be revised.

The Orbiter attitude at thrust initiation is 166.1 degrees pitch, 47.97 degrees yaw, and 100.4 degrees roll referenced to the local vertical, local horizontal coordinate system defined in reference 12, with a pitch, yaw, and roll sequence. The roll attitude is attained before the APU's are started, which is about 5 minutes before the deorbit maneuver, and is maintained throughout the burn and until the preentry trim maneuver at entry interface (EI -5 minutes). This procedure results in the APU venting to be out-of-plane as much as possible to minimize the effects of venting in determining the Orbiter state vector. The aerosurfaces are cycled before entry to thermally condition the hydraulic fluid lines. The targeting criteria for OFT-1 entry are presented in figure 4.2-1. Nominal conditions at entry interface are 3066 nautical miles range-to-go, 25 684 fps inertial velocity, and -1.527 degrees inertial flightpath angle.

4.3 Entry

4.3.1 Profile shaping.- The objective of the entry profile shaping for OFT-1 is to minimize the effects of the TPS thermal environment, maximize the flight control system performance margins, and minimize structural loads while providing sufficient maneuver margins to compensate for trajectory, navigation, aerodynamic, and environment dispersions. In some cases, these objectives result in conflicting requirements for the entry profile. For example, shortening the entry range reduces the TPS backface temperatures but increases the TPS surface temperatures unless the angle of attack profile is altered. Increasing the angle-of-attack profile reduces both the TPS surface and backface temperatures because energy is dissipated through the larger drag coefficient for the higher angle of attack rather than through increased atmospheric density by flying lower altitudes. But higher angles of attack also increase the problem of damping the phugoid motion introduced by the bank reversals used for crossrange trajectory control. In general, increasing the angle of attack reduces the aerodynamic crossrange capability, reduces the flight control system margins by reducing the angular acceleration about the stability axis, and if the high angle of attack is maintained to low speeds, reduces the postblackout maneuvering capability for removing navigation and other dispersions and for runway redesignation.

The OFT-1 entry interface through landing groundtrack is presented in figure 4.3-1.

The entry profile developed for OFT-1 is a compromise between the conflicting requirements for profile shaping. Minor modifications were made in two regions of the preliminary reference flight angle-of-attack profile (ref. 1) for this update. One change involves a more gradual quadratic transition from the 40-degree angle of attack to the linear ramp extending to TAEM interface. The updated pitchdown quadratic begins at 14 500 fps and intercepts the linear segment at 7789 fps. This more gradual angle-of-attack transition causes the drag profile to more accurately follow the reference profile in that velocity region. The second modification involves raising the angle-of-attack profile slightly in the latter part of the transition phase from 4500 fps to TAEM interface. This improves the equilibrium glide load factor/dynamic pressure corridor in this region. Basically, the angle-of-attack profile for OFT-1 differs from the design entry profile developed in order to achieve a high crossrange by maintaining the initial entry angle of attack to lower speeds, thus eliminating the ramp to the lower angle-of-attack levels required for high crossrange. The OFT-1 angle-of-attack profile is presented in figure 4.3-2.

With this angle-of-attack profile, the entry corridor as limited by TPS surface temperatures, structural loads, flight control considerations, and the equilibrium glide capability can be defined. This latter constraint must be met to ensure that the flight conditions can be sustained (i.e., no subsequent trajectory transients will necessarily occur) and that crossrange maneuvering is possible. The corridor, as limited by these considerations, is presented in figure 4.3-3 in the drag acceleration (D/m) Earth-relative velocity plane.

The TPS backface temperature is minimized by dissipating the Orbiter kinetic and potential energy as quickly as possible within the limits defined by systems and by flight dynamic constraints as illustrated in figure 4.3-3. This is achieved by maintaining the drag acceleration as high as possible throughout entry. The higher the TPS surface temperatures, the higher the permissible drag acceleration level in the critical high-speed region of entry; therefore, to minimize the backface temperatures, the TPS surface temperatures must be as high as possible. The backface temperature is more sensitive to the drag acceleration level at the higher speeds during entry and is relatively insensitive to the drag acceleration level at speeds below 10 000 to 12 000 fps. The entry trajectory shaping policy is to maintain high drag acceleration during entry consistent with the systems and flight dynamics constraints. This results in minimum entry range, entry flight time, and TPS backface temperatures.

The design drag velocity profile for this update differs from that of the preliminary reference flight profile (ref. 1) in the temperature control phase. This was accomplished to minimize the heat load increase while maintaining the same surface temperatures as on the previous profile considering the increases in vehicle weight and apogee altitude for this update. The temperature control phase of this entry profile is consistent with the philosophy used in shaping the preliminary reference flight profile to maintain margins in structural temperatures at the expense of higher surface temperatures and possible refurbishment of limited TPS surface tiles for OFT-1. In addition, the design constant drag level was increased from 31 fps^2 to 33 fps^2 to aid the heat load minimization The increase in weight and apogee altitude caused the heat load to increase by about 1100 Btu/ft^2 on the preliminary OFT-1 trajectory. Optimizing the drag-velocity profile in the temperature control phase and raising the constant drag level to 33 fps^2 reduced this heat load increase to 978 Btu/ft^2 over the preliminary reference profile (ref. 1).

In shaping the OFT-1 entry profile, the TPS surface temperatures were evaluated at five locations as illustrated in figure 4.3-4. The surface temperature limit is 2800 degrees, which for the high-temperature reusable surface insulation (HRSI) material is the limit for one-mission capability and greater than one-mission capability for the reinforced carbon-carbon (RCC) reusable material. Because the TPS surface temperatures are computed using a simplified TPS model, these limiting temperatures must be adjusted to account for the error in surface temperatures resulting from inaccuracies in temperature prediction. Further, in some cases, the point chosen for surface temperature evaluations in the simplified model is not the most critical point from a surface temperature standpoint, and adjustments in allowable temperatures must be made to compensate for this effect. This is true for control point 5 located at the RCC/HRSI interface on the underside of the fuselage on the Orbiter centerline. The most critical temperature in this region is not located at this interface but at the chine; thus, the allowable surface temperature at control point 5 is adjusted to ensure that the temperature at the RCC/HRSI interface at the chine remains within limits. Also, allowances must be made for the effects of trajectory dispersions and control surface (elevon and body-flap) deflection from the nominal setting required for aerodynamic trim. These effects on TPS surface temperatures and the resulting limits on the nominal value of surface temperatures, calculated using the simplified TPS model, are presented in table 4.3-I.

These limits on the nominal surface temperatures are translated into constraints on the entry corridor in figure 4.3-3. The limiting surface temperatures are for the RCC/HRSI interface on the underside of the fuselage (control point 5) and for the outboard tip of the elevon underside (control point 4). Also shown in figure 4.3-3 are the effects of the remainder of the constraints and the guidelines on the entry corridor. On the first orbital flight, it is desirable to limit the structural loads to 2.0g normal load factor, which is 80 percent of the design value of 2.5g's. Also shown for information purposes is the 1.5g normal load factor line.

The equilibrium glide lines define the minimum drag level that the time rate-of-change of flightpath angle, $\dot{\gamma}$, can be maintained equal to, or greater than, zero. Thus, this line defines the limit for sustaining equilibrium flight. Although flight conditions with lower values of drag acceleration can be achieved, this condition is temporary, and a subsequent trajectory transient to higher drag acceleration will occur. This equilibrium glide boundary is a function of bank angle as well as angle of attack and Earth-relative speed. Therefore, the boundaries were defined for the minimum bank angles used by the entry guidance to ensure a turning capability for crossrange maneuvering. This minimum bank angle is a function of entry speed with higher values required to overcome the higher inertia at high speeds. Thus, the entry guidance uses two discrete levels of minimum bank angle to achieve turning: 37 degrees at high speeds and 20 degrees at low speeds. These bank angle limits result in significant turning capability with little loss in entry corridor because turning capability and entry corridor are functions of the sine and cosine of the bank angle, respectively.

As mentioned earlier, this update to the OFT-1 reference trajectory reflects a weight increase to 183 839.8 pounds and an orbital apogee altitude increase to 150 nautical miles with the objective of maintaining the same maximum surface temperatures. The entry profile was reshaped to minimize the backface temperature increase. The resulting nominal entry profile is presented in figure 4.3-3 along with the entry corridor. The summary of the resulting thermal environment for several surface panels and the five control points is presented in table 4.3-II. The TPS panel locations are presented in figure 4.3-4.

The low-speed part of the entry profile, during transition to the low angle-of-attack and trajectory conditions at the TAEM interface, was shaped to achieve the desired TAEM initial flight conditions and to maintain the entry profile at the location in the entry corridor that maximizes the capability to compensate for navigation, aerodynamic, and environmental dispersions while providing a capability for postblackout runway redesignation. The flight conditions at this interface were defined by selecting the TAEM profile that properly positions the TAEM profile within the TAEM flight corridor and by designing the entry profile to achieve these conditions. The dynamic pressure at the interface is about 215 lb/ft^2 (sec. 4.4). During the transition phase, the entry profile must achieve this flight condition while maintaining the entry profile properly located within the flight corridor to provide maneuver capability to accommodate dispersions and runway redesignation. Because the bank angle essentially determines the location of the flight profile within the corridor, and hence the maneuver margins, the angle of attack is selected to achieve the desired dynamic pressure at the bank angle that provides the necessary maneuver margins. This angle of attack at the interface is compatible with the entry profile, at a higher speed, in that the angle-of-attack profile during transition provides maneuver margins for trajectory control and also results in a profile that provides good flight control characteristics. The resulting interface conditions are summarized in table 4.3-III. These flight conditions provide a smooth transition into the TAEM phase as illustrated in figure 4.3-5, which shows that the entry profile slope is the same as the desired or reference profile slope for the TAEM profile at the interface.

4.3.2 Control surface deflection schedules.- The nominal deflection schedules of the aerodynamic control surfaces are designed to aerodynamically trim the Orbiter to minimize the attitude control moments required from the RCS system and to maximize the effectiveness of the control surfaces to provide Orbiter attitude control while maintaining aerodynamic heating on the control surfaces within limits. The nominal and actual elevon, speedbrake, and body-flap deflection schedules to accomplish this are presented in figures 4.3-6, 4.3-7, and 4.3-8, respectively. During the period of high aerodynamic heating, the speedbrakes are fully retracted to minimize the aerodynamic heating on these surfaces, and the elevon and body-flap deflection schedules are balanced to control the surface temperatures of these two control surfaces. At speeds above 12 000 fps, the elevon is deflected 2 degrees up, and the body flap is deflected 5 degrees up during most of this region. There is a discontinuity in the elevon deflection at about 13 700 fps, which results from a discontinuity in the aerodynamic coefficients when the use of viscous aerodynamic effects is terminated in the simulation. A linear ramp is introduced in the elevon schedule at 12 000 fps to move the elevon to a 2.5-degree down deflection. This down deflection is necessary to ensure that the rolling moment, due to aileron deflection, is not balanced by the rolling moment from the yaw angle induced by the aileron deflection. This provides the capability to use the aileron to compensate for the aerodynamic moments caused by lateral center-of-gravity offset and aerodynamic asymmetries.

After switching to the late entry flight control system that uses the rudder to assist in attitude control, it is necessary to move the elevon to a small up deflection to prevent the ailerons from inducing an adverse yaw that must be compensated for by the rudder. In the subsonic speed range, the elevon is deflected down to reduce the elevon hinge moment. The transition between the different levels of constant elevon deflection is scheduled at approximately the maximum rate for which the body flap can drive to the required deflection to achieve aerodynamic trim.

The speedbrakes are deflected to a full out position at a speed of 8000 fps to induce a pitch up moment so that the elevon can normally be deflected down in this region. Conversely, at a speed of 3000 fps when the elevon is moved to an up position, the speedbrake is moved to a smaller deflection to reduce the pitch up tendency. At subsonic speeds, the nominal speedbrake deflection schedule is the midvalue to allow for modulation for speed control. The body-flap schedule is used to balance the pitching moment to trim the Orbiter.

4.3.3 Nominal trajectory data.- Significant trajectory parameters for the entry through landing are presented in tables 4.3-IV and figures 4.3-10 through 4.3-35. The constants for the entry guidance are presented in table 4.3-V.

4.3.4 Aerodynamic crossrange capability.- The aerodynamic crossrange capability for the OFT-1 is illustrated in table 4.3-VI. The maximum crossrange capability is 753 nautical miles. Allowing 95 nautical miles for entry dispersions and an additional 88 nautical miles for a first flight safety margin reduces the crossrange capability to 570 nautical miles. Allowing for a projected 20-nautical mile increase in crossrange dispersions, the recommended crossrange limit for OFT-1 is 550 nautical miles.

4.4 TAEM

The primary factors that influence the shape of the trajectory during the TAEM phase are aerodynamic maneuver capability, compartment venting, allowance for dispersions and winds, sonic boom overpressures, and flight control considerations. In some cases, these factors result in conflicting requirements on the trajectory shape. For example, the best profile for minimizing sonic boom overpressures and structural problems, which result from compartment venting, is a profile with low dynamic pressure and high angle of attack in the transonic region; whereas, the dynamic pressure should be higher and the angle of attack lower in this flight regime to optimize the flight control system performance and maneuver capability to compensate for winds and dispersions. The OFT-1 TAEM profile shaping objective is to provide flight conditions that result in a proper balance of these conflicting considerations.

The OFT-1 TAEM through landing groundtrack is presented in figure 4.4-1.

The constraints and guidelines that define the flight corridor during the TAEM region are presented in figures 4.4-2 and 4.4-3 in the dynamic pressure

Earth-relative velocity plane and in the angle-of-attack Mach number plane, respectively. Figure 4.4-2 presents the flight limits for the structural and flight control systems, the ground level sonic boom overpressure, the minimum dynamic pressure when constrained to operate on the front side of the L/D curve, and the descent rate guidelines for minimizing pressure differentials across the Orbiter structure and skin resulting from compartment venting. The sonic boom guideline is for a 2.0 lb/ft^2 ground level overpressure and is based upon the data and analysis presented in reference 13. Since the preliminary profile (ref. 1) was published, an assessment (ref. 2) of compartment venting has shown that acceptable venting conditions are maintained for dynamic pressures less than 300 psf in the transonic regime and that venting is less restrictive than the flight control system limit (fig. 4.4-2) in the supersonic and subsonic regimes.

The angle-of-attack corridor presented in figure 4.4-3 defines the angle-of-attack limit for the flight control system as defined in reference 2. Also shown in this figure are the regions where the Orbiter has a tendency for roll off, nose slice, buffet onset, and lateral directional instability. Although the effect of these characteristics on the flight control system performance is not expected to be unacceptable, these regions are avoided to the extent possible for OFT-1 to obtain flight performance data before full commitment to flying in these regions.

The nominal TAEM dynamic pressure profile is also presented in figure 4.4-2. The dynamic pressure at initiation of TAEM guidance is 215 psf and is approximately constant throughout the supersonic regime. This dynamic pressure profile results in an angle-of-attack profile (fig. 4.4-3) in the supersonic regime which provides improved flight control conditions for lateral directional stability. This profile is contingent on a modification to the TAEM guidance to provide an additional reference altitude versus range segment. During the transonic flight regime, the profile was biased toward the undershoot boundary to provide maneuver capability to compensate for wind dispersions in this flight regime. Detailed analysis is required to establish the actual sonic boom overpressure profile, but because the profile is similar to the preliminary flight profile (ref. 1), the sonic boom overpressure is expected to be about 2 psf. During the subsonic TAEM region, the dynamic pressure is ramped to the 285 lb/ft^2 level required by the approach and landing phase. The resulting angle-of-attack profile for OFT-1 is shown in figure 4.4-3 and is consistent with the constraints and guidelines defined for flight control considerations.

Significant trajectory parameters for the TAEM and approach and landing phases are presented in figures 4.4-4 through 4.4-25. Figure 4.4-7 illustrates no significant discontinuity in the angle-of-attack profile but illustrates a change in slope of the profile to achieve low angles of attack required during the transonic region.

Figure 4.4-8 shows a discontinuity in the bank angle at the entry/TAEM interface. Actually, this discontinuity would have been larger if the crossrange trajectory control resulted in a change in the sign of the bank command across this interface. This result would be similar to the effects of bank reversals that are a normal part of the entry control mode and should present no unusual problems.

The TAEM profile was shaped assuming that the TAEM guidance software would be modified to include a linear reference altitude segment as a function of range at initiation of the TAEM guidance. This modification is required to eliminate transients that might occur because the slope of the cubic reference altitude versus range relationship does not correspond to the flightpath angle at the entry/TAEM interface point. The TAEM guidance constants required for this profile are presented in table 4.4-I.

4.5 Approach and Landing

The approach and landing phase consists of a 22-degree steep glideslope followed by a preflare maneuver to a 1.5-degree shallow glideslope with a final flare maneuver just prior to touchdown. These glideslopes and the geometric parameters associated with them are designed specifically for the weight and configuration of the OFT-1 Orbiter vehicle.

The outer glideslope is designed to be as shallow as possible to provide the lowest descent rate and the least demanding maneuver in making a transition to the shallow glideslope and yet to be steep enough to maintain sufficient speedbrake reserves to cope with varying winds and dispersions. Additionally, an airspeed is maintained that provides the velocity at preflare that provides 10 seconds of flight time on the inner glideslope and the desired touchdown conditions. The design values of a 22-degree outer glideslope and 290 KEAS (285 psf dynamic pressure) satisfy these conditions.

The inner glideslope is designed to be as shallow as possible to minimize the sink rate when close to the ground and to require only a slight final flare prior to touchdown and yet to be steep enough to provide reasonable ground clearance while on final approach. A 1.5-degree shallow glideslope meets these conditions better than the 3.0-degree inner glideslope of the OFT-1 preliminary reference flight profile (ref. 1).

Flight profile design considerations associated with the inner glideslope include providing 10 to 15 seconds of flight time after completion of the preflare maneuver and prior to touchdown (ref. 14), both in the presence of 50-percent headwinds and in a no-wind condition, and to ensure MSBLS coverage is available down to an altitude at which the Orbiter is in stable flight on the inner glideslope and is receiving radar altimeter information.

The autoland guidance routines are presently designed such that four sets of approach and landing phase geometric parameters are available to account for two ranges of Orbiter weights and for varying wind conditions. The parameters used in this profile are designed to provide acceptable conditions for the OFT-1 Orbiter weight and zero- to 50-percent design headwinds. The geometry is designed such that with the 50-percent design headwind, enough energy is available at the preflare position to provide the desired final approach and touchdown conditions. For the no-wind environment, the speedbrake is held in its deployed state longer to reduce the energy available at the same preflare position resulting in approximately the same final approach and touchdown conditions.

TAEM/approach and landing interface conditions are presented in table 4.5-I. The groundtrack for approach and landing is presented in figure 4.5-1.

The targeted touchdown conditions are 190 KEAS, -3.0 fps altitude rate with touchdown at 2000 to 3000 feet down the runway from the threshold. This touchdown speed was determined by defining the "tailscrape" velocity (as a function of pitch angle, weight, and configuration) for this vehicle to accommodate either a hot or cold day at EAFB and adding a delta velocity that corresponds to 5 seconds of flight time as recommended in reference 13. The tailscrape airspeed (168 KEAS) and the 5-second extra flight time (about 22 KEAS) result in a targeted nominal touchdown airspeed of about 190 KEAS. The altitude rate at touchdown was chosen to assure a firm touchdown so that a "ground effect" float would not be probable. The touchdown position down the runway was chosen so that MSBLS coverage, because of its vertical coverage limitations, was available until stable flight conditions were achieved on the inner glideslope.

Since the aerodynamic drag increases when the landing gear is deployed, they are deployed as late as possible in the approach and landing phase at 300 feet altitude above the runway. This allows the energy to dissipate at a slower rate thus providing more time on the inner glideslope.

The OFT-1 autoland guidance parameters are designed for the 50-percent wind condition and were verified using a 6-degree-of-freedom simulation. Evaluation of the no-wind case has indicated that the load factor during the preflare maneuver (for the no-wind case) is marginal. The guidance constants must be refined to alleviate this problem. Touchdown conditions resulting from 6-degree-of-freedom simulations of the zero and no-wind cases are presented in table 4.5-2. Table 4.5-2 also includes the touchdown conditions resulting from the 3-degree-of-freedom SVDS simulation used to define the OFT-1 reference flight profile for deorbit through landing.

The variable speedbrake retraction altitude logic provided by the guidance is used to control the energy at preflare to the design conditions. This retraction logic causes the speedbrake to retract at 4000 feet and 1800 feet respectively, for the 50- and zero-percent design headwinds.

The steep glideslope ground intersection and the preflare geometry were determined so that a midrange speedbrake (55- to 60-degree "hinge line") would be utilized during equilibrium conditions (no-wind) on the steep glideslope and so that the preflare maneuver with a maximum normal acceleration of approximately 1.45g's, would result in an initial 1.5-degree glideslope airspeed of about 250 KEAS. This airspeed provides from 10 to 15 seconds of stabilized flight on the inner glideslope prior to main gear touchdown plus the 5 seconds of reserve flight time at touchdown.

The approach and landing geometry is presented in figure 4.5-2. TAEM/approach and landing guidance constants are presented in table 4.5-III. Figures 4.5-3 through 4.5-14 present detailed plots from the 3-degree-of-freedom simulation for some specific parameters describing approach and landing conditions.

TABLE 4-I.- SEQUENCE OF EVENTS FOR OFT-1

(a) Deorbit through landing

	Start time, hr:min:sec (GET)	Δt of event, min:sec	Altitude,[a] ft	Relative velocity, fps	Relative heading, deg	Relative flightpath angle, deg	Longitude +east, deg	Geodetic latitude, deg	Total vehicle weight, lb	c.g., location, percent x	OMS propellant used, lb	ΔV, fps	Maneuver parameters[b] Roll, deg	Pitch, deg	Yaw, deg
Deorbit burn initiation (TIG)	29:40:03	00:00	918 905	24 157	56.868	.011	103.635	-22.881	193 957	67.62			100.45	166.05	47.97
Deorbit burn termination	29:44:21	04:19	909 298	23 817	52.749	-.150	117.601	-13.397	184 057	67.62	9653	528	106.07	176.15	48.29
Initiate post-deorbit attitude maneuver	29:44:51	04:49	906 465	23 820	52.354	-.206	119.129	-12.249	184 055	66.25			106.03	176.13	48.29
Terminate post-deorbit attitude maneuver	29:46:21	06:19	894 035	23 836	51.398	-.375	123.631	-8.751	184 055	66.25			-90.56	-.73	-40.37
Guam S-band acquisition (elevation = 3 deg)	29:51:02	10:59	819 169	23 929	50.538	-.869	137.321	2.490	184 055	66.25					
Guam S-band LOS (elevation = 3 deg)	29:57:09	17:06	651 075	24 138	54.252	-1.358	155.961	16.925	184 055	66.25					
Initiate APU system warmup	29:52:53	-11:05	775 816	23 983	51.064	-1.038	142.762	6.948	184 055	66.25					
Maneuver to entry attitude completed	29:58:54	-08:59	591 085	24 213	56.495	-1.458	161.856	20.800	183 840	66.25					
Initiate entry guidance MM304	29:58:58	-04:59	588 712	24 216	56.590	-1.461	162.087	20.943	183 840	66.25					

[a]Altitude of c.g. above 1960 Fischer ellipsoid.
[b]Pitch, yaw, roll sequence defined in reference 12.

TABLE 4-I.- Continued

(b) Entry interface through landing

	Start time, hr:min:sec (GET)	Δt of event, min:sec	Altitude,[a] ft	Relative velocity, fps	Relative heading, deg	Relative flightpath angle, deg	Longitude +east, deg	Geodetic latitude, deg	Total vehicle weight, lb	c.g., location, percent x	Mach number
Entry interface	30:03:58	00:00	400 000	24 452	66.068	-1.604	-178.898	30.473	183 840	66.25	18.52
Activate aerocontrol surfaces	30:06:05	02:07	317 028	24 549	71.467	-1.591	-169.792	33.496	183 840	66.25	26.35
Deactivate RCS roll thrusters	30:07:24	03:26	304 438	24 559	72.363	-1.575	-168.341	33.892	183 840	66.25	27.16
Initiate temperature control phase; enter S-band communications blackout	30:07:29	03:31	264 217	24 493	75.532	-1.308	-163.300	35.094	183 840	66.25	27.71
Deactivate RCS pitch thrusters	30:07:59	04:02	250 205	24 318	77.087	-.870	-160.887	35.576	183 840	66.25	26.46
Initiate drag updating in navigation filter	30:08:26	04:29	242 806	24 062	78.969	-.553	-158.768	35.943	183 840	66.25	25.61
Initiate equilibrium glide phase	30:11:54	07:56	218 631	20 566	98.429	-.306	-143.161	36.382	183 840	66.25	20.44
Initiate constant drag phase	30:13:36	09:38	210 165	18 167	104.263	-.750	-136.748	35.184	183 840	66.25	17.72
Pt. Pillar C-band acquisition (AOS + 60 sec)	30:16:24	12:26	181 838	12 914	91.894	-.775	-128.300	34.034	183 840	66.25	12.06
Exit S-band communications blackout	30:16:50	12:52	176 848	12 041	89.009	-.934	-127.203	34..026	183 840	66.25	11.19

[a]Altitude of c.g. above 1960 Fischer ellipsoid.

TABLE 4-I.- Continued

(b) Entry interface through landing

	Start time, hr:min:sec (GET)	Δt of event, min:sec	Altitude,[a] ft	Relative velocity, fps	Relative heading, deg	Relative flightpath angle, deg	Longitude +east, deg	Geodetic latitude, deg	Total vehicle weight, lb	c.g., location, percent x	Mach number
Vandenberg C-band acquisition (AOS + 60 sec)	30:16:51	12:53	176 470	11 979	88.790	-.947	-127.127	34.047	183 840	66.25	11.13
Initiate transition phase	30:17:16.4	13:19	171 228	11 176	85.744	-1.162	-126.183	34.064	183 840	66.25	10.33
Exit L-band blackout	30:17:23	13:25	169 920	10 992	84.999	-1.199	-125.974	34.078	183 840	66.25	10.16
San Luis Obispo TACAN acquisition (range rate = 6300 kn)	30:17:24	13:26	169 489	10 930	84.768	-1.184	-125.906	34.084	183 840	66.25	10.10
Buckhorn S-band acquisition (masking + 30 sec)	30:17:55	13:58	163 445	9 968	80.68	-1.146	-124.864	34.193	183 840	66.25	9.21
Exit UHF blackout	30:18:01	14:03	162 313	9 795	79.833	-1.197	-124.678	34.219	183 840	66.25	9.05
Earliest opportunity for runway redesignation (Buckhorn AOS + 15 sec)	30:18:11	14:13	160 345	9 514	78.377	-1.306	-124.280	34.267	183 840	66.25	8.79
Initiate San Luis Obispo updating (range rate = 6300 kn) (Buckhorn AOS + 30 sec)	30:18:25	14:28	156 926	9 074	75.937	-1.528	-123.922	34.353	183 840	66.25	8.38
Incorporate MCC update (Buckhorn AOS + 50 sec)	30:18:45	14:48	151 569	8 488	72.300	-1.871	-123.335	34.491	183 840	66.25	7.89

[a]Altitude of c.g. above 1960 Fischer ellipsoid.

TABLE 4-I.- Continued

(b) Entry interface through landing

	Start time, hr:min:sec (GET)	Δt of event, min:sec	Altitude,[a] ft	Relative velocity, fps	Relative heading, deg	Relative flightpath angle, deg	Longitude +east, deg	Geodetic latitude, deg	Total vehicle weight, lb	c.g., location, percent x	Mach number
San Luis Obispo TACAN acquisition (range rate = 4500 kn)	30:19:13	15:15	144 733	7 757	67.357	-1.823	-122.660	34.695	183 840	66.25	7.29
Goldstone S-band acquisition (masking + 30 sec)	30:19:29	15:32	141 332	7 352	64.770	-1.450	-122.315	34.82	183 840	66.25	6.95
Initiate San Luis Obispo TACAN updating (range rate = 4500 kn AOS + 30 sec)	30:19:43	15:45	139 613	6 969	66.949	-.974	-121.979	34.949	183 840	66.25	6.61
San Luis Obispo elevation >45 deg	30:20:24	16:26	128 526	6 080	78.058	-3.046	-121.148	35.165	183 840	66.25	5.86
Initiate Fellows TACAN updating	30:21:16	17:19	115 326	4 913	93.849	-2.284	-120.208	35.228	183.840	66.25	4.85
Fellows elevation >45 deg	30:21:19	17:21	114 880	4 874	94.516	-2.731	-120.177	35.226	183 840	66.25	4.82
Initiate TACAN navigation region updating	30:21:24	17:26	113 503	4 755	96.603	-2.953	-120.085	35.219	183 840	66.25	4.71
Pt. Pillar C-band LOS (elevation = 3 deg)	30:21:59	18:01	103 928	4 063	109.630	-3.772	-119.595	35.135	183 840	66.25	4.09

[a]Altitude of c.g. above 1960 Fischer ellipsoid.

TABLE 4-I.- Continued

(b) Entry interface through landing

	Start time, hr:min:sec (GET)	Δt of event, min:sec	Altitude,[a] ft	Relative velocity, fps	Relative heading, deg	Relative flightpath angle, deg	Longitude +east, deg	Geodetic latitude, deg	Total vehicle weight, lb	c.g., location, percent x	Mach number	True airspeed, kn	Equivalent airspeed, kn
Gorman TACAN acquisition	30:22:26	18:28	98 618	3 515	109.192	-2.435	-119.279	35.022	183 840	66.25	3.55		
Entry/TAEM interface	30:23:23	19:25	84 377	2 487	83.518	-5.989	-118.716	34.965	183 076	66.17	2.54		
Mobil TACAN acquisition	30:23:38	19:40	80 644	2 268	82.099	-6.629	-118.604	34.978	183 076	66.17	2.32		
Deactivate RCS yaw thrusters	30:24:38	20:40	61 128	1 443	81.566	-14.465	-118.234	35.017	183 076	66:17	1.50		
Vandenberg C-band LOS (elevation = 3 deg)	30:25:04	21:07	52 779	1 118	81.315	-16.545	-118.145	35.030	183 076	66.17	1.15		
Initiate speedbrake modulation	30:25:36	21:39	43 061	869	81.310	-18.140	-118.034	35.042	183 076	66.17	.90		
Edwards TACAN acquisition	30:25:44	21:47	41 261	839	81.320	-18.321	-118.016	35.045	183 076	66.17	.87		
Initiate air data system updating	30:26:21	22:23	32 029	737	81.848	-19.536	-117.926	35.056	183 076	66.17	.75	437	258
Initiate TACAN landing site region updating	30:26:50	22:52	24 541	671	115.758	-20.724	-117.859	35.055	183 076	66.17	.66	398	270
Initiate MSBLS updating	30:27:09	23:11	20 464	645	146.017	-21.029	-117.833	35.037	183 076	66.17	.62	382	277
Goldstone S-band LOS	30:27:09	23:1	20 465	646	146.025	-21.035	-117.831	35.045	183 076	66.17	.62	383	277
TAEM/approach and landing interface	30:27:30	23:32	15 552	613	-178.641	-21.701	-117.821	35.005	183 076	66.17	.58	363	286

[a]Altitude of c.g. above 1960 Fischer ellipsoid.

TABLE 4-I.- Concluded

(b) Entry interface through landing

	Start time, hr:min:sec (GET)	Δt of event, min:sec	Altitude,[a] ft	Relative velocity, fps	Relative heading, deg	Relative flightpath angle, deg	Longitude +east, deg	Geodetic latitude, deg	Total vehicle weight, lb	c.g., location, percent x	Mach number	True airspeed, kn	Equivalent airspeed, kn
Initiate pre-flare	30:28:24	24:26	4 009	518	-169.910	-21.831	-117.837	34.927	183 076	66.17	.47	307	290
Landing gear deployment	30:28:35	24:38	2 544	488	-169.932	-8.206	-117.840	34.913	183 076	66.17	.44	289	279
Initiate radar altimeter up-dating	30:28:36	24:39	2 491	483	-169.936	-7.139	-117.841	34.912	183 076	66.17	.44	286	276
Initiate final flare	30:28:43	24:46	2 276	406	-169.936	-1.246	-117.842	34.903	183 076	66.17	.37	241	233
Weight on wheels (touchdown)	30:28:50	24:52	2 238	353	-169.995	-.053	-117.844	34.897	183 076	66.17	.32	209	201

[a]Altitude of c.g. above 1960 Fischer ellipsoid.

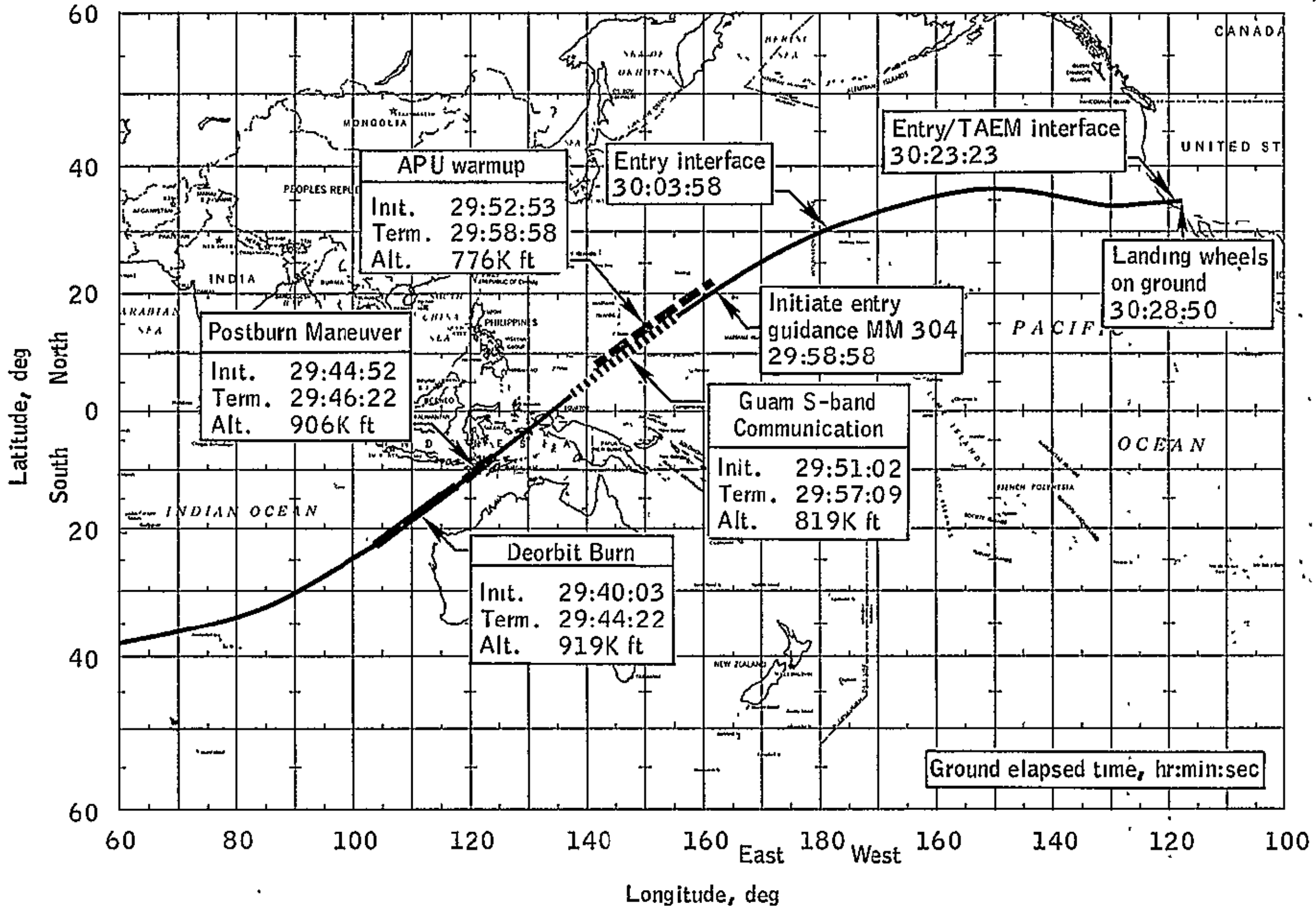

Figure 4-1.- OFT-1 deorbit through landing groundtrack.

TABLE 4.1-I.- MASS PROPERTIES FOR OFT-1

Event	Wt, lb	$X_{c.g.}$, in.	$Y_{c.g.}$, in.	$Z_{c.g.}$, in.
Predeorbit	193 957	1110.5	0.0	379.5
Entry interface	183 839.8	1092.8	.0	374.2
TAEM interface	183 076.8	1091.8	.0	373.8
Orbiter at landing	183 068.4	1093.0	.0	371.6

TABLE 4.1-II.- OMS LOADING PHILOSOPHY

Requirement	ΔV, fps
Insertion	192
Circulation (150 n. mi.)	176
Deorbit	364
OMS tank system failure	[a]164
Total ΔV	896
Reserved RCS	[b]100
One OMS tank	182
	282
Nominal required	364
Additional required per tank	82
Total system 82 x 2 =	164

[a]Backup deorbit requirement.

[b]2250 pounds planned reserved for entry. See open issues (sec. 6) for detailed discussion.

TABLE 4.1-III.- NAVIGATION SYSTEM MISSION PARAMETERS

Parameter	Data Type	Precision	Value	Units	Coord Frame	Definition
BASE_DEN	V(4)	DP	0.0, 0.00388747, 0.0011132, 0.03955768	slugs/ft^2		Vector of base densities for each layer to model drag
CORR_COEFF_UPDATE*	V(7)	S	0.0, 0.0, -.99, -.99, 0.0, 0.0, 0.0	vary	UYW	Correlation coefficients used to initialize covariance matrix for manual updat
DRAG_CONST	S	S	.23652181	ft^2/slugs		Drag constant equal to vehicle reference area divided by twice the vehicle mass
SIG DIAG UPDATE	V(6)	S	4.E6, 225.E6, 4.E6, 400., 9., 9.	ft, ft/s	UVW	Square root of diagonal elements to initialize covariance matrix for manual update
DENSITY_LIMIT	V(4)	S	0.0, 0.0, 135 000, 240 000	ft	-	Base altitude for drag model atmospheric layers

TABLE 4.1-IV.- NAVIGATION SYSTEM EXTERNAL MEASUREMENT CONSTRAINTS

TACAN:	
Maximum slant range, n. mi.	399
Maximum range rate, kn (fps)	4500 (7595)
Air data system:	
Deployment, Mach no.	3.0
Data accepted, Mach no.	0.75
MSBLS:	
Maximum slant range, n. mi.	20.7
Maximum range rate, kn (fps)	1185 (2000)
Maximum azimuth, deg.	15
Maximum elevation, deg.	29.3
Data accepted, ft. above runway	18 500
Radar altimeter:	
From end of runway (ref. 10), ft.	4000

TABLE 4.2-I.- OFT-1 LANDING OPPORTUNITIES AT EAFB

[March 30, 1979, 12:30 GMT Launch]

Entry orbit[a]	Crossrange[b] n. mi.	Time after sunrise, hr:min	Time before sunset, hr:min	GET of landing, day:hr:min	Local landing time, P.s.t., hr:min
2A	546	:35	11:53	0:01:44	6:14
3A	53	2:09	10:19	0:03:18	7:48
4A	-177	3:44	8:44	0:04:53	9:23
5D	-104	5:19	7:09	0:06:28	10.58
6D	259	6:54	5:34	0:08:03	12:33
18A	360	:35	11:53	1:01:44	6:14
19A	-54	2:10	10:18	1:03:19	7:49
20D	-187	3:45	8:43	1:04:54	9:24
21D	-15	5:20	7:08	1:06:29	10:59
22D	431	6:54	5:34	1:08:03	12:33
34A	198	:40	11:55	2:01:45	6:15
35A	-131	2:14	10:21	2:03:19	7:49
36D	-164	3:49	8:46	2:04:54	9:24
37D	103	5:24	7:11	2:06:29	10:59
50A	61	:40	11:55	3:01:45	6:15
51A	-176	2:15	10:20	3:03:20	7:50
52D	-109	3:50	8:45	3:04:55	9:25
53D	249	5:24	7:11	3:06:29	10:59

[a]Ascending (A) or descending (D) groundtrack at closest point of approach.

[b]Landing site north (+) or south (-) of groundtrack.

TABLE 4.2-II.- DEORBIT PARAMETERS

Parameter	2 OMS	1 OMS
ΔV_{min} for equal 2 and 1 OMS solutions, fps . . .	364	364
ΔV_{total} for c.g. control, fps	528	528
W predeorbit, lb	193 957	193 957
W entry interface, lb	183 840	183 840
T_{ig}, GET, hr:min:sec	29:40:03	29:40:03
Longitude, deg E at tig	103.635	103.635
Geodetic latitude, deg S at tig	-22.881	-22.881
Inertial velocity, fps at tig	25 399.3	25 399.3
Inertial flightpath angle, deg at tig	0.010883	0.010883
Inertial heading, deg at tig	58 679	58 679
Altitude above 1960 Fisher ellipsoid, ft at tig.	918 905	918 905
ΔT_{burn}, min:sec	4:18.4	8:36.8
ΔT_{coast}, min:sec	19:38.8	15:18.4
Entry range, n. mi.	3066	3066
V_{ei}, fps	25 684.9	25 683.8
γ_{ei}, deg	-1.527	-1.526

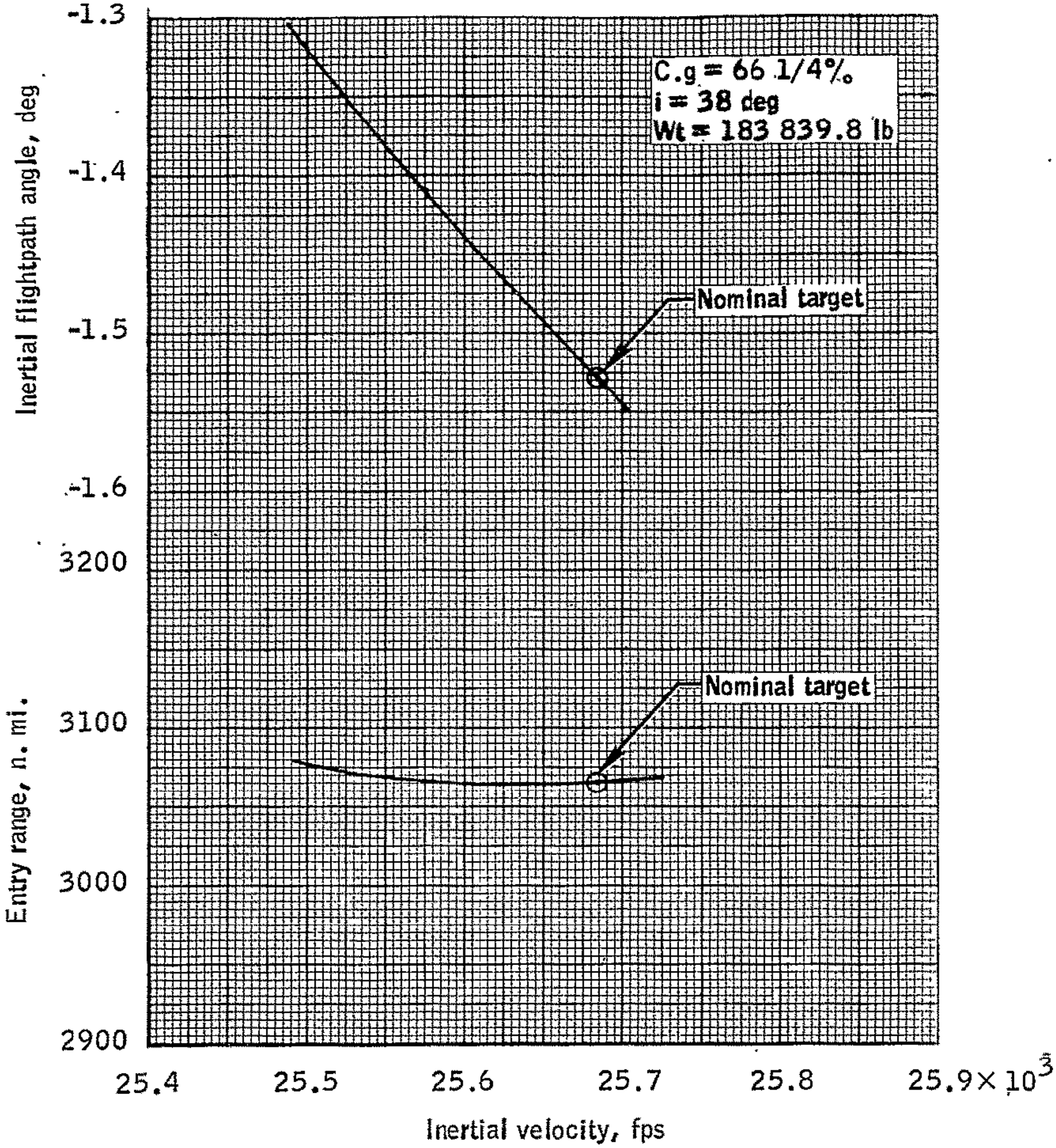

Figure 4.2-1.- Inertial velocity, inertial flightpath angle, and range target lines for orbiter OFT-1 entry interface.

TABLE 4.3-I.- ORBITER SURFACE TEMPERATURE LIMITS

Control point	Orbiter body location	Single mission maximum, °F	Equivalent simplified model, °F	Trajectory dispersion margin, °F (a)	Control surface deflection margin, °F	Maximum allowable nominal, °F
1	Nose RCC	2800	2950	80	-	2870
2	Body flap HRSI	2800	2800	150	185	2465
3	Wing RCC	2800	2950	85	-	2865
4	Elevon HRSI	2800	2800	195	100	2505
5	Nose RCC/HRSI interface	2800	2610	80	-	2530

[a]Preliminary.

TABLE 4.3-II.- THERMAL PROTECTION SYSTEM (TPS) SUMMARY

	In-flight Maximums				Weight/unit weight summaries			
Panel no.	Panel area, ft^2	Heating rate, Btu/ft^2/sec	Surface temperature, °F	Surface insulation type	Total heat load, Btu/ft^2	Insulation, lb/n.d.	Thickness, in.	Total weights, lb/n.d.
1	24.00	29.28	2456.56	RCC	15 098.33	164.08/6.84	1.86	164.08/6.84
2	362.00	15.41	2024.19 -74.06	HRSI	7 942.37	778.82/2.15	2.13	778.82/2.15
3	113.00	13.00	1920.68 -68.70	HRSI	6 693.03	225.91/2.00	1.95	225.91/2.00
4	446.00	12.13	1879.78 -66.86	HRSI	6 203.92	799.86/1.79	1.71	799.86/1.79
5	559.00	8.85	1702.22 -66.90	HRSI	4 655.38	792.18/1.42	1.26	792.18/1.42
6	403.00	6.43	1536.75 -65.97	HRSI	3 527.78	602.29/1.49	1.36	602.29/1.49
7	158.00	14.74	1996.73	RCC	8 498.97	1663.26/10534	.88	1663.26/***
8	435.00	17.54	2105.68 -68.26	HRSI	10 459.72	1105.06/2.54	2.59	1105.06/2.54
9	412.00	14.21	1974.06 -70.62	HRSI	7 981.12	949.13/2.30	2.31	949.13/2.30
10	641.00	17.68	2110.92 -41.19	HRSI	7 511.76	1410.74/2.20	2.19	1410.74/2.20
11	165.00	22.07	2257.58 -45.57	HRSI	8 698.40	398.80/2.42	2.44	398.80/2.42
12	360.00	9.99	1768.90 -51.41	HRSI	4 059.46	652.91/1.81	1.73	652.91/1.81
13	275.00	3.89	1300.39 -77.31	HRSI	2 001.70	313.96/1.14	.94	313.96/1.14
14	473.00	2.68	1144.23 -73.14	LRSI	1 406.75	292.86/.62	.38	292.86/.62
15	1631.00	.28	453.20	LRSI	149.74	777.50/.48	.20	777.50/.48
16	764.00	.10	247.25	LRSI	63.78	364.20/.48	.20	364.20/.48
17	114.00	.52	604.81	LRSI	237.76	54.34/.48	.20	54.34/.48
18	631.00	.40	535.31	LRSI	216.21	300.80/.48	.20	300.80/.48
19	155.00	6.96	1576.42 -95.01	HRSI	3 762.77	284.27/1.83	1.75	284.27/1.83
20	673.00	2.28	1080.36 -71.65	LRSI	1 305.81	433.93/.64	.41	433.93/.64
21	242.00	1.01	795.62 -72.88	LRSI	568.56	129.69/.54	.28	129.69/.54
22	610.00	1.01	795.38 -73.59	LRSI	517.84	290.79/.48	.20	290.79/.48
23	1132.00	.55	619.46	LRSI	285.08	539.62/.48	.20	539.62/.48

TABLE 4.3-II.- Concluded

	In-flight Maximums				Weight/unit weight summaries			
Panel no.	Panel area, ft^2	Heating rate, Btu/ft^2/sec	Surface temperature, °F	Surface insulation type	Total heat load, Btu/ft^2	Insulation, lb/n.d.	Thickness, in.	Total weights, lb/n.d.
24	372.00	.59	638.68 -73.53	LRSI	305.31	177.33/.48	.20	177.33/.48
25	82.00	33.82	2563.59 -53.94	HRSI	12 247.67	220.77/2.69	2.76	220.77/2.69
						13723.13		13723.13

Control point surface	CP1 (nose)	CP2 (body flap)	CP3 (wing leading)	CP4 (elevon)	CP5 (RCC/HRSI interface)
Temperature maximums	.2686526+04	.2242640+04	.2754700+04	.2431848+04	.2456563+04
Relative velocity	.2329445+05	.2052403+05	.2329445+05	.2004704+05	.2329445+05
Temperature limit	2870	2465	2865	2505	2530
Temperature margin	183.5	222.4	110.3	73.2	73.5

TABLE 4.3-III.- ENTRY/TAEM INTERFACE CONDITIONS

GET (rev 20), hr:min:sec.	30:23:23
Time from entry interface, min:sec	19:27
Relative velocity, fps	2488.84
Altitude of c.g. above runway, ft	82 118
Geodetic altitude, above 1960 Fisher ellipsoid, ft.	84 339
Geodetic latitude, deg N	34.966
Geocentric latitude, deg	34.786
Longitude, deg W	118.716
Relative heading from north, deg	83.250
Earth-relative flightpath angle, deg	-6.0587
Mach number	2.538
Angle of attack, deg	13.669
Dynamic pressure, psf	215.56
Range-to-runway threshold, n. mi.	52.08
Delta azimuth to HAC, deg	0.723
Weight, lbs	83 076

TABLE 4.3-IV.- ENTRY PARAMETERS

Initial conditions:	
Entry weight, lb	183 839.8
Longitude, deg W	179.098
Geodetic latitude, deg N	30.395
Geodetic latitude, deg N	30.231
Geodetic altitude, ft	401 863
Inertial velocity, fps	25 681.9
Inertial flightpath angle, deg	-1.527
Inertial heading, deg	67.175
Orbit inclination, deg	38
Entry range, n. mi.	3073.7
Target (runway threshold):	
Longitude, deg W	117.842
Geodetic latitude, deg N	34.902
Geodetic altitude, ft	2220.6
True heading, deg	190.068

Entry trajectory characteristics:	Nominal OFT-1			Design limits		
	Entry	TAEM	Autoland	Entry	TAEM	Autoland
Max dynamic pressures, lb/ft^2	232	276	287	300 for Mach >1	342 Mach <1	
Max normal load factors, g.	1.56			2.5	2.5	2.5
Max hinge moments, in-lb						
Inboard elevon x 10^6	-.329	.211	.216	±.93	±.78	±.55
Outboard elevon x 10^6	-.134	-.128	.045	±.43	±.35	±.25
Body flap x 10^6	-.374	-.432	-.279	±1.4	±.74	±.74
Speedbrake x 10^6	.577	.994	.915	±2.5	±2.1	±2.1
Max heating rate, Btu/ft^2/sec	81.7					
Heat load, Btu/ft^2	42 085			62 547		
Max surface temperature, deg F:						
Nose (RCC)	2 687			2 870		
Body flap	2 243			2 465		
Wing leading edge	2 755			2 865		
Elevon	2 432			2 505		
Nose (RCC/HRSI)	2 457			2 530		
Bondline temperature margin, deg F						
Panel 2	74.06					

TABLE 4.3-V.- DEFINITION OF ENTRY GUIDANCE CONSTANTS

Symbol	Description	Value	Units
AGN1	Time constant for $\dot{h}$ feedback	50.0	s
AK	Factor in dD/dV for temperature control guidance used to define C23	-2.460488	nd
AK1	Factor in dD/dV for temperature control guidance used to define C23	-2.961503	nd
ALFM	Desired constant drag level	33.0	ft/s^2
ALIM	Maximum sensed acceleration in transition	70.84	ft/s^2
ALMN1	Maximum L/D command outside of heading error deadband	0.7986355	nd
ALMN2	Maximum L/D command inside of heading error deadband	0.9659258	nd
ALMN3	Maximum L/D command below VELMN	0.93969	nd
ALMN4	Maximum L/D command above VYLMAX	1.0	nd
ASTART	Sensed acceleration to enter phase 2	5.66	ft/s^2
CALPO(1)	ALPCMD constant term in VE	0.85	deg
CALPO(2)	ALPCMD constant term in VE	18.37	deg
CALPO(3)	ALPCMD constant term in VE	4.47625	deg
CALPO(4)	ALPCMD constant term in VE	-9.933914	deg
CALPO(5)	ALPCMD constant term in VE	40.0	deg
CALPO(6)	ALPCMD constant term in VE	40.0	deg
CALPO(7)	ALPCMD constant term in VE	40.0	deg
CALP1(1)	ALPCMD rate term in VE	0.660E-2	deg-s/ft
CALP1(2)	ALPCMD rate term in VE	-0.242E-2	deg-s/ft

TABLE 4.3-V.- Continued

Symbol	Description	Value	Units
CALP1(3)	ALPCMD rate term in VE	0.31875E-2	deg-s/ft
CALP1(4)	ALPCMD rate term in VE	0.6887436E-2	deg-s/ft
CALP1(5)	ALPCMD rate term in VE	0	deg-s/ft
CALP1(6)	ALPCMD rate term in VE	0	deg-s/ft
CALP1(7)	ALDCMD rate term in VE	0	deg-s/ft
CALP2(1)	ALPCMD quadratic term in VE	-0.6E-6	deg-s^2/ft^2
CALP2(2)	ALPCMD quadratic term in VE	0.560E-6	deg-s^2/ft^2
CALP2(3)	ALPCMD quadratic term in VE	0	deg-s^2/ft^2
CALP2(4)	ALPCMD quadratic term in VE	-0.2374978E-6	deg-s^2/ft^2
CALP2(5)	ALPCMD quadratic term in VE	0	deg-s^2/ft^2
CALP2(6)	ALPCMD quadratic term in VE	0	deg-s^2/ft^2
CALP2(7)	ALPCMD quadratic term in VE	0	deg-s^2/ft^2
CDDOT1	CD velocity coefficient	1500.0	ft/s
CDDOT2	CD velocity coefficient	2000.0	ft/s
CDDOT3	CD velocity coefficient	0.15	nd
CDDOT4	CD alpha coefficient	0.0783	nd
CDDOT5	CD alpha coefficient	-8.165E-3	1/deg
CDDOT6	CD alpha coefficient	6.833E-4	1/deg^2
CDDOT7	CD coefficient	7.5E-5	s/ft
CDDOT8	CD coefficient	13.666E-4	1/deg^2
CDDOT9	CD coefficient	-8.165E-3	1/S
CNMFS	Conversion factor from feet to nautical miles	1.64579E-4	nm/ft

TABLE 4.3-V.- Continued

Symbol	Description	Value	Units
CT16(1)	C16 coefficient	0.1354	s^2/ft
CT16(2)	C16 power coefficient	-0.10	nd
CT16(3)	Gain on C16 drag error term	0.006	s^4/ft^2
CT17(1)	C17 coefficient	1.537E-2	s/ft
CT17(2)	C17 power coefficient	-5.8146E-1	nd
CT16MN	Minimum value of C16	0.025	s^2/ft
CT16MX	Maximum value of C16	0.35	s^2/ft
CT17MX	Minimum value of C17	0.0025	s/ft
CT17MN	Maximum value of C17	0.014	s/ft
CY0	Constant term in heading error deadband	-0.1308996939	rad
CY1	Slope of heading error deadband wrt VE	1.09083×10^{-4}	rad-s/ft
DDLIM	Maximum delta drag for $\dot{h}$ feedback	2.0	ft/s^2
DELV	Phase transfer velocity bias	2300.0	ft/s
DF	Final drag value in transition phase	21.0	ft/s^2
D230	Initial value of D23	23.2	ft/s^2
DRDDL	Minimum value of DRDD	-1.5	$nm\text{-}s^2/ft$
DTEGD	Entry guidance computation interval	1.92	s
DT2MIN	Minimum value of T2DOT	0.00231	ft/s^3
EEF4	Final reference energy level in transition phase	2.0×10^6	ft^2/s^2
ETRAN	Energy level at start of transition	60.71073E+6	ft^2/s^2

TABLE 4.3-V.- Continued

Symbol	Description	Value	Units
E1	Minimum value of DREFP and |DREFP-DF| in transition phase	0.01	ft/s^2
GS	Earth gravitational constant	32.174	ft/s^2
GS1	Factor in smoothing roll command	0.02	s^{-1}
GS2	Factor in smoothing roll command	0.02	s^{-1}
GS3	Factor in smoothing roll command	0.03767	s^{-1}
GS4	Factor in smoothing roll command	0.03	s^{-1}
HSMIN	Minimum value of scale height	20 500.0	ft
HS01	Scale height constant term	18 075.0	ft
HS02	Scale height constant term	27 000.0	ft
HS03	Scale height constant term	45 583.5	ft
HS11	Scale height slope wrt VE	0.725	s
HS13	Scale height slope wrt VE	-0.9445	s
LODMIN	Minimum L/D ratio	0.5	nd
NALP	Number of ALPCMD velocity segment boundaries	6	nd
PREBNK	Preentry bank angle command	0.0	deg
RADEG	Radian-to-degree conversion factor	57.29578	deg/rad
RLM	Maximum roll command in transition	70.0	deg
RPTI	Range bias term	22.068	nm
VA	Initial velocity for temperature quadratic, dD/dV-0	30 538.46	ft/s
VALP(1)	ALPCMD vs VE boundary	4000.0	ft/s

TABLE 4.3-V.- Continued

Symbol	Description	Value	Units
VALP(2)	ALPCMD vs VE boundary	4500.0	ft/s
VALP(3)	ALPCMD vs VE boundary	7789.412	ft/s
VALP(4)	ALPCMD vs VE boundary	14 500.0	ft/s
VALP(5)	ALPCMD vs VE boundary	30 000.0	ft/s
VALP(6)	ALPCMD vs VE boundary	30 000.0	ft/s
VA1	Boundary velocity between quadratic segments in temperature control phase	23 000	ft/s
VA2	Initial velocity for temperature quadratic, dD/dV-0	30 538.46	ft/s
VB1	Heat rate-equilibrium glide phase boundary velocity	20 000	ft/s
VC16	Velocity to start C16 drag error term	23 000.0	ft/s
VELMN	Maximum velocity for limiting LMN by ALMN3	8000.0	ft/s
VEROLC	Maximum velocity for limiting bank angle command	8000.0	ft/s
VHS1	Scale height vs VE boundary	12 310.34	ft/s
VHS2	Scale height vs VE boundary	19 675.5	ft/s
VQ	Predicted end velocity for constant drag phase	5000.0	ft/s
VROT	Velocity to start $\dot{h}$ feedback	23 000.0	ft/s
VSAT	Local circular orbit velocity	25 766, 1973	ft/s
VS1	Reference velocity for equilibrium glide	25 744.43	ft/s
V_TAEM	Reference velocity at entry-TAEM interface	2500.0	ft/s

TABLE 4.3-V.- Concluded

Symbol	Description	Value	Units
VTRAN	Nominal velocity at start of transition phase	10 500.0	ft/s
VYLMAX	Minimum velocity for limiting LMN by ALMN4	23 000.0	ft/s
YLMIN	YL bias used in test for LMN	0.03	rad
YLMN2	Minimum YL bias	0.07	rad
Y1	Maximum heading error deadband	0.30543262	rad
Y2	Minimum heading error deadband	0.17453292	rad
ZK1	Gain for $\dot{h}$ feedback	1.0	s

TABLE 4.3-VI.- ENTRY CROSSRANGE CAPABILITY FOR OFT-1

Maximum crossrange available, n. mi.	753
Less entry dispersions RSS, n. mi.	95
	658
Less margin for first flight safety, n. mi.	88
Maximum crossrange available, n. mi.	570
Recommended maximum crossrange for flight design, n. mi. . .	550

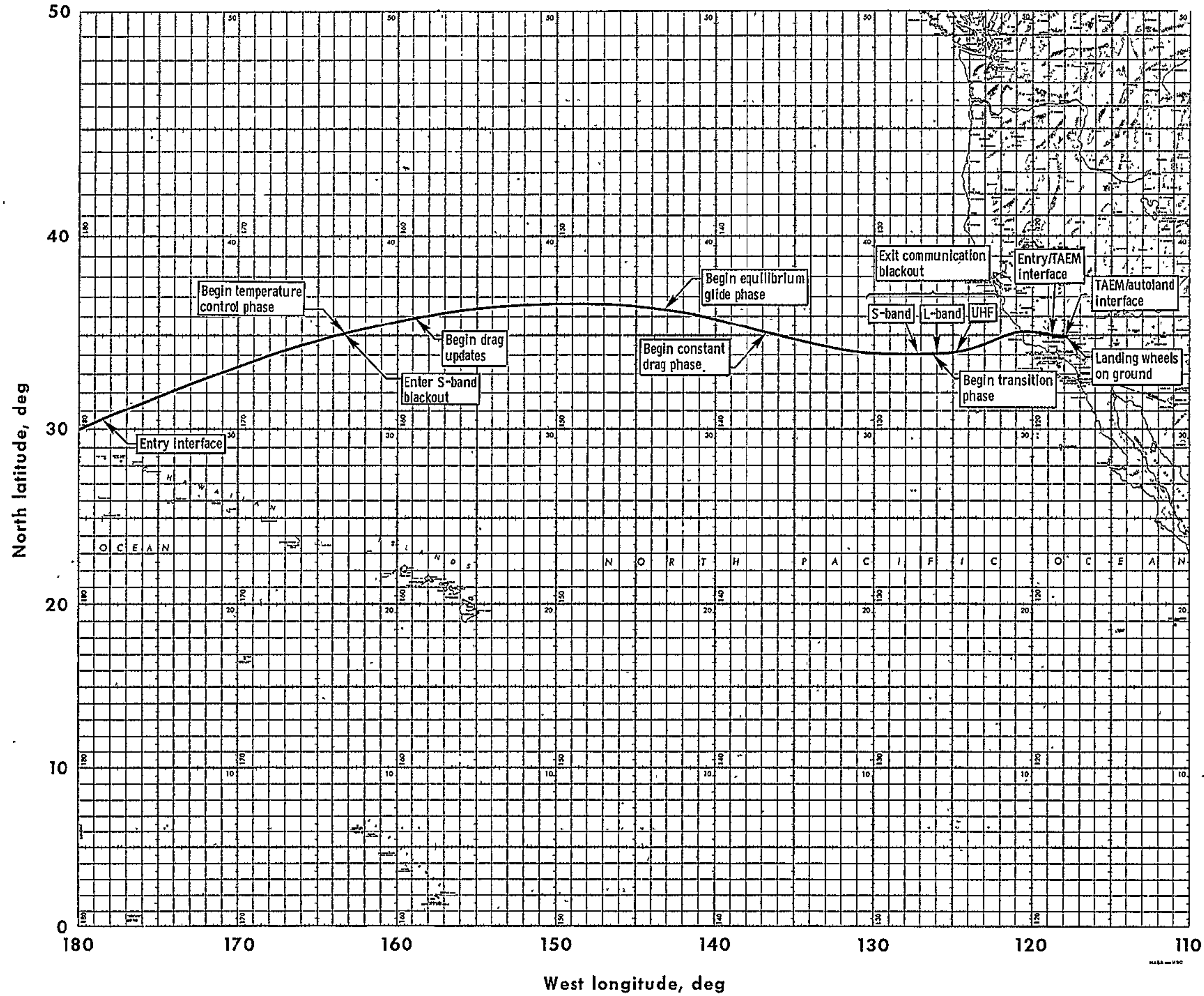

Figure 4.3-1.- OFT-1 entry interface through landing groundtrack.

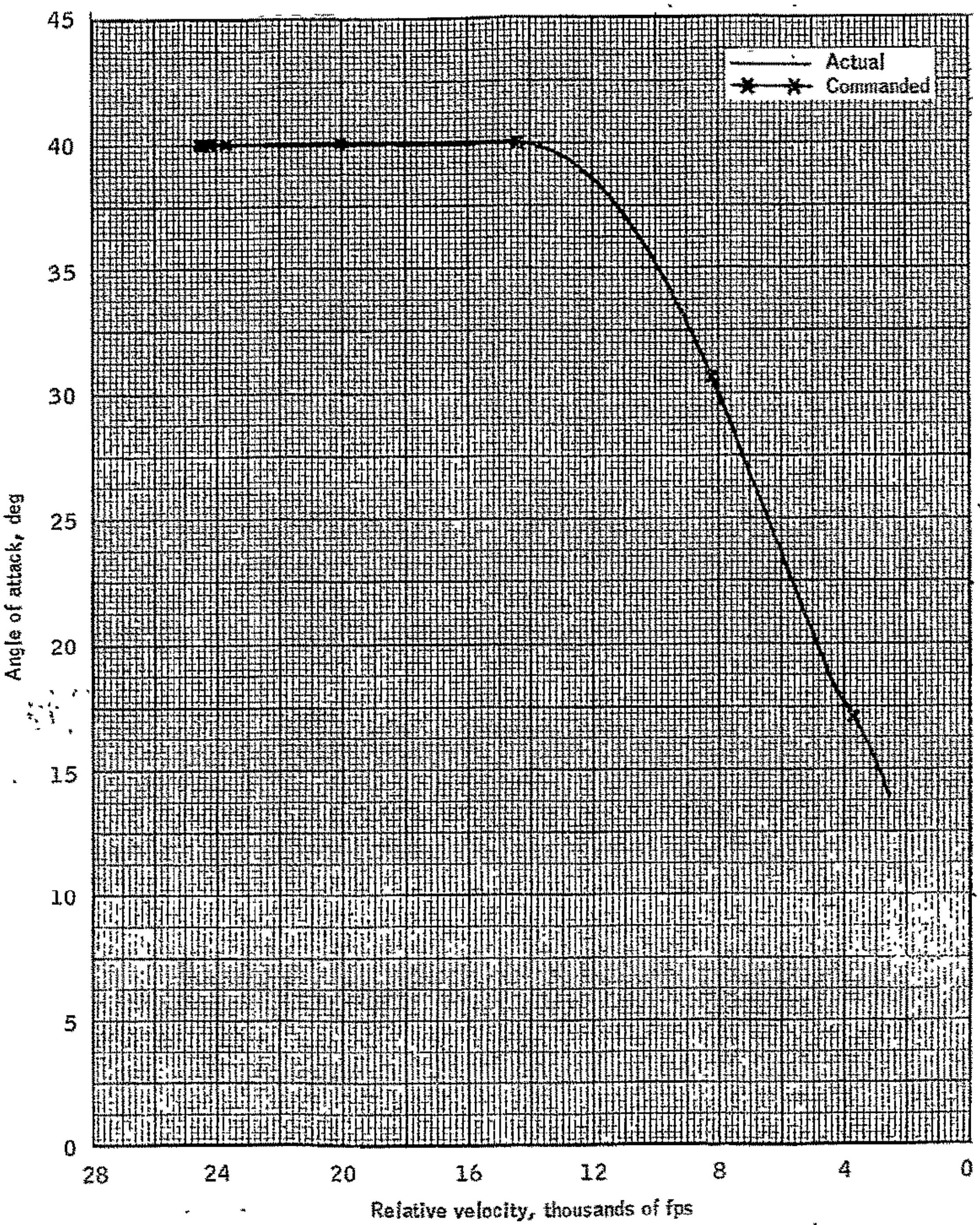

Figure 4.3-2.- Actual and commanded angle of attack versus relative velocity for orbiter OFT-1 entry.

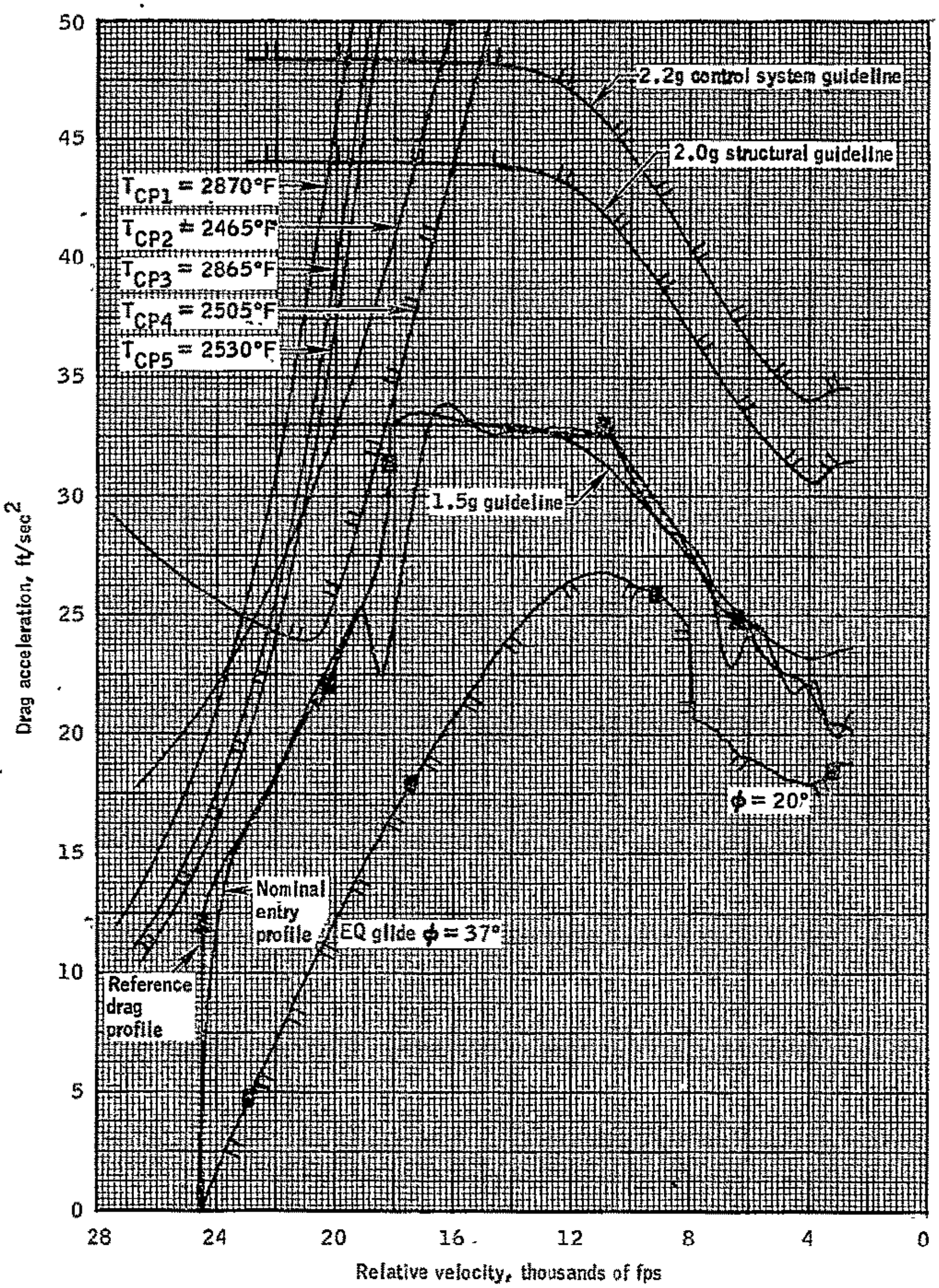

Figure 4.3-3.- Entry corridor and flight profile versus relative velocity for orbiter OFT-1 entry.

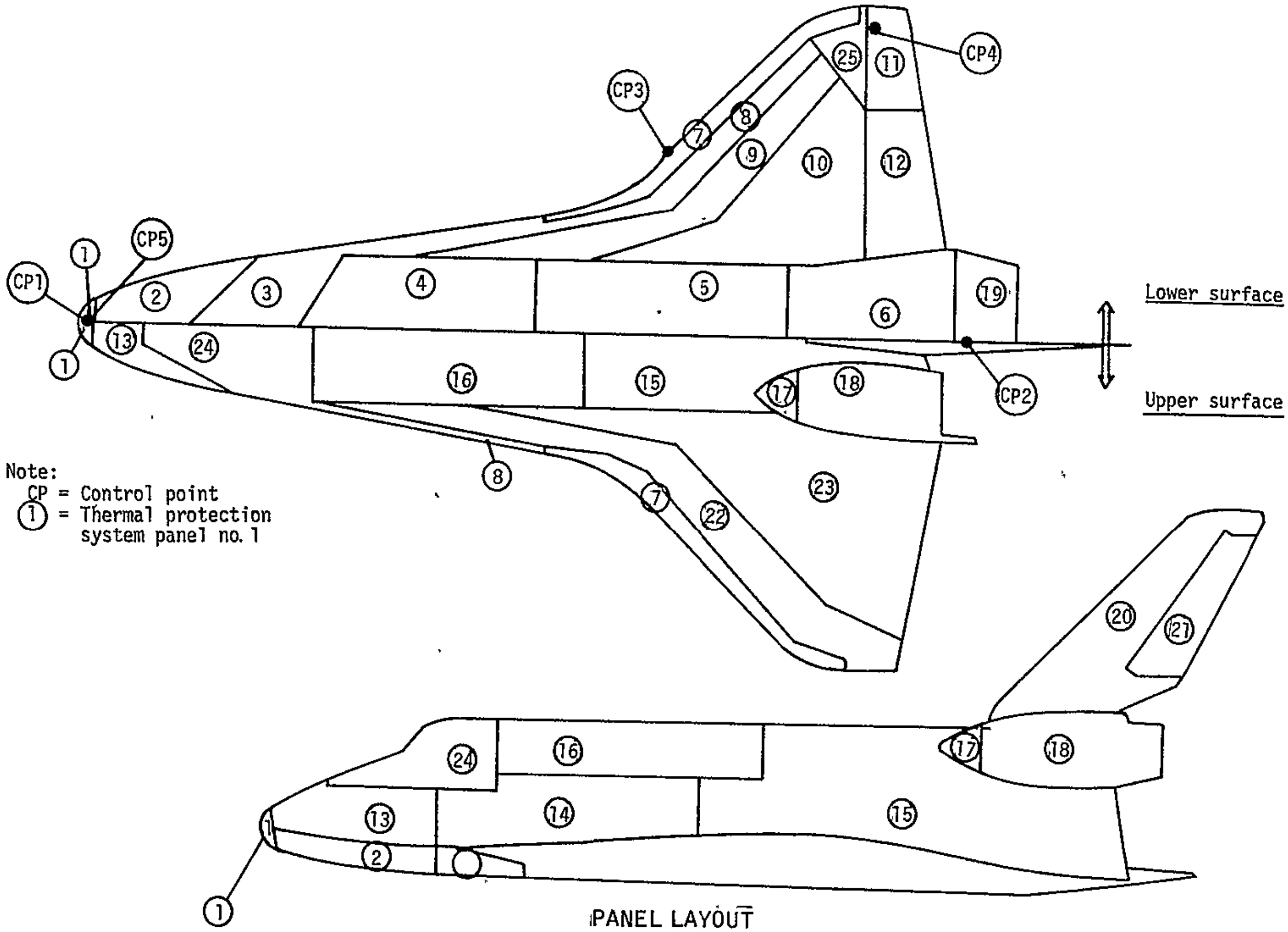

Figure 4.3-4.-Surface-temperature critical control points and various panel locations.

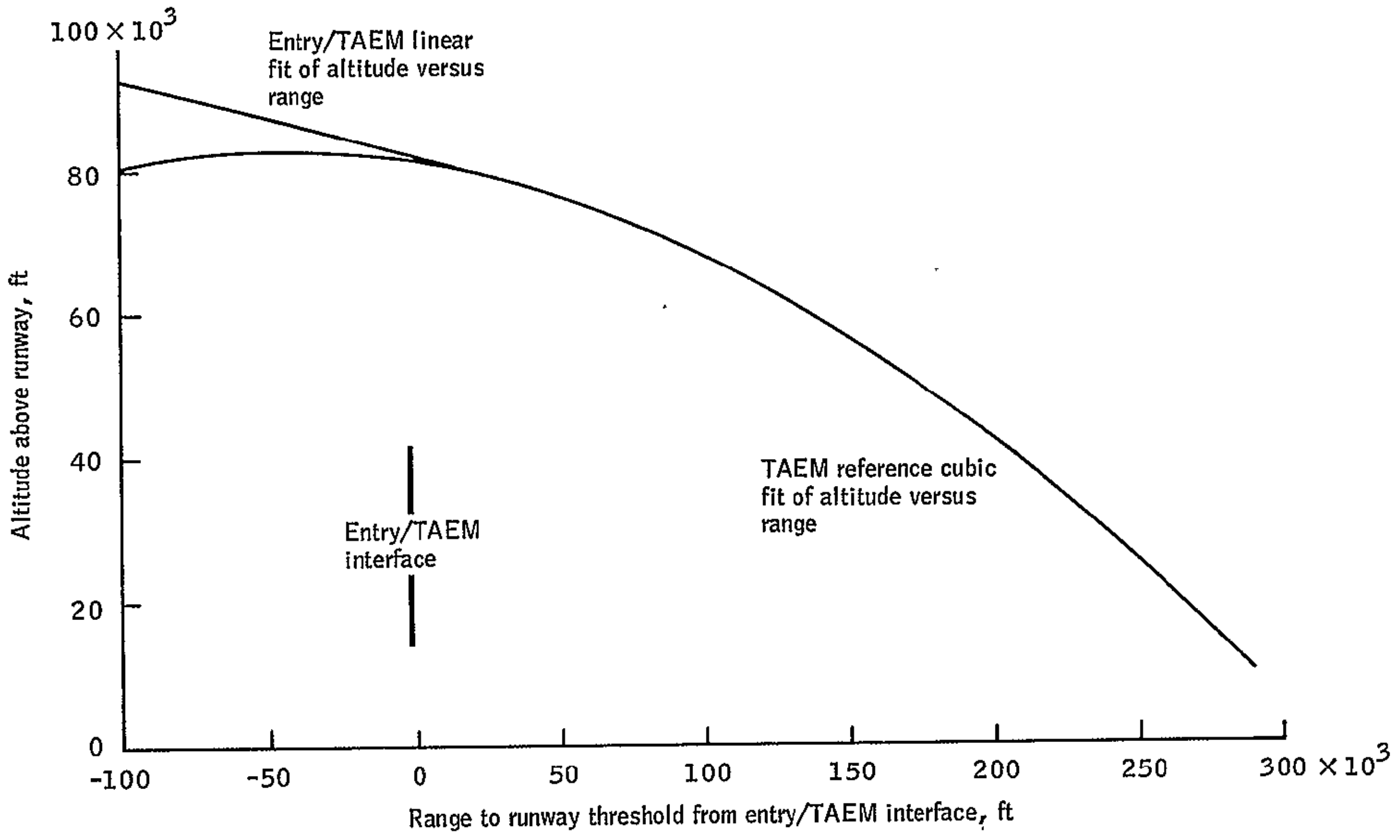

Figure 4.3-5.- Altitude versus range at entry/TAEM interface.

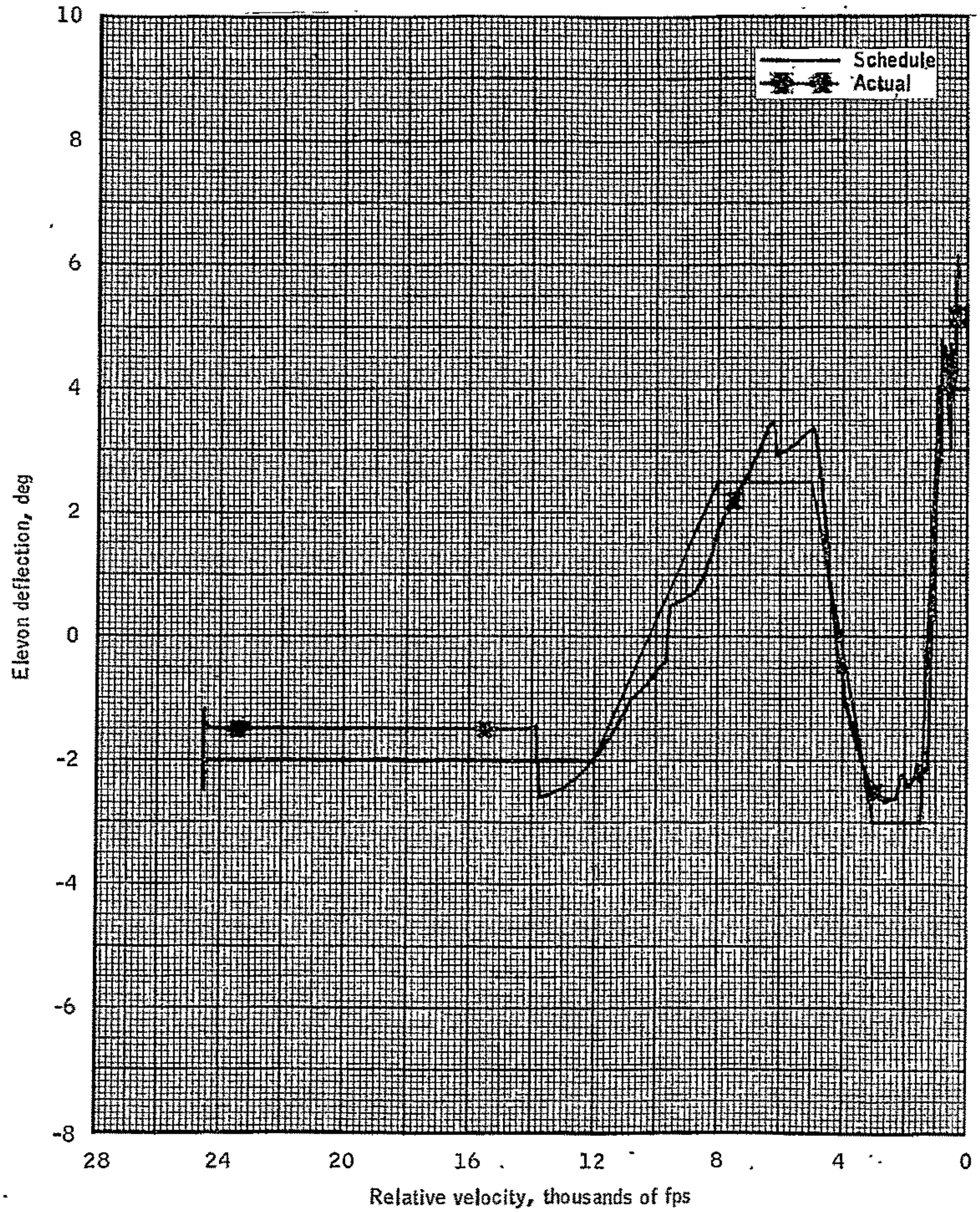

Figure 4.3-6.- Nominal elevon deflection schedule and actual elevon deflection for orbiter OFT-1.

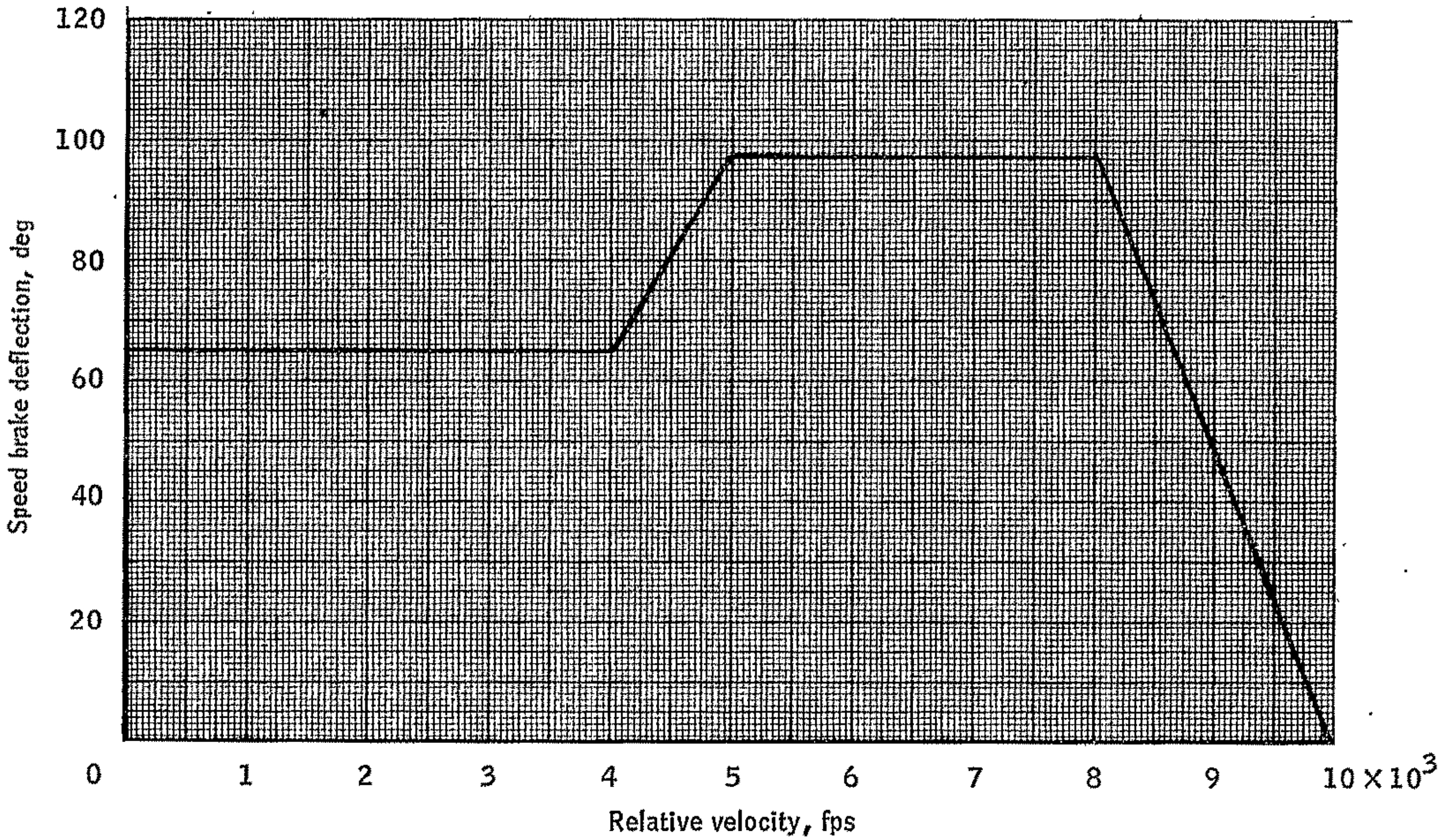

Figure 4.3-7.-Nominal speedbrake deflection schedule versus relative velocity.

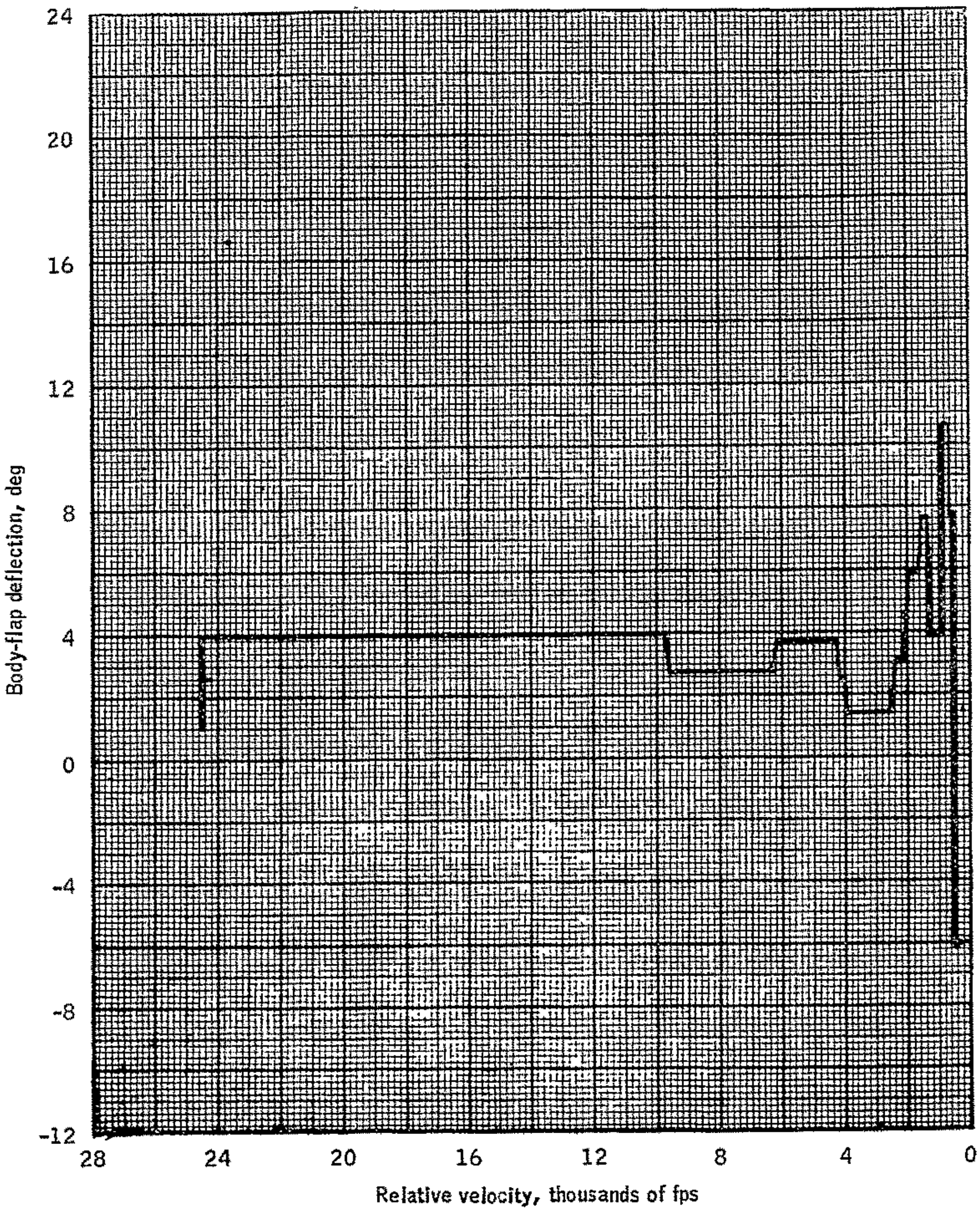

Figure 4.3-8.- Nominal body-flap deflection versus relative velocity for orbiter OFT-1.

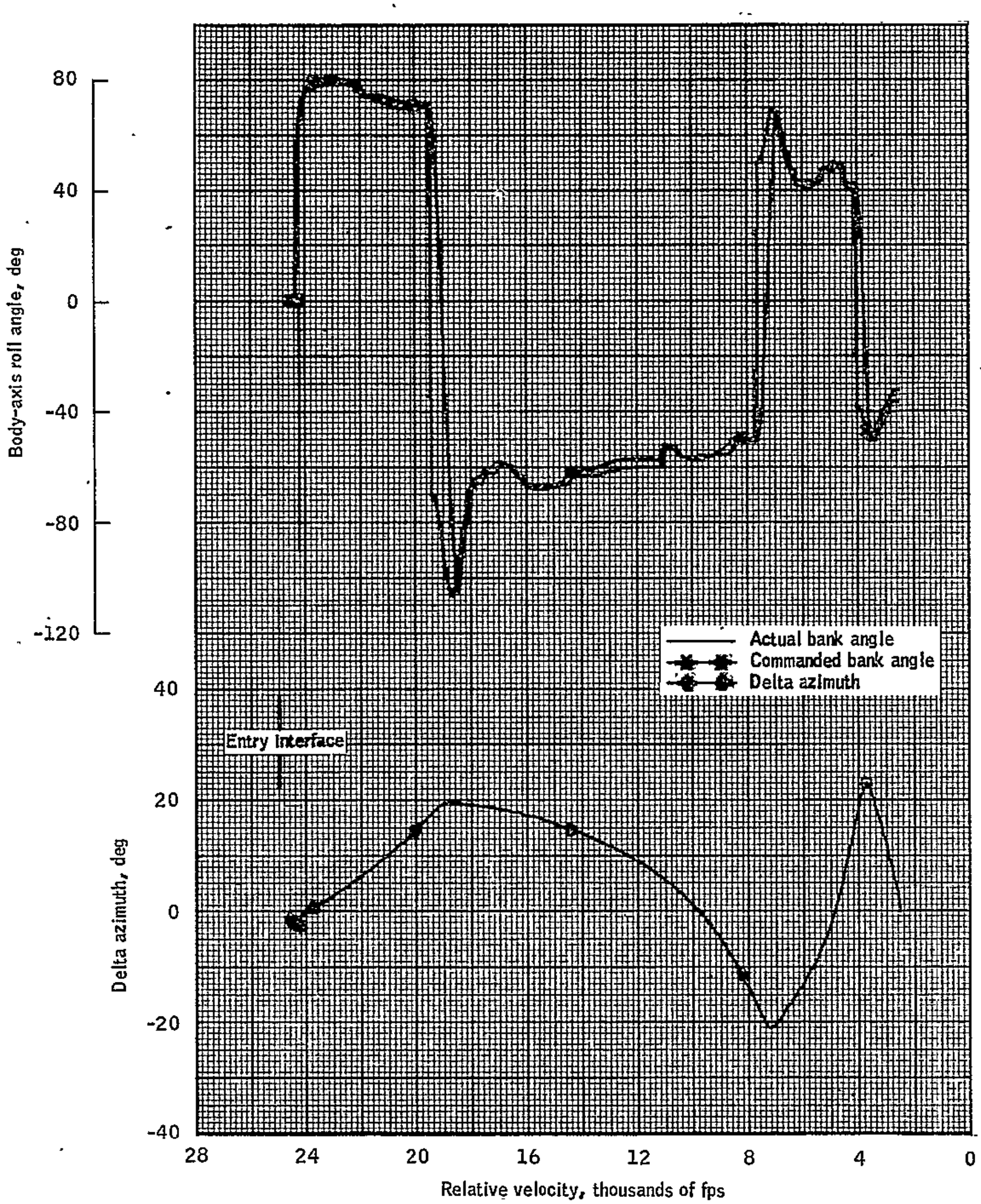

Figure 4.3-9.- Delta azimuth, actual and commanded bank angles versus relative velocity for orbiter OFT-1.

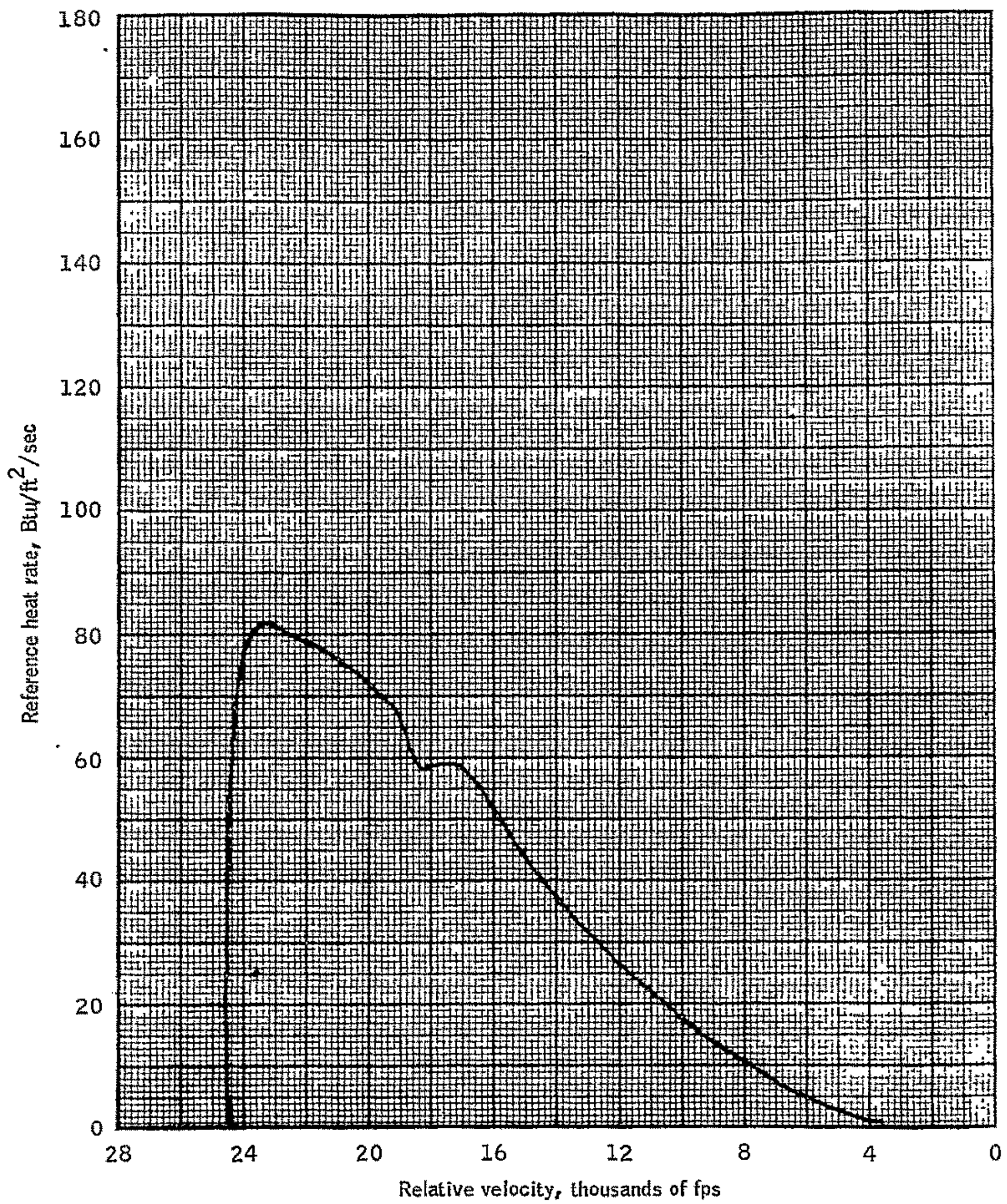

Figure 4.3-10.- Reference heating rate versus relative velocity for orbiter OFT-1.

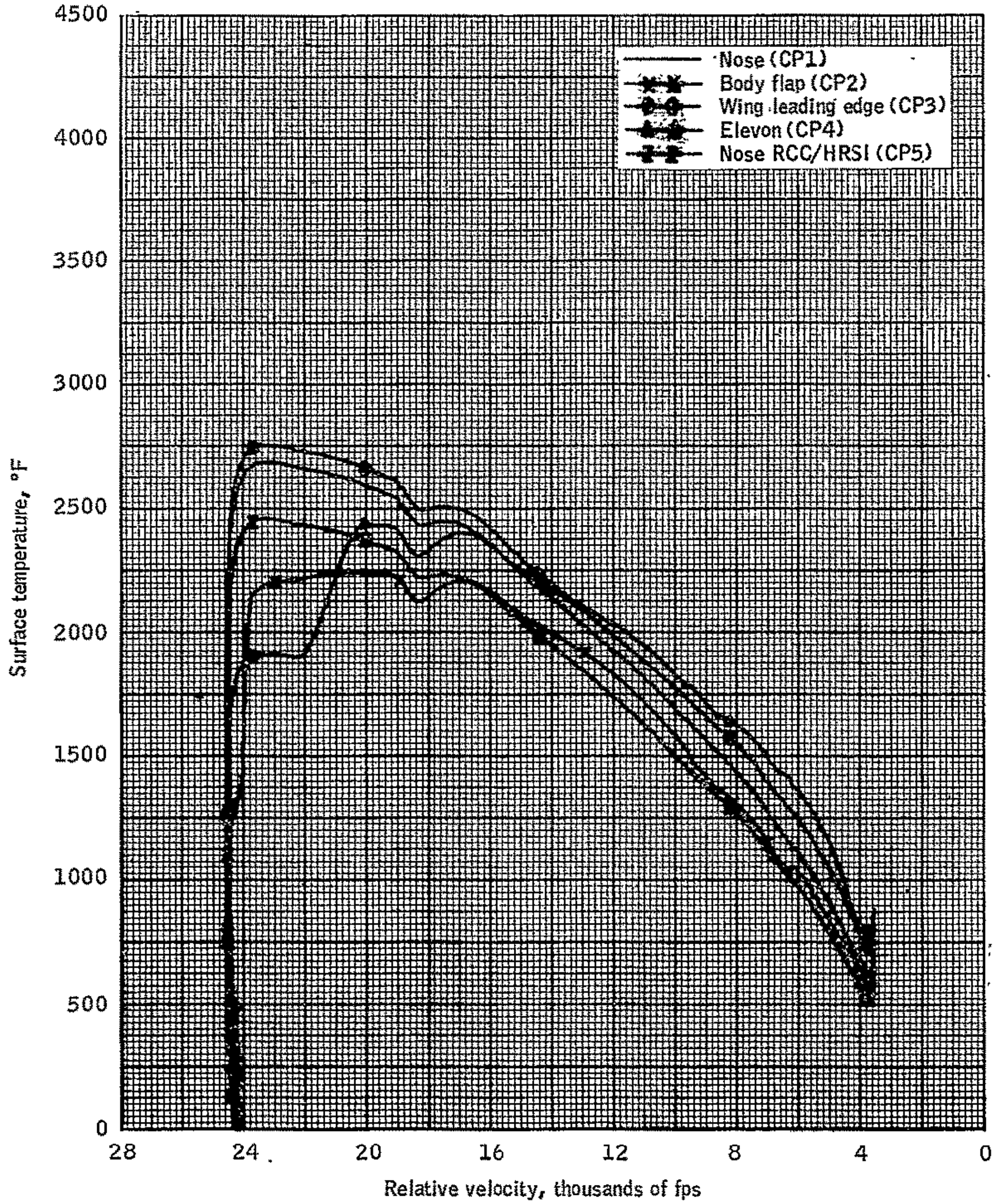

Figure 4.3-11.- Surface temperatures versus relative velocity for orbiter OFT-1.

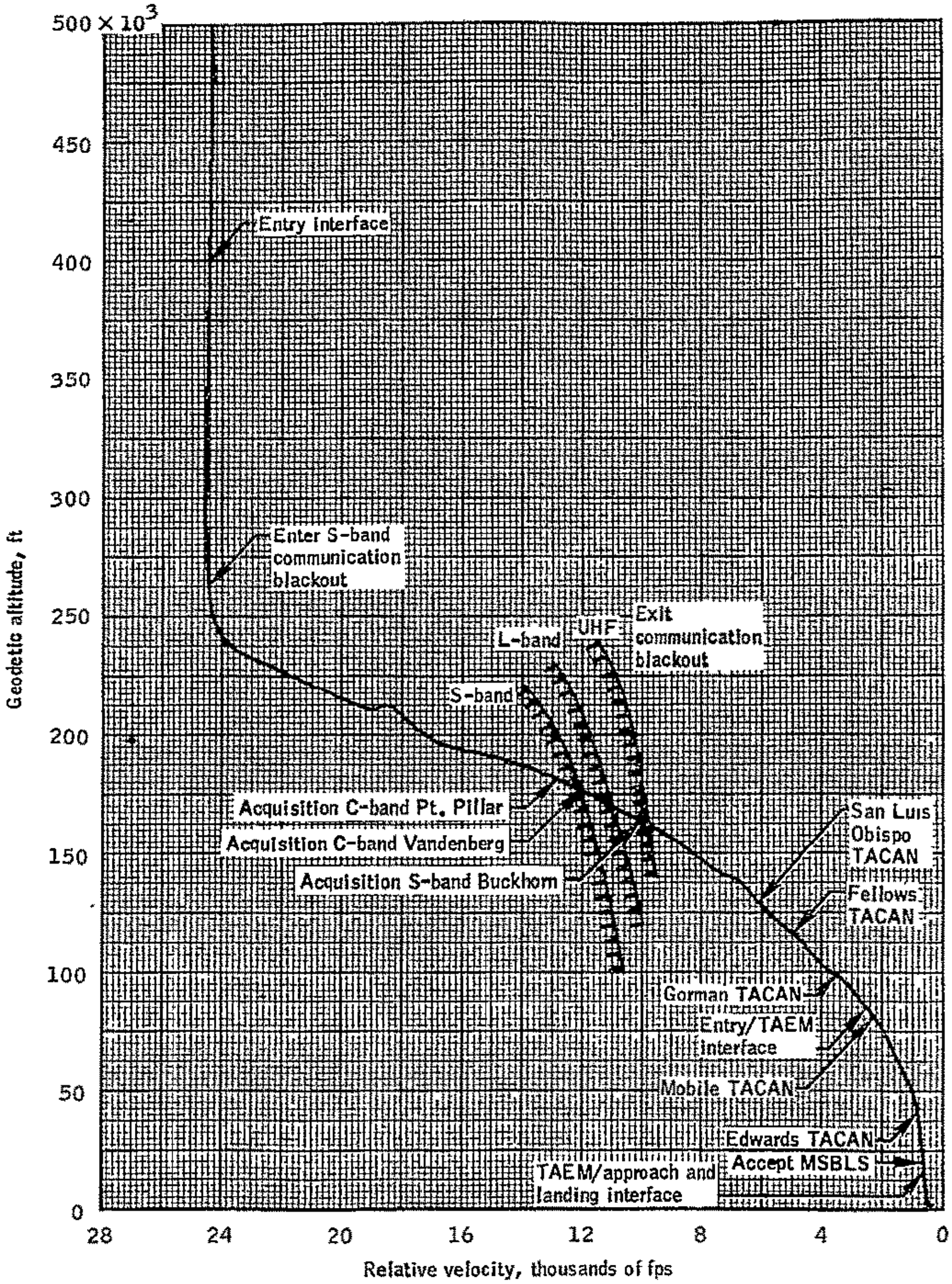

Figure 4.3-12.-Altitude versus relative velocity for orbiter OFT-1.

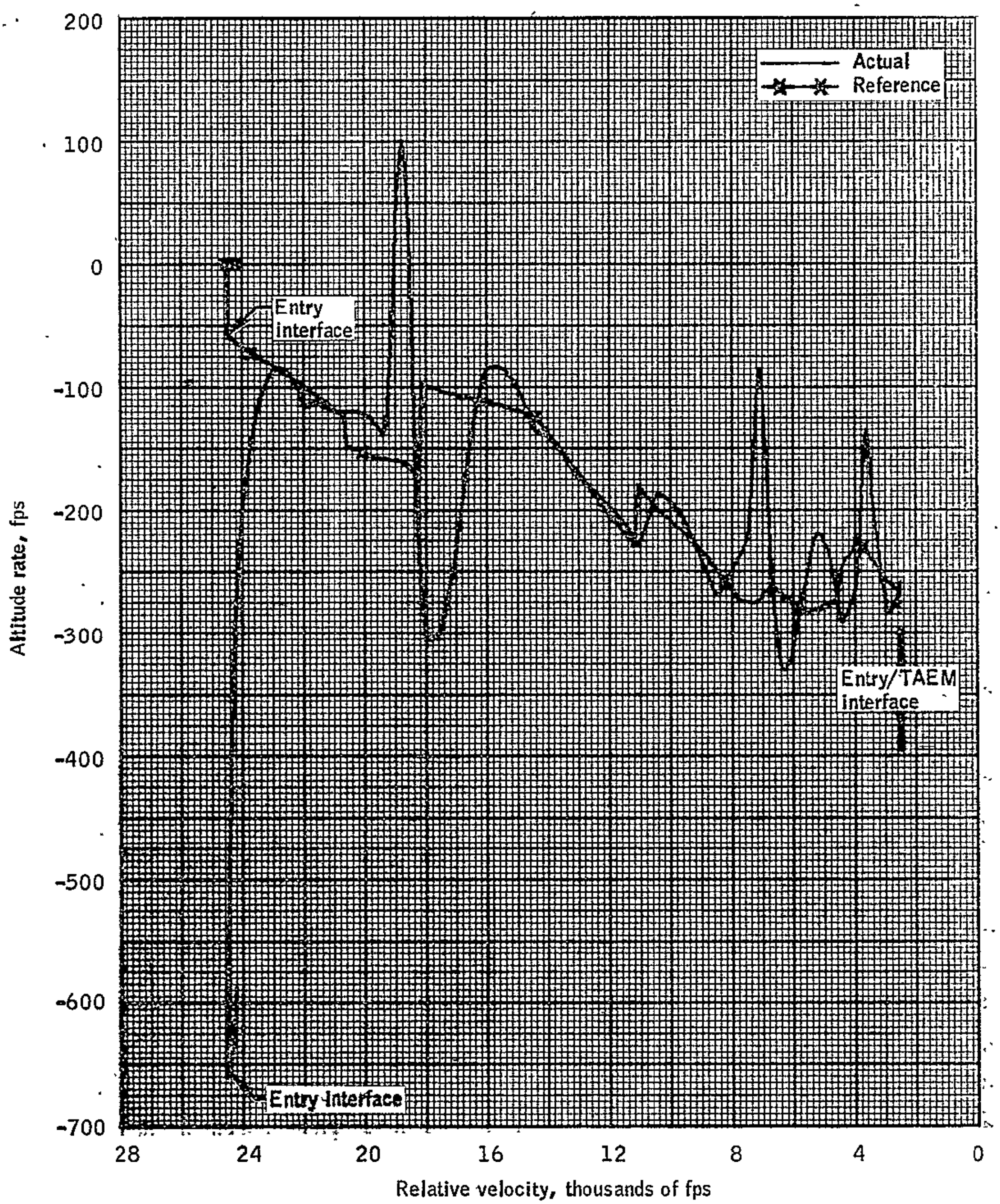

Figure 4.3-13.- Actual and reference altitude rate versus relative velocity for orbiter OFT-1.

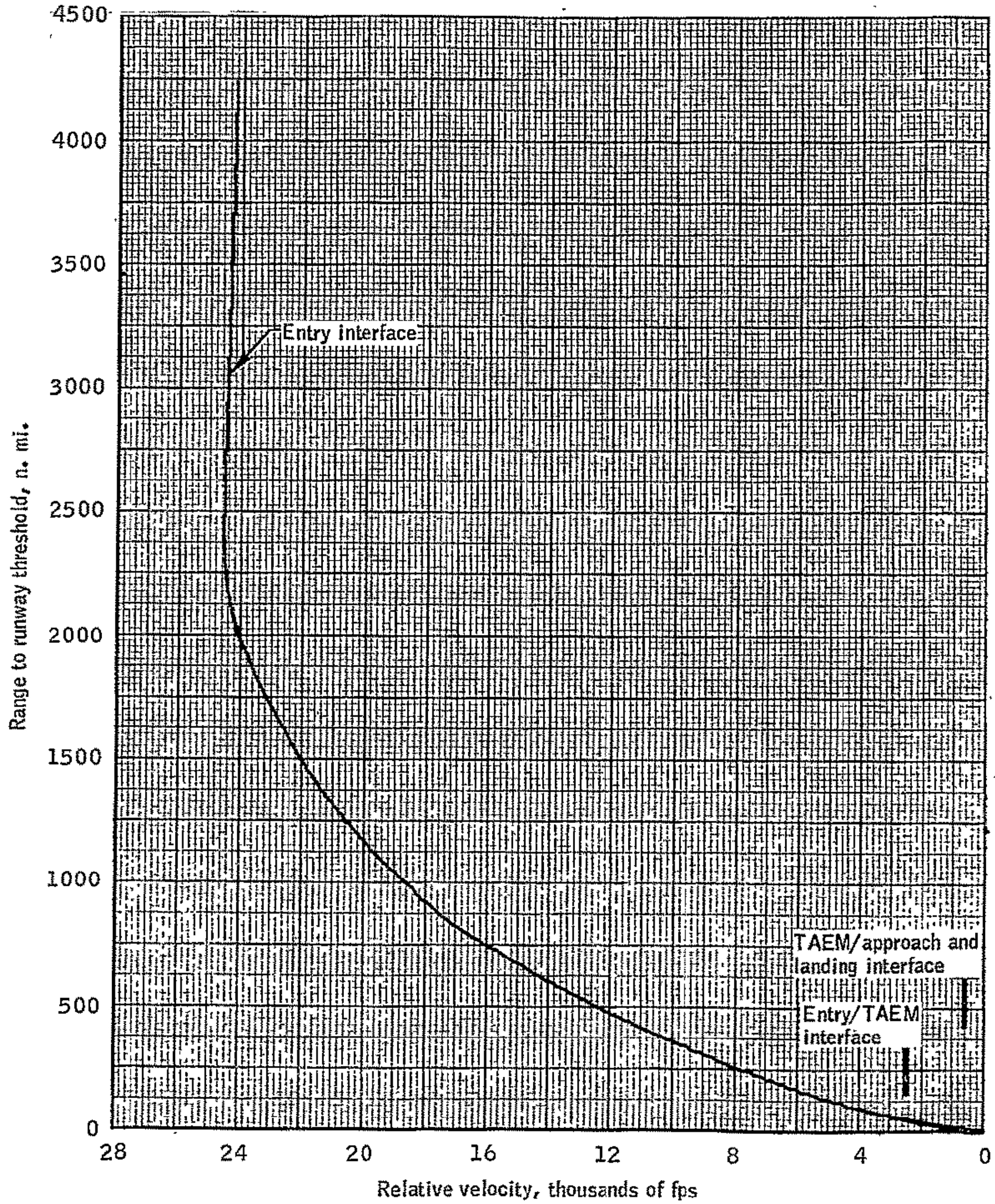

Figure 4.3-14.- Range to runway threshold versus relative velocity for orbiter OFT-1.

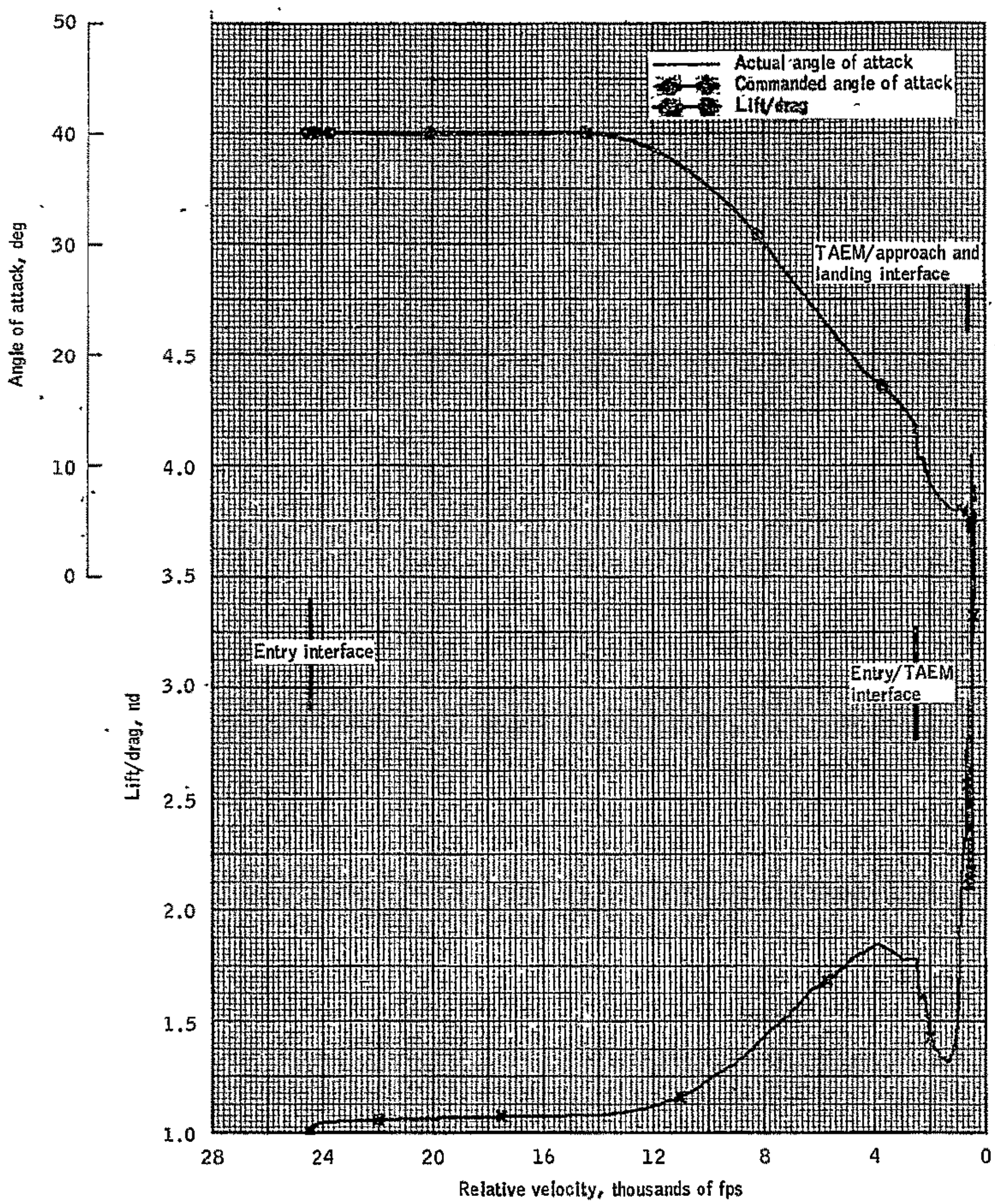

Figure 4.3-15.- Lift/drag actual and commanded angle of attack versus relative velocity for orbiter OFT-1.

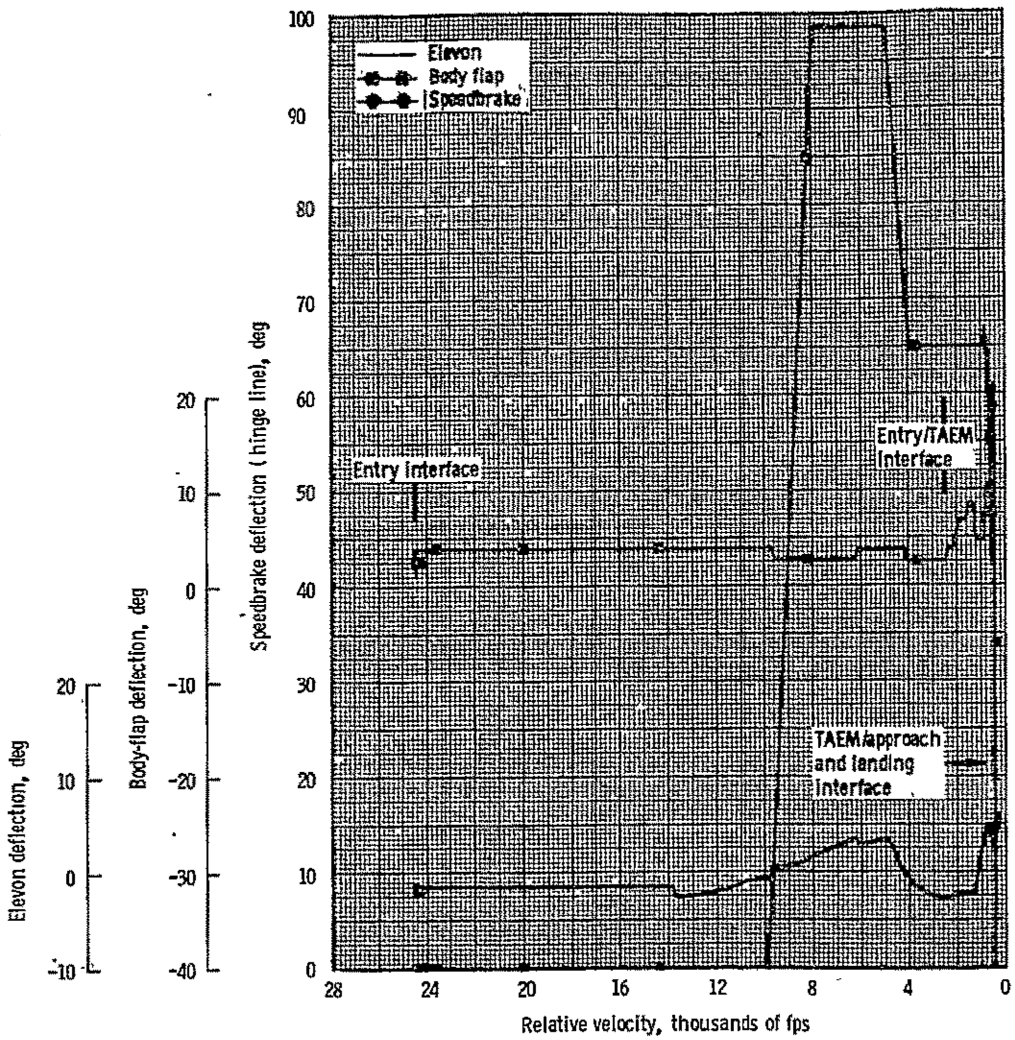

Figure 4.3-16.- Elevon, bodyflap, and speedbrake deflection versus relative velocity for orbiter OFT-1.

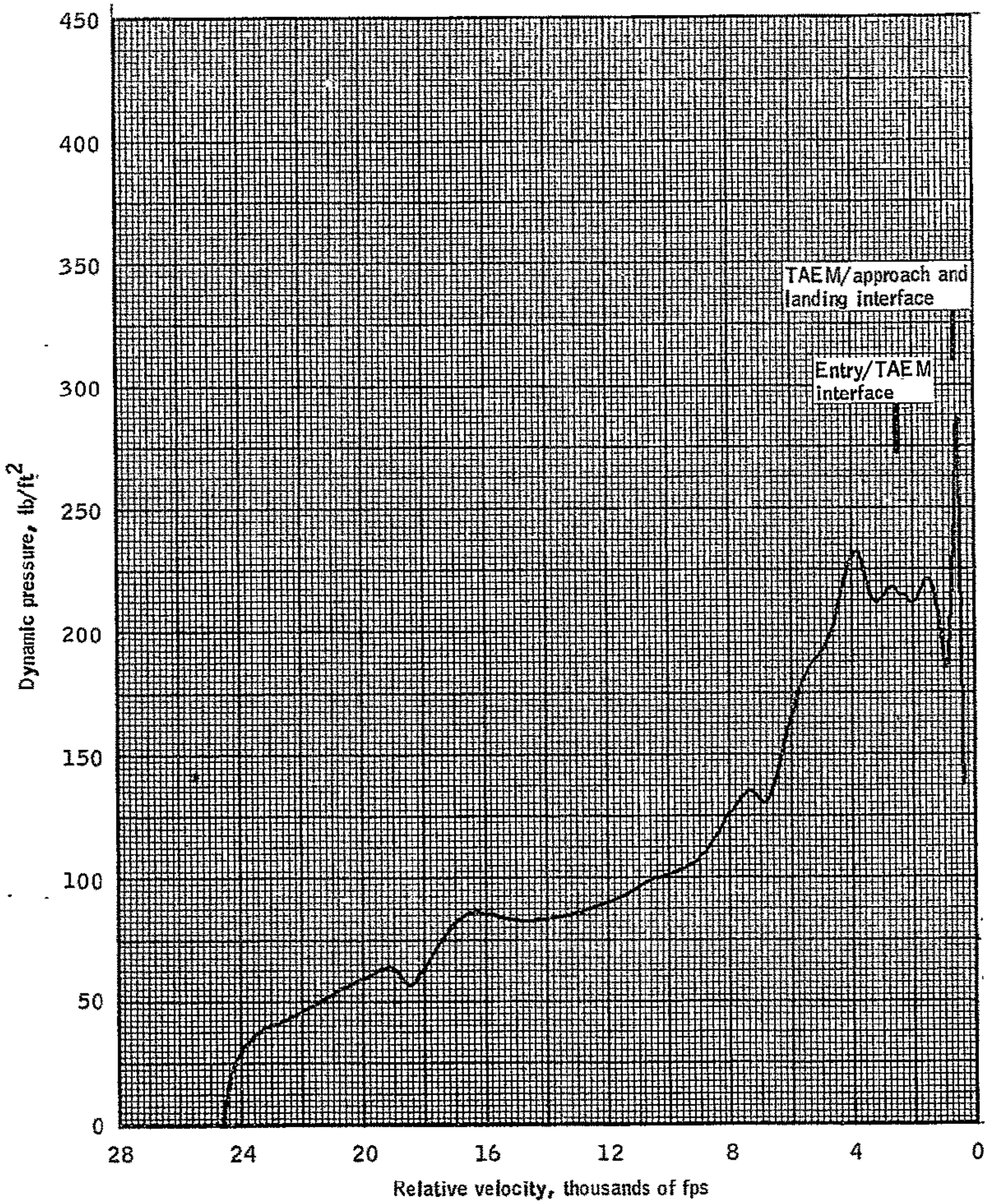

Figure 4.3-17.- Dynamic pressure versus relative velocity for orbiter OFT-1.

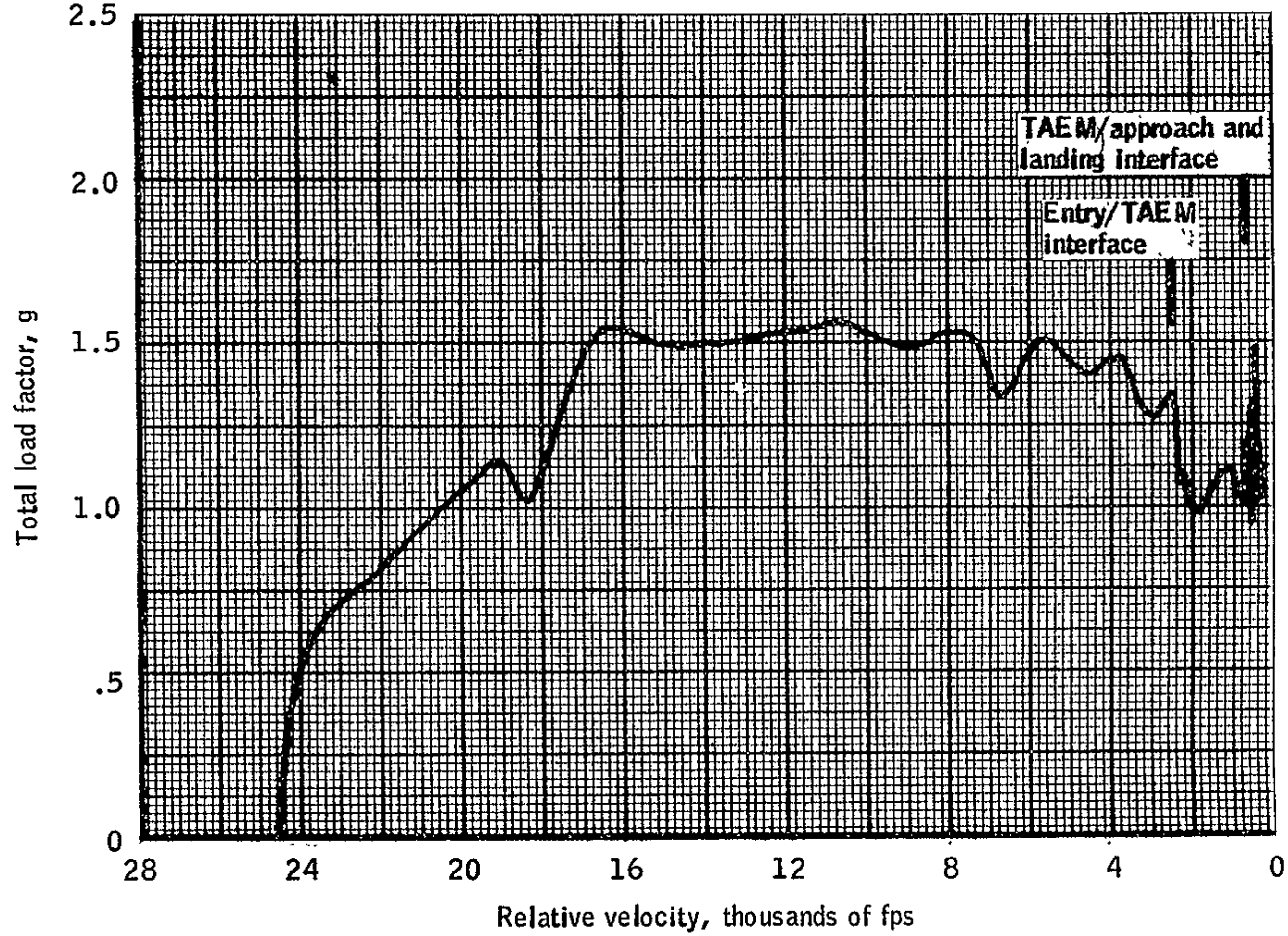

Figure 4.3-18.- Total load factor versus relative velocity for orbiter OFT-1.

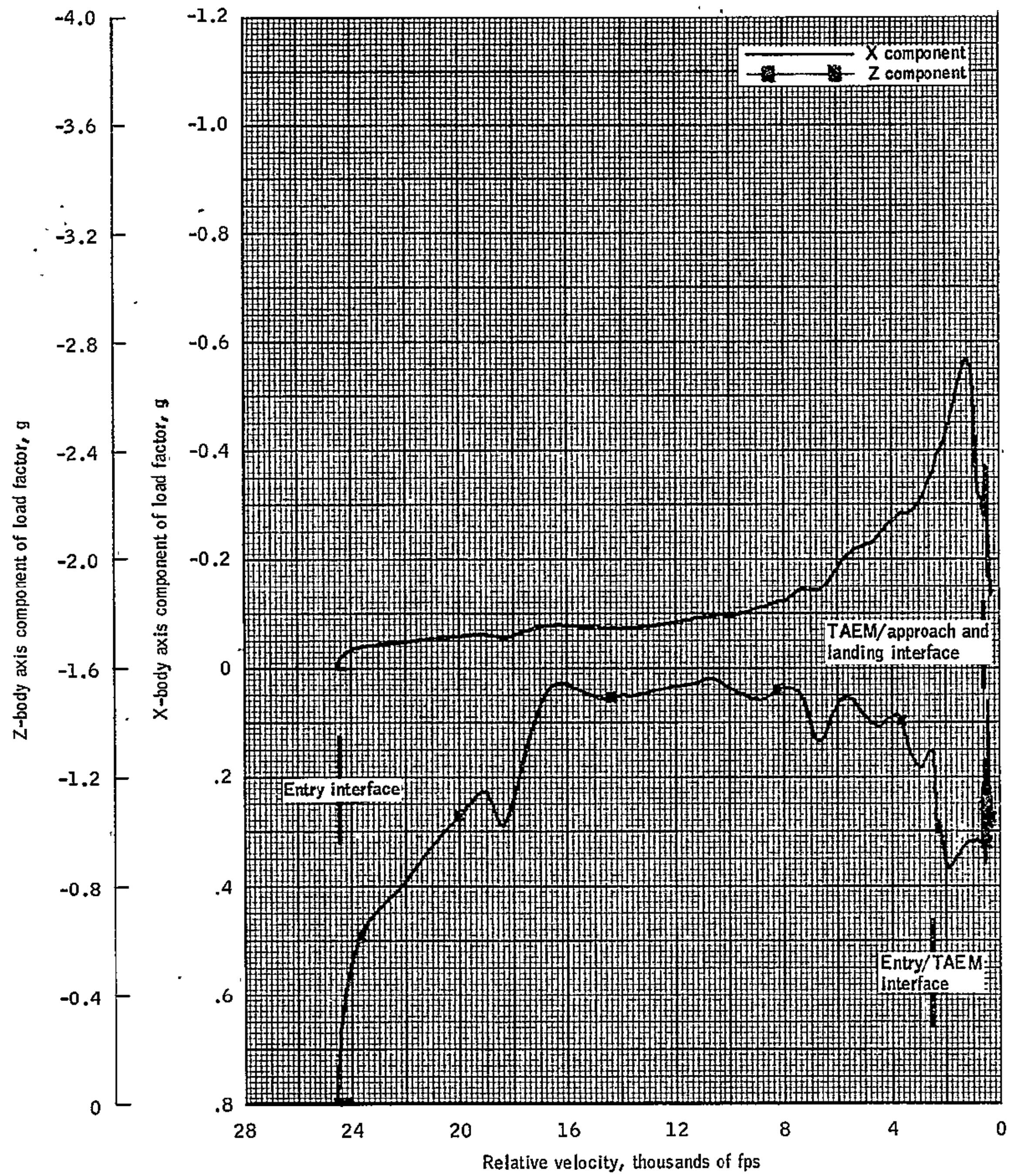

Figure 4.3-19.- X- and Z-body axis components of load factor versus relative velocity for orbiter OFT-1.

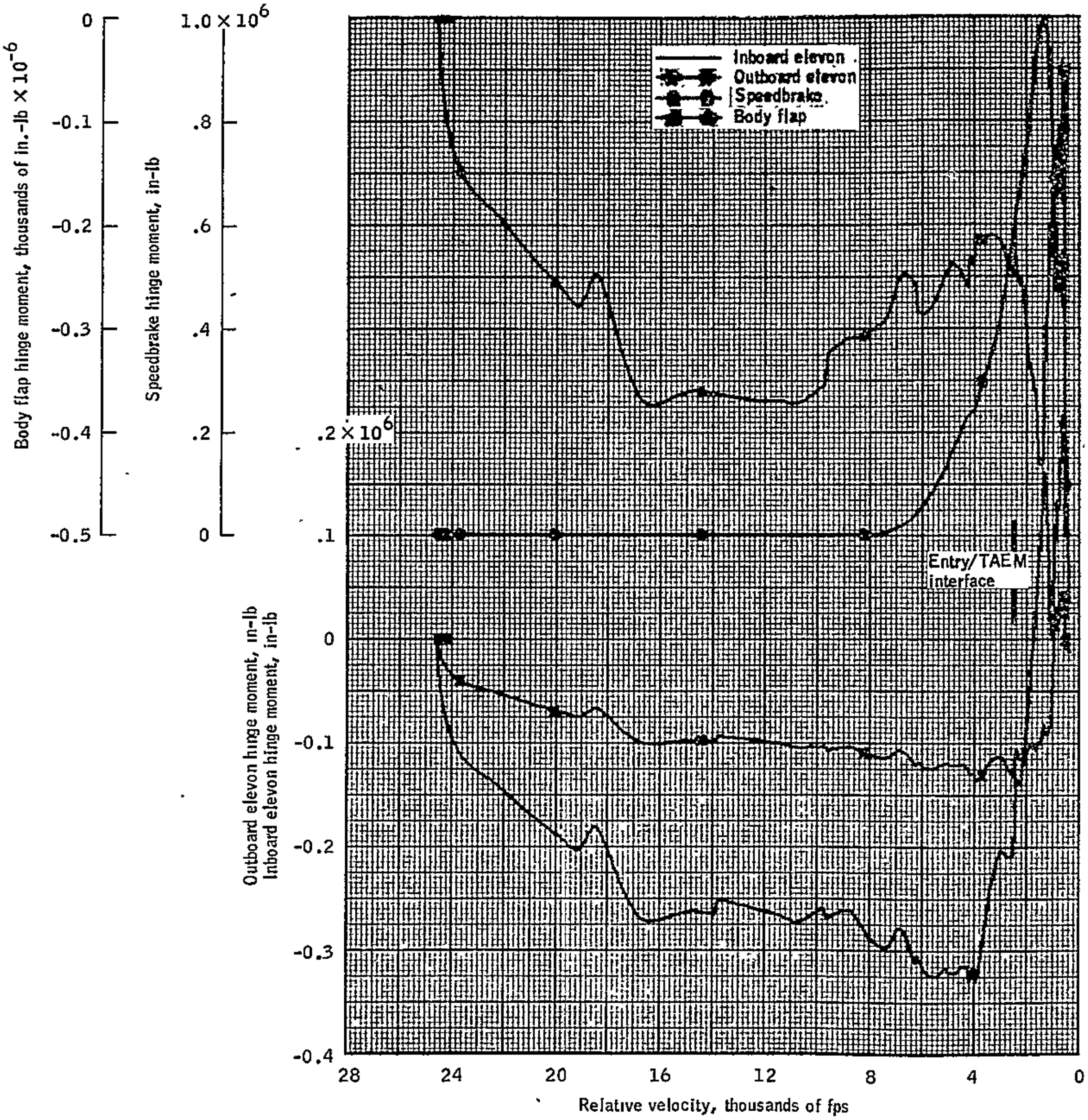

Figure 4.3-20.- Elevon, speedbrake and body-flap hinge moments versus relative velocity for orbiter OFT-1.

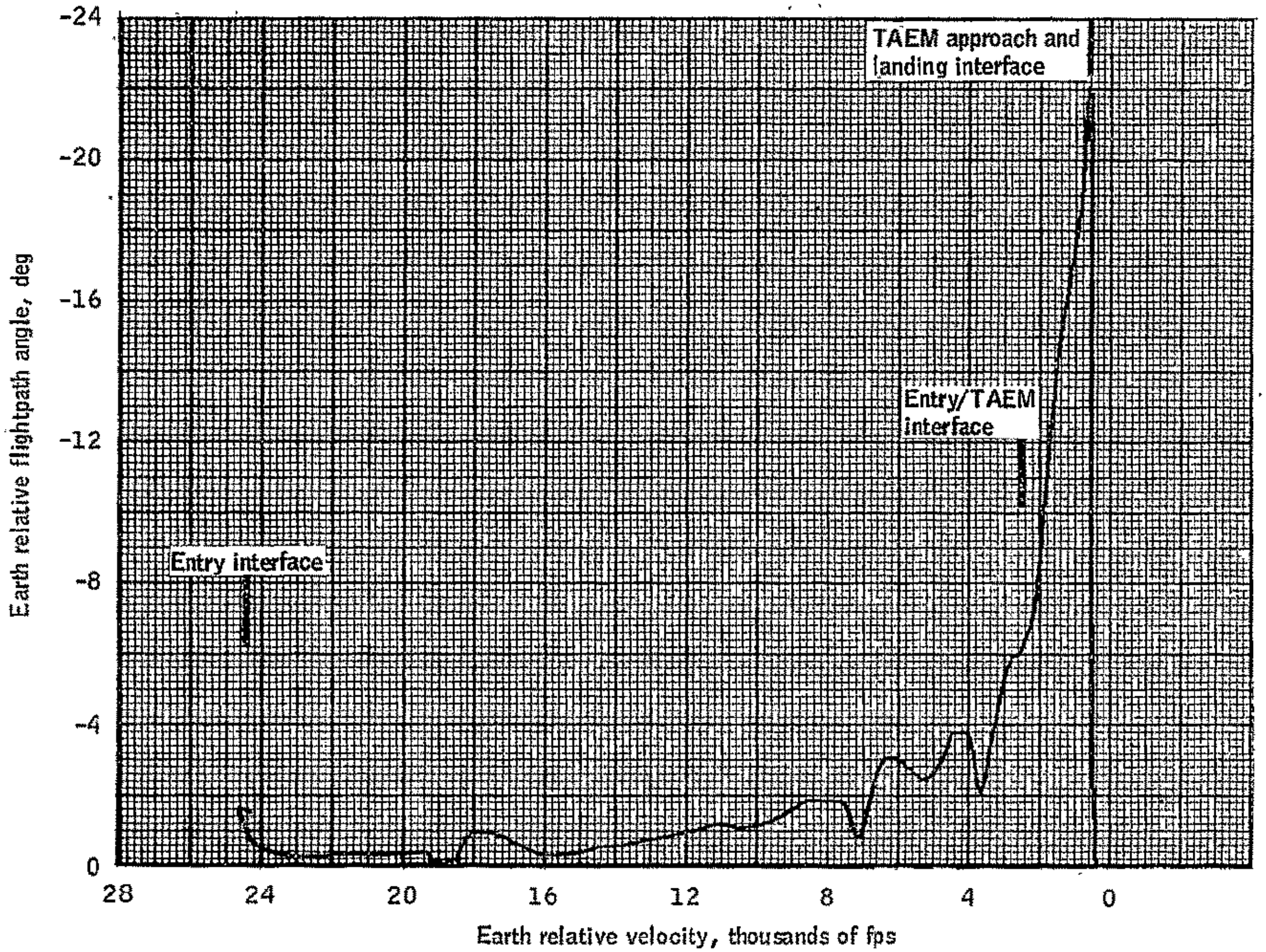

Figure 4.3-21.- Earth relative flightpath angle versus earth relative velocity OFT-1.

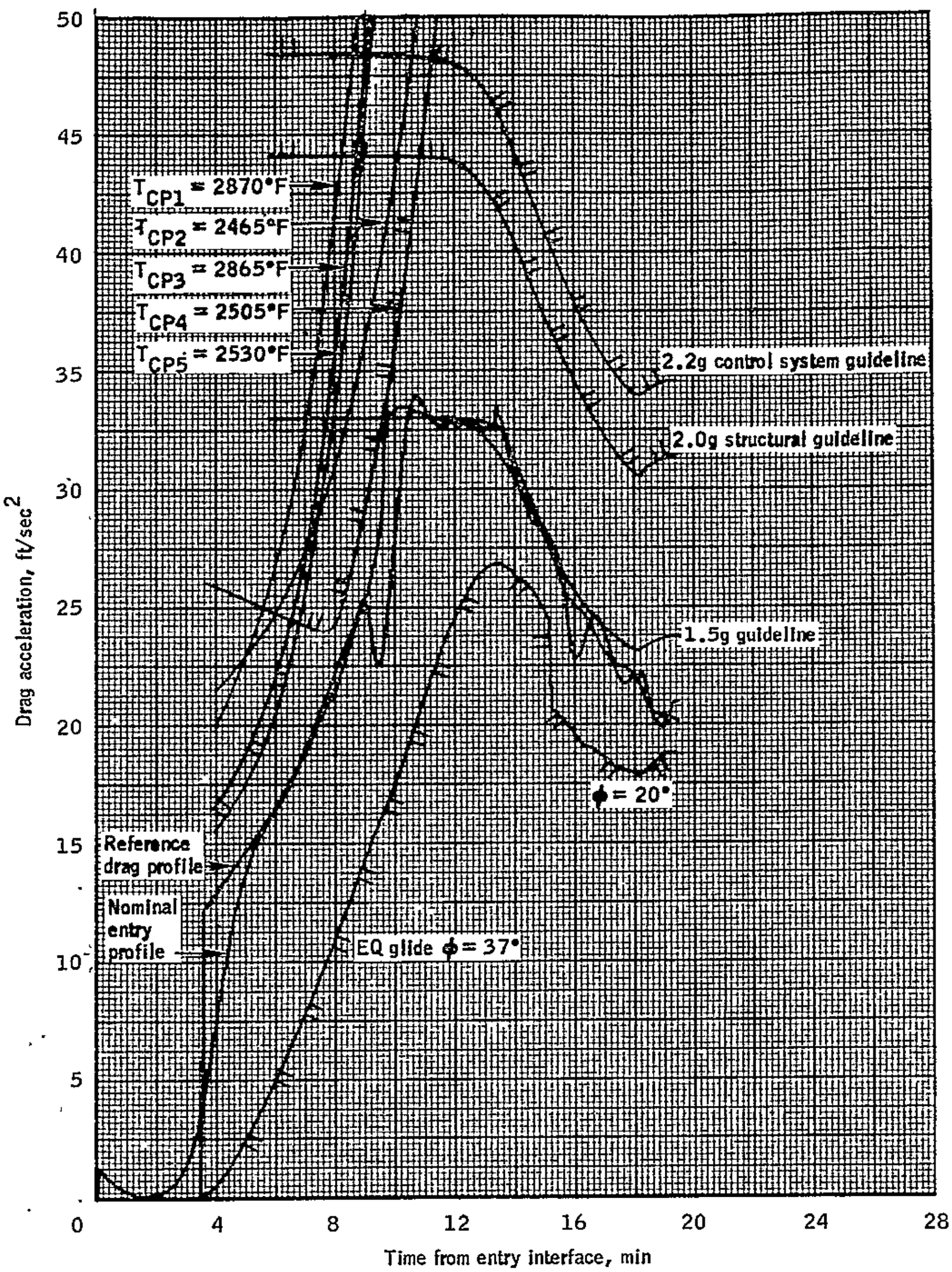

Figure 4.3-22.- Entry corridor and flight profile versus time from entry interface for orbiter OFT-1.

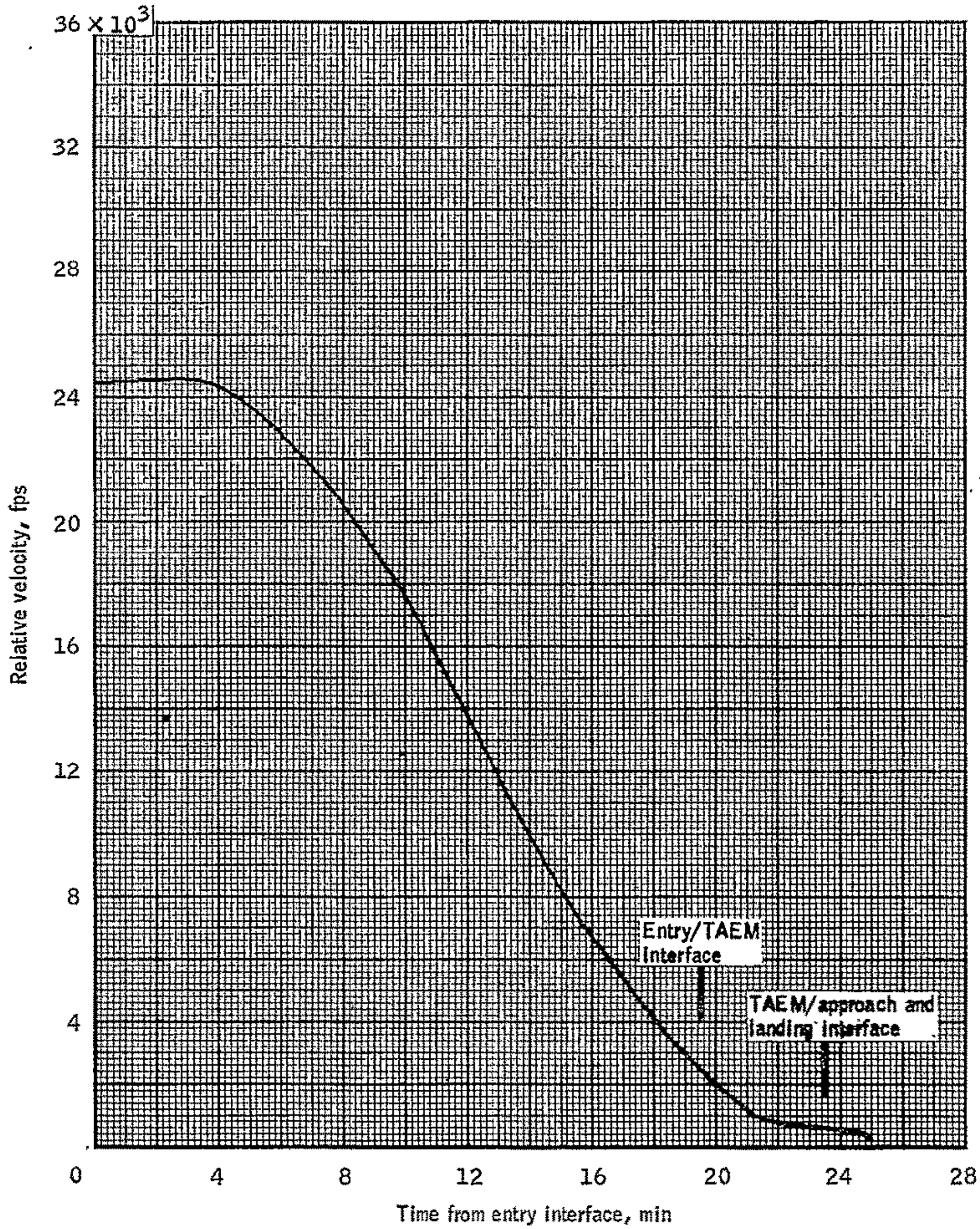

Figure 4.3-23.- Relative velocity versus time from entry interface for orbiter OFT-1.

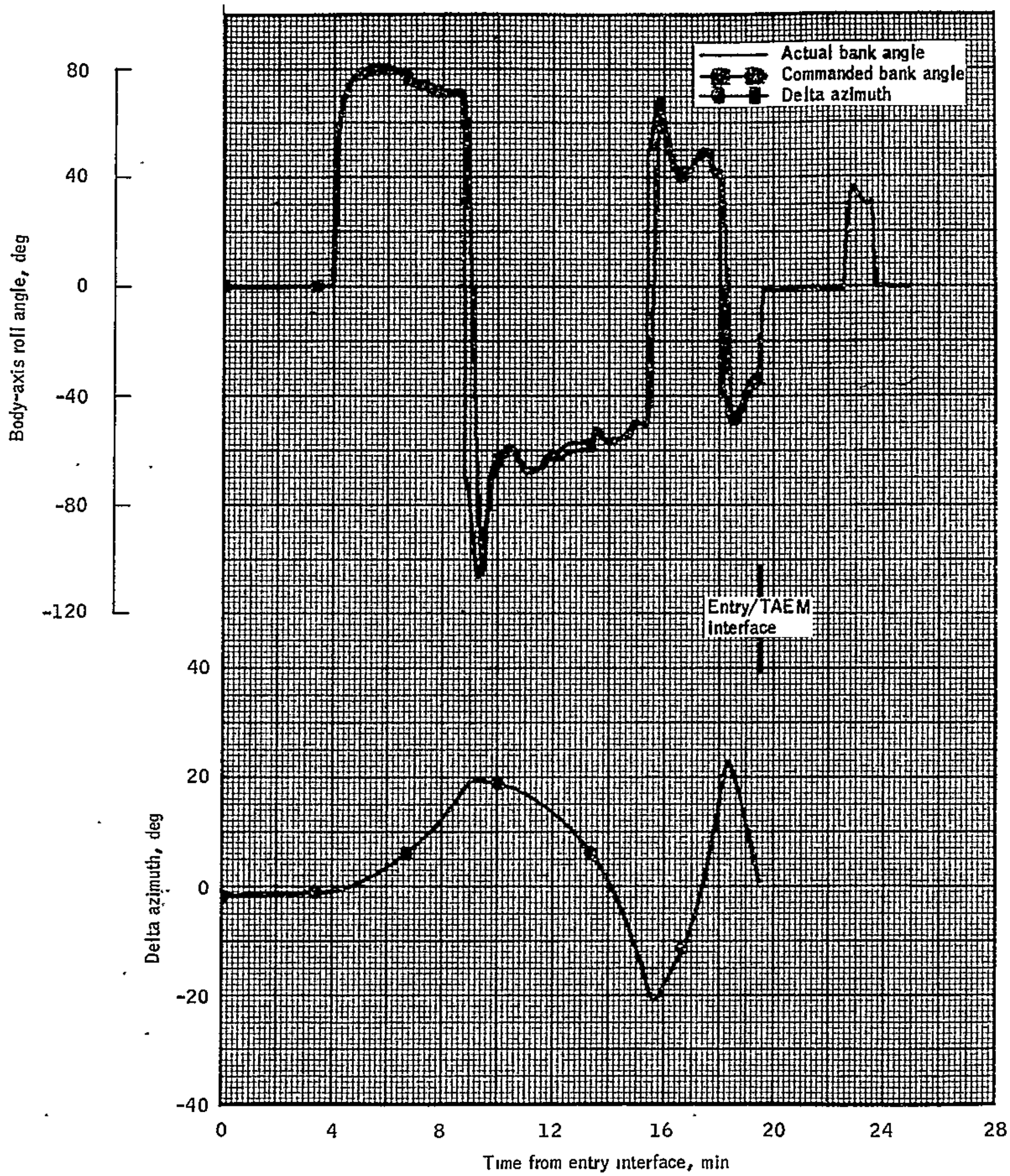

Figure 4.3-24.- Delta azimuth, actual and commanded bank angle versus time from entry interface for orbiter OFT-1.

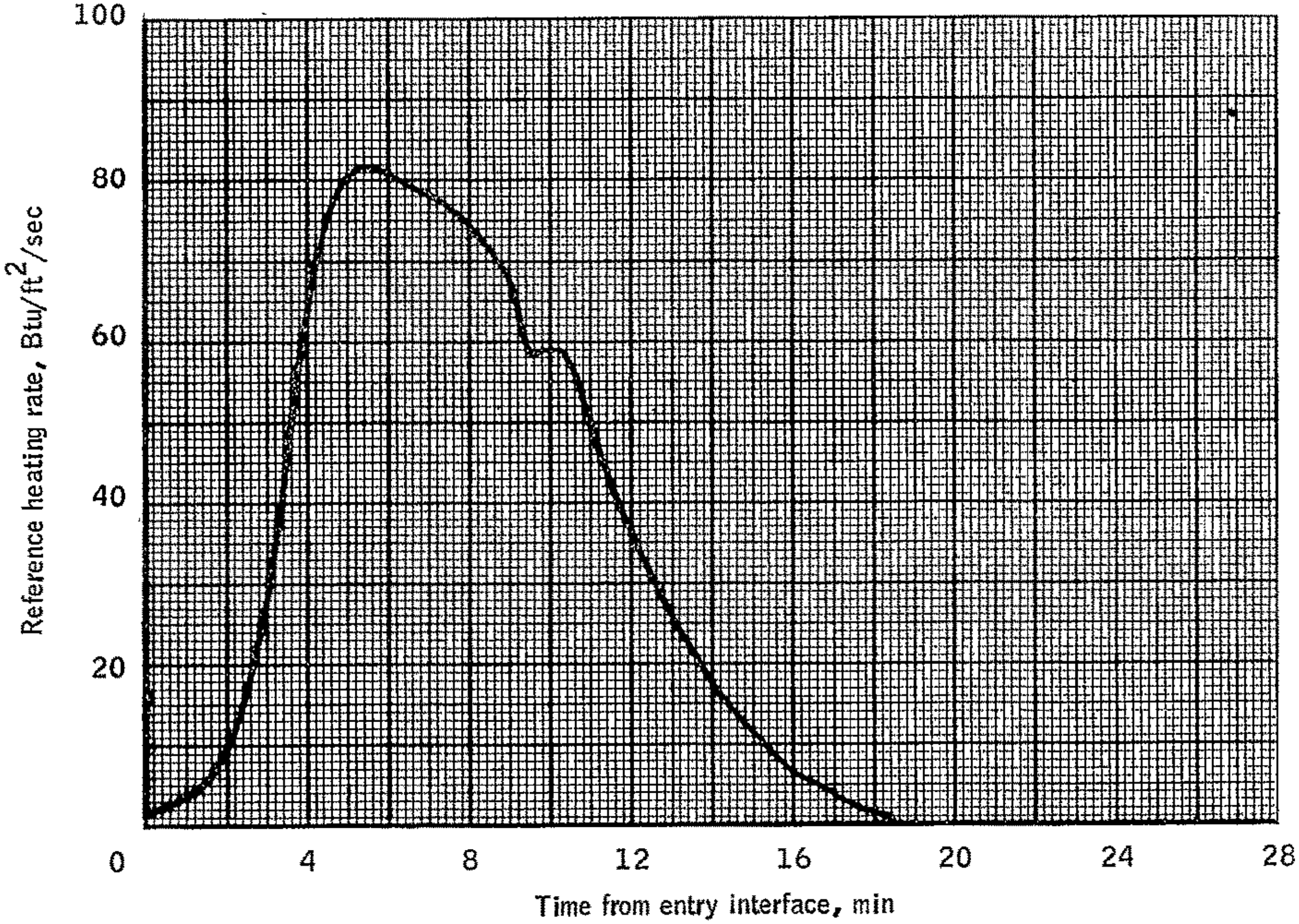

Figure 4.3-25.- Reference heating rate versus time from entry interface for orbiter OFT-1.

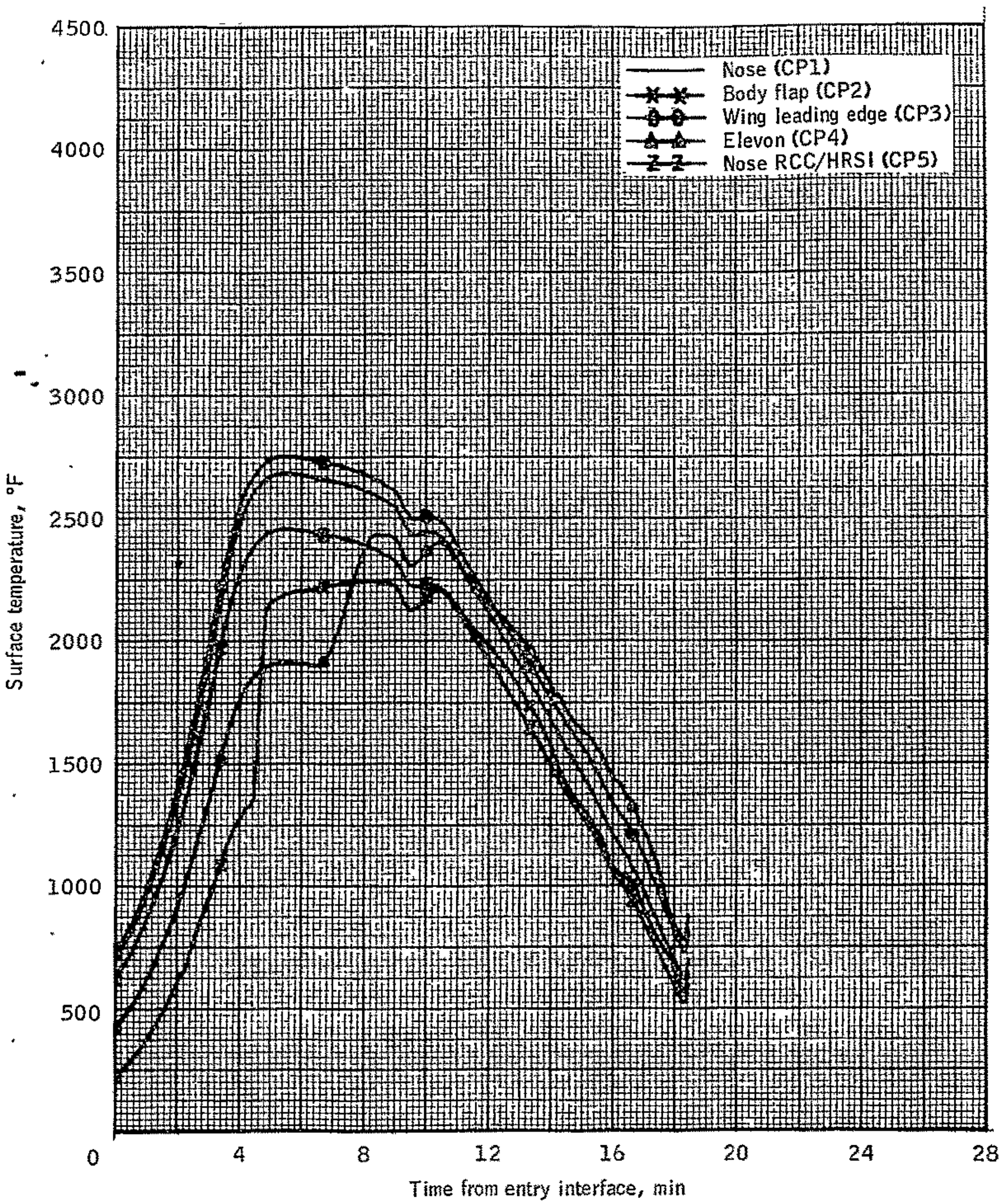

Figure 4.3-26.- Surface temperatures versus time from entry interface for orbiter OFT-1.

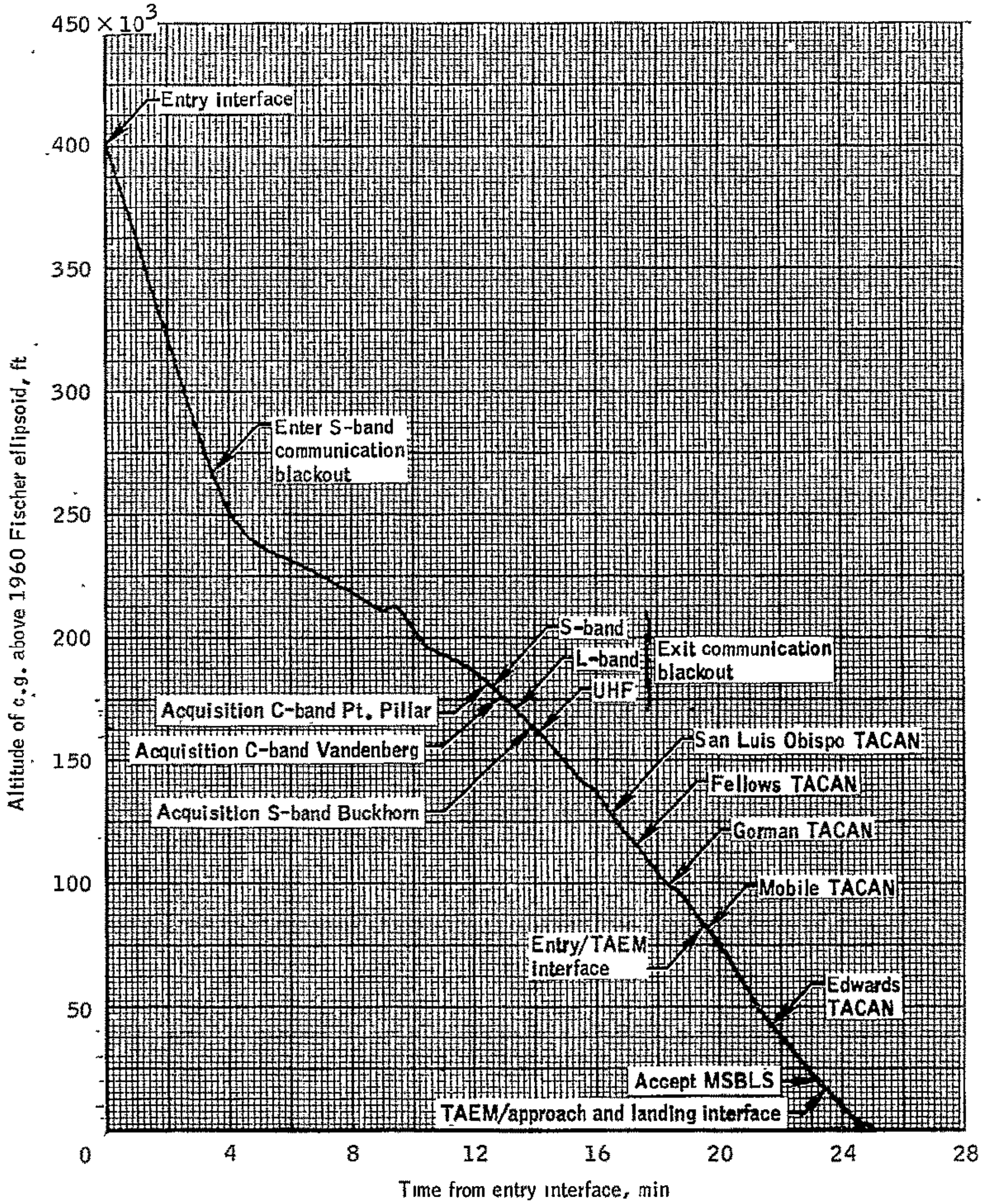

Figure 4.3-27.-Altitude versus time from entry interface for orbiter OFT-1.

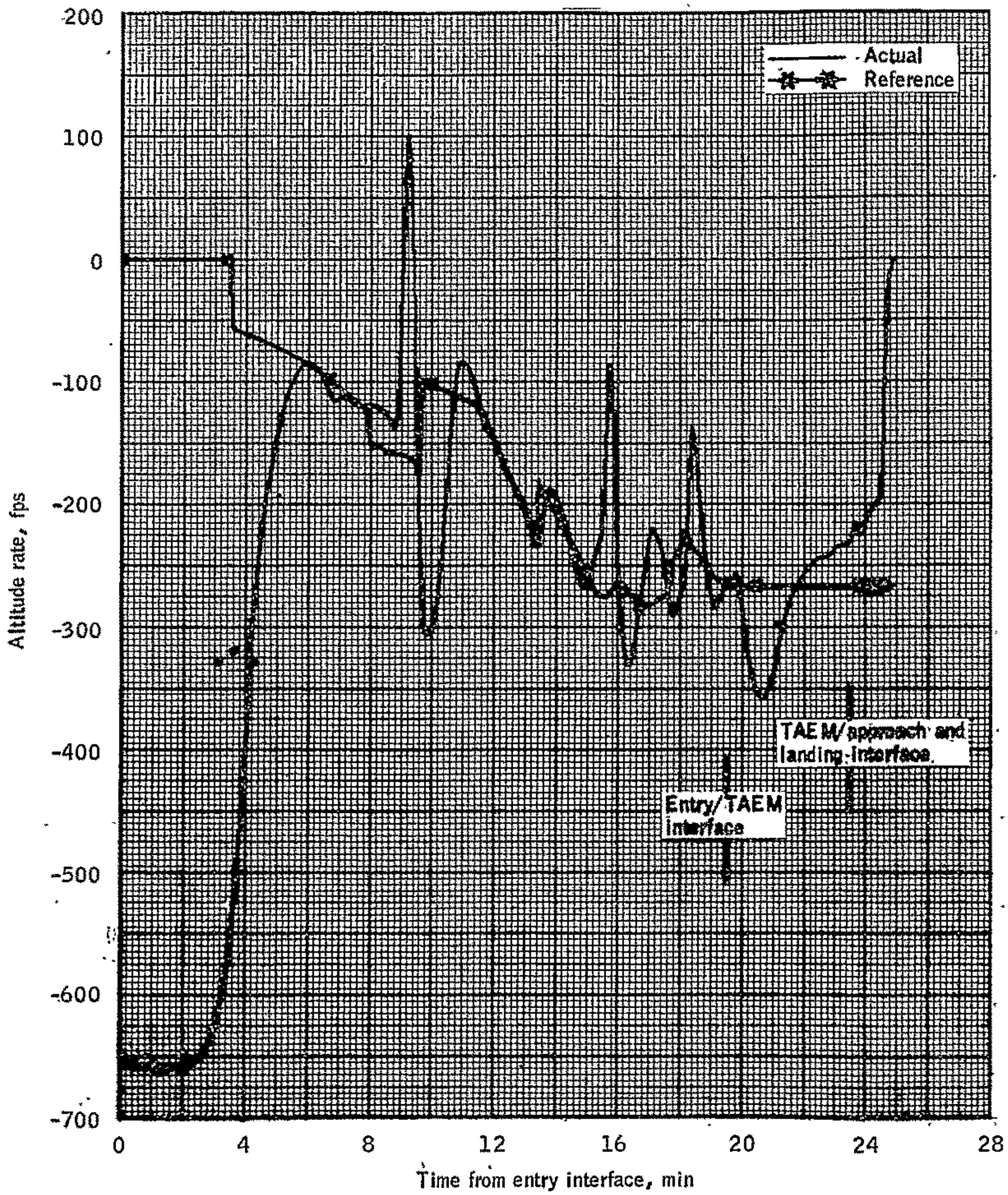

Figure 4.3-28.- Actual and reference altitude rate versus time from entry interface for orbiter OFT-1.

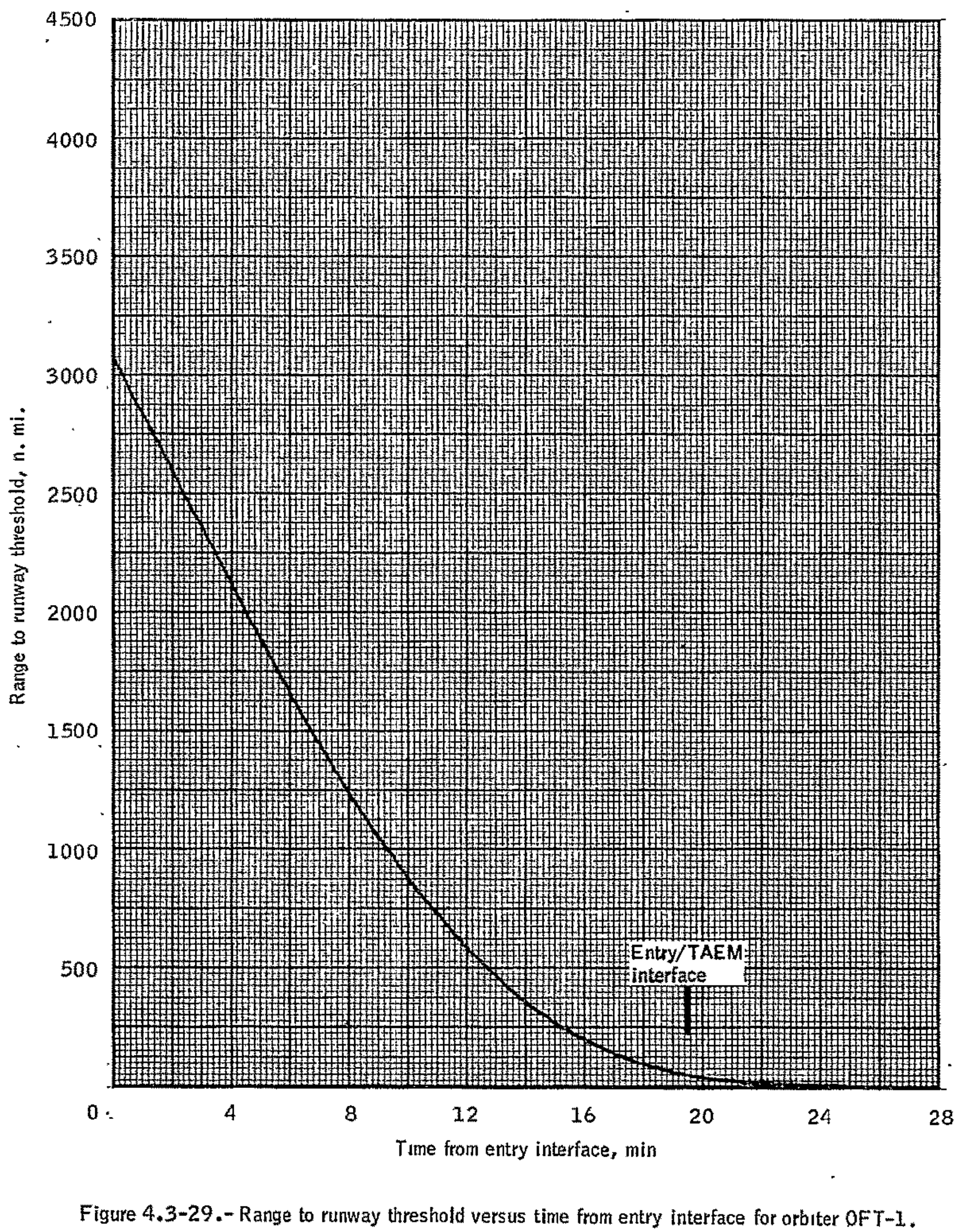

Figure 4.3-29.- Range to runway threshold versus time from entry interface for orbiter OFT-1.

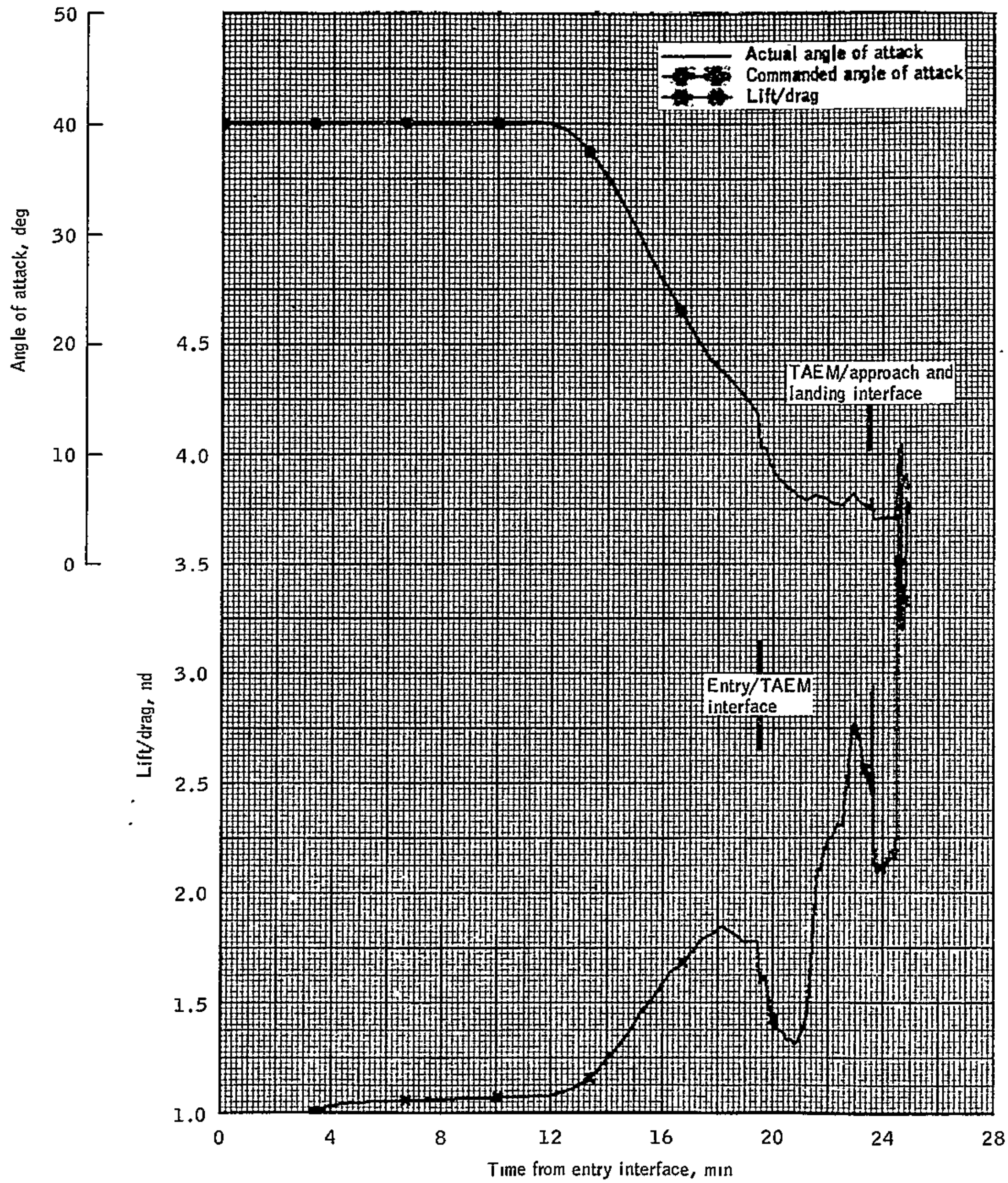

Figure 4.3-30.- Lift/drag, actual and commanded angle of attack versus time from entry interface for orbiter OFT-1.

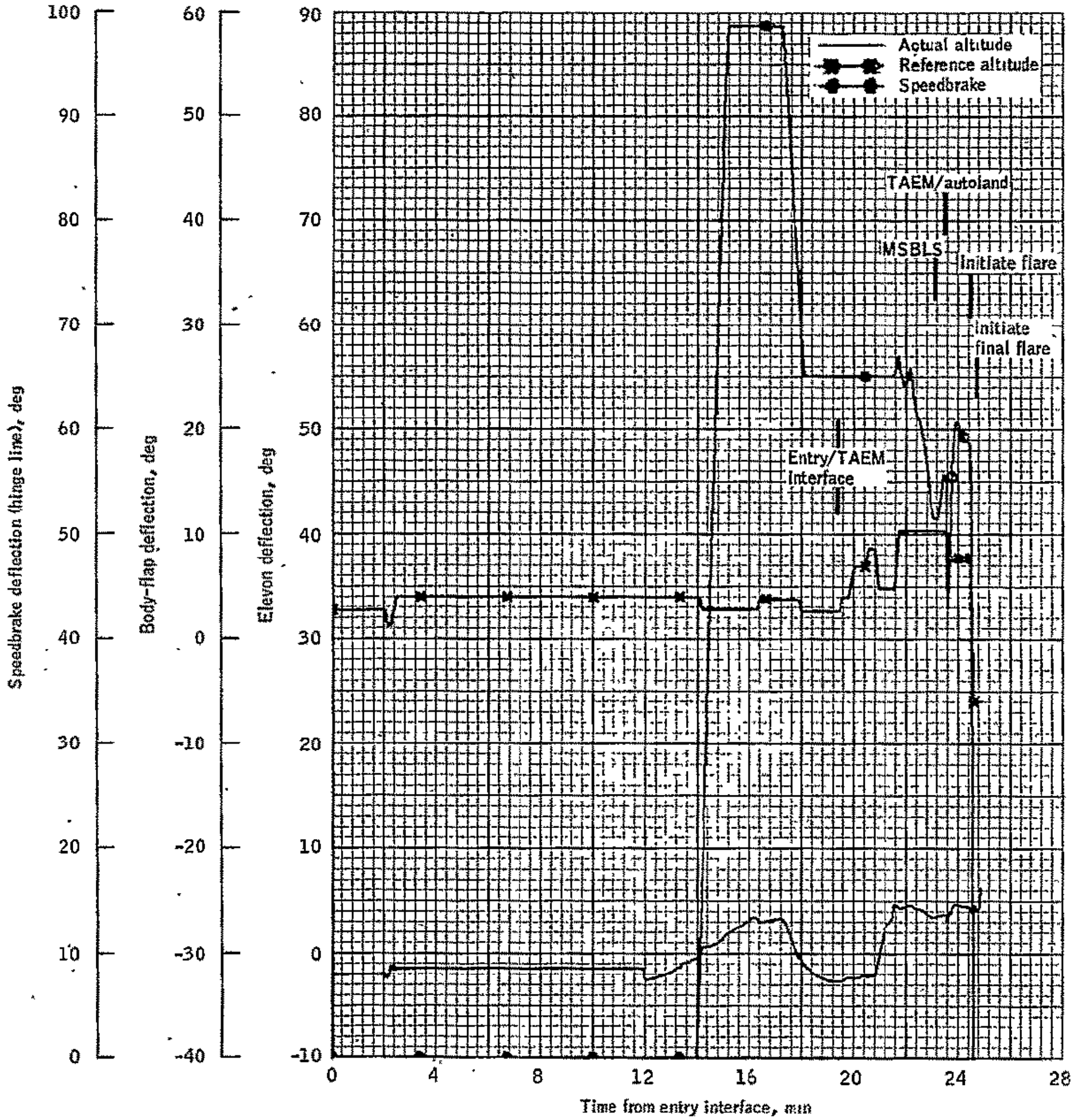

Figure 4.3-31.- Elevon, body-flap and speedbrake deflection versus time from entry interface for orbiter OFT-1 TAEM.

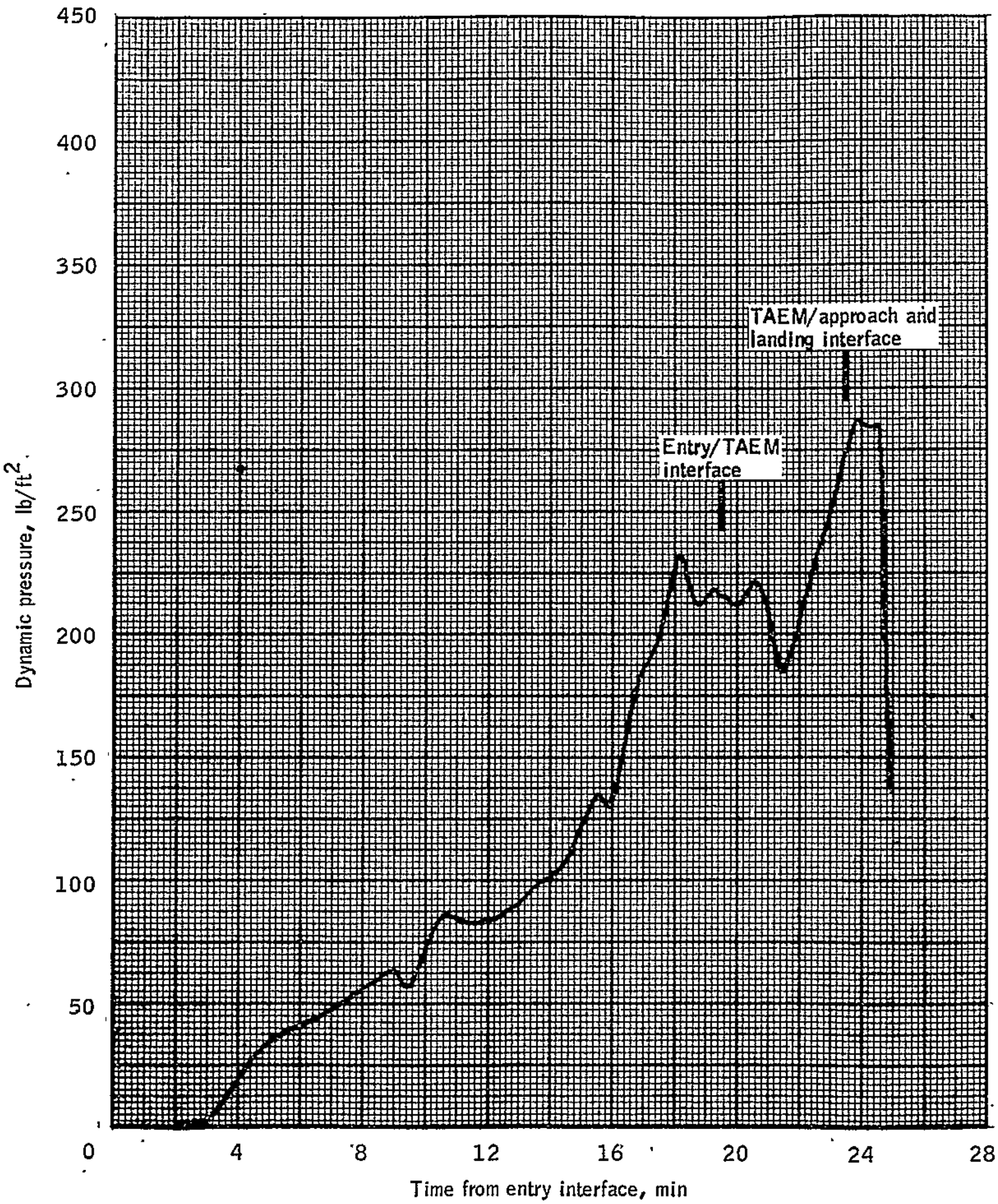

Figure 4.3-32.- Dynamic pressure versus time from entry interface for orbiter OFT-1.

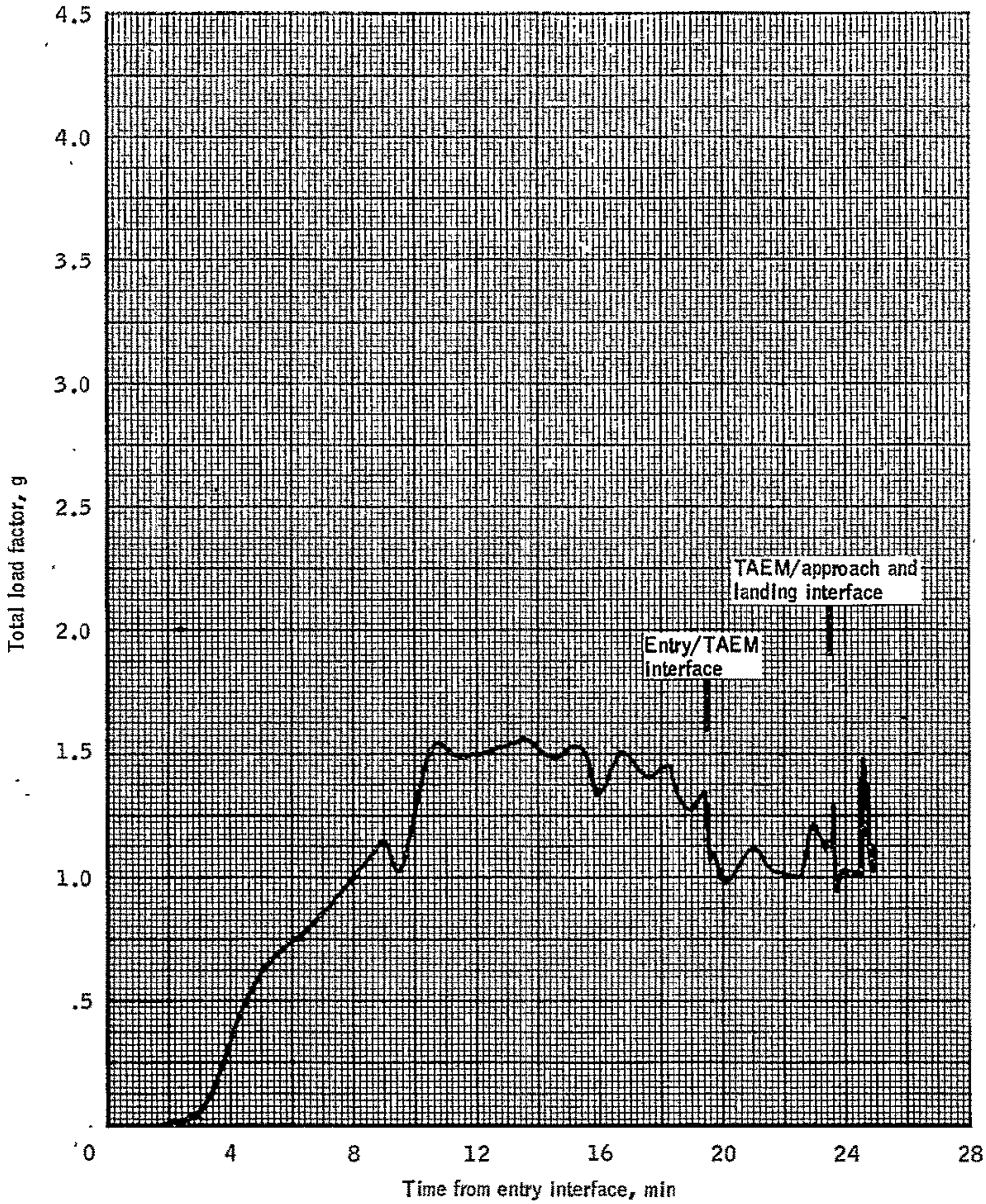

Figure 4.3-33.- Total load factor versus time from entry interface for orbiter OFT-1.

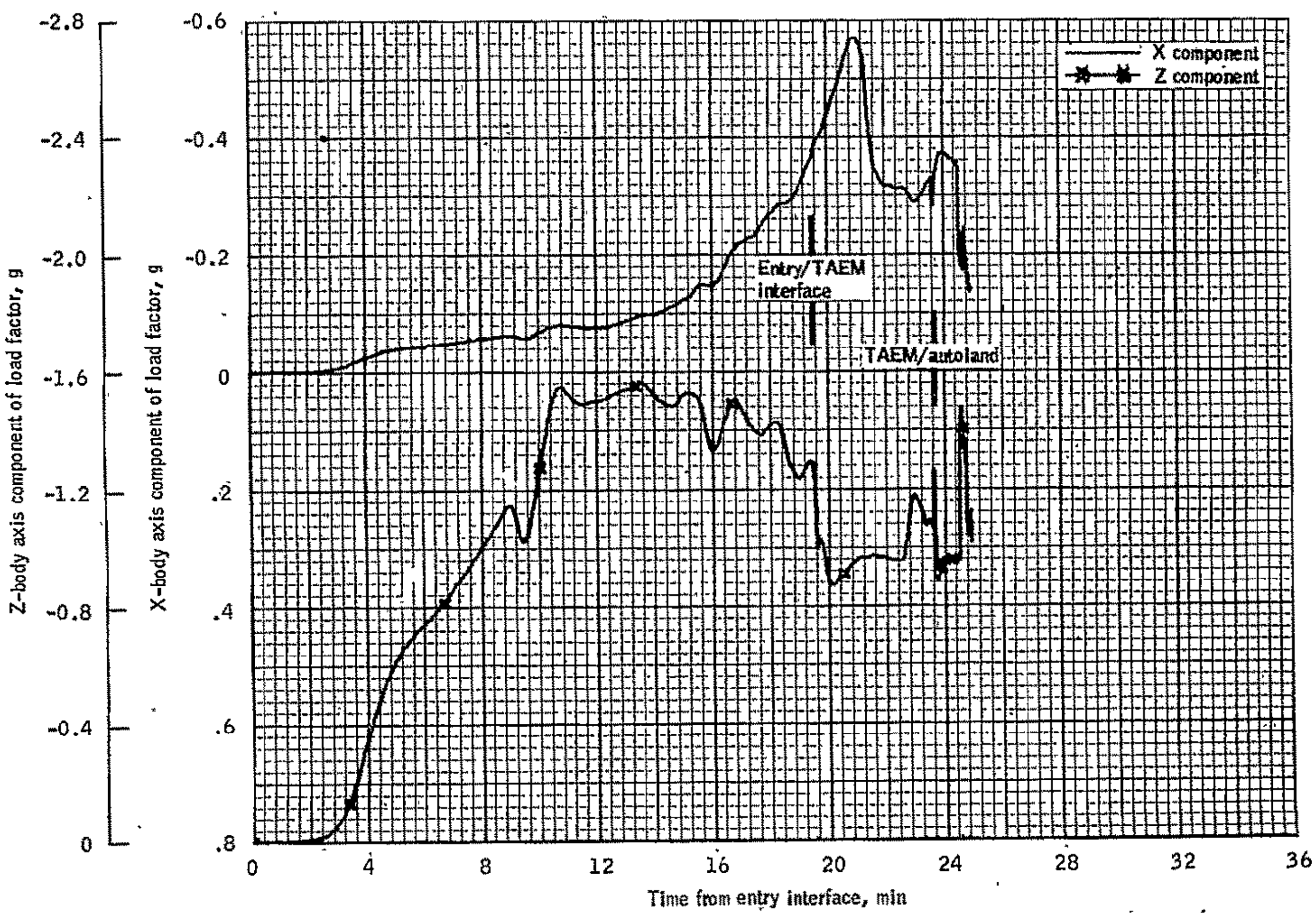

Figure 4.3-34.- X- and Z-body axis components of load factor versus time from entry interface for orbiter OFT-1.

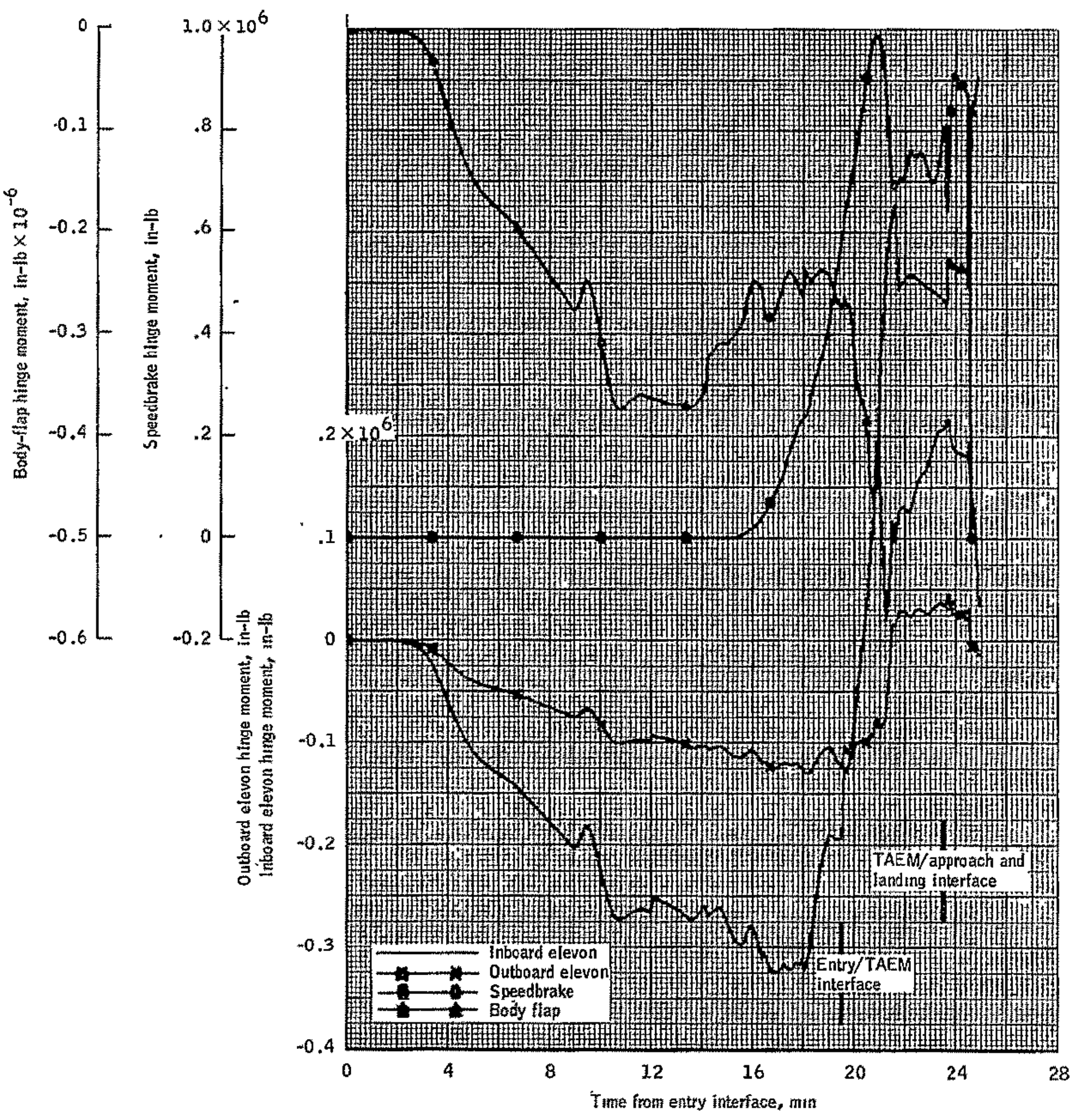

Figure 4.3-35.- Elevon, speedbrake, and body-flap hinge moments versus time from entry interface for orbiter OFT-1.

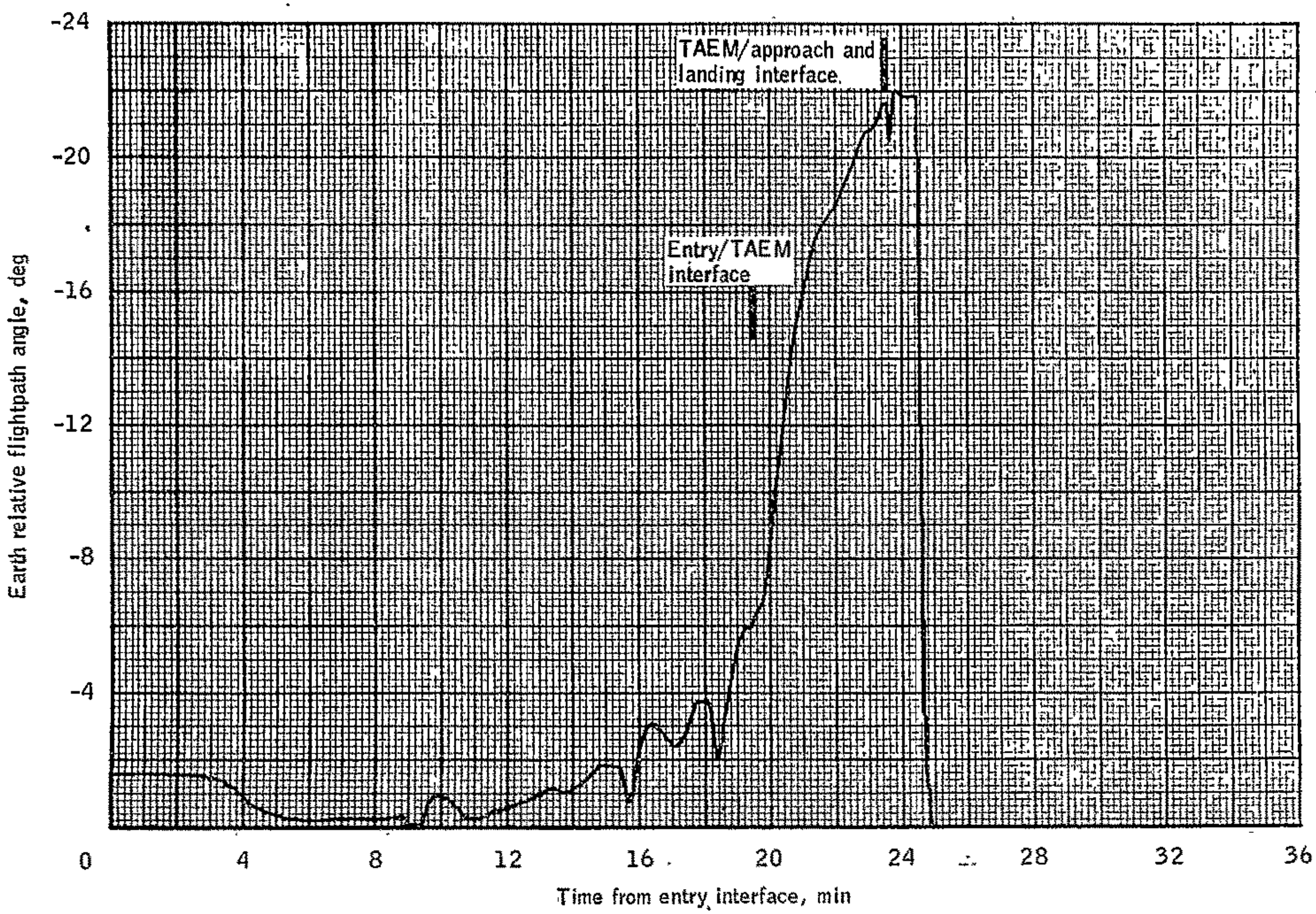

Figure 4.3-36.- Earth relative flightpath angle versus time from entry interface for OFT-1, entry.

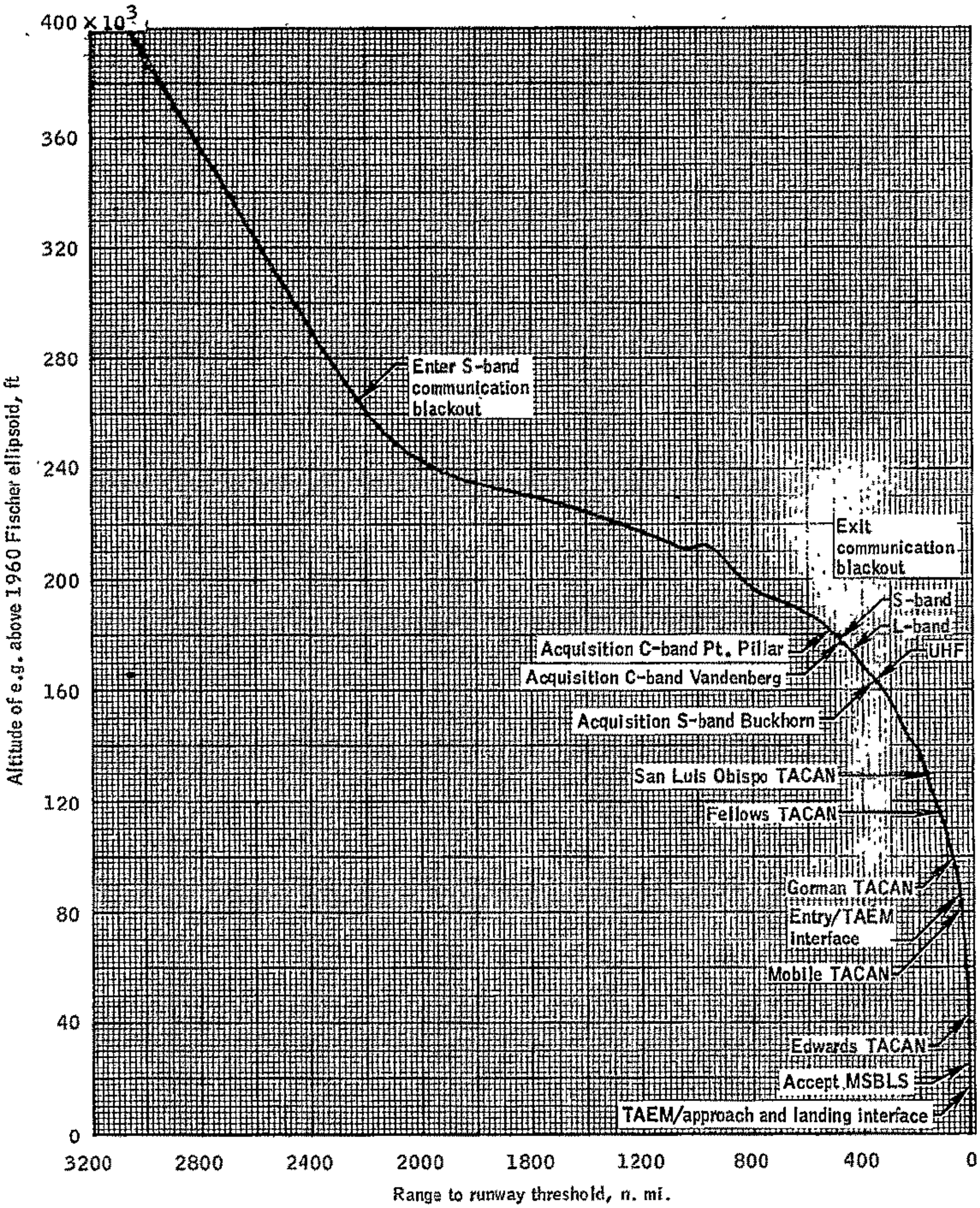

Figure 4.3-37.-Altitude versus range to runway threshold for OFT-1.

TABLE 4.4-I.- DEFINITION OF TAEM GUIDANCE CONSTANTS

Symbol	Description	Value	Units
CDEQD	Constant gain used to compute QBD (= EXP (-0.4 DTG))	0.68113143	nd
CPMIN	Minimum value of COSPHI	0.707	nd
CQDG	Constant gain used to compute QBD (= 1 - CDEQD)	0.31886857	nd
CQG	Constant gain used to compute QBARD and DNZCD (= (1 - EXP (-0.08 DTG))/DTG)	0.5583958	-1
CUBIC_C3 (1,2)	Coefficient used to compute HREF and DHDRRF	-4.7714787E-7, TBD	ft^{-1}
CUBIC_C4 (1,2)	Coefficient used to compute HREF and DHDRRF	-2.4291527E-13, TBD	ft^{-2}
DEL_H1	Altitude error coefficient	0.19	nd
DEL_H2	Altitude error coefficient	900.0	ft
DEL_R_EMAX (1,2)	Delta range used to compute EMAX	54 000.0, TBD	ft
DNZCG	Gain used to compute DNZC	0.01	g-s/ft
DNZLC1	Phases 0,1, and 2 lower NZC limit	-0.5	g
DNZLC2	Phase 3 lower NZC limit	-0.75	g
DNZUC1	Phases 0,1, and 2 upper NZC limit	0.5	g
DNZUC2	Phase 3 upper NZC limit	1.5	g
DSBCM	Mach value to initiate speedbrake modulation	0.9	nd
DSBIL	Limit on integral component of speedbrake command	20.0	deg
DSBLIM	Maximum value for speedbrake command	98.6	deg

TABLE 4.4-I.- Continued

Symbol	Description	Value	Units
DSBNOM	Nominal speedbrake command value	65.0	deg
DSBSUP	Mach > DSBCM speedbrake command	65.0	deg
DSHPLY	Delta range value used to compute SHPLYK	4000.0	ft
DTG	TAEM guidance cycle time interval	0.96	s
DTR	Degrees to radians conversion factor	0.0174533	deg^{-1}
EDELNZ (1,2)	Delta energy over weight used to compute EMAX and EMIN	4000.0, TBD	ft
EDRS (1,2)	Slope of ES with range	0.69946182, TBD	nd
EMEP_C1 ((1,1), (1,2),(2,1), (2,2))	Constant energy over weight used to compute EMEP	2702.1202 13859.314 TBD, TBD	ft
EMEP_C2 ((1,1),(1,2), (2,1),(2,2))	Slope of EMEP with range	0.5155494, 0.265521, TBD, TBD	nd
EN_C1 ((1,1), (1,2),(2,1), (2,2))	Constant energy over weight used to compute EN	6854.7826, 18 272.012, TBD, TBD	ft
EN_C2 ((1,1), (1,2),(2,1), (2,2))	Slope of EN with range	0.60776028, 0.44326307, TBD,TBD	nd
EOW_SPT (1,2)	Range used for IEL selection	105 863.43, TBD	ft

TABLE 4.4-I.- Continued

Symbol	Description	Value	Units
ES1 (1,2)	Constant energy over weight used to compute ES	90 000.0, TBD	ft
G	Gravitational acceleration at sea level	32.174	ft/s^2
GAMMA_COEF1	Flightpath error coefficient	0.0007	deg/ft
GAMMA_COEF2	Flightpath error coefficient	3.0	deg
GAMMA_ERROR	Flightpath error band	4.0	deg
GAMSGS (1,2)	Steep glideslope angle	-22.0, TBD	deg
GDHC	Constant used to compute GDH	2.0	nd
GDHLL	Lower limit on GDH	0.3	nd
GDHS	Slope of GDH with altitude	0.00007	ft^{-1}
GDHUL	Upper limit on GDH	1.0	nd
GEHDLL	Gain used to compute EOWNZLL	0.01	g-s/ft
GEHDUL	Gain used to compute EOWNZUL	0.01	g-s/ft
GELL	Gain used to compute EOWNZLL	0.1	s^{-1}
GEUL	Gain used to compute EOWNZUL	0.1	s^{-1}
GPHI	Gain on heading error for phase 1 roll command	2.5	nd
GR	Gain on radial error for phase 2 roll command	0.02	deg/ft
GRDOT	Gain on radial rate error for phase 2 roll command	0.2	deg-s/ft
GSBE	Speedbrake proportional gain on QBERR	1.5	deg/psf

TABLE 4.4-I.- Continued

Symbol	Description	Value	Units
GSBI	Speedbrake integral gain on QBERR	0.1	deg-s/psf
GY	Phase 3 lateral error gain	0.05	deg/ft
GYDOT	Phase 3 lateral rate error gain	0.6	deg-s/ft
H_ERROR	Altitude error bound for transition to autoland	1000.0	ft
H_REF1	Altitude reference for transition to autoland	10 000.0	ft
H_REF2	Altitude reference for transition to autoland	5000.0	ft
HALI (1,2)	Altitude used to compute XALI and HREF	10 018.0, TBD	ft
HDREQG	Gain on HERROR to compute DNZC	0.1	s^{-1}
HFTC (1,2)	Altitude used to compute XFTC	12 018.0, TBD	ft
MXQBWT	Constant used to compute QBLL = (140./190000 psf/lb m)	0.7368421E-03	psf/lb m
PBGC (1,2)	Lower limit on DHDRRF = (TAN (5.5 DTR), TBD)	0.11126660, TBD	nd
PBRCQ(1,2)	Range break point for QBREF	89 971.082, TBD	ft
PBHC (1,2)	Altitude reference for DRPRED = PBRC	78 161.826, TBD	ft
PBRC (1,2)	Maximum range for cubic altitude reference	256 527.82, TBD	ft
PHAVGC	Constant used to compute PHAVG	63.33	deg
PHAVGLL	Lower limit on PHAVG	30.0	deg
PHAVGS	Slope of PHAVG with Mach	13.33	deg
PHAVGUL	Upper limit on PHAVG	50.0	deg

TABLE 4.4-I.- Continued

Symbol	Description	Value	Units
PHILMSUP	Supersonic roll command limit	30.0	deg
PHILMO	Saturn roll command limit	50.0	deg
PHILM1	Acquisition roll command limit	50.0	deg
PHILM2	Heading alinement roll command limit	60.0	deg
PHILM3	Prefinal roll command limit	30.0	deg
PHIM	Mach value for PHILIMIT test	0.9	nd
PHIP2C	Nominal roll command during phase 2	30.0	deg
P2TRNC1	Constant used in phase 2 initiation test	1.1	nd
P2TRNC2	Constant used in phase 2 initiation test	1.01	nd
QB_ERROR1	Dynamic pressure error bound for transition to autoland	24.0	psf
QB_ERROR2	Dynamic pressure error bound for transition to autoland	24.0	psf
QBARDL	Limit on QBARD	5.0	psf/s
QBC1 (1,2)	Slope of QBREF with DRPRED > PBRCQ	3.6086999E-4 TBD	psf/ft
QBC2 (1,2)	Slope of QBREF with DRPRED < PBRCQ	-1.1613301E-3, TBD	psf/ft
QBG1	Gain used to compute QBNZLL and QBNZUL	0.1	s^{-1}
QBG2	Gain used to compute QBNZLL and QBNZUL	0.125	s-g/psf
QBMXS	Slope of QBMXNZ with Mach > QBM2	0.0	psf

TABLE 4.4-I.- Continued

Symbol	Description	Value	Units
QBMX1	Constant used to compute QBMXNZ	340.0	psf
QBMX2	Constant used to compute QBMXNZ	300.0	psf
QBMX3	Constant used to compute QBMXNZ	300.0	psf
QBM1	Mach breakpoint for computing QBMXNZ	1.0	nd
QBM2	Mach breakpoint for computing QBMXNZ	1.7	nd
QBRLL (1,2)	QBREF lower limit	180.0, TBD	psf
QBRML (1,2)	QBREF middle limit	220.0, TBD	psf
QBRUL (1,2)	QBREF upper limit	285.0, TBD	psf
RERRLM	Limit on RERRC	50.0	deg
RFTC	Roll fader time constant	5.0	s
RMINST (1,2)	Minimum range to initiate Saturn phase	152 000.0, TBD	ft
RN1 (1,2)	Constant range used in computing EN, EMEP, and EMAX	36 456.6, TBD	ft
RTBIAS	Constant used in Phase 2 initiation test	3000	ft
RTD	Conversion factor for radians to degrees	57.29578	deg
RTURN	HAC radius	20 000.0	ft
TGGS (1,2)	Tangent of steep glideslope (= TAN(GAMSGS(1)DTR), TAN(GAMSGS(2) DTR))	-0.40402623, TBD	nd

TABLE 4.4-I.- Concluded

Symbol	Description	Value	Units
VCO	Constant used to compute GCONT (= RTD G/GQN, where GQN = GQN (FCS))	548.7	ft/sec
WT_GS1	Weight used for IGS selection	250 000.0	lb m
XA (1,2)	Steep glideslope ground intercept	-5000.0, TBD	ft
Y_ERROR	Crossrange error bound for autoland initiation when H > H_REF1	1000.0	ft
Y_RANGE1	Coefficient on H used to compute crossrange error bound when H < H_REF1	0.18	nd
Y_RANGE2	Constant used to compute crossrange error bound when H < H_REF1	800.0	ft
YERRLM	Limit on YERRC	120.0	deg

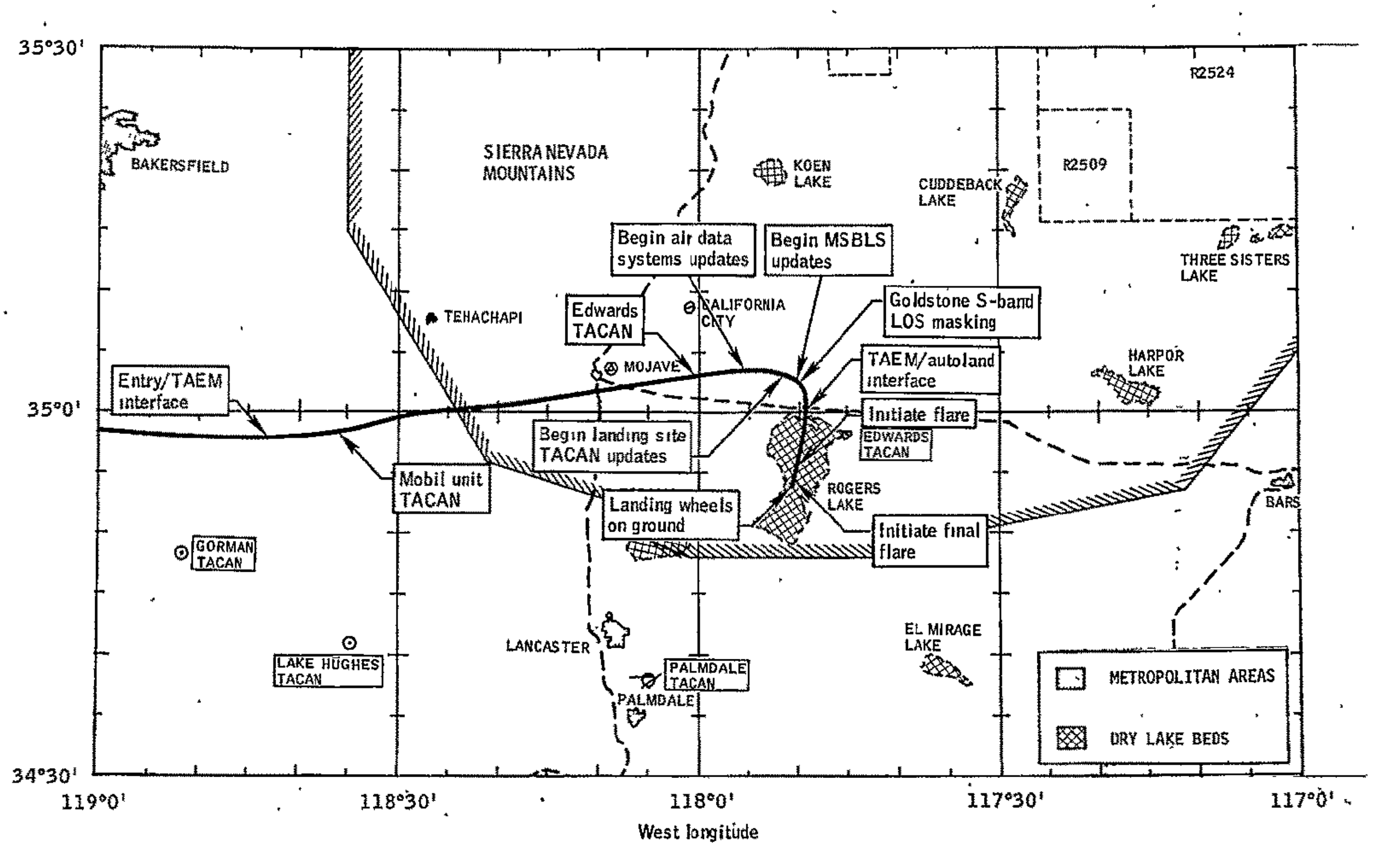

Figure 4.4-1.-TAEM through landing groundtrack.

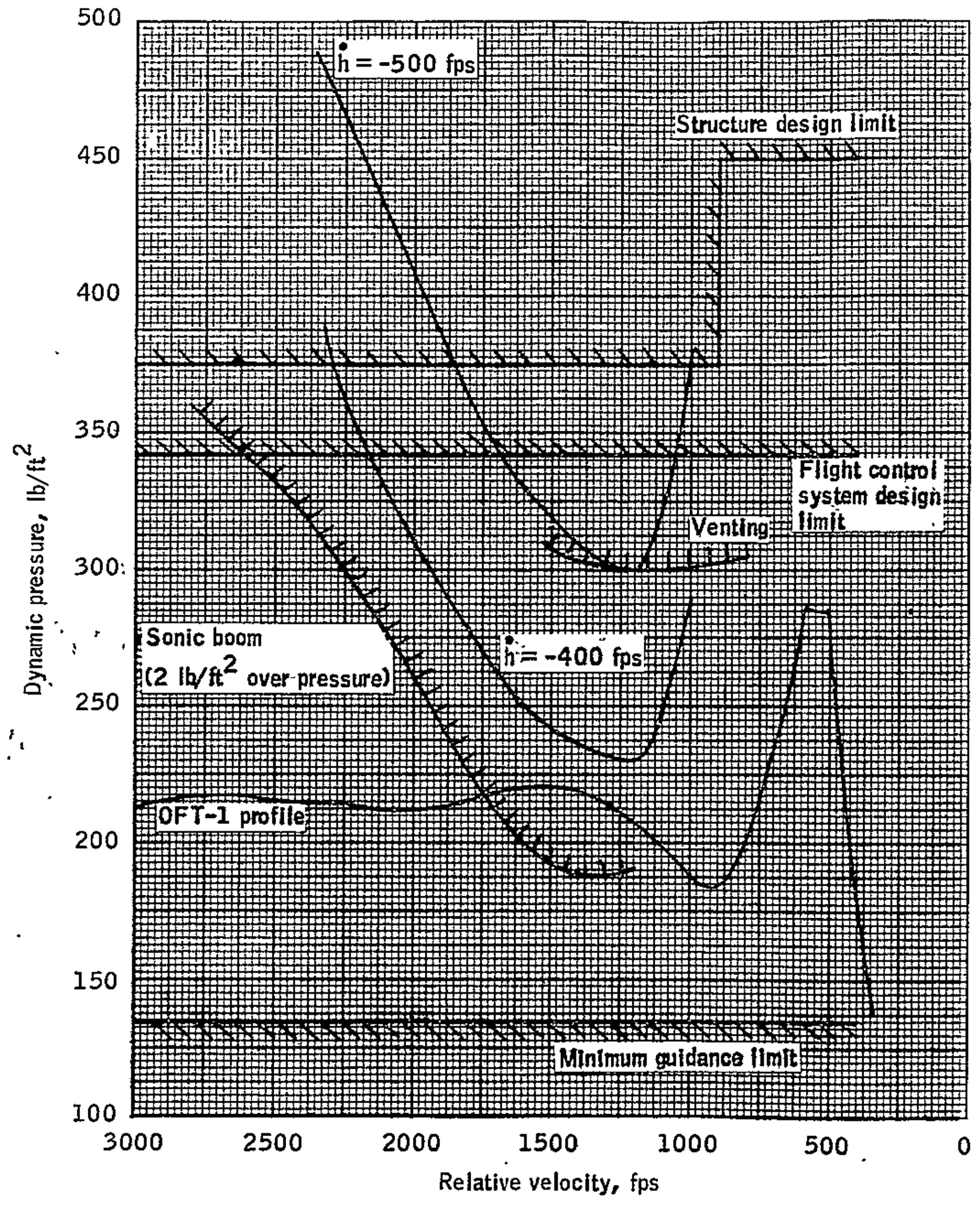

Figure 4.4-2.- TAEM dynamic pressure corridor.

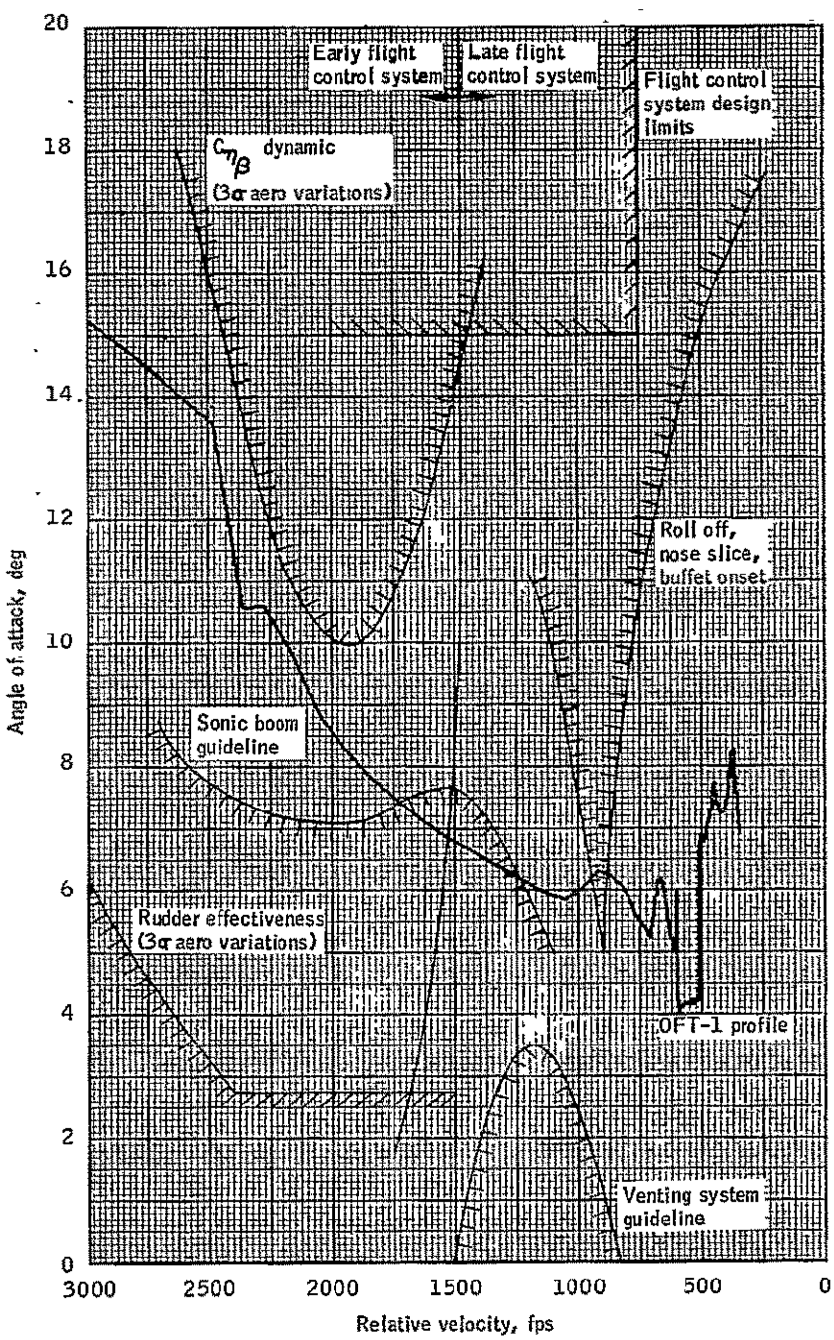

Figure 4.4-3.- TAEM angle of attack corridor.

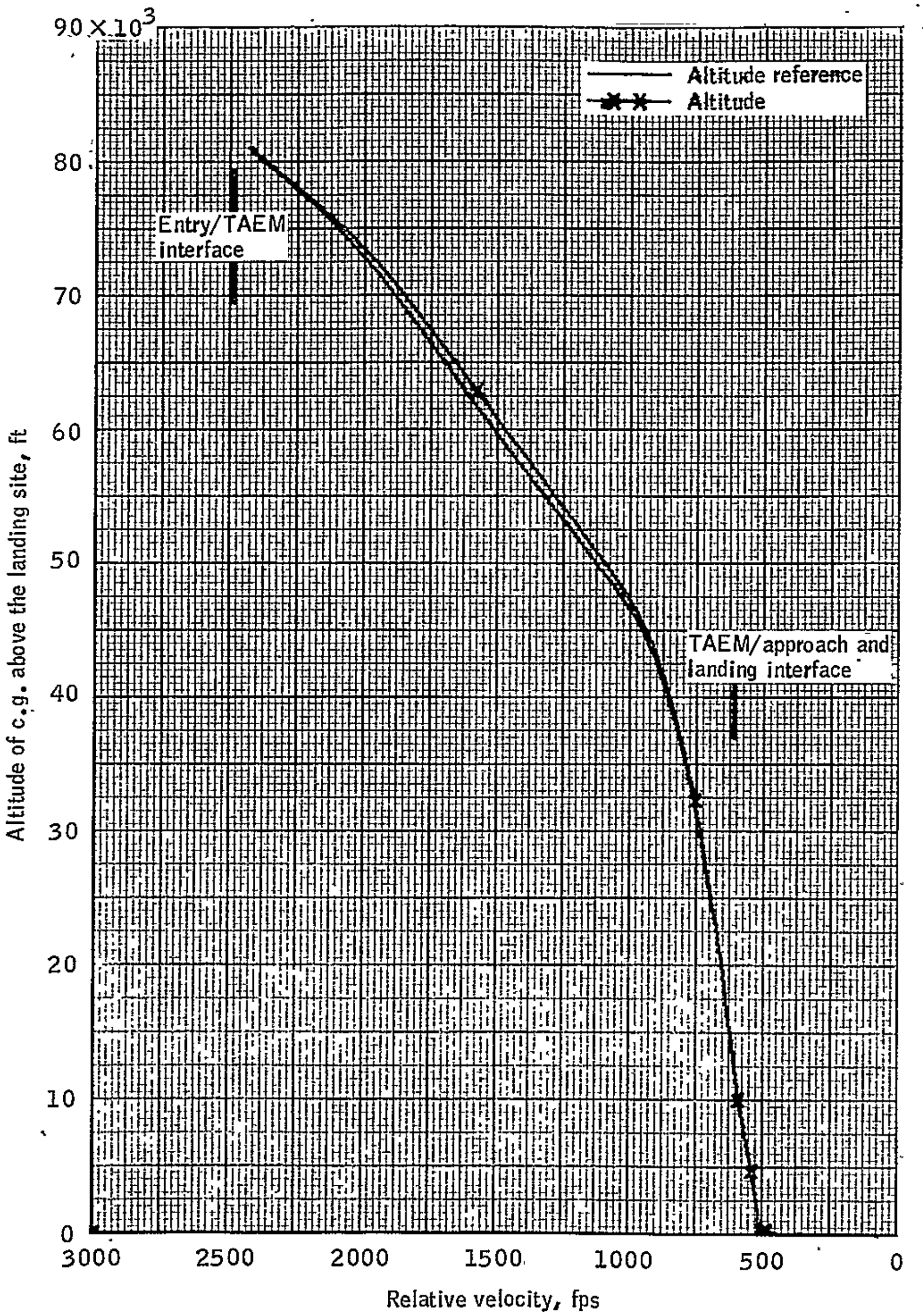

Figure 4.4-4.- Altitude and altitude reference (above landing site) versus relative velocity for orbiter OFT-1 TAEM.

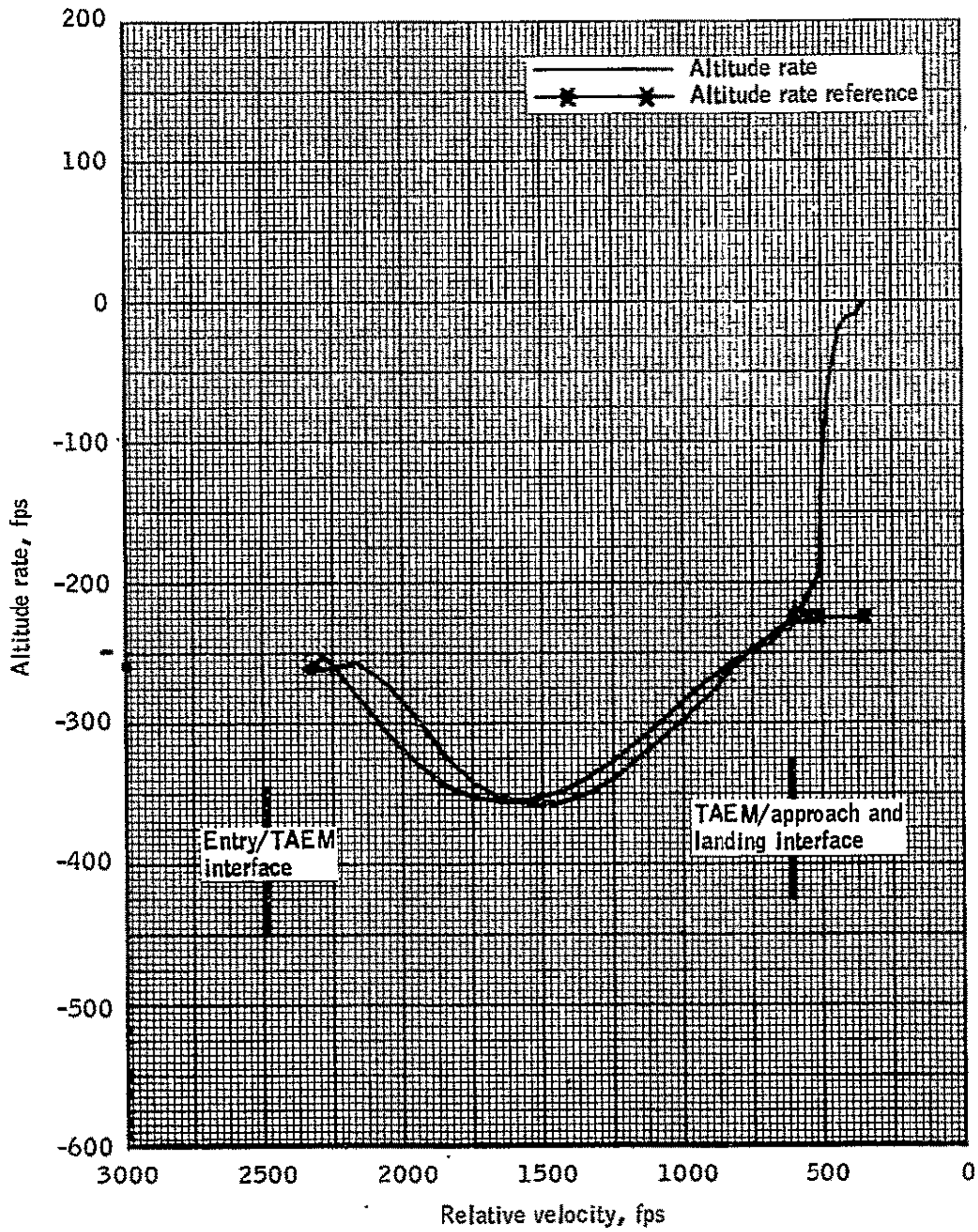

Figure 4.4-5.- Altitude rate and altitude rate reference versus relative velocity for orbiter OFT-1 TAEM.

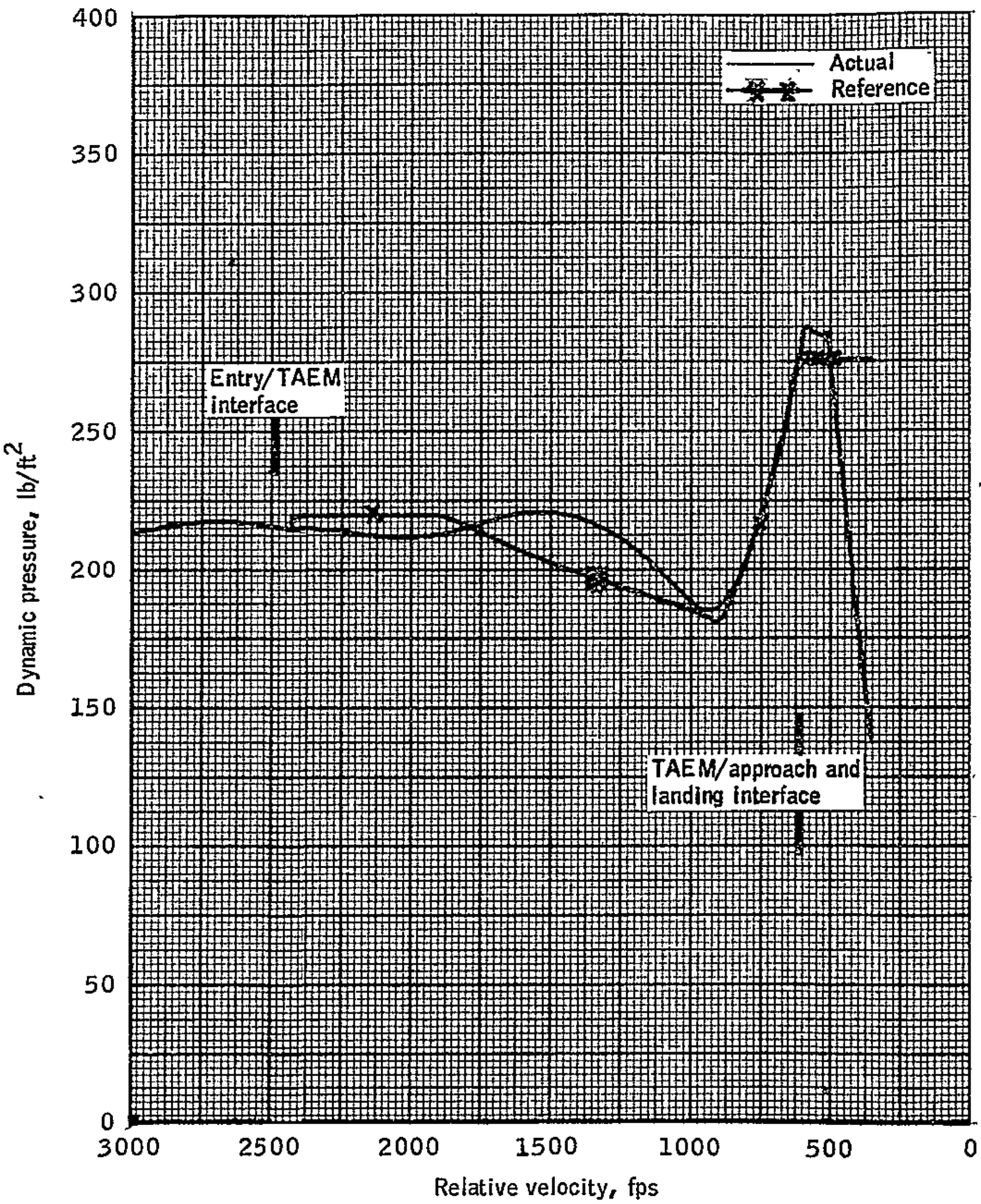

Figure 4.4-6.- Actual and reference dynamic pressure versus relative velocity for orbiter OFT-1 TAEM.

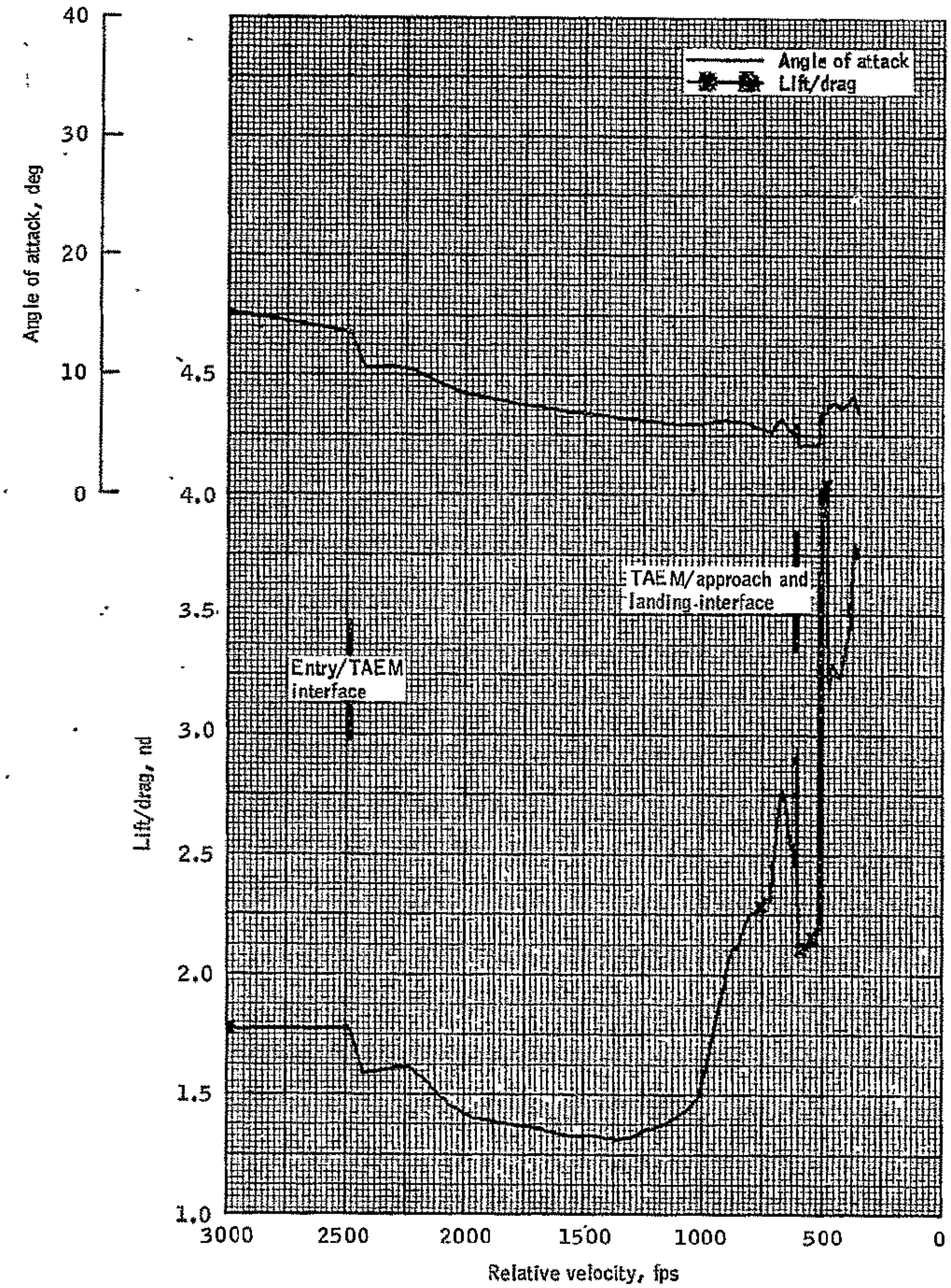

Figure 4.4-7.- Lift/drag and angle of attack versus relative velocity for orbiter OFT-1 TAEM.

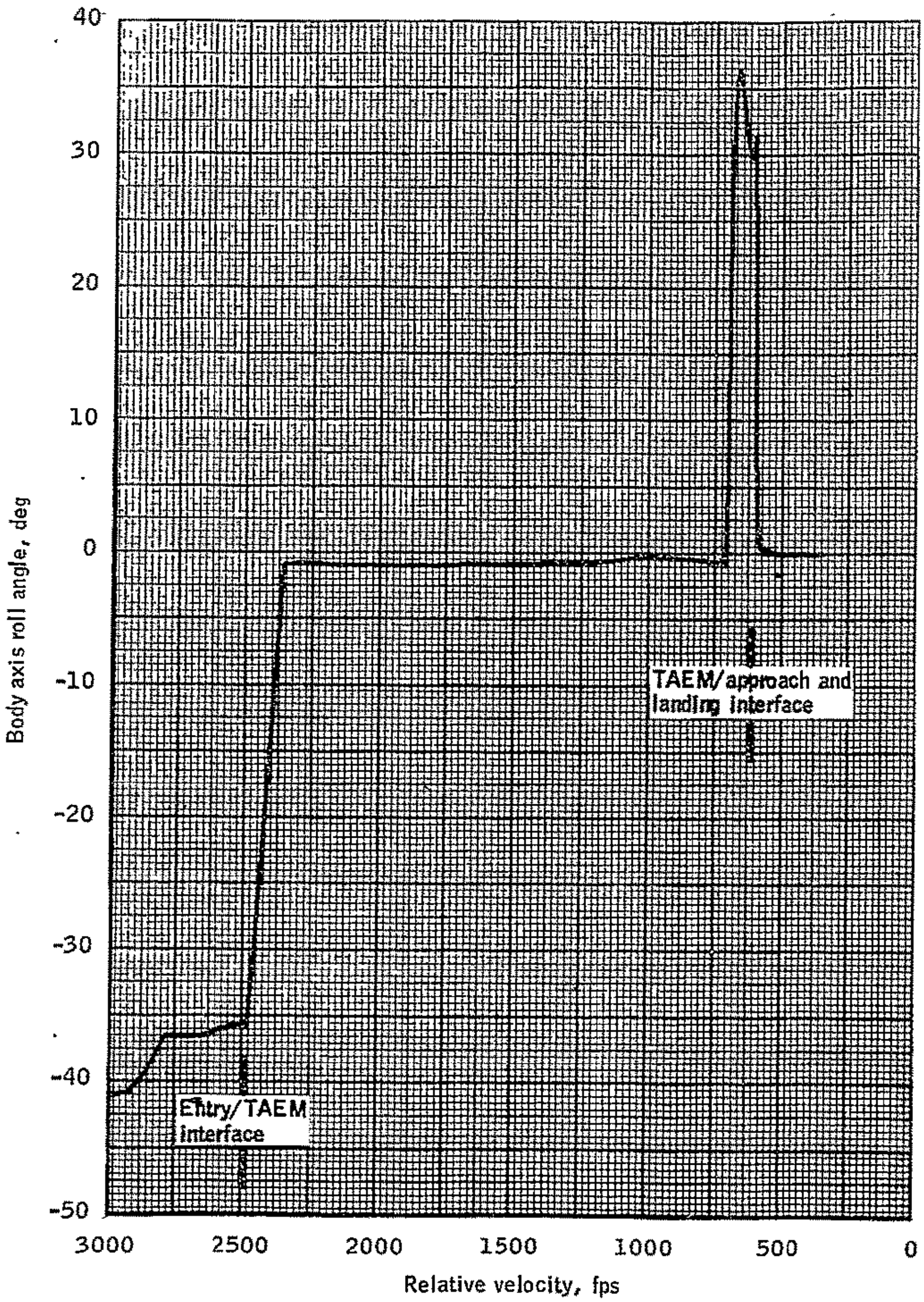

Figure 4.4-8.- Bank angle versus relative velocity for orbiter OFT-1 TAEM.

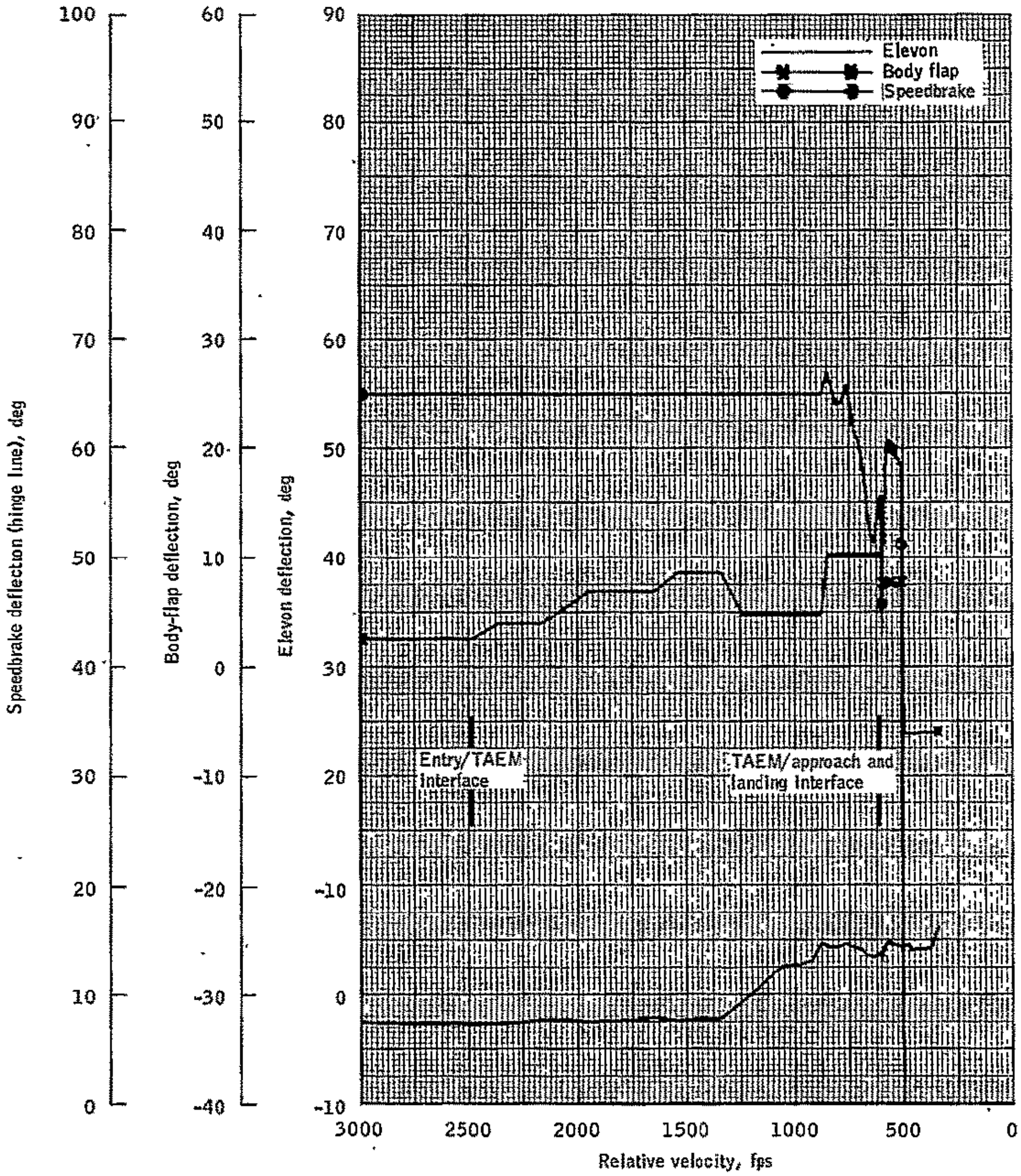

Figure 4.4-9.- Elevon, bodyflap, and speedbrake deflection versus relative velocity for orbiter OFT-1 TAEM.

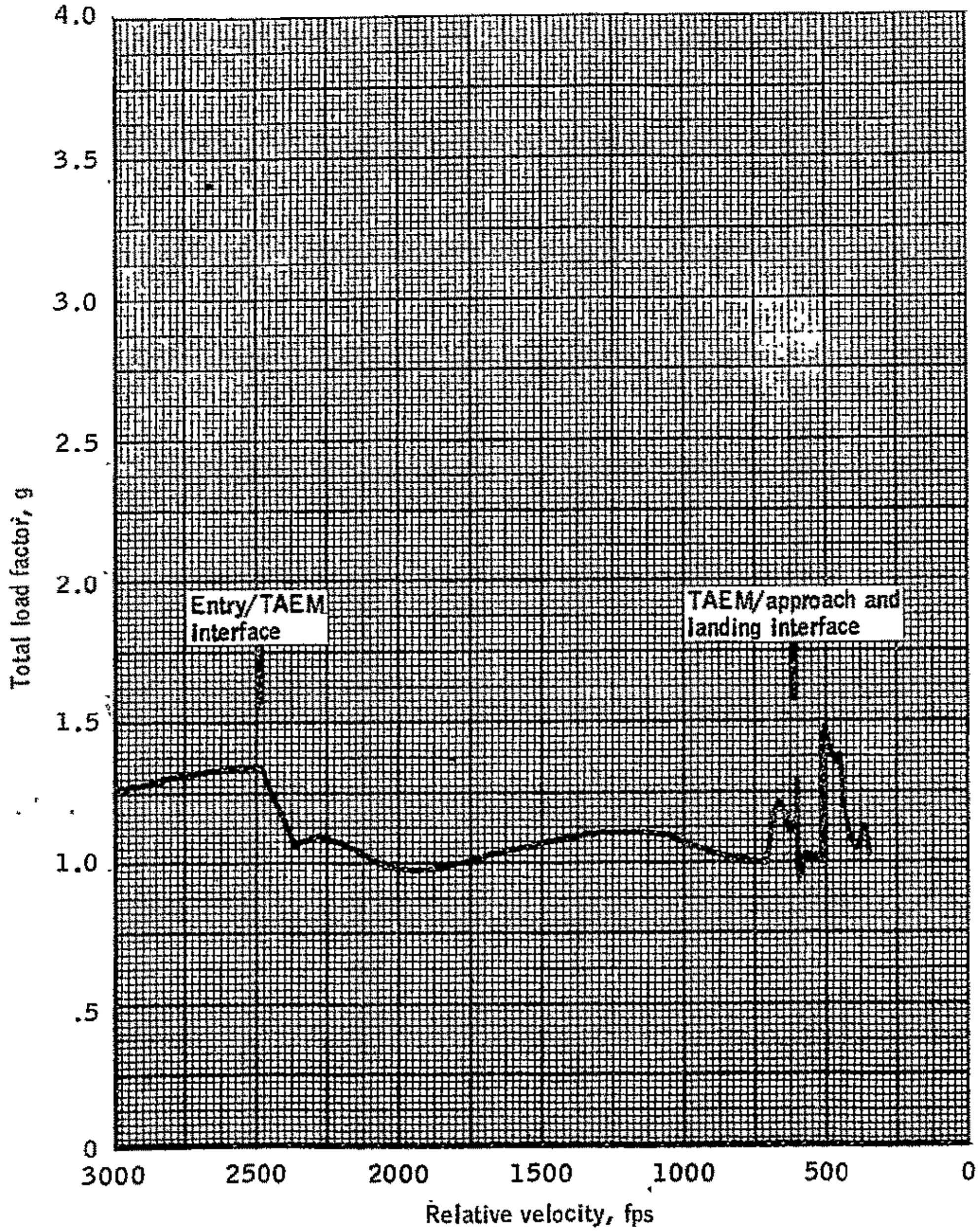

Figure 4.4-10.- Total load factor versus relative velocity for orbiter OFT-1 TAEM.

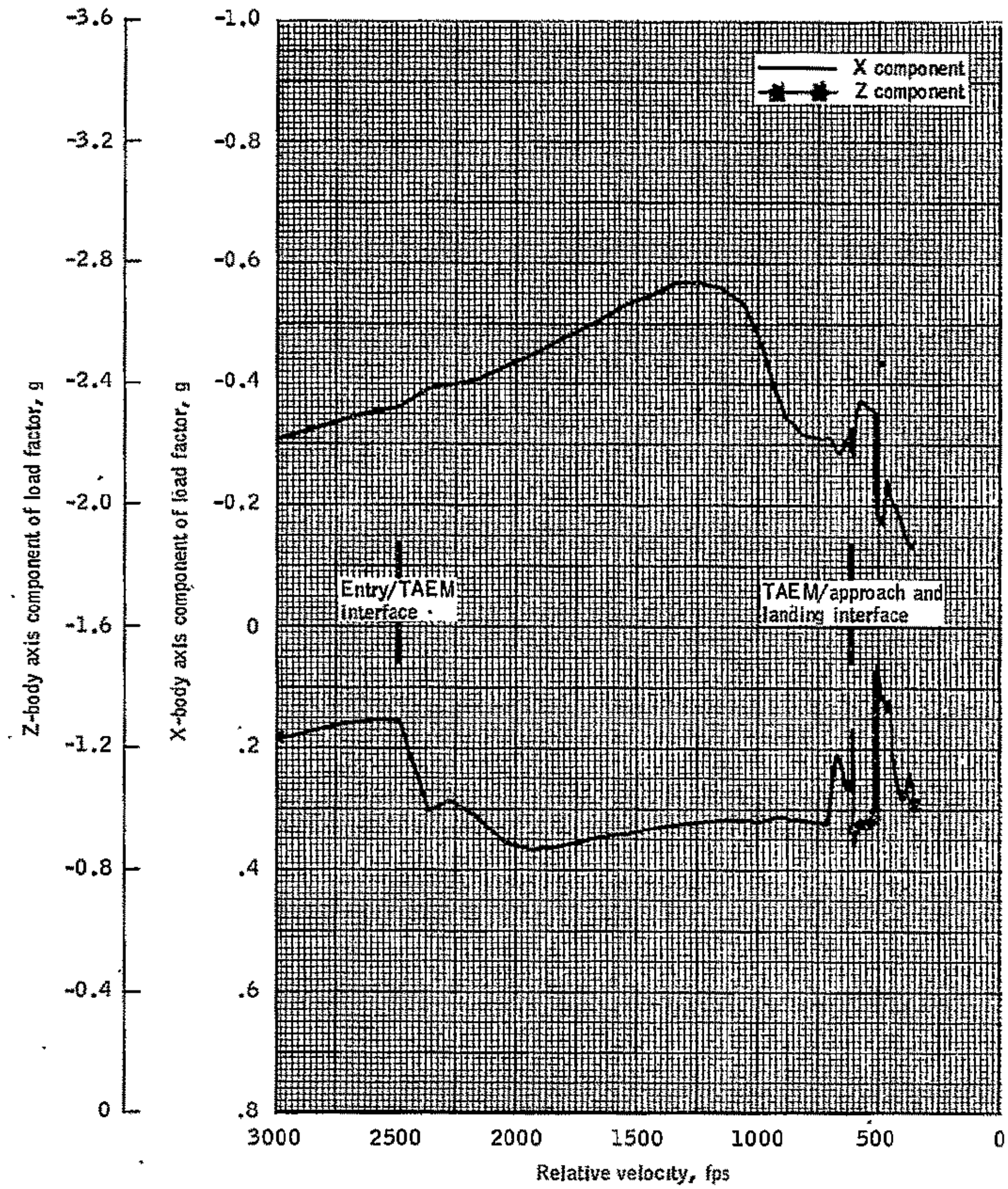

Figure 4.4-11.- X- and Z-body axis components of load factor versus relative velocity for orbiter OFT-1 TAEM.

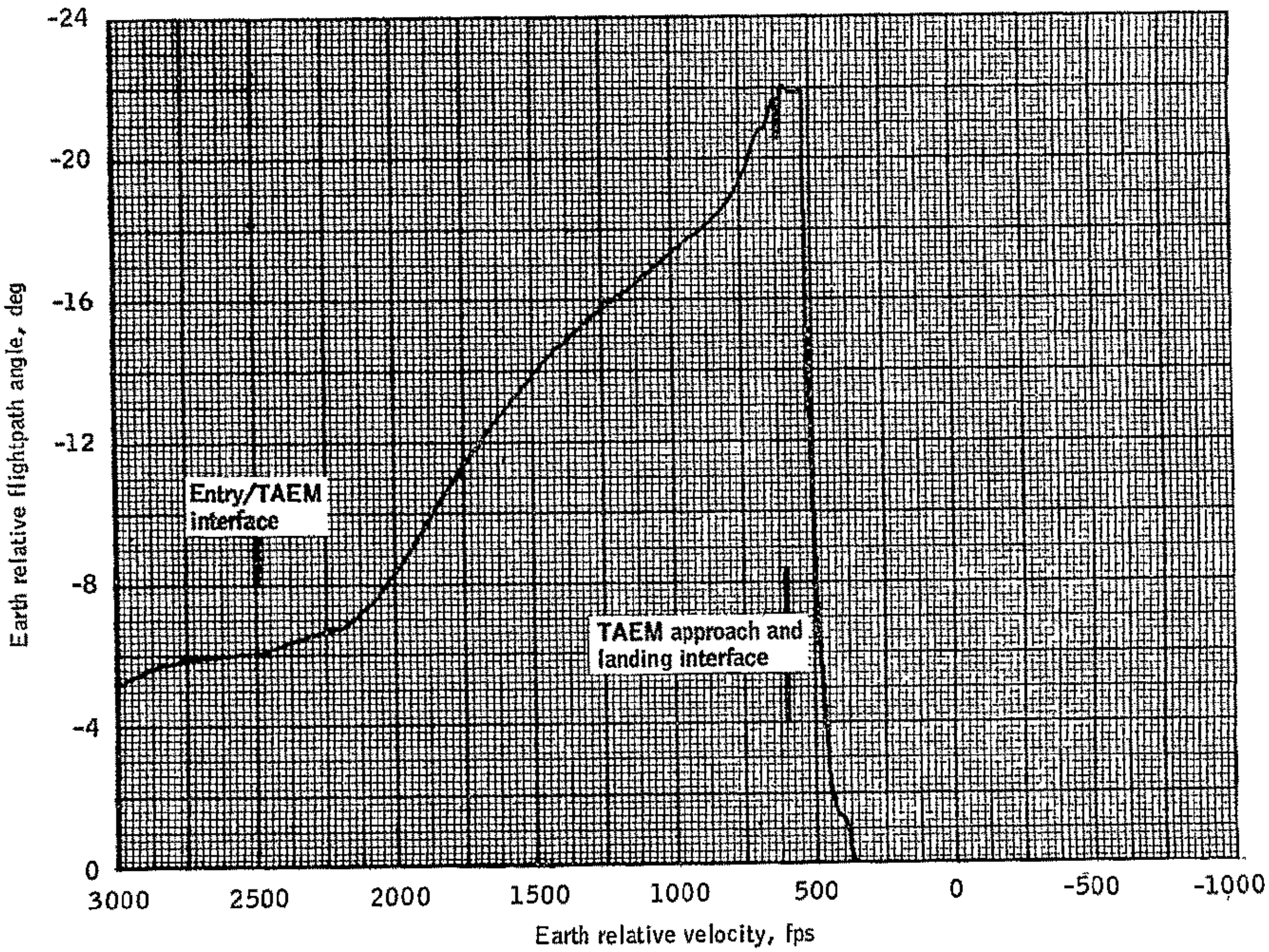

Figure 4.4-12.- Earth relative flightpath angle versus earth relative velocity OFT-1, TAEM.

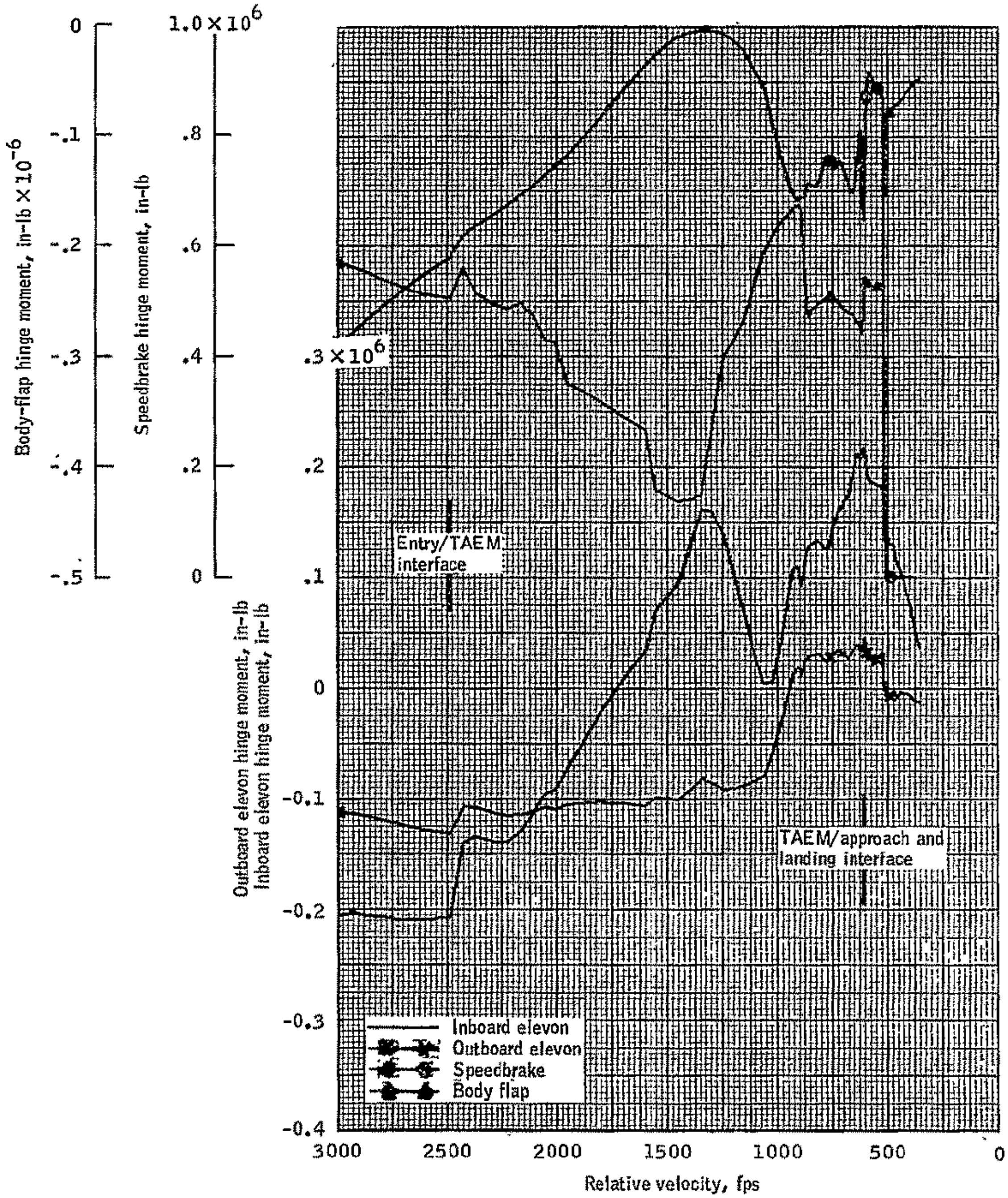

Figure 4.4-13.- Elevon, speedbrake, and body-flap hinge moments versus relative velocity for orbiter OFT-1 TAEM.

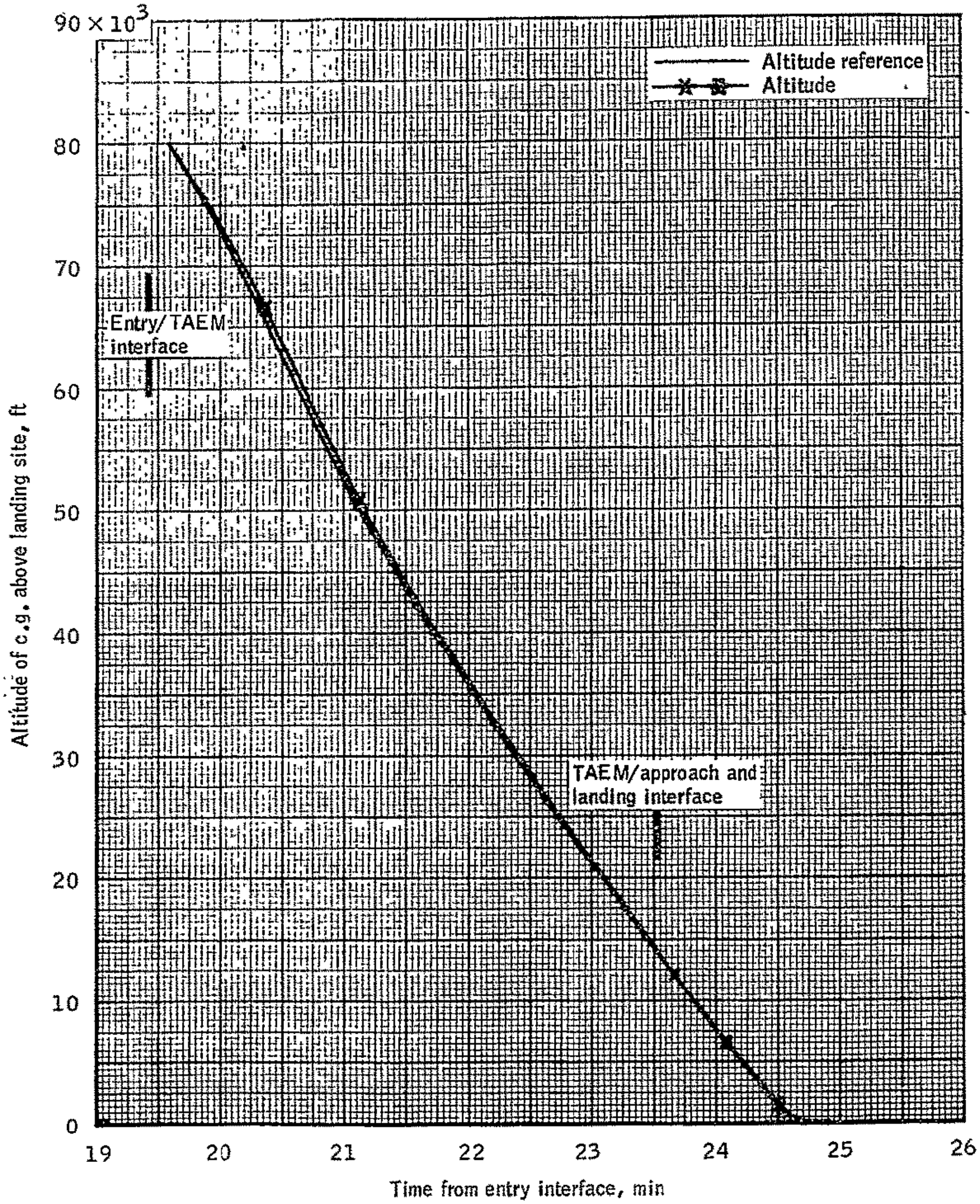

Figure 4.4-14.- Altitude and altitude reference (above landing site) versus time from entry interface for orbiter OFT-1 TAEM.

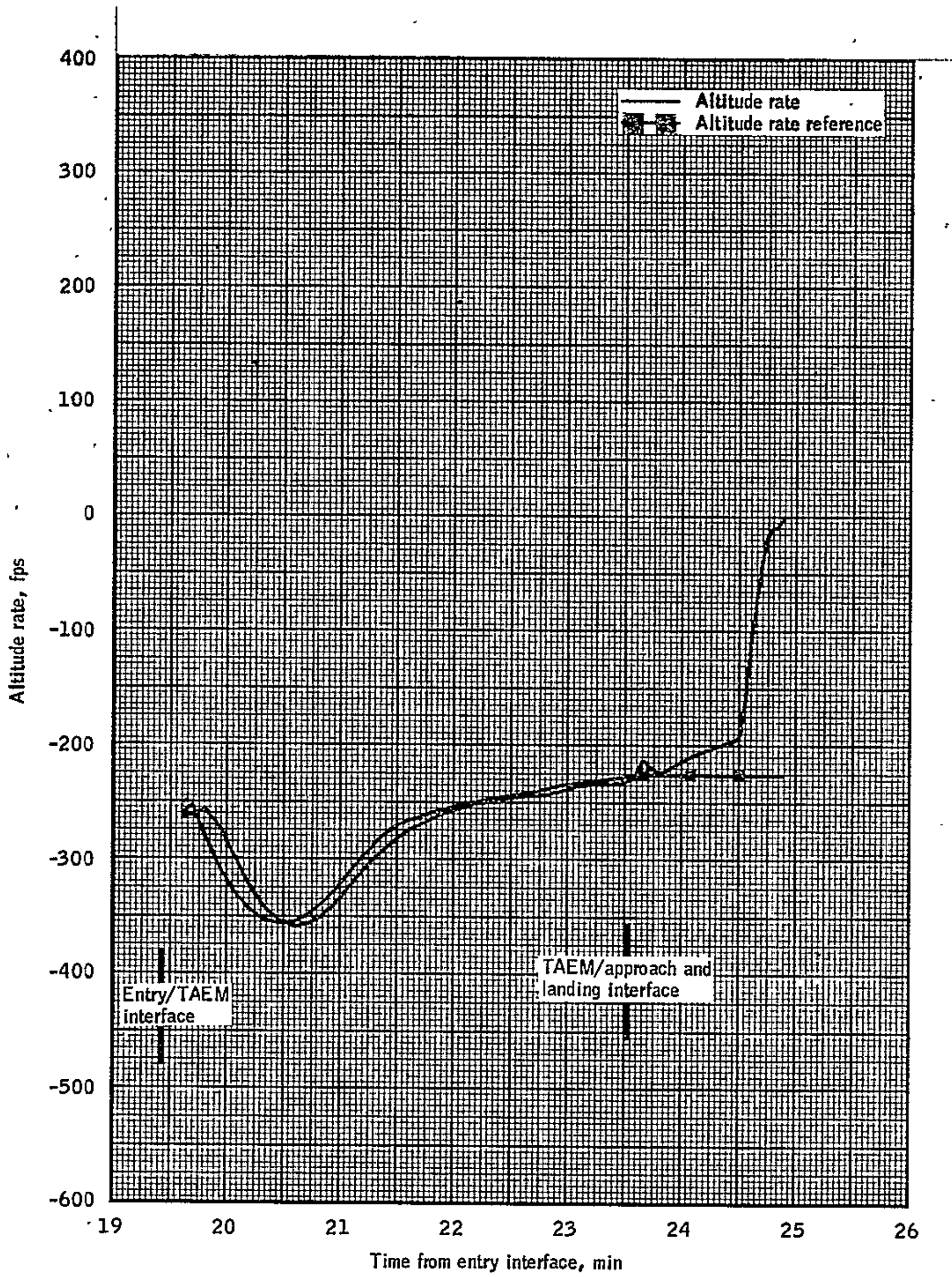

Figure 4.4-15.- Altitude rate and altitude rate reference versus time from entry interface for orbiter OFT-1 TAEM.

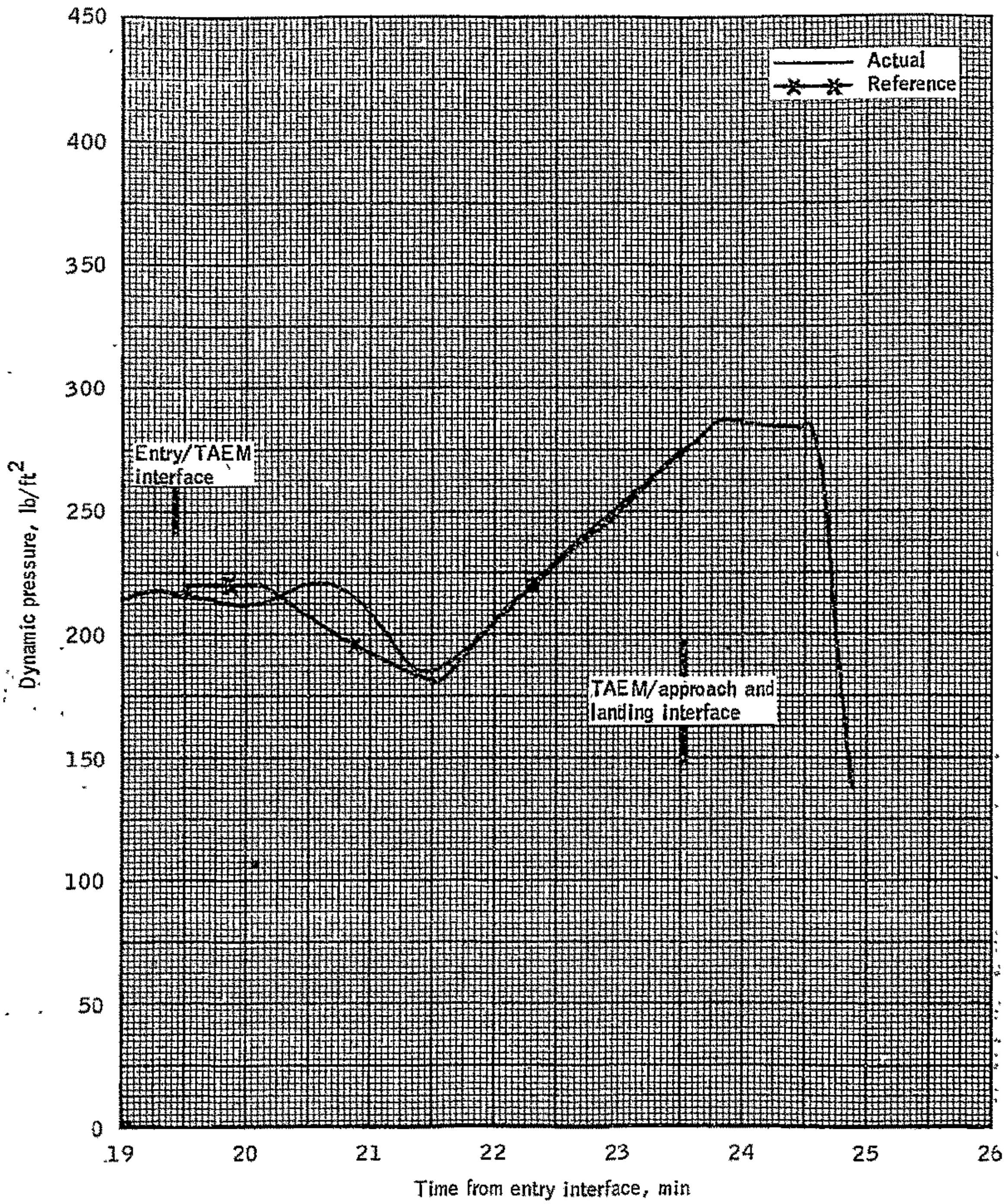

Figure 4.4-16.- Actual and reference dynamic pressure versus time from entry interface for orbiter OFT-1 TAEM.

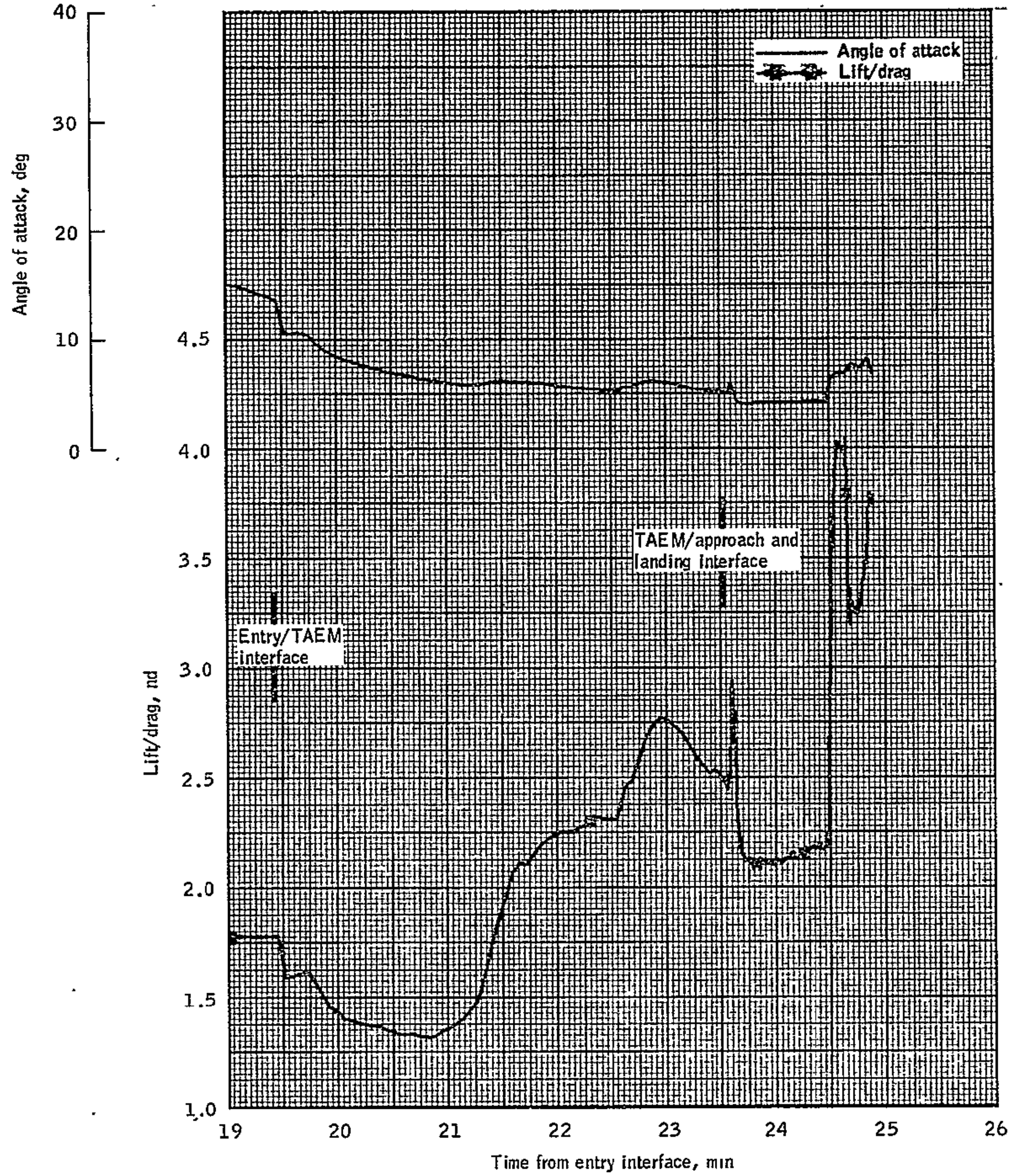

Figure 4.4-17.- Lift/drag and angle of attack versus time from entry interface for orbiter OFT-1 TAEM.

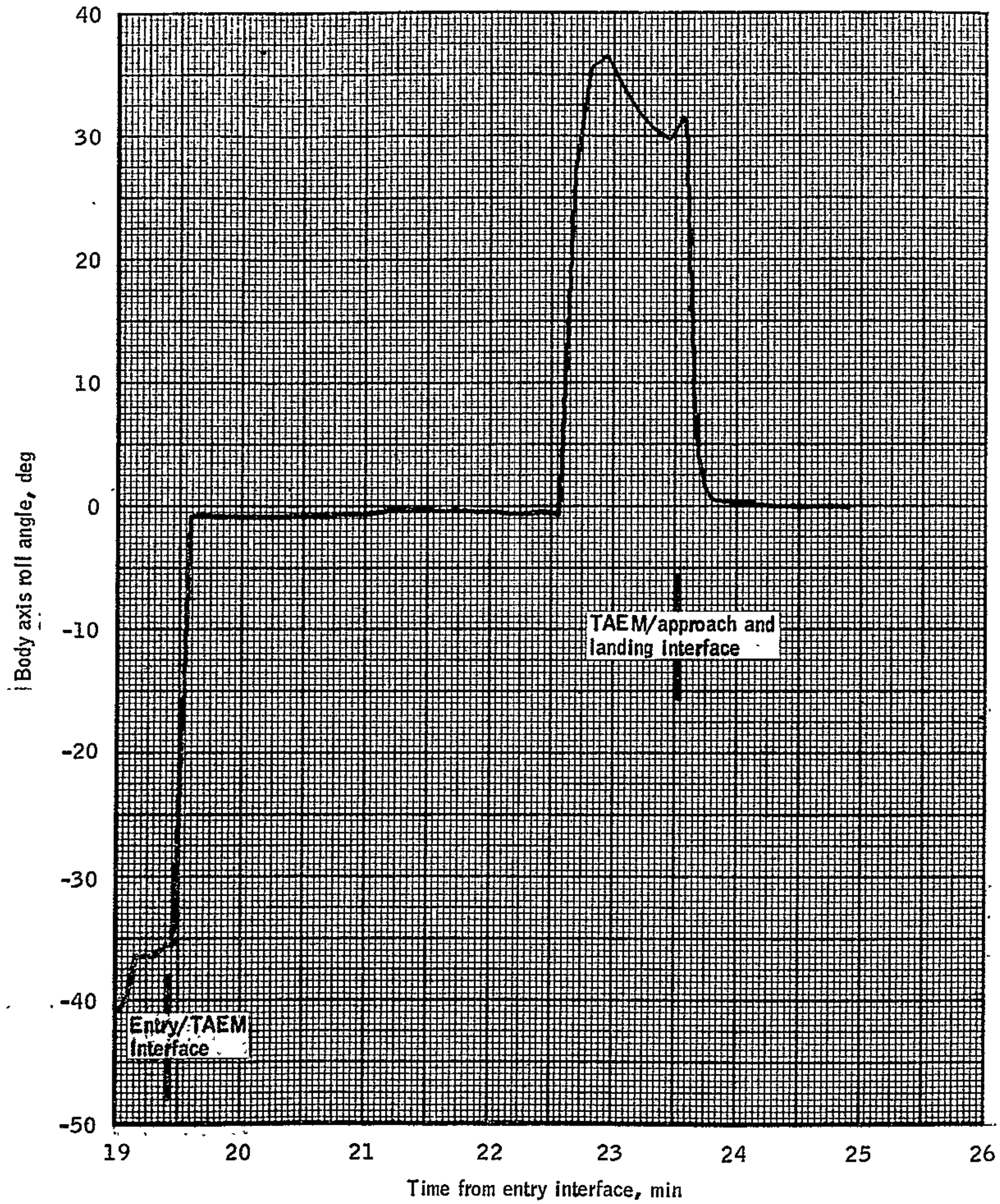

Figure 4.4-18.- Body-axis bank angle versus time from entry interface for orbiter OFT-1 TAEM.

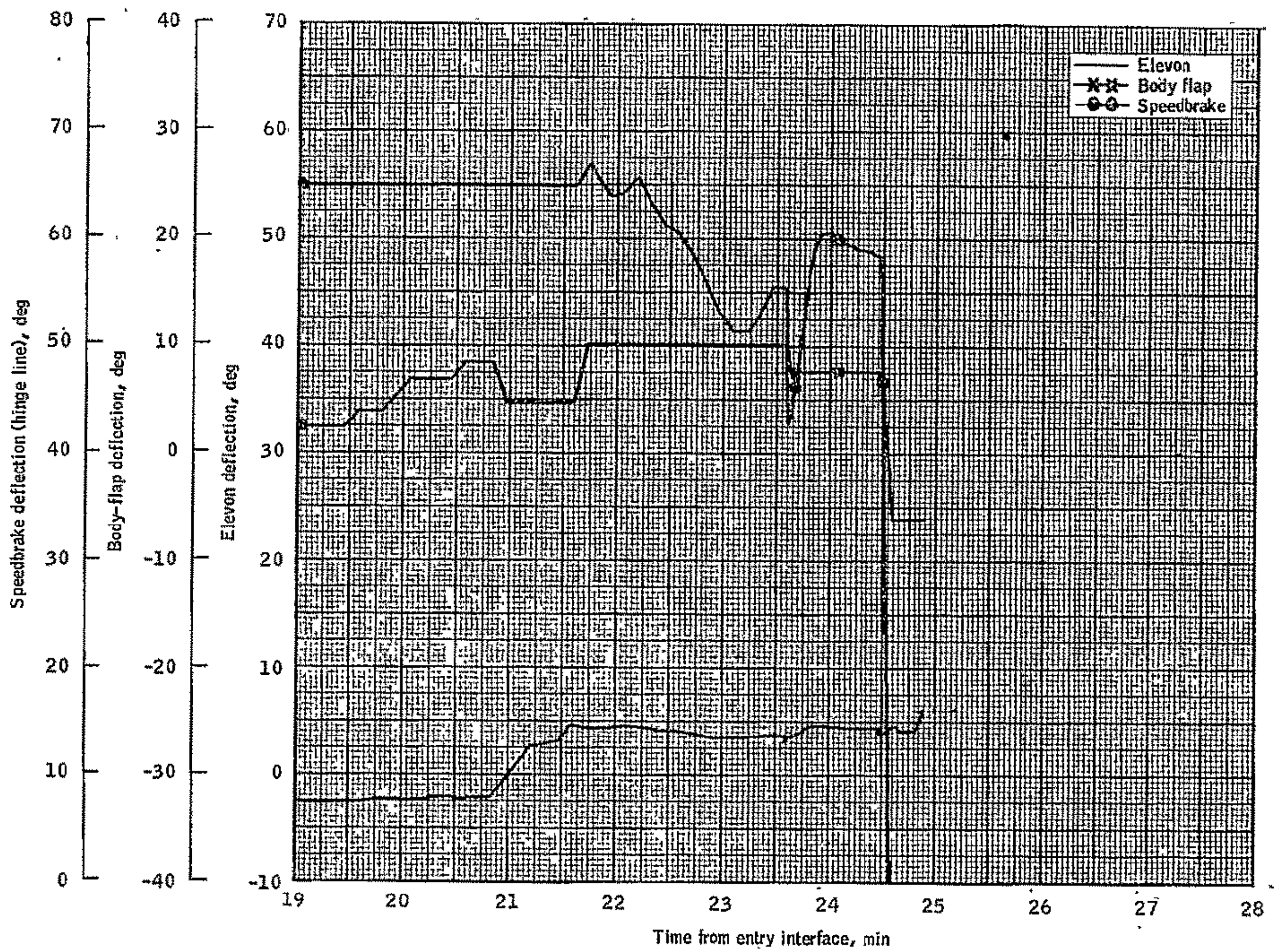

Figure 4.4-19.- Elevon, body-flap, and speedbrake deflection versus time from entry interface for orbiter OFT-1 TAEM.

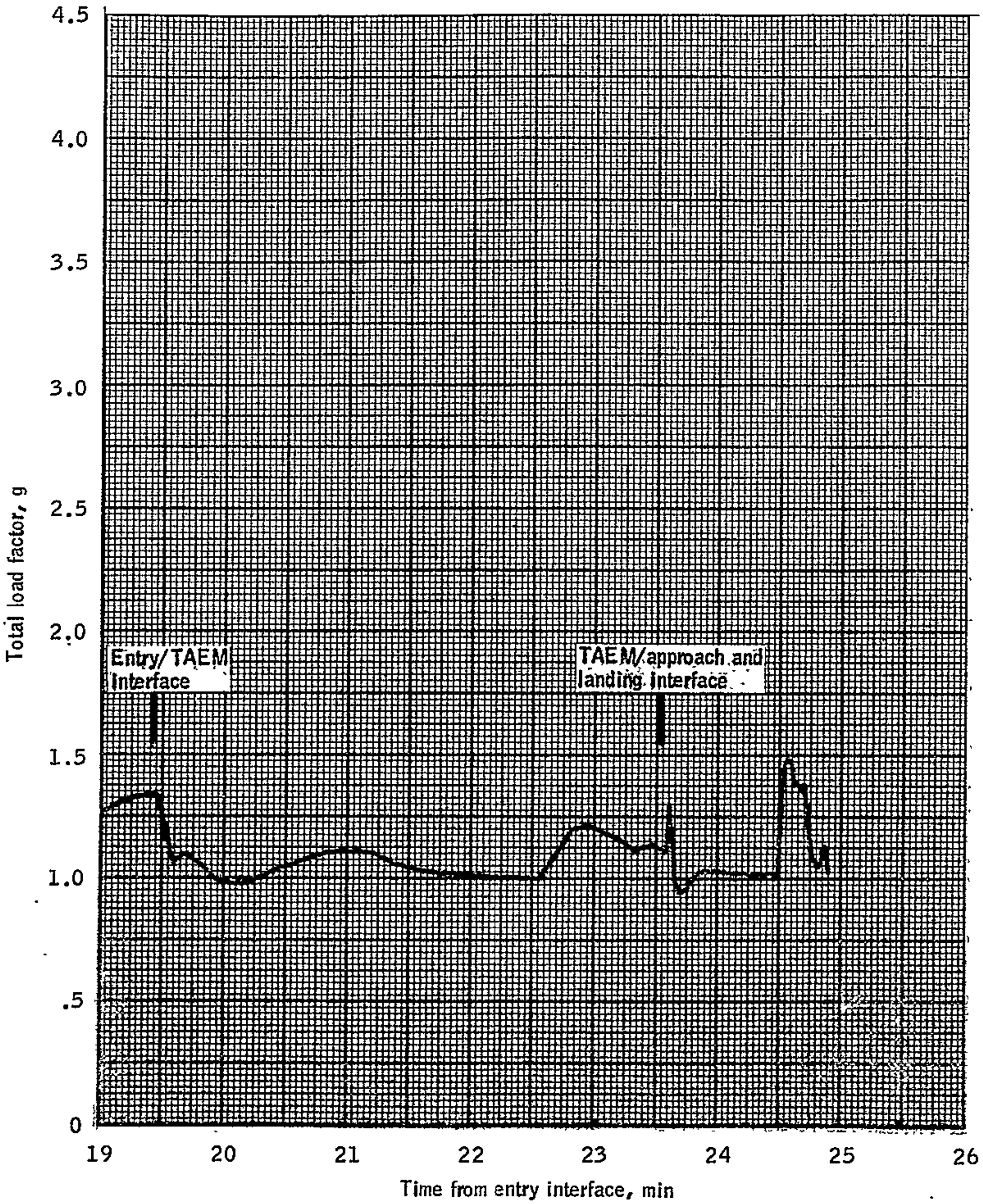

Figure 4.4-20.- Total load factor versus time from entry interface for orbiter OFT-1 TAEM.

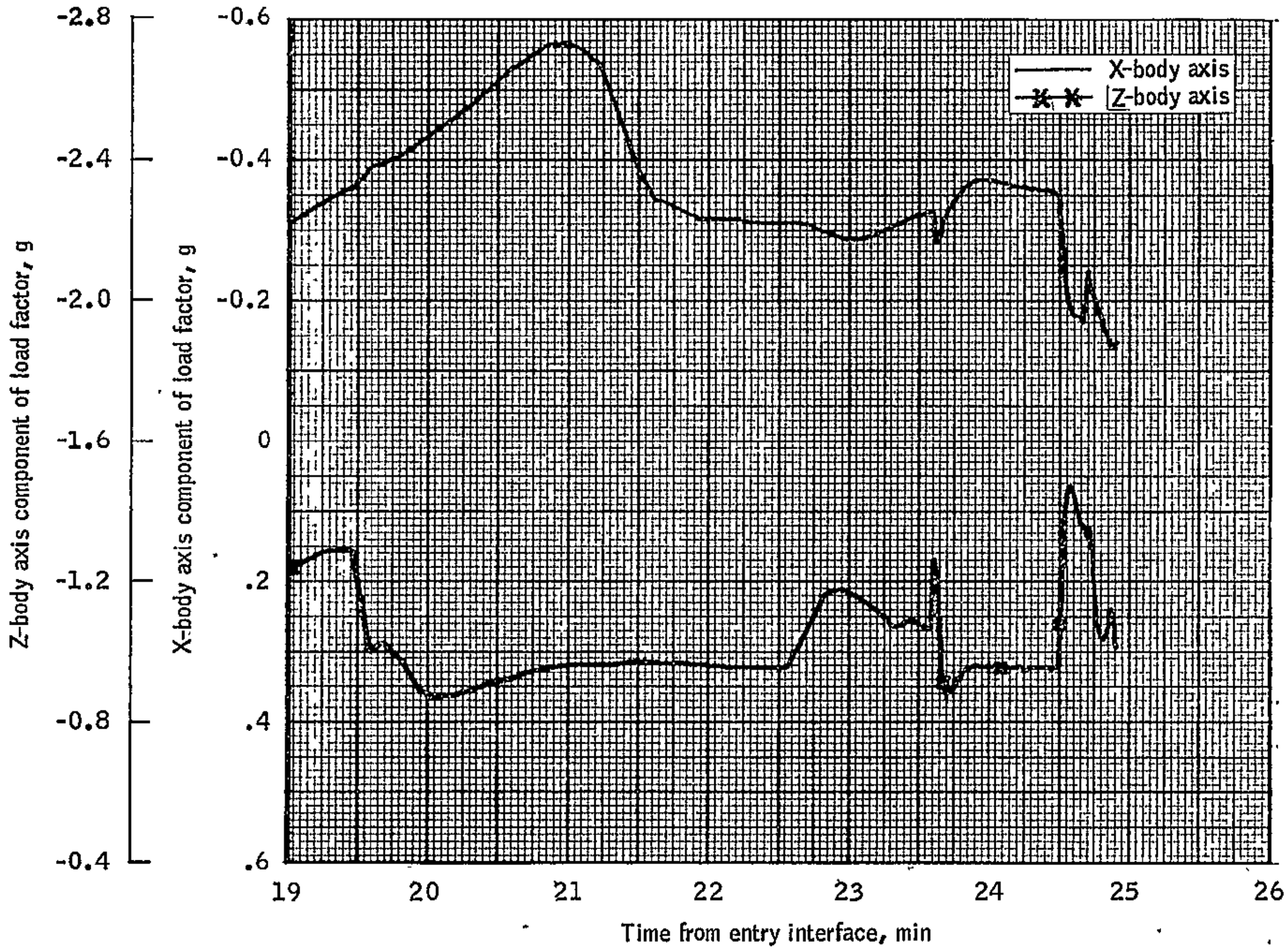

Figure 4.4-21.- X- and Z-body axis components of load factor versus time from entry interface for orbiter OFT-1 TAEM.

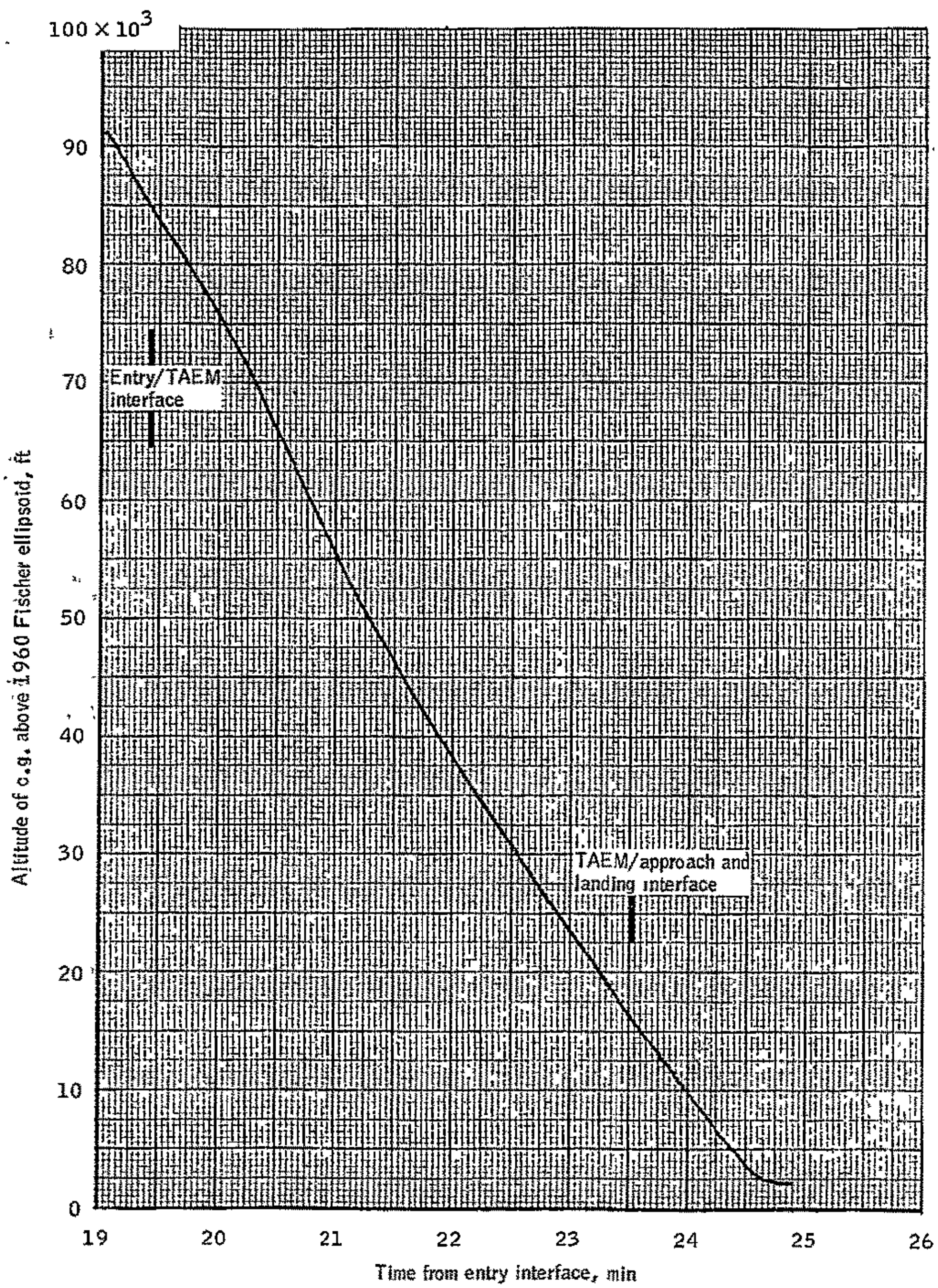

Figure 4.4-22.- Geodetic altitude versus time from entry interface for orbiter OFT-1 TAEM.

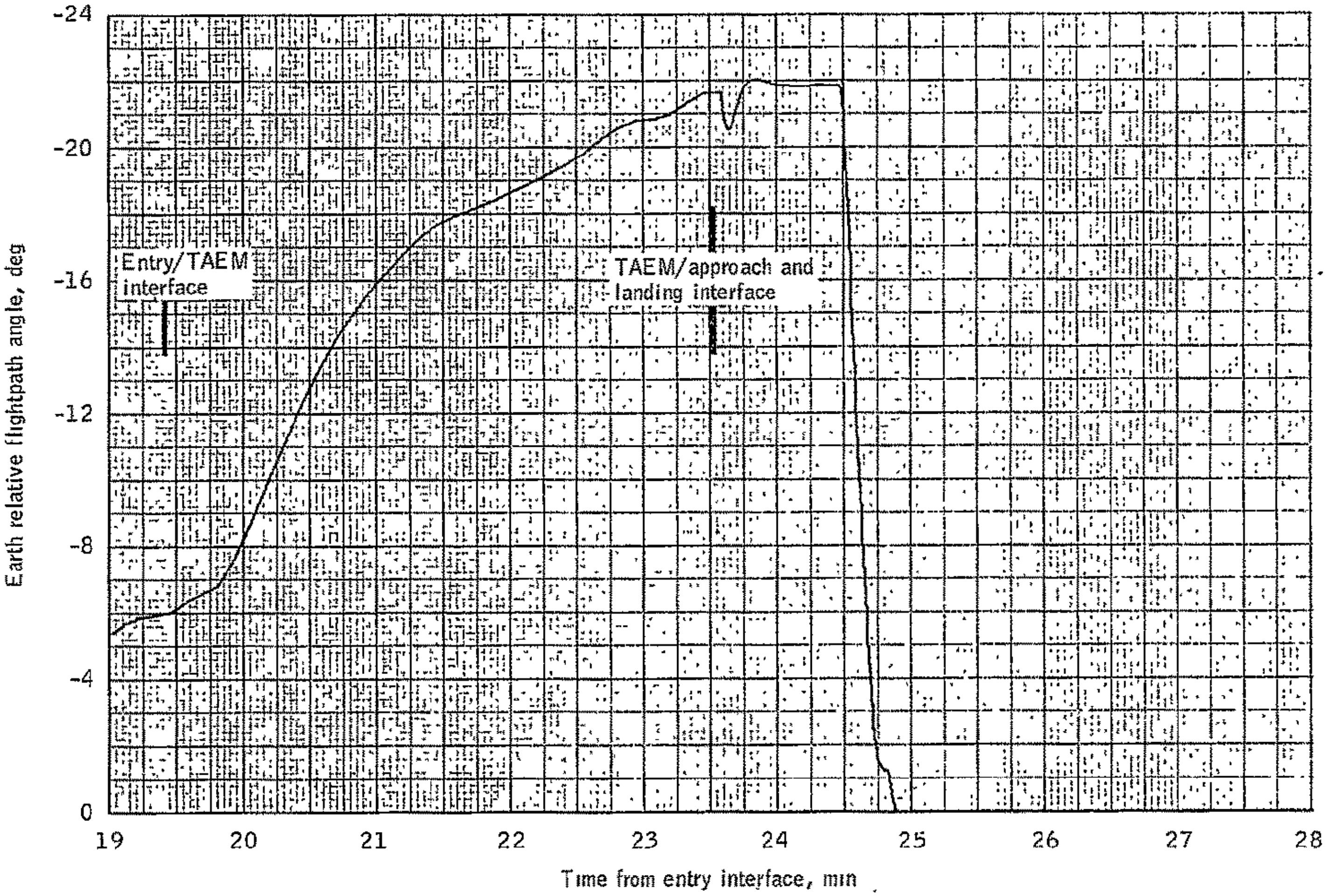

Figure 4.4-23.- Earth relative flightpath angle versus time from entry interface for OFT-1 TAEM

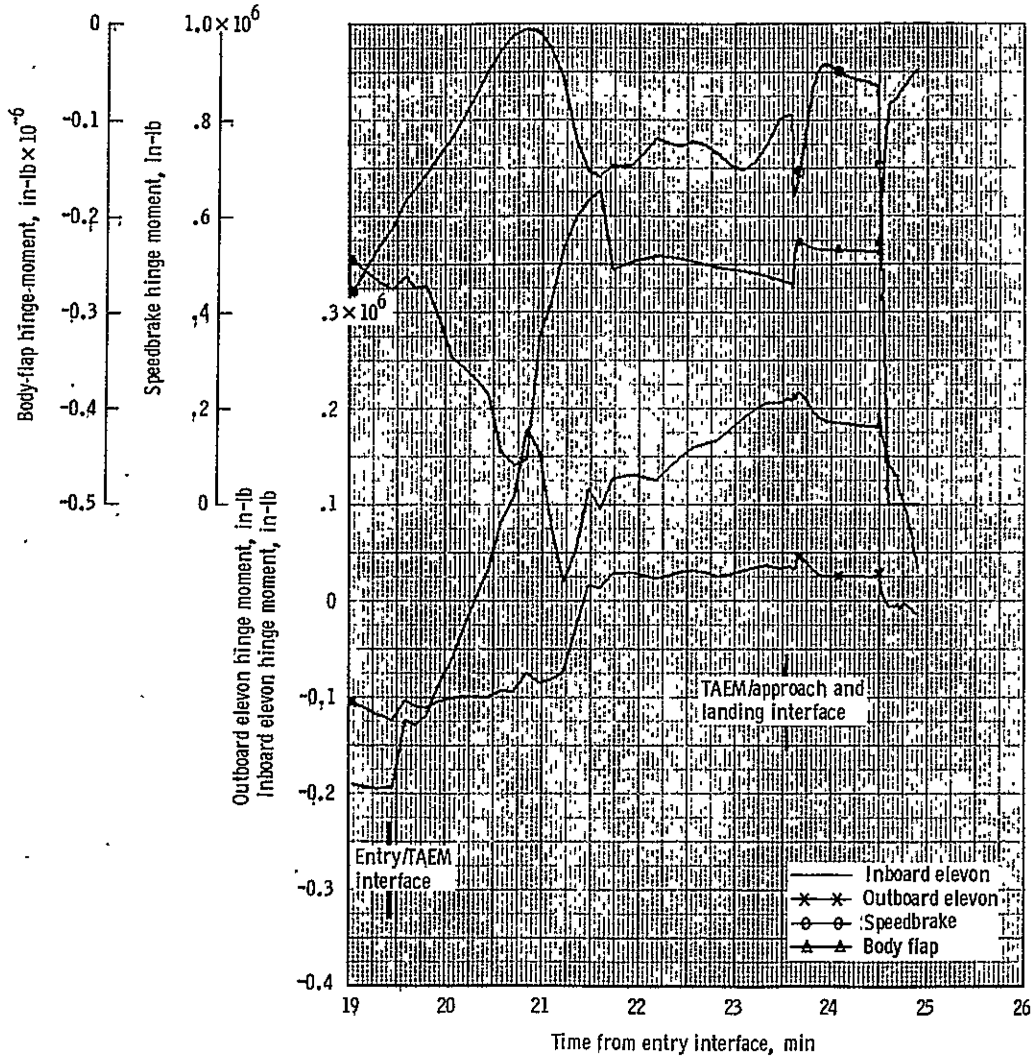

Figure 4.4-24.- Elevon, speedbrake, and body-flap hinge moments versus time from entry interface for orbiter OFT-1 TAEM.

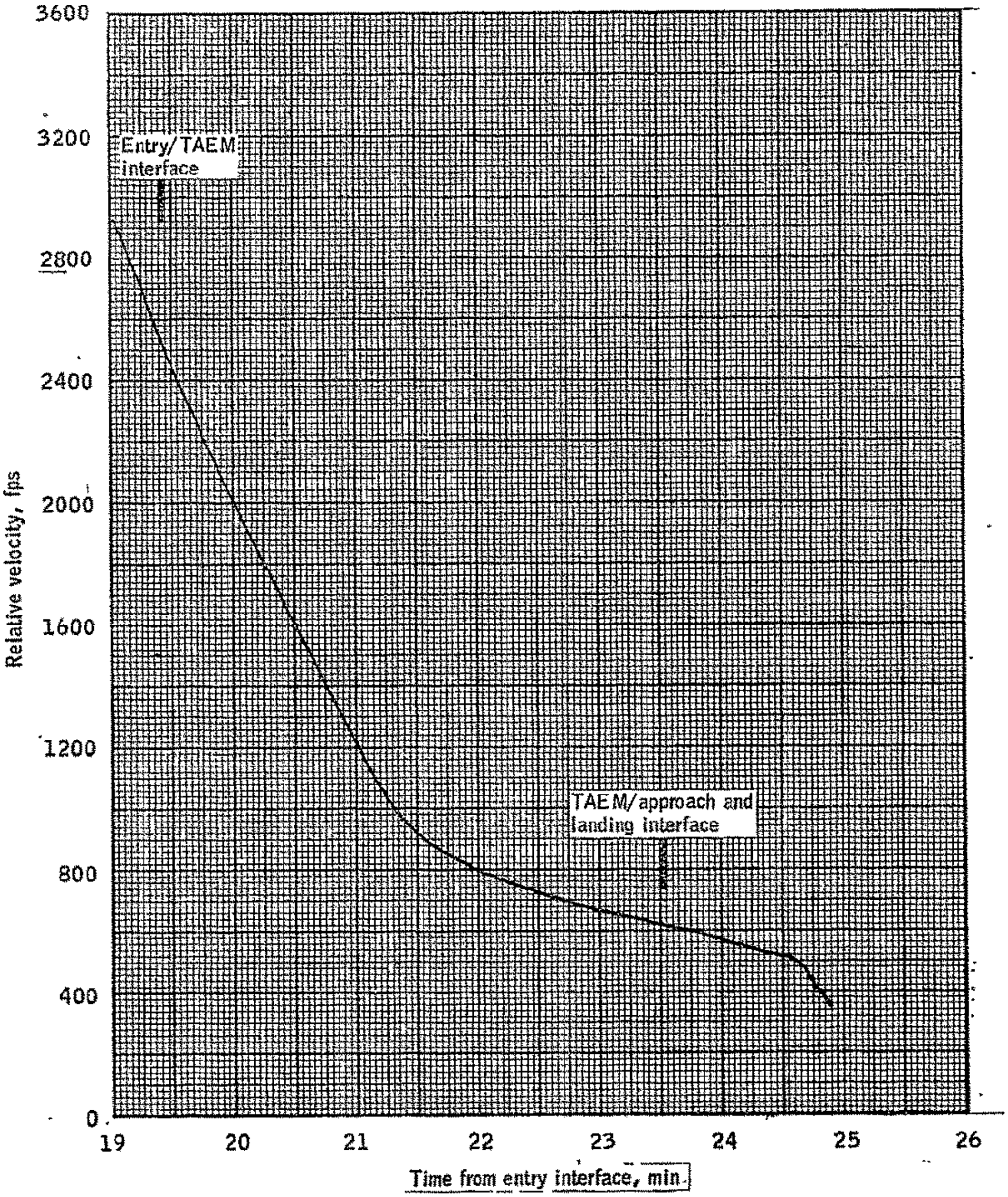

Figure 4.4-25.- Relative velocity versus time from entry interface for orbiter OFT-1 TAEM.

TABLE 4.5-I.- TAEM/APPROACH AND LANDING INTERFACE CONDITIONS

GET (rev 21), hr:min:sec	30:27:30
Time from entry interface, min:sec	23:43
Ground relative velocity, fps	612.72
Ground relative flightpath angle, deg	-21.65
Altitude above 1960 Fischer ellipsoid, ft	15 493
Altitude above runway, ft.	13 291
Geodetic latitude, deg N	35.004
Longitude, deg W	117.822
Downrange, ft	-37 387
Heading wrt runway centerline, deg	-8.7

TABLE 4.5-II.- OFT-1 FINAL APPROACH AND TOUCHDOWN CONDITIONS

Parameter	3-degree-of-freedom simulation		6-degree-of-freedom simulation		Design value
	50 percent wind	No wind	50 percent wind	No wind	
Speedbrake deflection after airspeed stabilized, deg.	45.9	57.7	46.9	59.1	55-60
Preflare velocity, KEAS	297	290	298	290	290
Initial inner glide-slope velocity, KEAS	249	252	255	257	250
Maximum normal acceleration during pre-flare maneuver, gs	1.39	1.45	1.52	1.77	1.5
Time on inner glide-slope, sec	9.8	9	12.6	11.7	10-15
Velocity at touchdown, KEAS	194	202	188	194	190
Altitude rate at touch-down, fps	-1.38	-1.4	-3.51	-3.91	-3.0
Alpha at touchdown, deg	7.85		8.24	7.86	< 11
Range from threshold at touchdown, ft.	1792	1960	2460	2655	2000-3000

TABLE 4.5-III.- DEFINITION OF APPROACH AND LANDING CONSTANTS

Symbol	Value	Units	Description
A_3	10.0	l/s	Final flare filter constant
A_INT	0.002	$deg/ft\text{-}s^{-1}$	Crossrange error integrator gain
A_SBF	0.5	1/s	Speedbrake command filter constant
A_13	1.0	1/s	Airspeed filter constant
A_14	1.0	1/s	Speed control filter constant
A_40	1.0	1/s	Open loop filter constant
DELTA_SB	2.8	deg	Speedbrake threshold angle
DEG_TO_RAD	0.0174533	deg^{-1}	Degrees to radians conversion factor
DSBC_TD(1,2)	0.0, TBD	deg	Speedbrake angle at TD
DT	0.16	s	Guidance sampling interval
G	32.174	ft/s^2	Gravitational constant
GAMMA_CAPTURE	2.0	deg	Maximum gamma error to engage steep glideslope
GAMMA_REF_1(1,2)	-22.0, TBD	deg	Steep glideslope flight path reference
GAMMA_REF_2	-1.5	deg	Shallow glideslope flightpath reference
H_CLOOP	1534.0	ft	Altitude at which start closed loop pullup
H_DECAY	70.0	ft	Exponential capture altitude reference
H_ERROR_CAPTURE	50.0	ft	Maximum altitude error to engage steep glideslope
H_ERROR_MAX	300.0	ft	Maximum altitude error

TABLE 4.5-III.- Continued

Symbol	Value	Units	Description
H_FF	60.0	ft	Altitude to start checking final flare altitude
H_FLARE	1784.0	ft	Flare altitude
H_INTMX	50.0	ft	Altitude error integrator maximum
H_K((1,1),(1,2),(2,1),(2,2))	20031.0, TBD, TBD, TBD	ft	Constant G circle center altitude
H_MIN	30.0	ft	Minimum altitude for final flare
H_NO_ACC	5.0	ft	Altitude for zero acceleration
H_SBR_TABLE(1,2,3)	4000.0, 3000.0, 1800.0	ft	Table of speedbrake retract altitudes
H_TD1_DOT	-30.0	ft/s	Touchdown altitude rate, reference 1
H_TD2_DOT	-3.0	ft/s	Closed-loop touchdown altitude rate
H_WL	5000.0	ft	Altitude reference for limiter
K_ALT_1	0.003	g/ft	Altitude error gain, SGS
K_FLR	-0.01	g-s^2/ft	Feed-forward gain, F-F
K_H	0.0036	g/ft	Altitude error gain, FSGS
K_H	0.003	g/ft	Altitude error gain, TC, SGS
K_HDOT	0.0175	g-s/ft	Vertical velocity gain, FF
K_HDOT	0.015	g-s/ft	Vertical velocity gain, FSGS
K_HDOT_SGS	0.015	g-s/ft	Vertical velocity gain, SGS
K_HDOT_TC	0.015	g-s/ft	Vertical velocity gain, TC

TABLE 4.5-III.- Continued

Symbol	Value	Units	Description
K_HINT1	1.5 x 10^{-4}	g/ft-s	Integrator gain, SGS
K_IFLR	0.0	g/ft	Integrator gain, FF
K_INT	0.05	s	Integral gain, FSGS
K_R1	0.5	s	Yaw rate command gain, flat turn
K_R2	1.0	s	Yaw rate command gain, touchdown
K_SB	2.0	deg/ft-s^{-1}	Speedbrake gain
K_SBI	0.1	1/ft	Speedbrake integral gain
K_Y1	0.05	deg/ft	Crossrange error integrator gain
K_YDOT	12.0	s	Crossrange rate gain
N_FADER	0	nd	Roll fader constant
NSB	3	nd	Maximum value of ISB
NZ_MAX	1.0	g	Max-G limit for NZC
PHI_M1	30.0	deg	Maximum roll attitude command
PHI_M2	15.0	deg	Maximum roll attitude command
PHI_M3	90.0	deg	Maximum roll attitude command
P_MODE_INITIAL	1	nd	Initial pitch subphase indicator
PSI_CAP	2.0	deg	Maximum heading error (RC)
R((1,1),(1,2) (2,1),(2,2))	19 950.0, TBD, TBD, TBD	ft	Constant-G circle radius
RAD_TO_DEG	57.29578	deg/rad	Radian-to-degree conversion

TABLE 4.5-III.- Continued

Symbol	Value	Units	Description
SB_MAX	98.6	deg	Maximum speedbrake angle
SB_RATE	10.0	deg/s	Speedbrake retract rate
SB_REF	55.0	deg	Speedbrake reference
SBF_TABLE(1, 2,3)	40.0, 55.0, 98.6	deg	Table of reference speed brake positions for retraction altitude
SIGMA(1,2)	837.1, TBD	ft	Exponential distance
T_Q	4.0	s	Minimum time with bounded errors for transition to steep glideslope phase
TAU_GAMMA	2.0	s	Time constant, FSGS
TAU_TD	4.88	s	Time constant, FSGS
TAU_TD1	5.0	s	Time constant, FF
TAU_TD2	4.88	s	Time constant, FF
TQ_LAT	4.0	s	Minimum time with bounded error to engage lateral track
V_LIMIT	10.0	ft/s	Maximum error velocity limit
V_REF(1,2)	489.0, TBD	ft/s	Reference airspeed
WT_GS1	250 000.0	lbm	Weight for glideslope selection
X_AIM_PT	1500.0	ft	Aim point X-distance
X_EXP((1,1), (1,2),(2,1), (2,2))	-3552.0, TBD,TBD, TBD	ft	Exponential capture X-distance

TABLE 4.5-III.- Concluded

Symbol	Value	Units	Description
X_K((1,1),(1,2),(2,1)(2,2)	-1339.0, TBD,TBD, TBD	ft	Constant-G circle center range
X_ZERO(1,2)	5000.0, TBD	ft	Steep glideslope intercept
Y_INLIM	50.0	ft	Crossrange error integration limit
Y_CAP	50.0	ft	Lateral capture distance (RC)
Y_LIMIT	1000.0	ft	Crossrange error limit

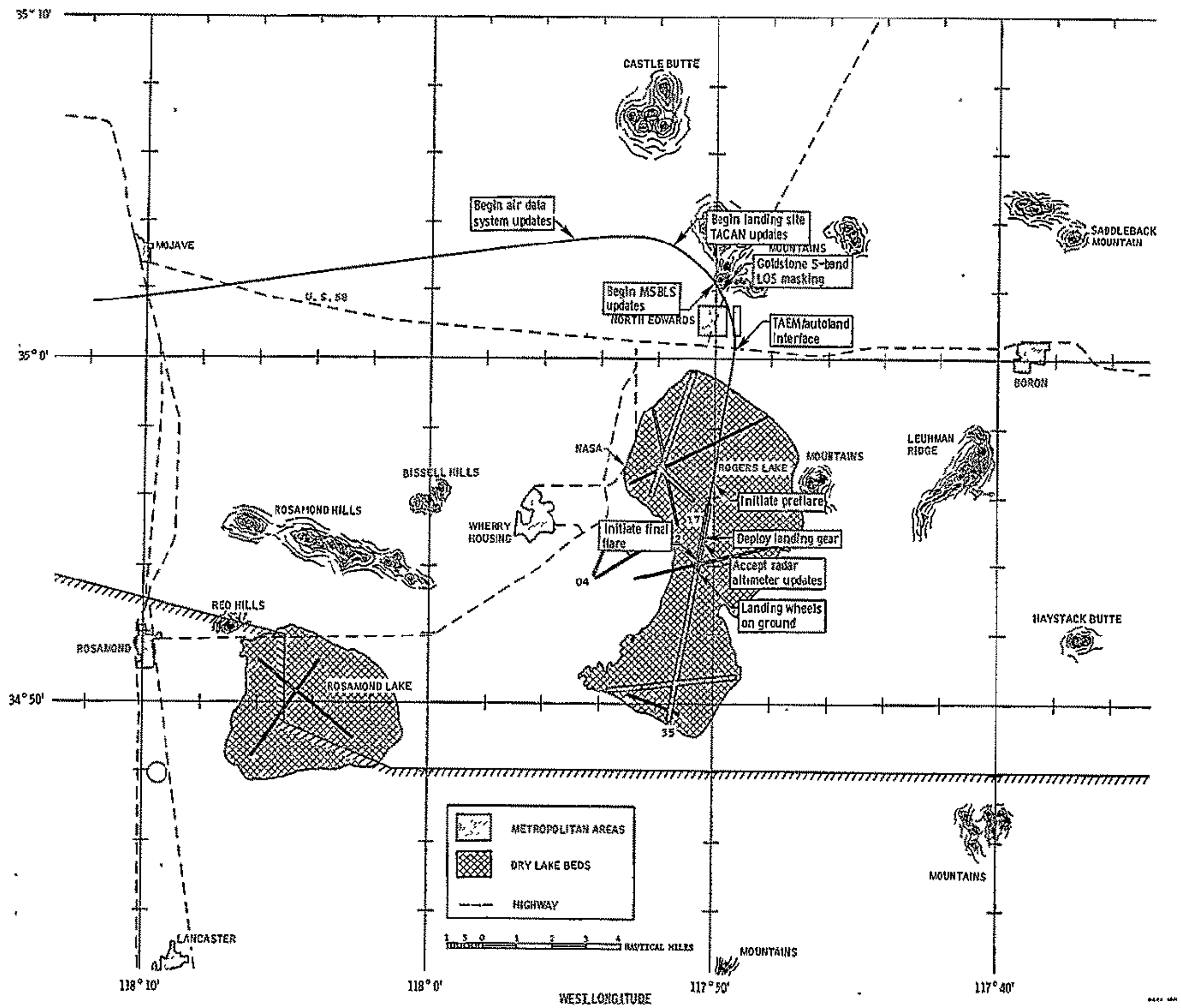

Figure 4.5-1.- Approach and landing groundtrack.

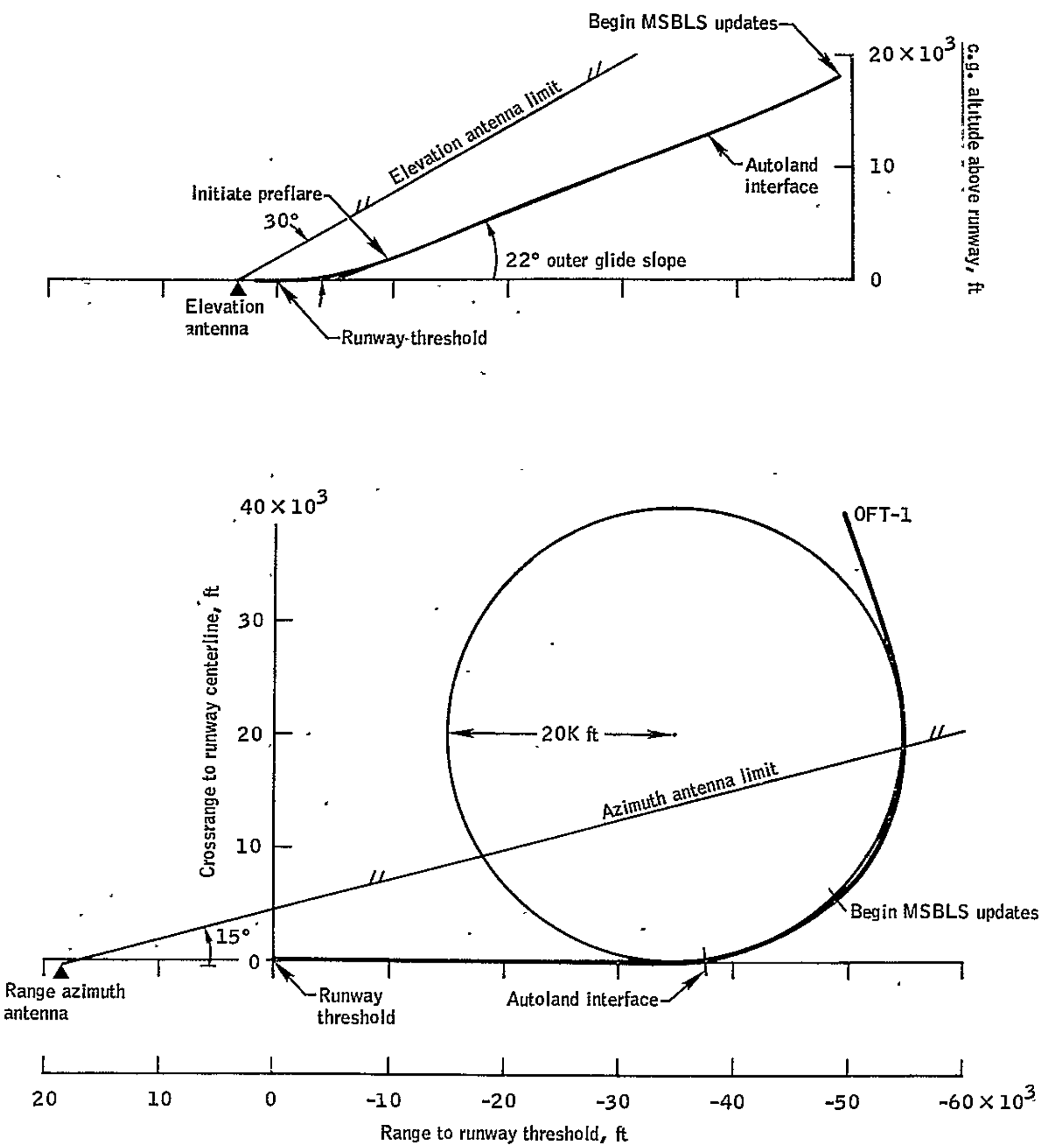

Figure 4.5-2.- Approach and landing geometry.

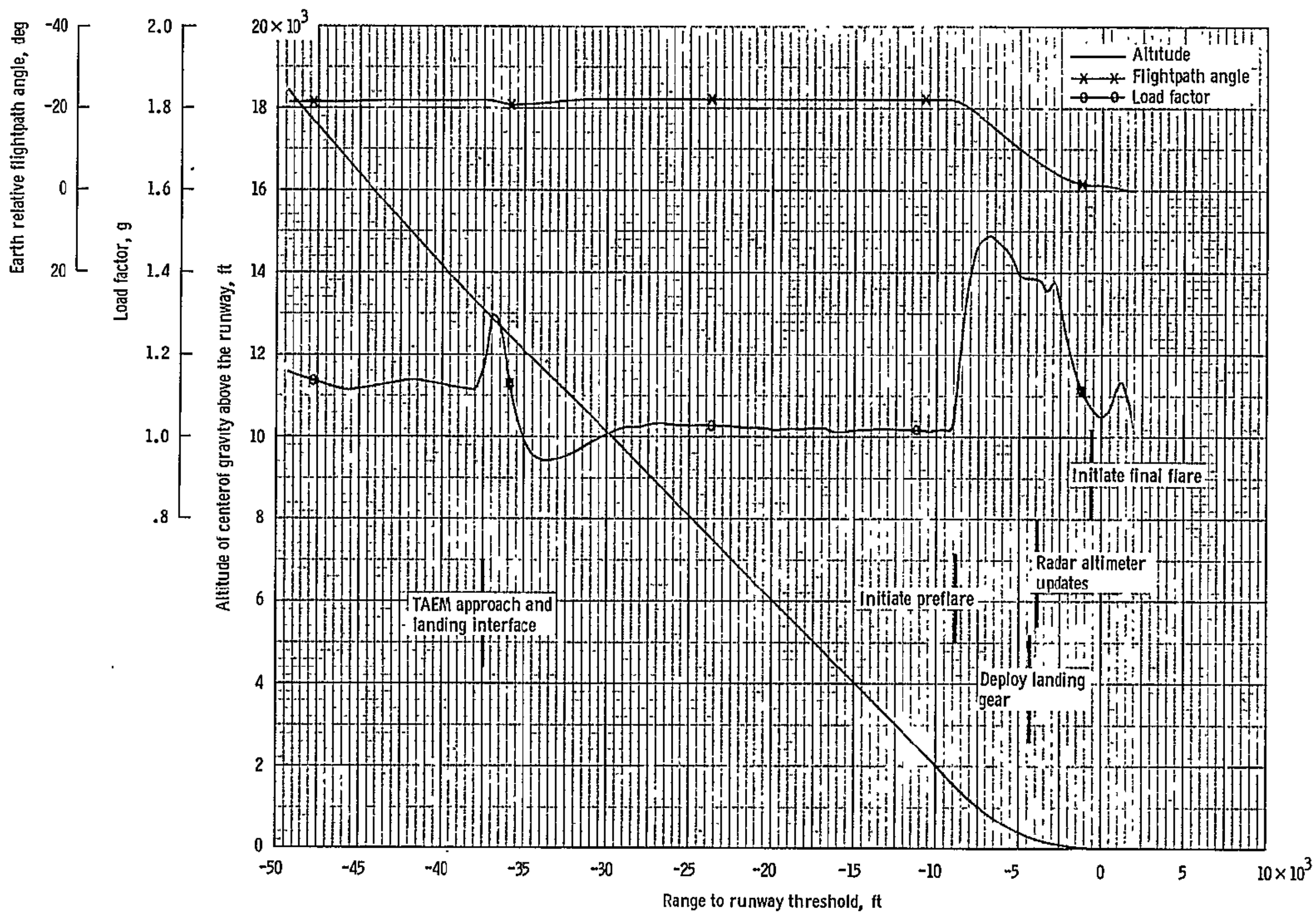

Figure 4.5-3.- Altitude of center of gravity above the runway, earth relative flightpath angle, and load factor versus range to runway threshold for OFT-1 approach and landing.

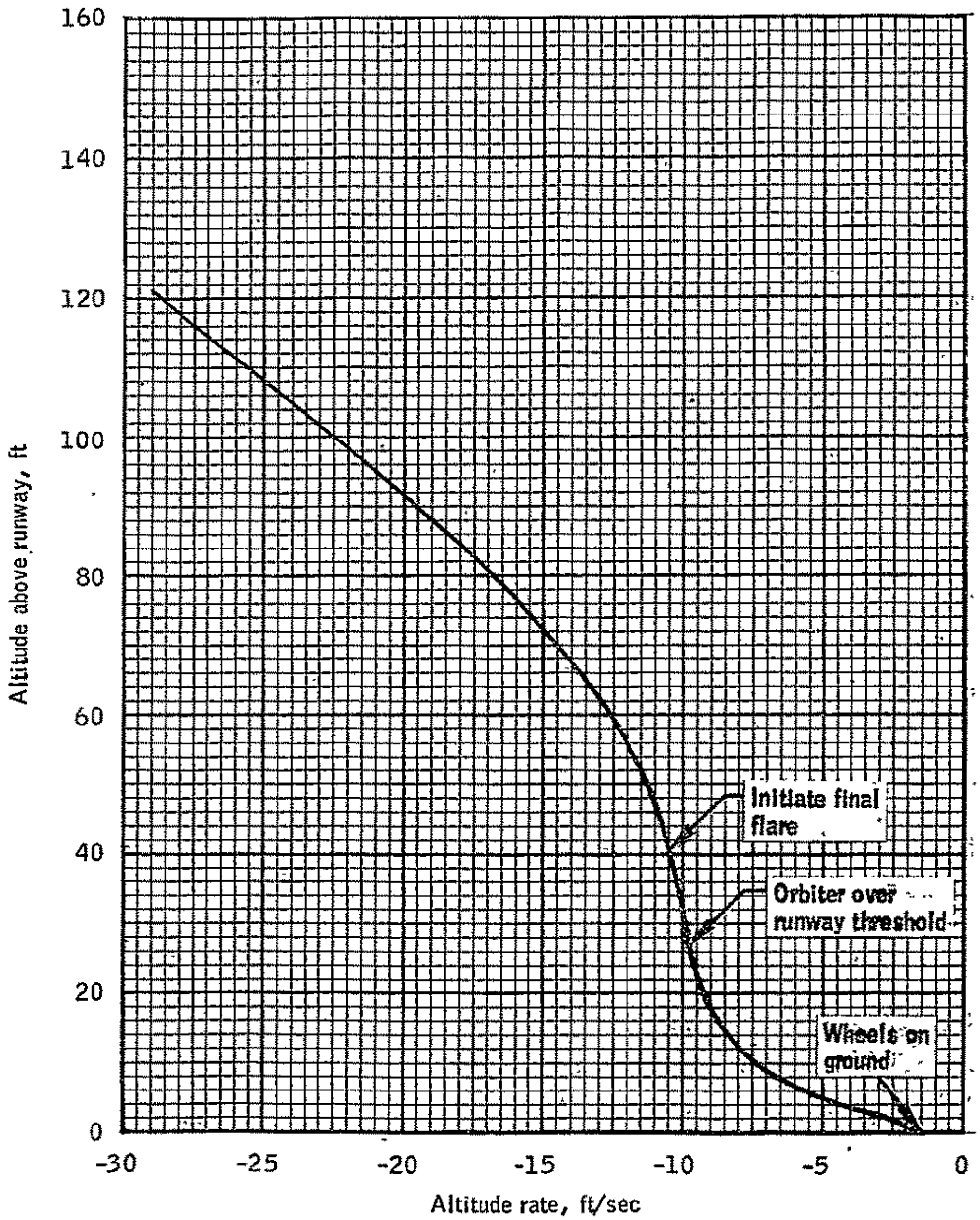

Figure 4.5-4.- Altitude above runway versus altitude rate for orbiter OFT-1 approach and landing.

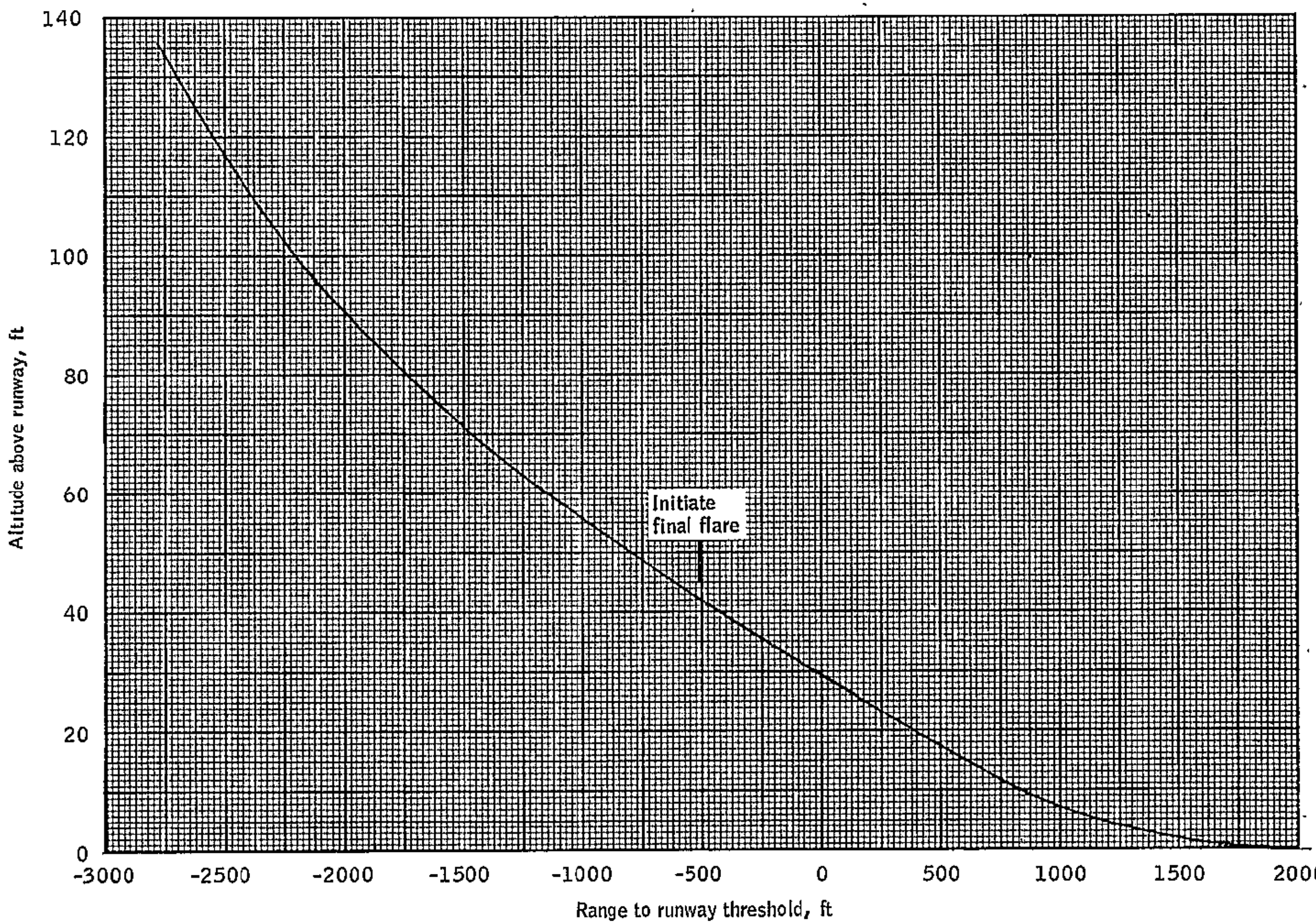

Figure 4.5-5.- Altitude above runway versus range to runway threshold OFT-1 approach and landing.

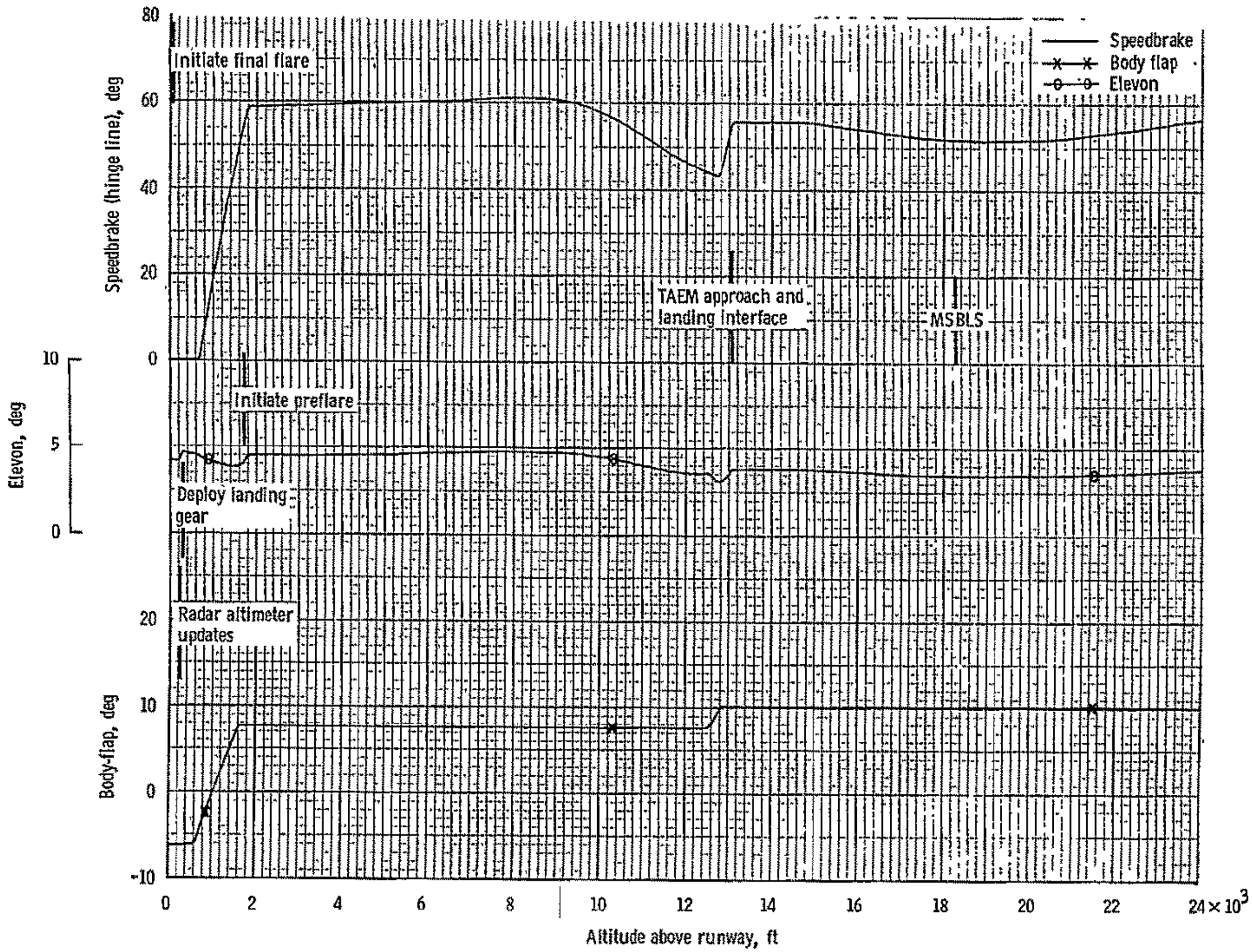

Figure 4.5-6.- Speedbrake, body-flap, elevon versus altitude above the runway for orbiter OFT-1 approach and landing.

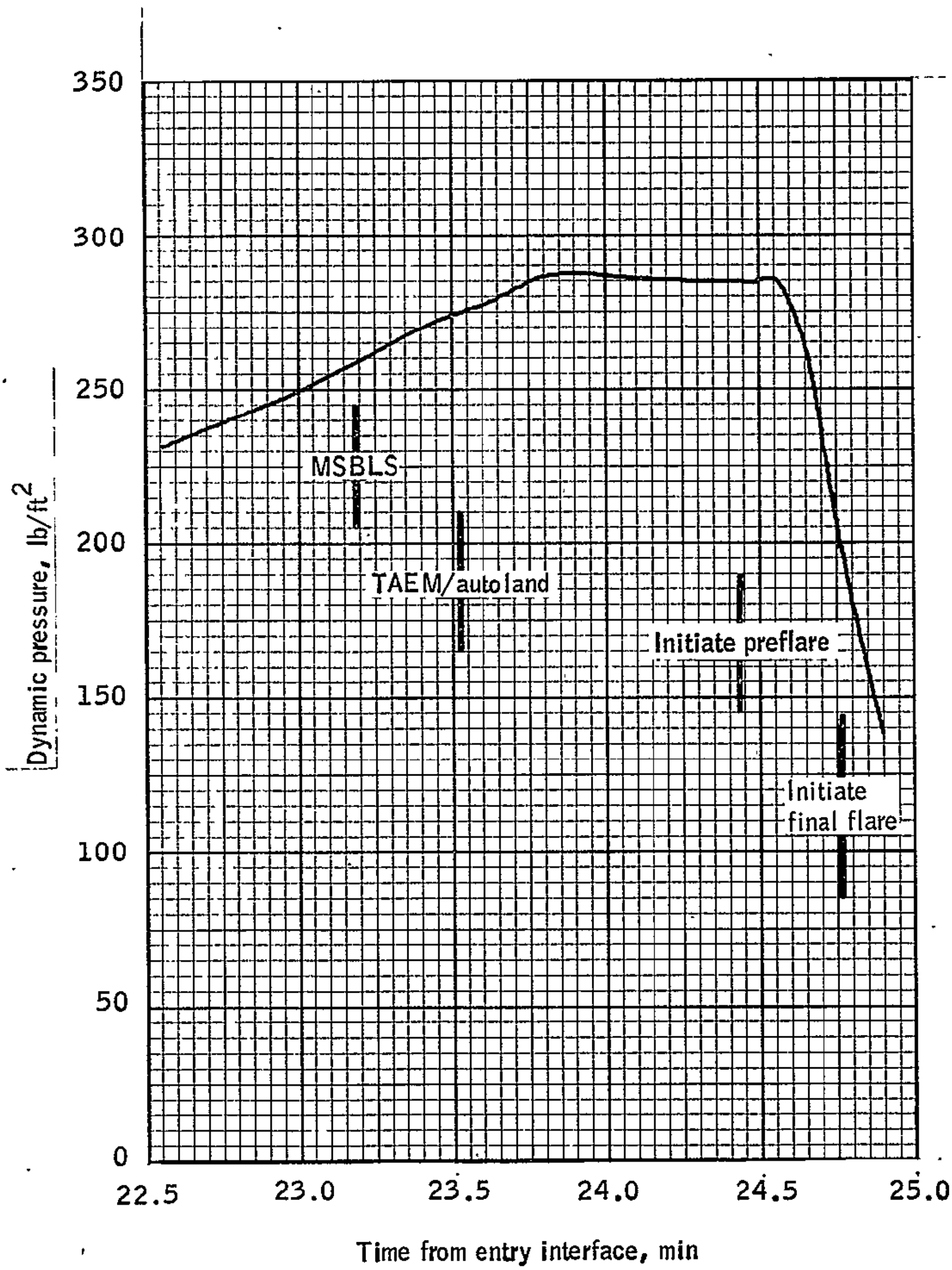

Figure 4.5-7.- Dynamic pressure versus time from entry interface for orbiter OFT-1 approach and landing.

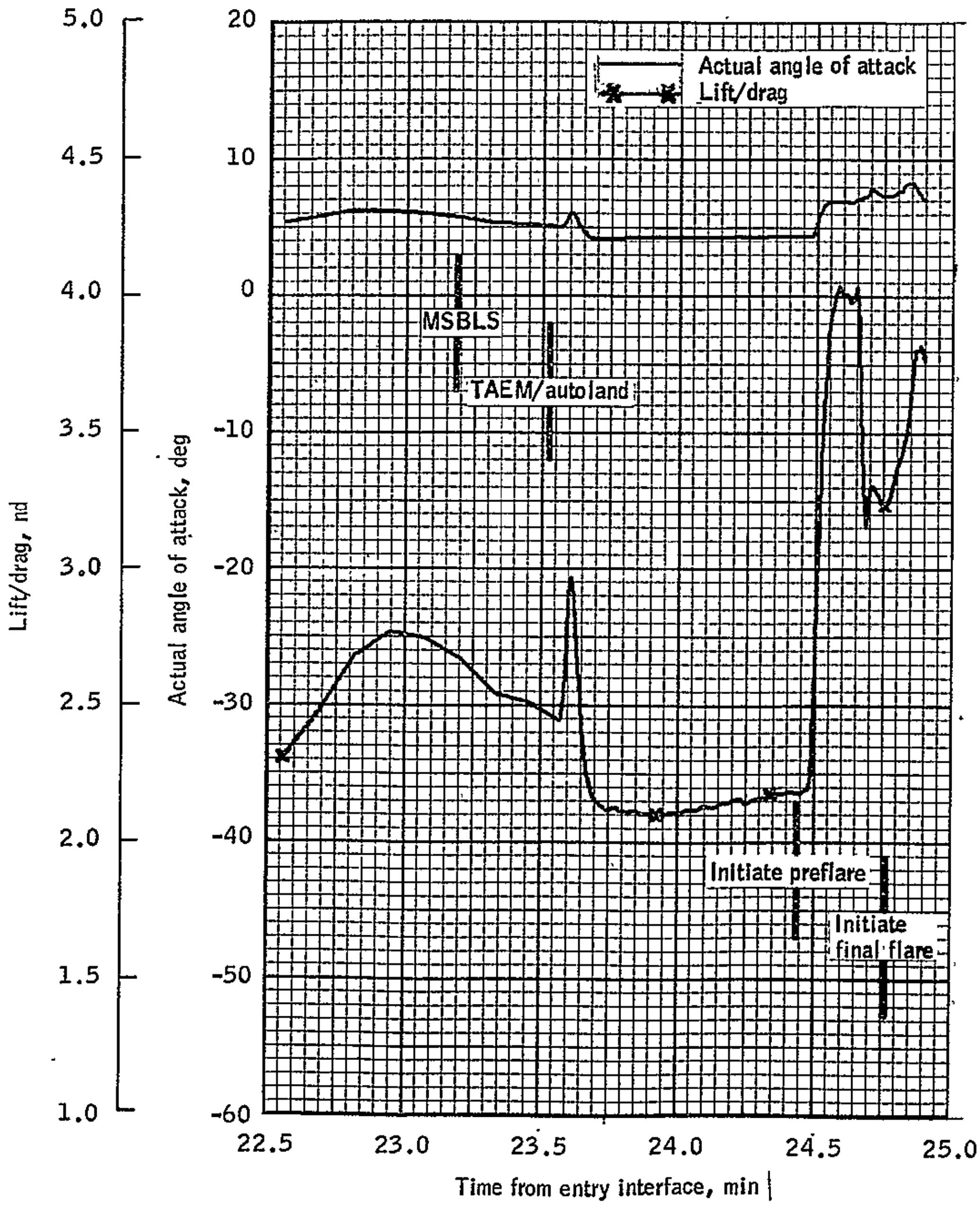

Figure 4.5-8.- Lift/drag and actual angle of attack versus time from entry interface for orbiter OFT-1 approach and landing.

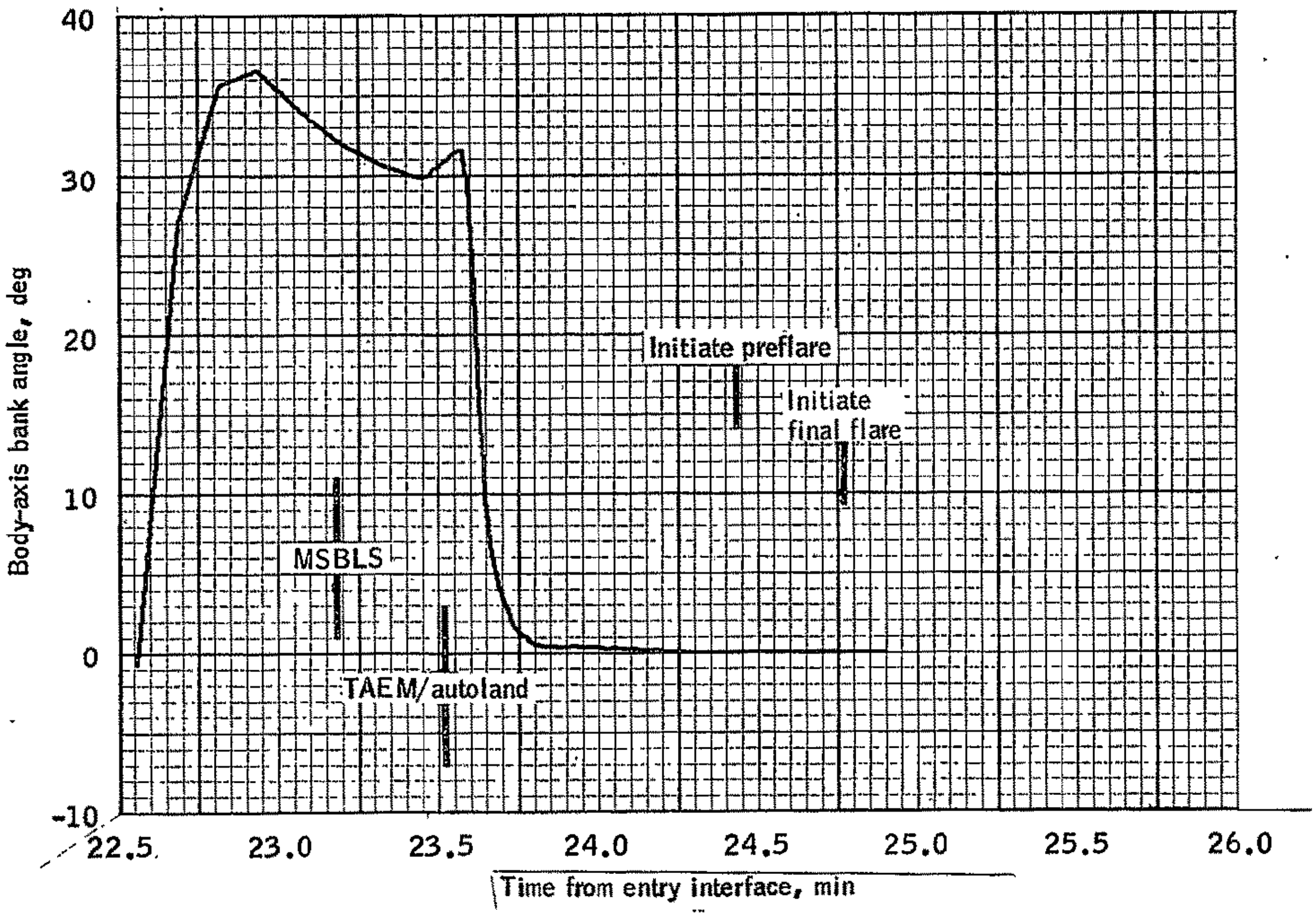

Figure 4.5-9.- Body-axis bank angle versus time from entry interface for orbiter OFT-1 approach and landing.

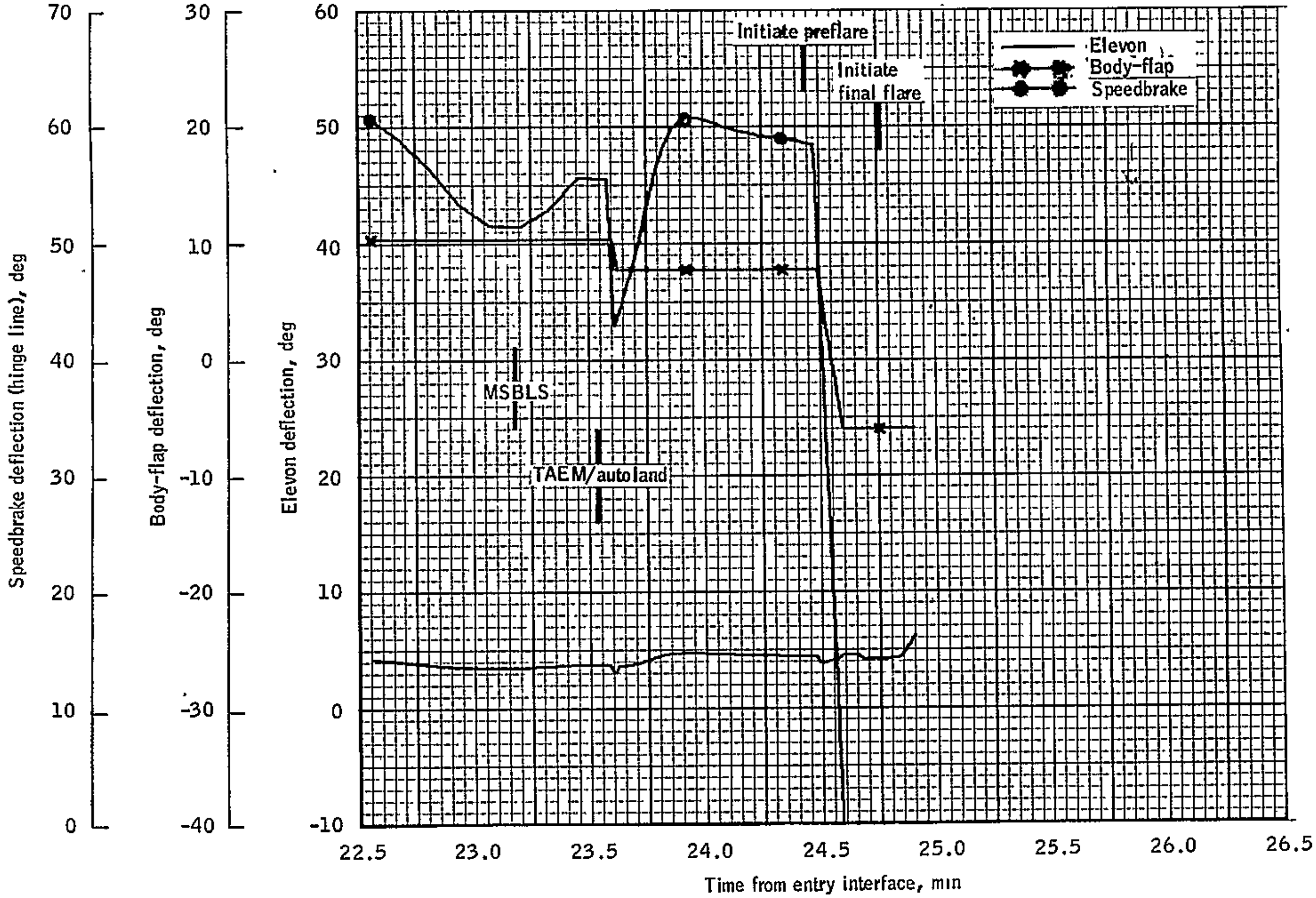

Figure 4.5-10.- Elevon, body-flap and speedbrake deflections versus time from entry interface for orbiter OFT-1, approach and landing.

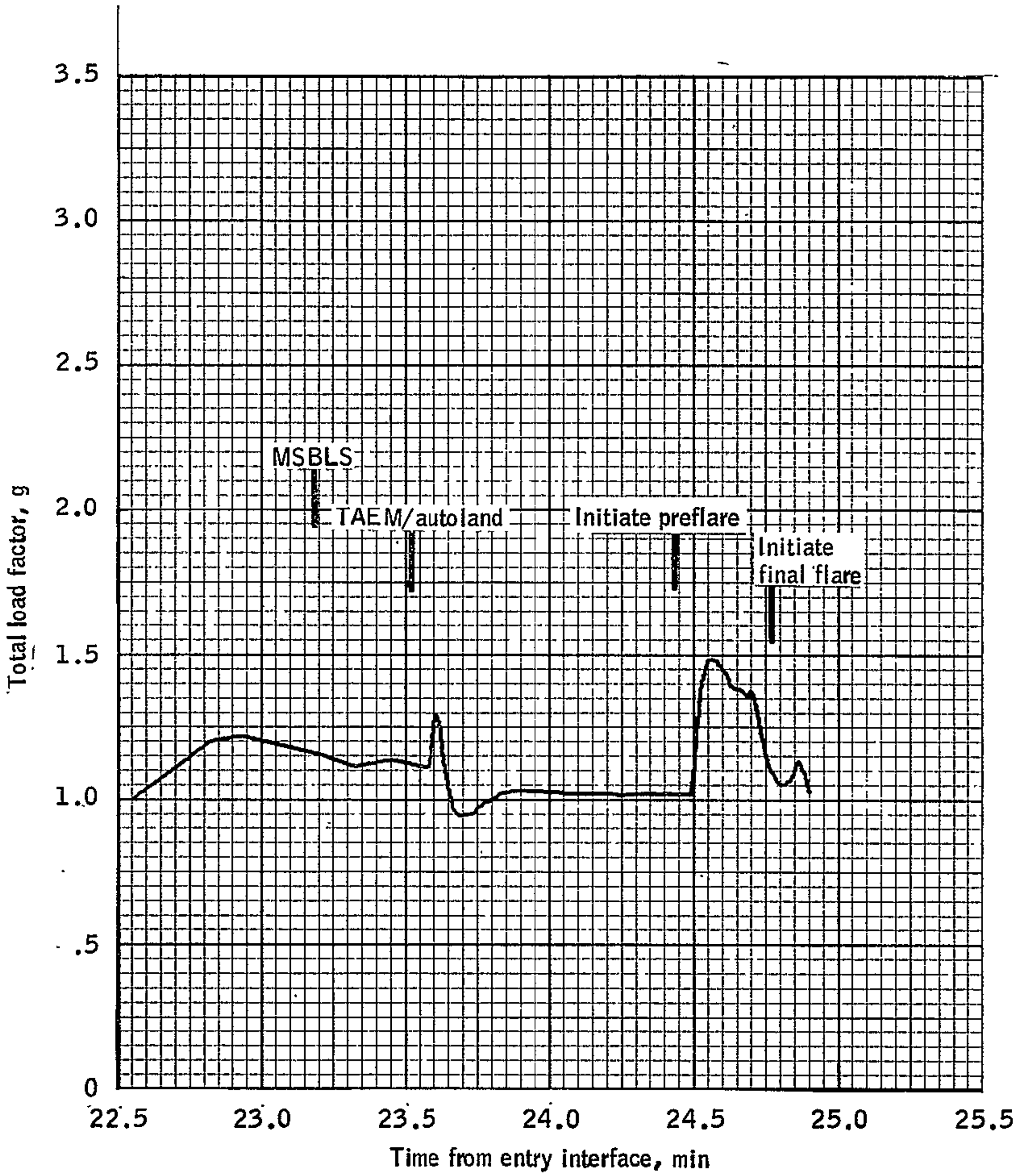

Figure 4.5-11.- Total load factor versus time from entry interface for orbiter OFT-1 approach and landing.

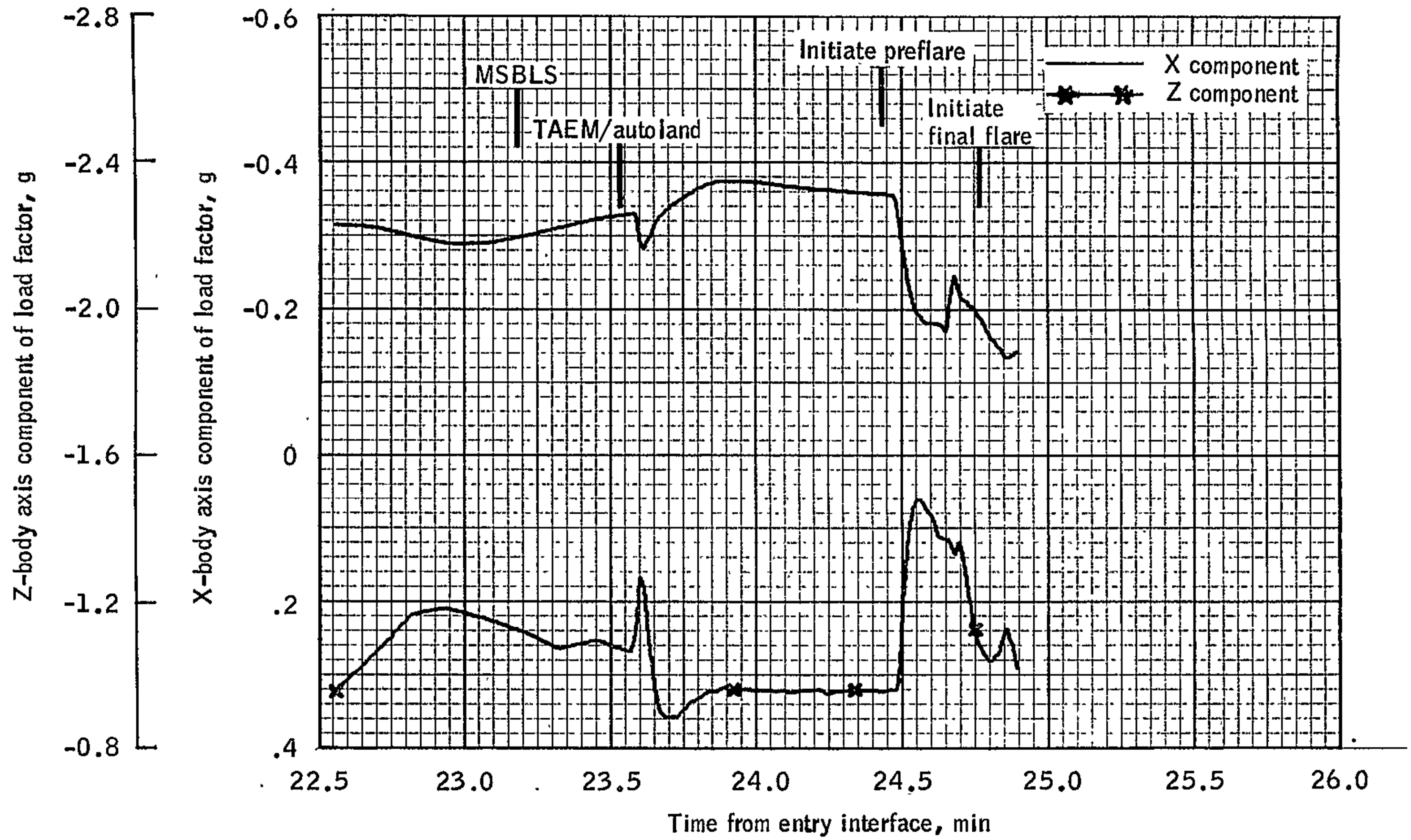

Figure 4.5-12.- X- and Z-body axis components of load factor versus time from entry interface for orbiter OFT-1 approach and landing.

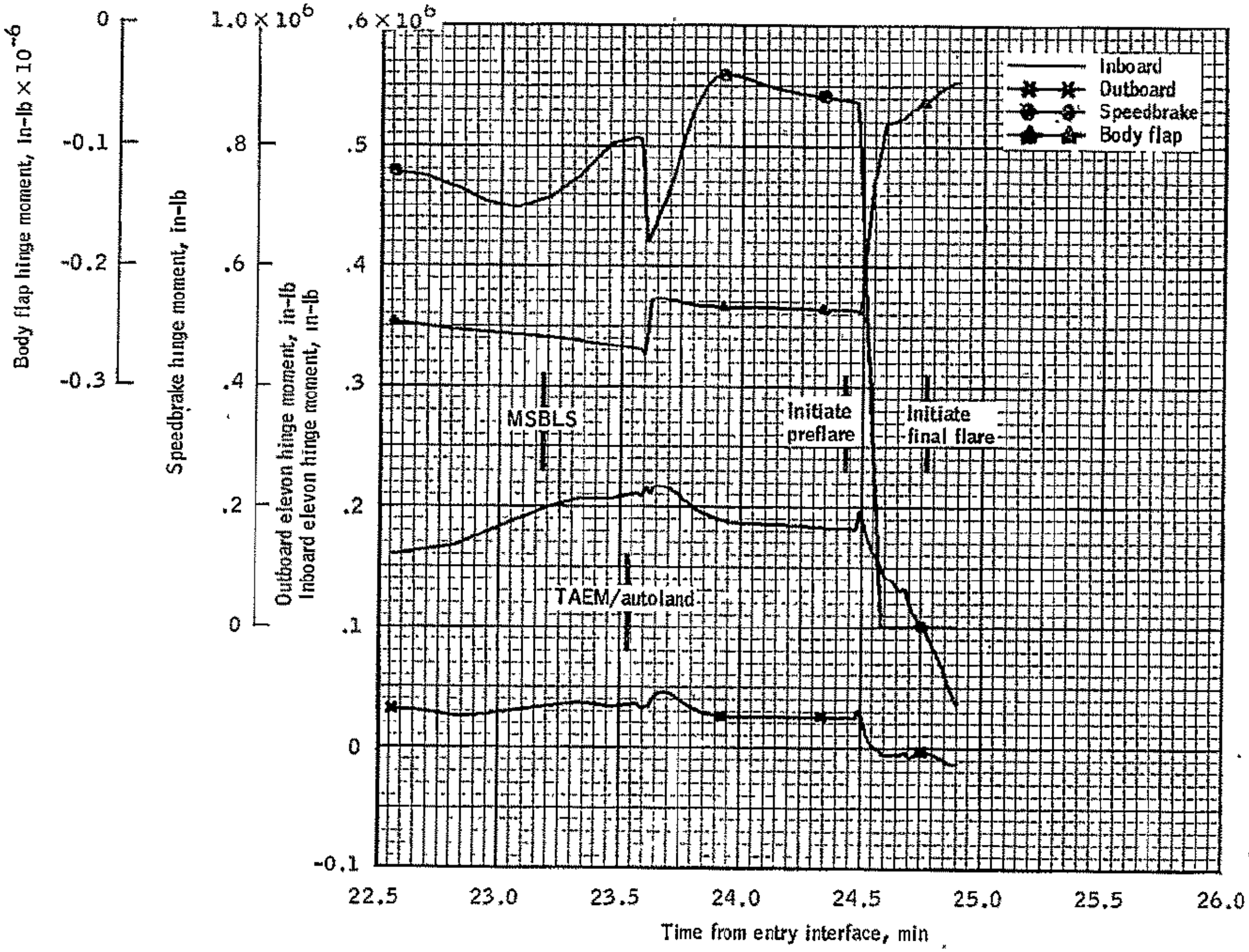

Figure 4.5-13.- Elevon, speedbrake, and body flap hinge moments versus time from entry interface for orbiter OFT-1 approach and landing.

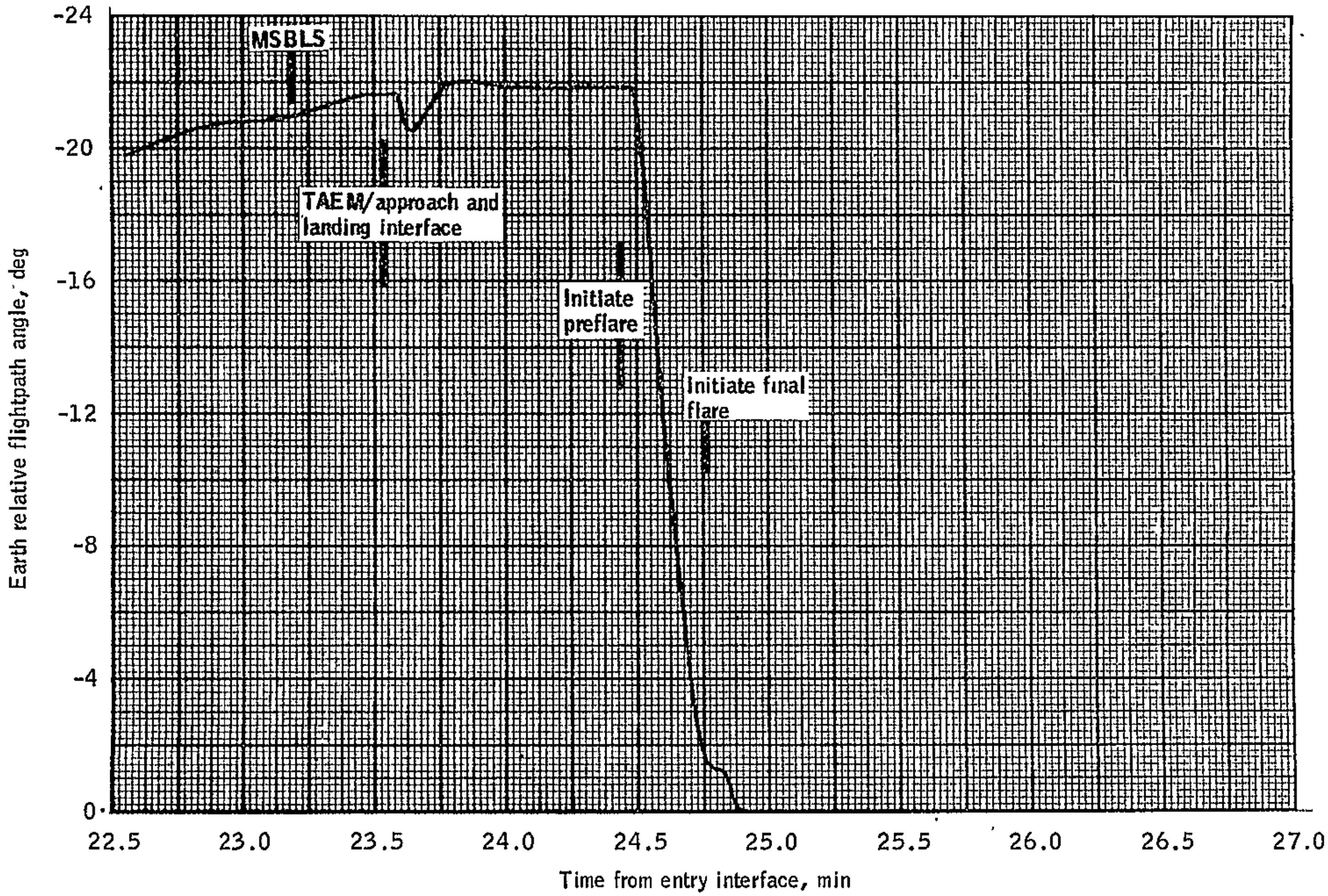

Figure 4.5-14.- Earth relative flightpath angle versus time from entry interface for OFT-1 approach and landing.

5.0 COMMUNICATIONS AND TRACKING

A summary of OFT-1 S-band and C-band data is presented in table 5-I. TACAN data are presented in table 5-II and station locations are presented in table 5-III. The data for the Buckhorn and Goldstone S-band communications stations are based on detailed analyses of terrain masking with 30 seconds allowed for lockup after clearing masking. The Pt. Pillar and Vandenberg C-Band tracking stations acquisition of signal (AOS) is based on a 0-degree elevation angle with 60 seconds allowed for firm lockup using skin tracking.

Approximately 6 minutes after the deorbit maneuver, communications and tracking by the Guam station is established with AOS based on a 3-degree elevation angle at 29 hours 51 minutes 07 seconds GET. This communication and tracking lasts for 6 minutes 07 seconds with loss of signal (LOS) based on a 3-degree elevation angle occurring 6 minutes 49 seconds prior to reaching the entry interface.

The Orbiter enters S-band blackout approximately 3 minutes 31 seconds after entry interface when the Orbiter is at an altitude of 264 217 feet and an Earth-relative speed of 24 493 fps. There are no S-band stations available for communications after Guam until Buckhorn acquisition.

The theoretical S-band blackout exit occurs 52 minutes 46 seconds after entry interface at an altitude of 176 848 feet and an Earth-relative speed of 12 042 fps. The theoretical blackout exit for L-band communication used by the TACAN station occurs about 13 minutes 25 seconds after entry interface at an altitude of 169 920 feet and an Earth-relative speed of 10 992 fps. Communications blackout entry and exit computations are based on the criteria presented in reference 13 and are presented in the altitude/relative velocity plane and altitude/range plane in figures 4.3-12 and 4.3-37, respectively.

Figures 5-1 and 5-2 present the OFT-1 trajectory profile in the elevation-azimuth plane for the Buckhorn and Goldstone stations, respectively.

C-band tracking by the Pt. Pillar station is established at about 181 838 feet altitude and an Earth-relative speed of 12 914 fps and by the Vandenberg station at about 176 470 feet altitude and Earth-relative speed of 11 979 fps. The data from these two C-band stations are available to provide an estimate of the state vector by the Mission Control Center (MCC) before establishing the S-band communications lockup with Buckhorn station. Fifteen seconds later, after communication is established through the Buckhorn station, the crew could initiate a runway redesignation if given a ground command, at an altitude of 160 345 feet and an Earth-relative speed of 9514 fps. The first MCC state vector update will occur about 50 seconds after the Buckhorn S-band communication at an altitude of 151 569 feet and an Earth-relative speed of 8488 fps.

The TACAN acquisition logic is based on the three-tier concept. A total of 10 TACAN stations are used for navigation with acquisition and switching of these stations based on the arrangement within three tiers or regions; the acquisition region, the navigation region, and the landing region. The acquisition region includes the San Luis Obispo, Avenal, and the Gaviota stations and is used for ranges greater that 120 nautical miles. The navigation region includes the Fellows, Gorman, Lake Hughes, and Santa Barbara stations and a mobile TACAN station and is used for ranges between 120 and 10 nautical miles. The landing region includes the Palmdale and EAFB stations and is used for ranges less than 10 nautical miles. Table 5-I and figure 5-3 present TACAN station usage and switching times. The TACAN data from San Luis Obispo are inhibited in this trajectory until the altitude decreases to 129 144 feet which allows time for crew evaluation prior to incorporation into the onboard navigation state vector. Since this profile was generated, the criteria for incorporating TACAN data into the onboard navigation system have changed allowing incorporation based on a range rate limit of 6300 knots provided the data have been verified by the MCC. Based on this criteria, TACAN data could have been incorporated at 156 926 feet altitude, which allows 30 seconds for evaluation by the MCC after acquisition by the Buckhorn station. This 30 seconds is required for the TACAN range and bearing data to be telemetered to the MCC through the Buckhorn station.

Figures 5-3 and 5-4 present significant communications and tracking events relative to the OFT-1 groundtracks.

TABLE 5-I.- OFT-1 C-BAND AND S-BAND COMMUNICATION SEQUENCE OF EVENTS

Time from 400K, min:sec	Site[a]	Event	G.m.t., hr:min:sec	g.e.t., hr:min:sec	Elevation, deg	Azimuth from north, deg	Slant range, n. mi.	Range rate, fps	Surface range, n. mi.	Relative velocity, fps	Altitude[b], ft	Longitude, deg	Geodetic latitude, deg
-13:43	GWM	AOS contact	42:20:15	29:50:15	.0	218.0	980.	-22 432.	954.	23 909.	835 322.	135.03	.59
-12:56	GWM	AOS data	42:21:02	29:51:02	3.0	214.9	807.	-22 130.	782.	23 929.	819 169.	137.32	2.49
-09:40	GWM	Max elevation	42:24:18	28:54:18	26.3	143.2	258.	-889.	223.	24 030.	738 136.	147.00	10.31
-06:49	GWM	LOS data	42:27:09	29:57:09	3.0	70.3	703.	21 973.	686.	24 138.	651 075.	155.96	16.92
-06:13	GWM	LOS contact	42:27:45	29:57:45	.2	67.1	837.	22 441.	820.	24 164.	630 829.	157.96	18.28
11:26	PTP	AOS contact	42:45:23	30:15:23	.0	246.1	465.	-11 863.	462.	14 844.	190 515.	-130.99	34.22
11:53	VDB	AOS contact	42:45:50	30:15:50	.1	268.4	458.	-13 573.	456.	13 972.	187 009.	-129.73	34.11
13:06	FRC	AOS contact	42:46:03	30:17:03	.0	265.3	441.	-11 449.	438.	11 608.	173 134.	-126.68	34.04
13:06	BUC	AOS contact	42:47:03	30:17:03	.0	265.3	441.	-11 450.	438.	11 608.	174 134.	-126.68	34.04
13:06	PTP	AOS data	42:47:03	30:17:03	3.0	224.5	300.	-8 098.	298.	11 608.	174 134.	-126.68	34.04
13:12	VDB	AOS data	42:47:09	30:17:09	3.0	264.5	297.	-11 287.	295.	11 422.	172 915.	-126.47	34.05
13:42	GDS	AOS contact	42:47:39	30:17:39	.0	262.7	429.	-10 342.	426.	10 441.	166 355.	-125.37	34.13
14:51	FRC	AOS data	42:48:49	30:18:49	3.0	265.7	269.	-8 252	267.	8 436.	151 053.	-123.29	34.50
14:51	BUC	AOS data	42:48:49	30:18:49	3.0	265.7	269.	-8 252.	267.	8 436.	151 053.	-123.29	34.50
15:47	GDS	AOS data	42:49:44	30:19:44	3.0	266.1	254.	-6 652.	252.	6 970.	139 613.	-121.98	34.95
15:53	PTP	Max elevation	42:49:50	30:19:50	6.6	168.8	165.	-1 266.	163.	6 838.	138 763.	-121.86	34.99
16:50	VDB	Max elevation	42:50:48	30:20:48	30.3	349.3	39.	-571.	34.	5 549.	121 927.	-120.71	35.22
18:01	PTP	LOS data	42:51:59	30:21:59	3.0	136.3	208.	3 511.	207.	4 063.	103 928.	-119.59	35.13
20:03	GDS	Max elevation	42:54:01	30:24:01	7.7	255.5	81.	-1 925.	80.	1 942.	74 401.	-118.45	35.00
20:29	PTP	LOS contact	42:54:27	30:24:26	.2	126.7	259.	1 030.	258.	1 601.	65 724.	-118.30	35.01
21:07	VDB	LOS data	42:55:04	30:25:04	3.0	79.0	123.	1 039.	123.	1 118.	52 779.	-118.14	35.03
22:02	BUC	Max elevation	42:55:60	30:25:60	41.6	329.9	9.	-378.	6.	790.	37 296.	-117.98	35.05
22:03	FRC	Max elevation	42:56:01	30:26:01	42.1	329.7	8.	-379.	6.	787.	37 053.	-117.97	35.05
23:07	GDS	LOS data	42:57:04	30:27:04	3.0	249.7	51.	-239.	51.	653.	21 587.	-117.84	35.04
23:12	VDB	LOS contact	42:57:09	30:27:09	.2	79.9	138.	249.	137.	646.	20 465.	-117.83	35.04
24:13	GDS	LOS contact	42:58:10	30:28:10	.2	243.7	53.	299.	53.	543.	6 908.	-117.83	34.95
24:27	FRC	LOS data	42:58:25	30:28:25	3.0	119.1	4.	146.	4.	519.	3 979.	-117.84	34.93
24:27	BUC	LOS data	42:58:25	30:28:25	3.0	116.6	4.	126.	4.	519.	3 979.	-117.84	34.93
24:35	FRC	LOS contact	42:58:32	30:28:32	.2	126.6	4.	219.	4.	503.	2 784.	-117.84	34.92
24:35	BUC	LOS contact	42:58:32	30:28:32	.2	124.5	4.	203.	4.	502.	2 767	-117.84	34.92

[a]C-Band Stations
Pt. Pillar (PTP)
Vandenberg (VDB)
FRC (FRC)

S-Band Stations
Buckhorn (BUC)
Goldstone (GDS)
GUAM (GWM)

[b]Altitude of c.g. above 1960 Fischer ellipsoid.

TABLE 5-II.- OFT-1 TACAN SEQUENCE OF EVENTS

Time from 400K, min:sec	Site[a]	Event	G.m.t., hr:min:sec	g.e.t., hr:min:sec	Elevation, deg	Azimuth from north, deg	Slant range, n. mi.	Range rate, fps	Surface range, n. mi.	Relative velocity, fps	Altitude[b], ft	Longitude, deg	Geodetic latitude, deg
11:49	SBP	AOS contact	42:45:46	30:15:46	.0	264.1	460.	-13 416.	458.	14 097.	187 551.	-129.91	34.12
12:06	GVO	AOS contact	42:46:03	30:16:03	.1	269.0	453.	-13 240.	450.	13 536.	185 026.	-129.13	34.07
12:14	FLW	AOS contact	42:46:11	30:16:11	.1	264.5	449.	-12 826.	447.	13 288.	183 806.	-128.79	34.05
12:14	SBA	AOS contact	42:46:11	30:16:11	.0	271.8	452.	-13 115.	450.	13 288.	183 806.	-128.79	34.05
12:39	GMN	AOS contact	42:46:36	30:16:36	.0	266.5	446.	-12 244.	443.	12 478.	179 410.	-127.74	34.02
12:49	LHS	AOS contact	42:46:46	30:16:46	.0	267.3	440.	-11 998.	438.	12 166.	177 594.	-127.36	34.02
13:00	PMD	AOS contact	42:46:57	30:16:57	.0	267.8	443.	-11 672.	441.	11 793.	175 319.	-126.90	34.03
13:10	EDW	APS contact	42:47:07	30:17:07	.0	265.3	441.	-11 339.	439.	11 484.	173 325.	-126.54	34.05
13:10	SBP	AOS data	42:47:07	30:17:07	3.0	257.5	297.	-11 121.	295.	11 484.	173 325.	-126.54	34.05
13:27	GVO	AOS data	42:47:24	30:17:24	3.0	266.3	293.	-10 852.	290.	10 930.	169 489.	-125.91	34.08
13:38	FLW	AOS data	42:47:36	30:17:36	3.0	259.8	288.	-10 418.	285.	10 563.	167 087.	-125.50	34.12
13:38	SBA	AOS data	42:47:36	30:17:36	3.0	271.2	288.	-10 456.	286.	10 563.	167.087	-125.50	34.12
14:13	GMN	AOS data	42:48:10	30:18:10	3.0	264.9	278.	-9 440.	275.	9 514.	160 345.	-124.38	34.27
14:25	LHS	AOS data	42:48:22	30:18:22	3.0	267.1	274.	-9 055.	271.	9 183.	157 817.	-124.03	34.33
14:44	PMD	AOS data	42:48:41	30:18:41	3.0	269.2	271.	-8 390.	269.	8 647.	153 103.	-123.49	34.45
14:59	EDW	AOS data	42:48:56	30:18:56	3.0	266.2	267.	-7 992.	265.	8 225.	149 026.	-123.09	35.56
16:49	SBP	Max elevation	42:50:46	30:20:46	83.6	158.5	20.	-91.	2.	5 593.	122 416.	-120.74	35.22
17:27	GVO	Max elevation	42:51:24	30:21:24	23.6	.3	45.	-575.	41.	4 755.	113 503.	-120.09	35.22
17:42	FLW	Max elevation	42:51:39	30:21:39	71.8	5.7	18.	-438.	6.	4 447.	109 376.	-119.85	35.19
17:52	SBA	Max elevation	42:51:49	30:21:49	15.1	2.4	63.	-1 036.	61.	4 256.	106 599.	-119.72	35.16
19:09	GMN	Max elevation	42:53:06	30:23:06	55.8	358.0	17.	-323.	9.	2 794.	89 080.	-118.87	34.96
19:31	LHS	Max elevation	42:53:28	30:23:28	35.3	343.7	22.	-434.	18.	2 410.	83 152.	-118.68	34.97
20:15	PMD	Max elevation	42:54:12	30:24:12	22.2	325.3	29.	-864.	27.	1 790.	70 724.	-118.38	35.00
20:55	SBP	LOS data	42:54:52	30:24:52	3.0	95.3	128.	1 138.	128.	1 260.	56 569.	-118.18	35.03
21:32	GVO	LOS data	42:55:29	30:25:29	3.0	72.5	105.	826.	105.	904.	45 402.	-118.06	35.04
21:35	SBA	LOS data	42:55:32	30:25:32	3.0	57.4	101.	751.	101.	890.	44 608.	-118.05	35.04
21:50	FLW	LOS data	42:55:47	30:25:47	3.0	91.2	92.	751.	91.	829.	40 506.	-118.01	35.05
22:33	EDW	Max elevation	42:56:30	30:26:30	26.3	305.3	10.	-549.	9.	718.	29 676.	-117.91	35.06
22:57	GMN	LOS data	42:56:54	30:26:54	3.0	73.0	52.	418.	52.	668.	23 853.	-117.85	35.05
22:59	SBP	LOS contact	42:56:56	30:26:56	.2	94.0	144.	539.	144.	665.	23 396.	-117.85	35.05
23:10	LHS	LOS data	42:57:07	30:27:07	3.0	59.5	42.	62.	42.	648.	20 913.	-117.84	35.04
23:26	GVO	LOS contact	42:57:23	30:27:23	.2	74.8	116.	-50.	116.	625.	17 103.	-117.82	35.02
23:27	SBA	LOS contact	42:57:24	30:27:24	.2	61.2	110.	-201.	110.	623.	16 880.	-117.82	35.01
23:33	FLW	LOS contact	42:57:30	30:27:30	.2	92.4	101.	12.	101.	613.	15 516.	-117.82	35.00
23:56	PMD	LOS data	42:57:53	30:27:53	3.0	29.8	23.	-512.	23.	575.	10 361.	-117.83	34.97
24:05	GMN	LOS contact	42:58:02	30:28:02	.2	79.4	52.	-181.	52.	558.	8 594.	-117.83	34.96
24:06	LHS	LGS contact	42:58:03	30:28:03	.2	65.9	40.	-289.	40.	554.	8 227.	-117.83	34.96
24:28	EDW	LOS data	42:58:25	30:28:25	3.0	236.9	5.	318.	5.	518.	3 885.	-117.84	34.93
24:31	PMD	LOS contact	42:58:28	30:28:28	.2	32.5	21.	-451.	21.	515.	3 354.	-117.84	34.92
24:39	EDW	LOS contact	42:58:36	30:28:36	.2	230.3	6.	363	6.	479.	2 463.	-117.84	34.91

[a]San Luis Obispo (SBP) | Gorman (GMN)
Gavioto (GVO) | Lake Hughes (LHS)
Avenal (AVE) | Mobil Unit, AF (MBL)
Fellows (FLW) | Palmdale (PMD)
Edwards (EDW)

[b]Altitude of c.g. above 1960 Fischer ellipsoid.

TABLE 5-III.- S-BAND, C-BAND, and TACAN STATION LOCATIONS USED FOR OFT-1 DEORBIT THROUGH LANDING

Station name	Latitude, deg	Longitude, deg	Altitude, ft
C-band radar station			
FRC, Calif.	34.9608N	117.9114W	2480.3
KPT, Kaena Pt., Oaho, Hawaii	21.5721N	158.2666W	931.7
PTP, Pt. Pillar, Calif.	37.4979N	122.4995W	-39.4
SNI, San Nicholas Is., Calif.	33.2470N	119.5200W	731.6
VDB, Vandenberg, Calif.	34.6659N	120.5814W	200.1
S-band communications stations			
GWM, Guam	13.3106N	144.7268E	380.6
GDS, Goldstone, Calif.	35.3414N	116.8736W	3064.3
BUC, Buckhorn, Calif.	34.9578N	117.9117W	2647.
Tacan stations			
SBP, San Luis Obispo	35.2523N	120.7603W	1433
GVO, Gavioto	34.5324N	120.0906W	2654
AVE, Avenal	35.6469N	119.9779W	670
FLW, Fellows	35.0933N	119.8652W	3903
GMN, Gorman	34.8039N	118.8610W	4875
LHS, Lake Huges	34.6831N	118.5766W	582
MBL, Mobil Unit, AF	35.0166N	118.1167W	4875
PMD, Palmdale	34.6321N	118.0634W	2469
EDW, Edwards	34.9824	117.7542W	2301

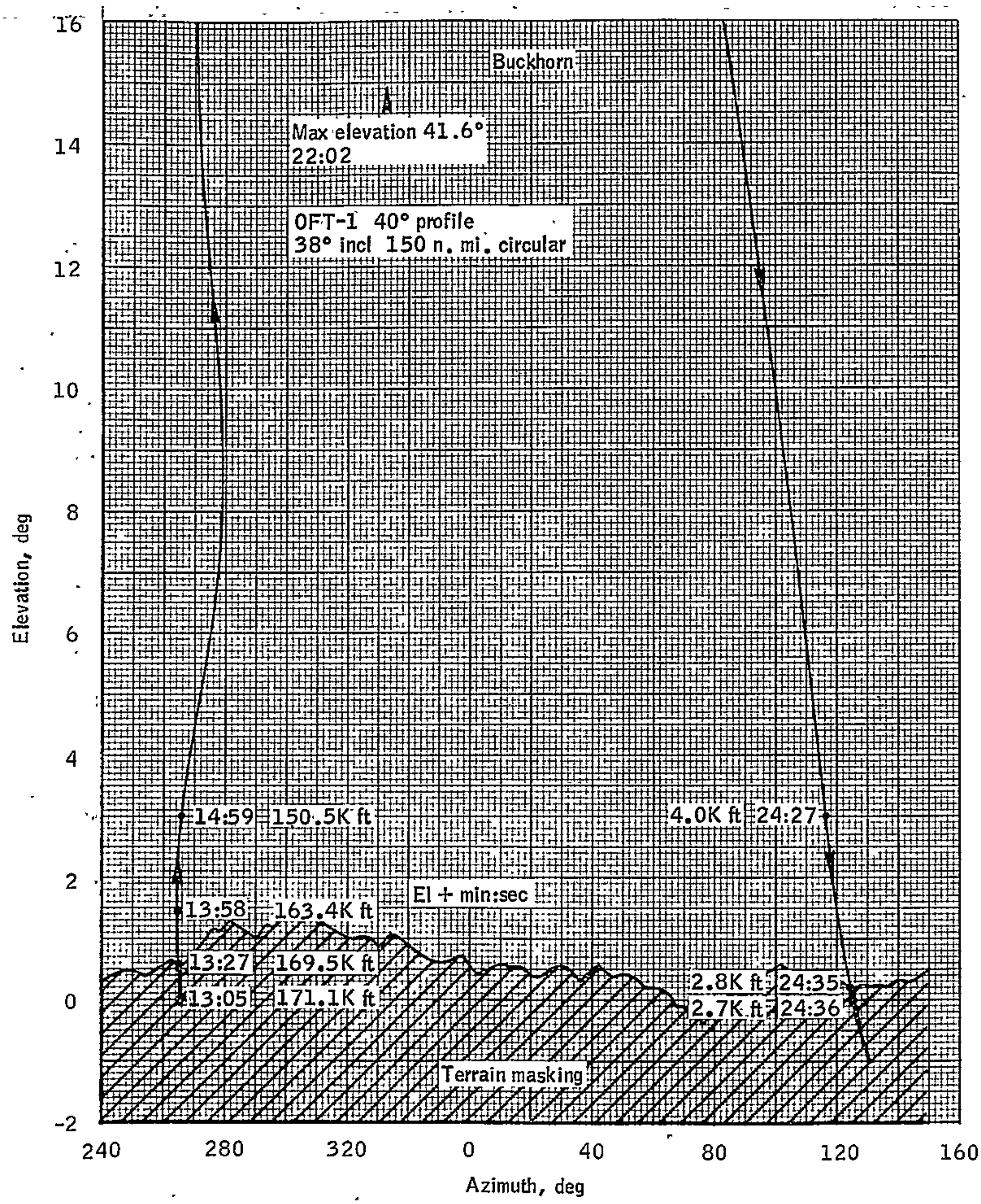

Figure 5-1.- Buckhorn elevation versus azimuth for orbiter OFT-1.

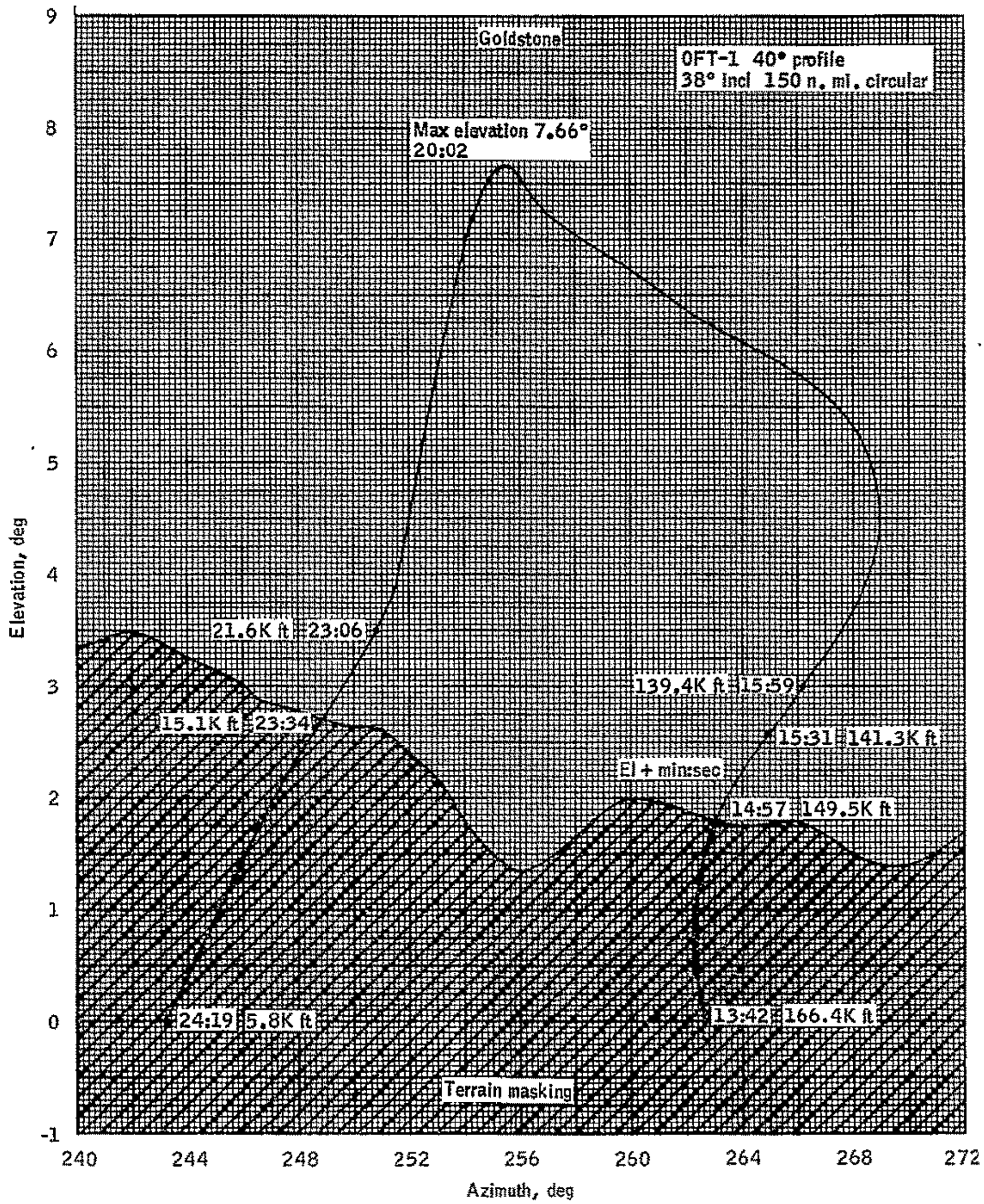

Figure 5-2.- Goldstone elevation versus azimuth for orbiter OFT-1.

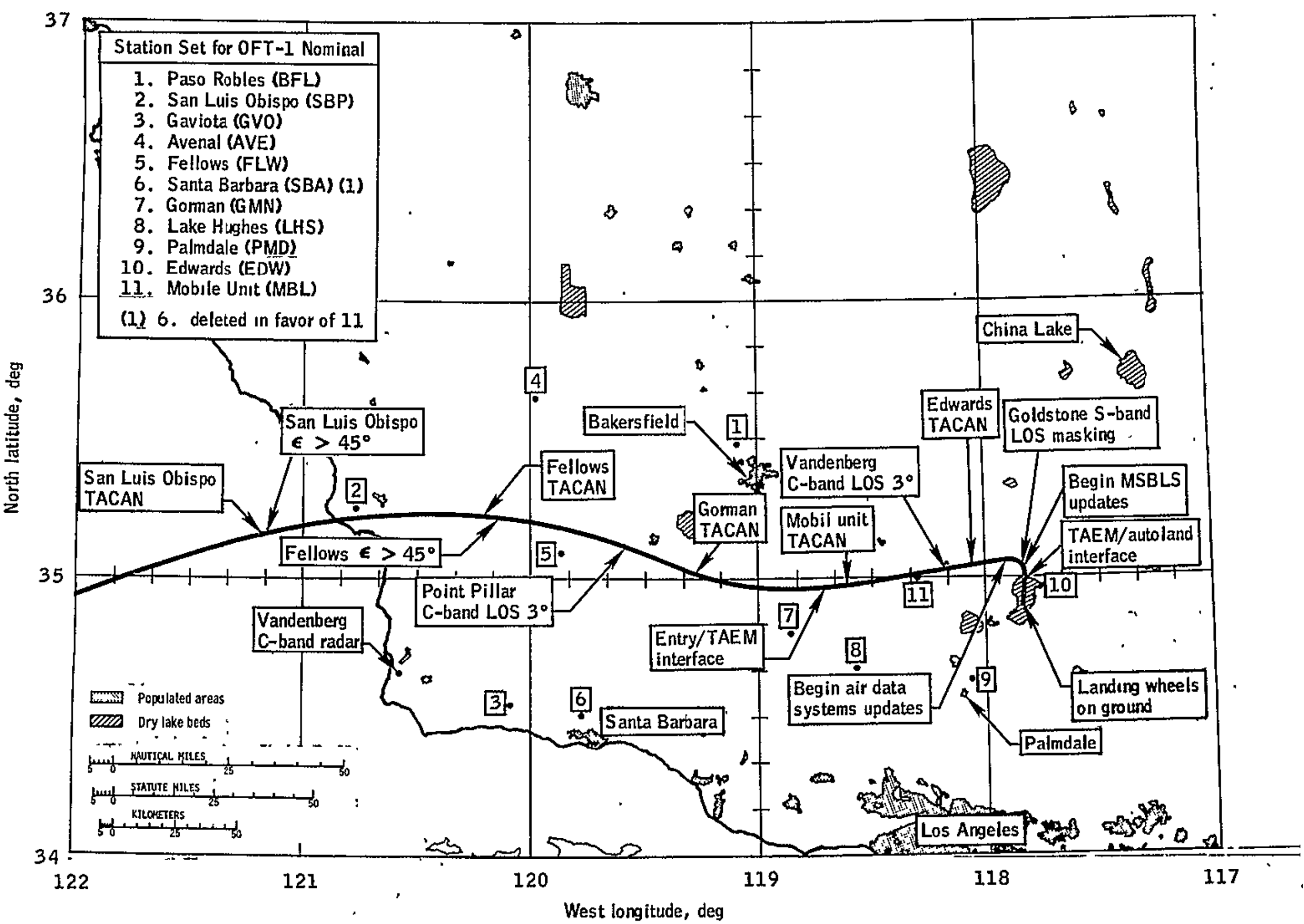

Figure 5-3.- OFT-1 entry groundtrack and TACAN events.

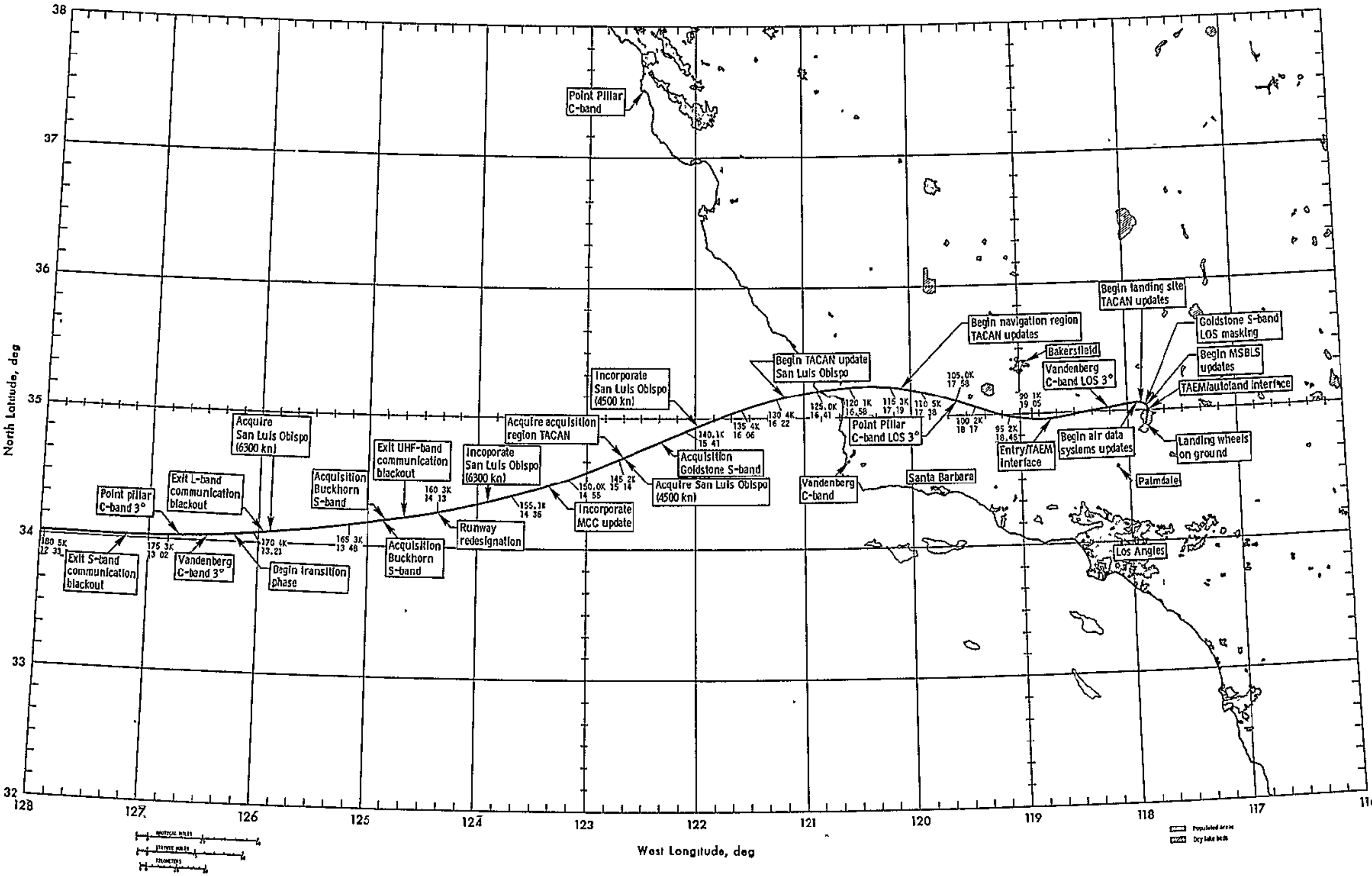

Figure 5-4.- Postblackout entry groundtrack for orbiter OFT-1.

NASA JSC

6.0 OPEN ISSUES

Several issues related to entry must be resolved prior to OFT-1. The OMS loading philosophy must be finalized. The modification to the TAEM guidance software to allow matching of the slopes of the entry and TAEM profiles at the entry/TAEM interface must be approved and verified. The autoland guidance constants for 50-to 100-present headwinds must be defined. Communication and tracking analysis of the deorbit-through-landing trajectory is required to determine if communications and tracking coverage is adequate. Dispersion analysis of the deorbit-through-landing trajectory and the performance evaluation of Shuttle Orbiter systems over the resulting flight regime is required to determine if the profile is adequate. Maneuver capability during TAEM must be determined and the TAEM HAC geometry defined to provide optimum MSBLS acquisition conditions consistent with TAEM guidance performance. Detailed venting and structural analysis of the TAEM profile are required. The sensitivity of sonic boom overpressure to variations in the trajectory must be defined and further optimization of the angle-of-attack profiles for the flight control constraints and limits will have to be incorporated into the OFT-1 deorbit-through-landing profile when it is reworked.

7.0 CONCLUSIONS

The OFT-1 deorbit-through-landing profile presented in this document has been designed to reach a good trade-off of conflicting requirements, considering all systems and operational guidelines and constraints. The 40-degree angle-of-attack profile for OFT-1 departs from the expected operational mission angle-of-attack profile in order to minimize TPS environment effects.

Two issues have been resolved since the OFT-1 Preliminary Reference Flight Profile for Deorbit Through Landing (ref. 1) was published. Flight software logic has been implemented to provide yaw steering during ascent if an AOA to EAFB is required. This reduces the crossrange-at-entry interface to within the 550 nautical mile crossrange requirement for OFT-1. The approach and landing profile has been shaped to provide a 22-degree outer glideslope and a 1.5-degree inner glideslope that is compatible with manual flight.

Several assumptions and simplifications in systems modeling were made in developing flight corridors and flight profiles for the OFT-1 deorbit-through-landing profile. Also, constraints and guidelines for different Orbiter systems and for operational considerations resulted in conflicting requirements in the OFT-1 flight profile development. Therefore, detailed Orbiter systems and operations evaluation of the profile is required to determine the adequacy of the profile.

The OFT-1 deorbit-through-landing profile will be refined and updated as issues are resolved.

8.0 REFERENCES

1. Hiott, James M.: OFT-1 Preliminary Reference Flight Profile for Deorbit Through Landing. JSC IN 76-FM-68, Sept. 1976.

2. Minutes of the OFT Entry-Through-Landing Working Group Meeting on Feb. 2, 1977. JSC memorandum.

3. Mission Integration Branch: Preliminary Reference Profile Design Considerations and Flight Summary for OFT-1. JSC IN 76-FM-54, Aug. 1976.

4. Flight Planning Branch: Reference Flight Profile for OFT-1 - Integrated Profile. JSC IN 77-FM-15, Mar. 1977.

5. Software Development Branch: Space Vehicle Dynamics Simulation (SVDS) Program Description, Revision 2. JSC IN 73-FM-85, Dec. 1975.

6. Rockwell International: Aerodynamic Design Data Book - Volume I, Orbiter Vehicle, Revision 5. SD72-SH-0060-1J, Dec. 1975.

7. Rockwell International: Space Shuttle Flight Control System Data Book, Volume II, Orbiter. SD 73-SH-0097-2E, June 1976.

8. Rockwell International: RI/Houston Simplified Weight Synthesis Program, Revision 3. SEH-ITA-75-192, July 1975.

9. Space Shuttle Orbiter Orbital Flight Test Level C Functional Subsystem Software Requirements Document, Guidance, Navigation and Control, Part A, Guidance, Entry through Landing. SD-76-SH1-0001, Nov. 1975.

10. Space Shuttle Orbital Flight Test Level C Functional Subsystem Software Requirements Document, Guidance, Navigation and Control, Part B, Entry through Landing Navigation, Dec. 17, 1976, SD 76-SH-0004B.

11. Lowes, Flora B.: Preliminary Coordinates of Landing Site Origins (Runway Thresholds) for Various ALT Runways. JSC memorandum FM86 (76-65), Mar. 1976.

12. Coordinate Systems for the Space Shuttle Program. NASA TM X-58153, 1974.

13. Minutes of the OFT Entry-Through-Landing Working Group Meeting on Feb. 24 and 25, 1976. JSC memorandum FM41 (76-20).

14. Trajectory Optimization/Autoland Study Report, HAD-1.6-120, McDonnell Douglas Technical Services Co., Inc., Dec. 3, 1976.

APPENDIX

OFT-1 DEORBIT-THROUGH-LANDING GUIDELINES AND CONSTRAINTS FOR MISSION PLANNING

APPENDIX

OFT-1 DEORBIT-THROUGH-LANDING GUIDELINES AND CONSTRAINTS FOR MISSION PLANNING

1.0 GENERAL

Orbit inclination will be 38 degrees. The inclination has been selected to optimize insertion and onorbit Spaceflight Tracking and Data Network (STDN) coverage within limits resulting from entry crossrange and aerodynamic heating considerations.

For all OFT flights, AOA landings will be on runway 17L on Rogers Lake bed at EAFB, and landings for RTLS will be on runway 15 at KSC. Because of the high probability of landing on either runway 15 or 33 for RTLS, OFT performance assessment will be based on the capability to achieve either runway for RTLS.

The time from the end of the last sleep period prior to deorbit to touchdown will not exceed 12 hours.

Nominal landing, landing following AOA, and RTLS aborts will be no earlier than 0.5 hour after sunrise nor later than 0.5 hour prior to sunset. It is desirable that landings at EAFB occur prior to 1000 hours local time.

The onorbit attitude time line and predeorbit thermal conditioning will minimize TPS backface temperature at entry interface within acceptable limits.

AOA capability and contingency deorbit capability on at least the first four revolutions following lift-off will be provided with landing at EAFB.

At all points on the ascent profile, the Orbiter will have RTLS or AOA capability, and the RTLS/AOA abort overlap will be maximized consistent with system margins and AOA crossrange limitations.

2.0 DEORBIT

Propulsive maneuvers, venting, and attitude time lines shall be designed to enhance state vector determination during atmospheric descent for nominal end-of-mission flight termination and contingencies.

The IMU alinement shall be designed to minimize the IMU misalinement at the entry interface. The maximum platform misalinement at entry interface for a star tracker alinement shall be TBD.

An IMU alinement will be made as close as possible to deorbit burn but no longer than 1.5 hours before the deorbit burn.

The auxiliary power units (APU's) will be assumed to be turned on one orbit before deorbit TIG and will remain on for approximately 8.5 minutes for APU and flight control system checkout. They will then be shut down until 5 minutes before deorbit ignition and will remain on throughout landing and rollout.

The deorbit attitude will be achieved at a minimum of 5 minutes prior to deorbit burn initiation.

Deorbit burns will be targeted out of plane, if necessary, to provide acceptable center-of-gravity conditions at entry interface.

The deorbit maneuver will be performed with both OMS engines, but an acceptable deorbit must be achieved even if one of these engines does not operate successfully.

Propellant-critical contingency deorbit will be based on a shallower-than-nominal targeting criteria where this targeting provides the best compromise between deorbit capability, RCS propellant availability for attitude control during atmospheric descent, and entry thermal environment.

All nominal deorbit opportunities will be planned so that a backup opportunity exists on the next revolution with a crossrange of less than 550 nautical miles.

A minimum free-fall time of 15 minutes between the termination of the deorbit maneuver with one OMS failure and entry interface is required for entry preparation.

APU hydraulic thermal conditioning will be performed between deorbit and entry interface.

In addition to satisfying the entry velocity, flightpath angle, and range requirements, the deorbit maneuver will reduce the OMS propellant remaining to achieve an acceptable Orbiter entry weight and center of gravity.

3.0 ENTRY

The entry profile will be shaped to minimize TPS bondline temperatures while maintaining surface temperatures within limits and providing acceptable systems and trajectory margins to compensate for dispersions.

The Orbiter entry weight will be minimized by reducing residual consumables, such as OMS and forward RCS propellant, within safe limits. Nominal RCS propellant allowance for attitude control for entry through landing will be 2250 pounds in the aft RCS propellant tanks. However, maximum aft RCS propellant, consistent with mission objectives and center-of-gravity considerations, will be maintained for entry-through-landing attitude control.

The entry-through-landing profile will conform to structural load limits corresponding to a -0.8 to 2g normal load factor, to control surface hinge moment aerodynamics load limits, and to actuator rate limits.

The maximum normal load factor with Orbiter weight equal to or less than 189 000 pounds shall be limited to 2g's nominally and 2.5g's for contingencies. Planned nominal entry crossrange will be $\leq$ 550 n.mi. with an angle-of-attack profile of 40 degrees.

Optimization of the entry profile will include consideration of sonic boom ground-level overpressures.

Nominal and abort targeting will be designed so that postblackout target changes are not nominally required. This does not preclude targeting to provide profile shaping to maximize the capability to redesignate after exit from voice communications blackout.

The nominal Orbiter center of gravity will be 66.25 percent longitudinally at entry with no lateral center-of-gravity displacement. The nominal vertical center of gravity will be 375 $\pm$ 3 inches.

The TAEM guidance target dynamic pressure will be based on the concept of flying directly to the HAC without employing a procedural turn in tailwind conditions. Additionally, this dynamic pressure will avoid undershoot conditions in the presence of severe headwinds. The energy control will provide conditions suitable for the initiation of autoland on the final approach.

The terminal area profile will be compatible with either a manual or an automatic mode of operation.

The maximum dynamic pressure during TAEM will be limited to 342 psf. The choice of minimum dynnamic pressure assures that terminal area maneuvers are limited to the front side of the lift/drag curve. Therefore, the minimum dynamic pressure is a function of Orbiter weight and varies from 138 psf to 161 psf as the orbiter weight varies from 188K to 218K lbs.

Terminal area maneuvers will not require operation on the backside of the lift/drag curve.

Nominal touchdown speed and altitude rate will provide adequate pitch margins for structural clearance, maximum tire speed margins, and landing gear structural load margins.

The TAEM guidance will not command a bank angle greater than 30 degrees for Mach numbers above 0.9 nor 60 degrees below Mach 0.9.

The maximum descent rate at landing shall be limited to 7 fps for an Orbiter weight $\leq$ 187 800 pounds.

The design landing weight of 188 000 pounds will not be exceeded for nominal landings. For AOA and RTLS 193 000 pounds will not be exceeded.

It is desirable that the atmospheric descent for nominal end-of-mission flight termination and AOA have the same angle-of-attack profile of 40 degrees during the critical TPS region of entry.

AOA targeting shall be based on a zero bank angle between entry interface and a dynamic pressure of 10 psf.

☆ U.S. GOVERNMENT PRINTING OFFICE. 1977 – 771-015/1656

DISTRIBUTION FOR JSC INTERNAL NOTE NO. 77-FM-36

JM6/Technical Library (2)
JM61/Center Data Mgmt. (3)
CA3/H. M. Draughon
CB/K. Bobko
V. D. Brand (2)
R. Crippen
H. W. Hartsfield (2)
K. Mattingly
J. Young
CF/M. P. Frank
CF3/W. Bolt
R. Epps
J. E. Ferguson
J. Greene
J. E. I'Anson
N. Griffith
CF6/H. F. Clancy
N. Hutchinson
CF7/E. I. Fendell
CG5/B. Anderson
D. L. Bentley
T. W. Holloway
D. K. Warren
CG6/C. R. Lewis
EJ/W. C. Bradford
EJ2/L. McWhorter
J. A. Porter
EJ3/K. J. Cox
M. C. Contella (3)
D. A. Dyer
T. E. Moore
E. E. Smith
EK/R. W. Kubicki
EK3/P. M. Deans
EP4/D. L. Connelly
ES/R. E. Vale
D. H. Greenshields
ES2/P. C. Glynn
A. C. Mackey
S. P. Weiss
ES3/D. B. Lee
R. C. Reid
G. Strouhal
J. A. Smith
EX/B. Redd
EX3/P. O. Romere
D. E. Tymms
J. M. Underwood
J. C. Young
EX4/R. L. Barton
F. Garcia
J. D. Gamble
K. M. Morrison
P. G. Thomas
FA/R. G. Rose
H. W. Tindall, Jr.
FA2/J. P. Mayer
FE3/B. Davila
R. Duval
FM/R. L. Berry
J. C. McPherson
Branch Chiefs (5)
FM2/L. D. Davis
G. L. Hunt
B. O. McCaffety
K. A. Young
FM4/A. J. Bordano
R. D. Davis
D. Ives
FM8/B. F. Cockrell
R. E. Eckelkamp
M. L. Heck
P. T. Pixley
R. Savely
FM14/Report Control Files (100)
G. Steeley
FM15/D. A. Nelson
FM17/B. Conway
R. M. Moore
FM42/J. C. Harpold (50)
G. L. Carman
H. Garcia
Garland
L. Gonzales
C. R. Halliman
J. A. Hansen
D. W. Heath
O. Hill
Lang
W. C. Lamey
M. N. Montez
J. D. Payne
Silvestri
J. V. West
FS5/J. W. Bormann
FS15/T. Sheehan
LN/H. E. Whitacre
LT/R. H. Kohrs
J. M. Peacock
MG/F. Littleton
WC6/E. R. Hischke
J. W. Mistrot
R. S. Morton
IBM/M. Bunde
B. Mills
A. Kuhn
D. Ramsey
T. Keller
Lockheed/Y. C. Loh
G. Volentine
MDAC/G. Bell
R. Hamilton
J. Hiott (20)
Langely
H. Kyle
R. Ruda
R. Spier
J. Treybig
H. Stone (2)
W. E. Hayes
E. A. Thompson
L. J. Drapela
R. K. Hamilton
G. Bell
R. Hamilton
R. Spier
H. C. Kyle
R. R. Ruda
W. W. Hinton
J. M. Hiott (20)
J. M. Treybig
K. R. Frohme
J. R. Weyraugh
M. E. Fowler
M. A. Culp
D. E. Wade
J. Treybig
R. M. Blackstock
J. F. Dubel
J. J. Ewell

DISTRIBUTION FOR JSC INTERNAL NOTE NO. 77-FM-36

JM6/Technical Library (2)
JM61/Center Data Mgmt. (3)
~~CA37/H. M. Draughon~~
CB/K. Bobko
V. D. Brand (2)
R. Crippen
H. W. Hartsfield (2)
K. Mattingly
J. Young
CF/M. P. Frank
CF3/W. Bolt
R. Epps
J. E. Ferguson
J. Greene
J. E. I'Anson
N. Griffith
CF6/H. F. Clancy
N. Hutchinson
CF7/E. I. Fendell
CG5/B. Anderson
D. L. Bentley
T. W. Holloway
D. K. Warren
CG6/C. R. Lewis
EJ/W. C. Bradford
EJ2/L. McWhorter
J. A. Porter
EJ3/K. J. Cox
M. C. Contella (3)
D. A. Dyer
T. E. Moore
E. E. Smith
EK/R. W. Kubicki
EK3/P. M. Deans
EP4/D. L. Connelly
ES/R. E. Vale
D. H. Greenshields
ES2/P. C. Glynn
A. C. Mackey
S. P. Weiss
ES3/D. B. Lee
R. C. Reid
G. Strouhal
J. A. Smith
EX/B. Redd
EX3/P. O. Romere
D. E. Tymms
J. M. Underwood
J. C. Young
EX4/R. L. Barton
F. Garcia

K. M. Morrison
P. G. Thomas
FA/R. G. Rose
H. W. Tindall, Jr.
FA2/J. P. Mayer
FE3/B. Davila
R. Duval
FM/R. L. Berry
J. C. McPherson
Branch Chiefs (5)
FM2/L. D. Davis
G. L. Hunt
B. O. McCaffety
K. A. Young
FM4/A. J. Bordano
R. D. Davis
D. Ives
FM8/B. F. Cockrell
R. E. Eckelkamp
M. L. Heck
P. T. Pixley
R. Savely
FM14/Report Control Files (100)
G. Steeley
FM15/D. A. Nelson
FM17/B. Conway
R. M. Moore
FM42/J. C. Harpold (50)
G. L. Carman
H. Garcia
Garland
L. Gonzales
C. R. Halliman
J. A. Hansen
D. W. Heath
O. Hill
Lang
W. C. Lamey
M. N. Montez
J. D. Payne
Silvestri
J. V. West
FS5/J. W. Bormann
FS15/T. Sheehan
LN/H. E. Whitacre
LT/R. H. Kohrs
J. M. Peacock
MG/F. Littleton
WC6/E. R. Hischke
J. W. Mistrot

IBM/M. Bunde
B. Mills
A. Kuhn
D. Ramsey
T. Keller
Lockheed/Y. C. Loh
G. Volentine
MDAC/G. Bell
R. Hamilton
J. Hiott (20)
Langely
H. Kyle
R. Ruda
R. Spier
J. Treybig
H. Stone (2)
W. E. Hayes
E. A. Thompson
L. J. Drapela
R. K. Hamilton
G. Bell
R. Hamilton
R. Spier
H. C. Kyle
R. R. Ruda
W. W. Hinton
J. M. Hiott (20)
J. M. Treybig
K. R. Frohme
J. R. Weyraugh
M. E. Fowler
M. A. Culp
D. E. Wade
J. Treybig
R. M. Blackstock
J. F. Dubel
J. J. Ewell